UNIVERSITY OF BIRMINGHAM

BOND AND DUCTILITY OF CONCRETE REINFORCED WITH VARIOUS STEEL BARS SURFACE AND DUCTILITY CONDITIONS

by

Mohamad Wassouf

A thesis to be submitted to
The University of Birmingham
for the degree of

DOCTOR OF PHILOSOPHY

Supervisors:
Prof. Jian Yang and Prof. Les Clark

The University of Birmingham
School of Engineering
Department of Civil Engineering
Edgbaston
Birmingham
B15 2TT
United Kingdom

September 2015

Table of Contents

Acknowledgment

I owe big and grateful thanks to my idol in this life, Prof. Jian Yang. I will not be able to complete this work without his help, guidance, patience and amazing supervisions. He has helped me through this long journey and given me all the required assistance and attentions. He guides me to learn from his great personality and patience how to deal with life, to meet goals, to work hard and to love your work. In addition to the massive academic knowledge that I learned from him, he put me on the right track in this life. I will always repeat his words regarding life and how to deal with it during the rest of my journey in this world. I really cannot express my deepest gratitude and thankful feelings for him, and would say to him “you are a great supervisor and it is an honour to be next to you for those years of my life”.

My great appreciations go to Prof. Les Clark for his support and great advices during the years of this research.

I would also like to express my thanks to David Cope and all the Civil Engineering staff for the effort they spent and the help they showed me during my research.

Big thanks will go to the University of Birmingham for giving me the chance to work in this great department. Thanks to Celsa group for providing the required materials to finish all the laboratories tests. My appreciation to all my friends and everyone who showed me a smile during my study.

Finally, I would like to extend my deepest thanks to the amazing parents ”Yasser Wassouf & Alisar Jourya”. Without their support I will not be able to write this acknowledgment and reach this point in my life. A big thank you for my great and most adorable sister “Kinda Wassouf”, who was the reason for my smile whenever I faced troubles during my study. Also big thanks to my brother in law “Wissam Issa” for all the support and attention which he gave to me.

Abstract

Reinforced concrete is a wide field for researches and studies in civil engineering subject. It is due to the fact that reinforced concrete is a most widely used material for the infrastructure in the world. Reinforced concrete consists of two main materials: reinforcing steel and concrete, each of those two materials has its own effect on the performance of the structure.

In this thesis, the change in RC performance due to different steel properties and specifications will be investigated. The study focuses on the bond interaction between steel and concrete and the flexural behaviour of RC beams.

Pull-out forces have been exerted on the reinforcing bars in RC blocks to examine the impact of steel properties on the bond strength and failure mode of the blocks. In addition to that, flexural testes have been conducted on simply supported RC beams to investigate how reinforcement properties can affect the ductility of reinforced concrete.

Comparison of results of the previous two tests with codes and analytical models have been carried out to verify the outcome of this research.

On the basis of the investigations that this study carried out, it is found that steel properties have direct impact on the bond behaviour of reinforced concrete. It has been discovered that ribs patters can affect the bond failure mode. Another factor which can affect the bond failure mode of reinforced concrete is the presence of shear links; they

can provide constraining effect and hence enhance the bond performance and allow the RC specimen to have pull-out failure rather than splitting.

The location of reinforcement plays an important role in the bond performance as it has been recorded in this study that the bars placed far from the casting surface showed better bond strength and behaviour comparing to bars closer to the casting surface. As a result of this work, it has been noticed that larger concrete cover has positive effect on the failure mode and can reduce the probability of ending up with splitting failure.

Regarding ductility, it has been proved in this study that reinforcement class and ductility have a positive effect on the ductility and load resistance of RC beams.

Different types of reinforcement have been used to conduct three point loading tests on simply supported beams in order to investigate the impact of reinforcement type on the ductility of RC beams. Single steel bars and welded steel meshes have been used as reinforcement; it was noticed that beams reinforced with steel meshes showed better performance in terms of ductility comparing to those reinforced with single bars

KEYWORDS: bond, ductility, failure mode, steel properties, reinforced concrete, flexural behaviour, splitting failure, pull-out failure, rotational capacity, steel classes, rib pattern, steel meshes, shear links, concrete cover, experimental studies, simply supported beams, pull-out test, one point loading test.

LIST OF FIGURES

LIST OF TABLES

Chapter 1: Introduction

1.1 General Background

Reinforced concrete is a mixture of cement, sand, gravel and water reinforced with steel elements. As tensile strength of the concrete is around 10% of its compressive strength, it is assumed that concrete will not resist any tensile stresses and all tensile resistance will be provided by the steel elements.

Steel elements such as steel bars have different properties and specifications, which may have different effects on the performance of the RC members. Studies and researches have been conducted to study the effect of bar properties on the structural behaviour of RC members. This study will examine three steel classes A, B, C that are classified based on the ductility of each class as shown in Table 1.1. In addition to those classes, another steel type that is produced by Celsa Ltd. will be examined in the study to for comparative study.

Table 1.1: Characteristics of class A, B, C in BS EN 1992-1-1:2004

Class	A	B	C
f_{yk} or $f_{0.2,k}$	400-600	400-600	400-600
$(f_t/f_y)_k$	≥1.05	≥1.08	≥1.15 and <1.35
ε_{uk} (%)	≥2.5	≥5.0	≥7.5

Where:

A, B and C: standard classes of steel reinforcement.

f_{yk}: Characteristic yield strength.

$f_{0.2,k}$: Characteristic values of 0.2% proof stress.

f_t: maximum tensile strength of the steel bar.

f_y: yield strength of the steel bar.

ε_{uk}: Characteristic strain of reinforcement at maximum load.

1.2 Backgrounds of Celsa-max steel bars

Recently a new series of steel reinforcement called as CELSA-max (referred to bar C' in this study) has been produced. This type of new bar has a new surface rib pattern with denser spiral and longitudinal as shown in Figure 1.1, and as such it is expected to provide improved performance and productivity benefits in de-coiling, bending and even in transport and storage. Another benefit is the reduced wear on the straightening machine rolls when producing cut and bent materials and hence results in prolong life for the rollers.

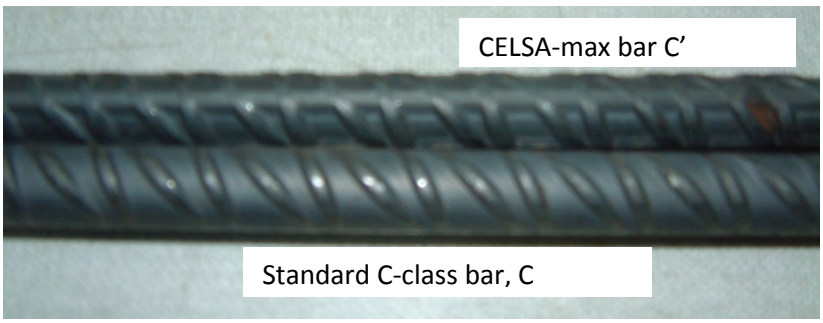

Figure 1.1: ribs pattern for C & C' reinforcing bars

The structural performance of this new bar, such as bond strength and ductility has yet been well known. This work is to address this deficit of knowledge.

This project will investigate the properties of this new type of bars and the resulting reinforced concrete beams by comparing with conventional bar types with particular references to the bond and ductility behaviours. This thesis summarizes

the work that has been carried out and report the findings obtained from the work. In addition, the future work is also proposed.

1.3 Aims and objectives of the study

The primary aim of the research is to study the impact of the steel properties on the bond and ductility performances of reinforced concrete beams. The studied variables include the ductility behaviour of steel bars, the surface pattern, and amount of shear links or other lateral restraining bars (steel mesh). It is well understood that the latter two variables have direct impact on bond strength and bond-slip relationship. So it has been decided that the bond and ductility behaviours of RC beams including various steel bars will be first examined separately with the same variables and then the interactions between both bond and ductility will be examined. It is believed that there is a transition zone of bond strength beyond which the increase of bond strength will have detrimental effect on ductility of reinforced concrete beams and the current work will also identify the transition zone.

To achieve the above aim, the primary objectives are as follows:

- To examine the bond behaviour between steel and concrete in RC beams.
- To characterize the flexural behaviour of RC beams using different types of reinforcing steel under different conditions.
- Based on the above two results, to find the effect of steel properties and the bond interaction between steel and concrete on the ductility of reinforced concrete members.

1.4 Thesis Layout

The above mentioned aim and objectives will be achieved through experimental and analytical methods. The experimental and analytical work is presented as follows:

- Conducting a series of pull-out and ductility tests to investigate the bond strength and ductility of reinforced concrete slabs and beams using different types of steel bars and meshes. Evaluating the influence of reinforcement types and different spacing values on the ductility and bond strength. This part of experimental work consists of two phases:
  - *Phase 1*: bond strength or pull-out test of RC beams and slabs will be conducted to study the effects of variables on bond performance, such as the steel bars surface rib pattern, steel mesh size, shear links spacing and the presence of steel mesh.
  - *Phase 2*: RC beams and slab ductility tests to investigate how the reinforcement ductility influences beam or slab ductility.
- Carrying out parametric studies to propose general design information. The behaviour and results for bond and ductility tests will be calculated by using design models and results will be compared with test dat

Chapter 2: Literature Review

2.1 Bond interaction between steel and concrete

2.1.1 Introduction

Reinforced concrete is concrete in which steel is embedded in such a manner that the two materials act together in resisting forces. Steel provides added strength by taking up the tension, while the concrete withstand the compression. The key to ensure that these two materials work together is the stress transfer between them. Many researches such as Hamad (1995, 1998, and 2004), Cairns and Abdullah (1994 and 1996), Darwin (1993 and 2000) and Tepfers (1973, 1979, 1981 and 2000) have studied the interaction between steel and concrete and its effect on loading capacity and ductility of RC beams. The stress transfer along the steel-concrete interface is always accompanied with a relative movement or slip, and resulting interfacial stress is known as bond stress (Hamad, 1995).

2.1.2 Bond mechanism and influencing factors

The movement of both concrete and steel materials at the interface are different which results in a relative displacement of the steel bar in respect to the surrounding concrete. This movement or displacement is called slip; bond stress arises to resist the interfacial slip resulting in tensile stress transfer into the concrete that ends up with highly-localized strains in the concrete layer close to the reinforcement (interface). The bond action between the steel and concrete can be idealized as a shear force at the circumferential surface of reinforcement (Wang,

2009). Although it is believed that there is also normal action at the interface, which is often ignored in engineering practice.

Portland Cement Association (PCA), as Azizinamini et al (1993) stated, defined the bond as a result from a combination of several parameters, such as the chemical adhesion between the concrete and steel interfaces and the friction caused by pressure of the hardened concrete against the steel bar due to the drying shrinkage of the concrete. In addition, friction interlock or mechanical interaction between the bar ribs and the concrete caused by the relative movements of the tensioned bar results in an increased resistance to slip.

As Mendis and French (2000) reported, it is important that reinforcement force is transferred to the concrete to maintain the structural integrity. The steel bar force is transferred to the concrete by adhesion, friction and mechanical bearing between bar ribs and the surrounding concrete.

Ozoden and Akpinar (2006) defined the major factors that influence the bond strength as follows:

- Casting method (pouring, shot concrete, sliding formwork method).
- Position of reinforcing bar during casting.
- Level of compression and tension strength of concrete. Shrinkage gives rise to the tensile stresses in concrete around the bars which may lead to cracking along the bars thereby causing a reduction in bond resistance, Tepfers (1973).
- Admixtures and enhancing materials for concrete.
- Concrete cover and bar spacing.

- Development length, splicing, hooks and cross bars.
- Diameter and shape (rib pattern) of the reinforcing bars, (in case steel bars are used for reinforcement).
- Adhesion between the concrete and the reinforcing bars.

Bars with ribbed surface are more beneficial for bond than using plain bars. Sofi et al (2007) reported that the most effective means of achieving an effective bond is the use of deformed bars which have a pattern of large deformation rolled onto the surface. Smooth surface allows higher slip of steel bars and leads to a lower bond strength compared to deformed bars which limit the slip of a steel bar while providing higher bond strength.

2.1.3 Types of bond tests

Bond tests are used in the laboratories by all the researches who are interested in defining the strength, behaviour and failure modes of the bond action between reinforcing steel and the surrounding concrete. The bond can be examined in different ways as the use of each of those tests is based on the results that the researcher is intending to study as will be discussed later in each of them.

2.1.3.1 Pull-out test

The tested steel bar is usually loaded by reacting off the concrete surrounding the bar as shown in figure 2.1. Direct pull-out test is useful and cost effective method towards evaluating preliminary relative comparisons.

Williamson (1999) states that the pull-out test method represents the basis for both American and British Standard bond tests; however this test is useful for comparative purposes only as the bar is pulled in tension while the surrounding

concrete will be in almost pure compression which is not a popular or even a rare situation to be found in the real designed structures.

Other researchers, Okelo and Yaun (2005), considered the pull-out method as a popular way of testing bond because it provides a simple means of comparing the relative bond developed by different types of steel bars and concrete. The confining action provided by the surrounding concrete mass or reinforcement should be adequate so as to minimise the risk of splitting the concrete by bond forces.

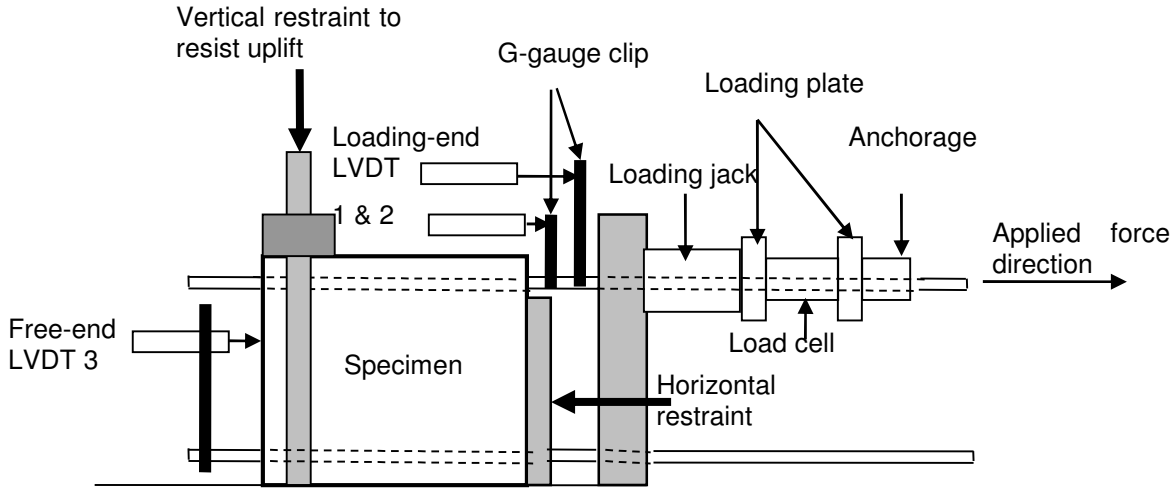

Figure 2.1: Pullout test arrangement.

2.1.3.2 Beam test

Beams can be tested for bond using two different ways as follows:

1. Beam-end test: It is used as a more realistic bond test. They are used extensively in experiments to evaluate the bond strength of steel bars in a reinforced concrete beams. The beams are tested as a simply

supported beams, load will be applied at the end of the cantilevered regions as shown in figure 2.2.

2. RELIM beam test: RELIM beam test shown in figure 2.3 was used by Cairns and Plizzari (2003). It consists of two separated blocks. In this test the bars are de-bonded except for the central portion and are confined by stirrups in both longitudinal and transverse directions.

In general, beam tests have the disadvantage of being costly and time consuming. In addition to that, beam tests were found to have contradictions in their results unlike the pullout tests which seem to be more consistent and popular for bond testing.

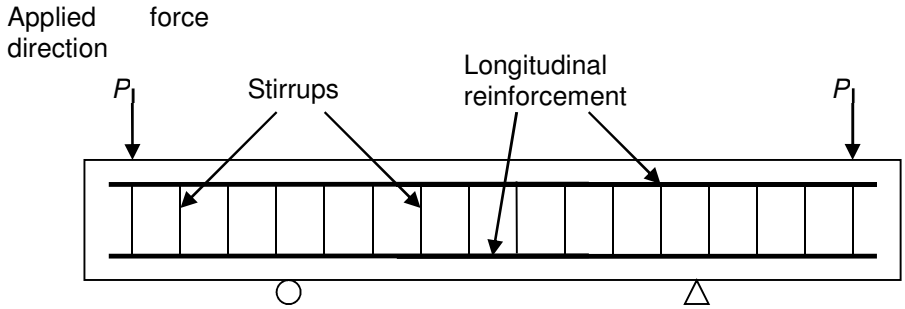

Figure 2.2: Side view of beam-end test arrangement (Darwin, 2000)

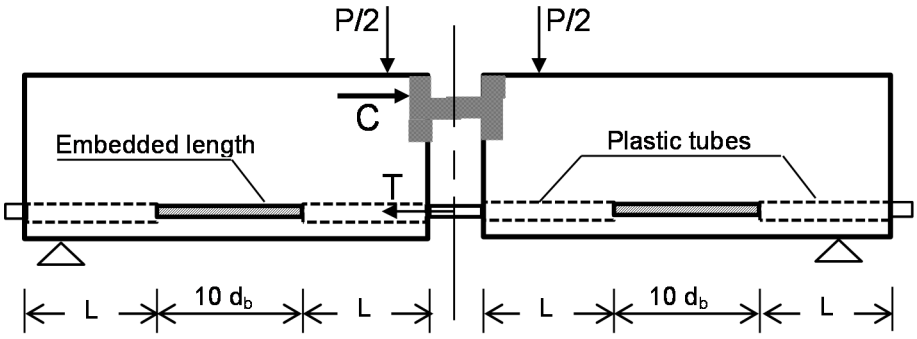

Figure 2.3: RELIM beam test (Cairns and Plizzarie, 2003)

As both bond and structural constitutive behaviours of the specimen will be included in beam tests results; it is difficult to compare bars with different nominal diameters using the beam test. This was the main reason for choosing the pull out method to examine the bond strength and behaviour of the reinforcing bars in this study. Another reason for choosing the pull-out test is the fact that it is more economical and can be done in less time comparing with the beam test.

2.1.4 Bond strength and interaction behaviour

Bond between reinforcement and concrete may conveniently be regarded as a shear stress over the surface of the bar (Cairns and Abdullah, 1996). They also defined the bond strength as the maximum bond stress developed by friction or interlocking mechanism along the reinforcing bar interfaces with surrounding concrete.

Cairns and Jones (1995) defined bond as a transfer of force between a ribbed bar and the surrounding concrete and can be achieved by bearing of the ribs on the concrete. Cairns and Plizzari (2003) stated that the bearing action of ribs generates bursting forces which tend to split the surrounding concrete. As clear from Figure 2.4, the resultant compressive force exerted by the ribs on the concrete is inclined at an angle α to the bar axis. A ring tension in the concrete cover around the bar is created by the radial component of the exerted force. As soon as tensile capacity of the ring is exceeded during the development of the bond action, a splitting failure occurs by fracturing the concrete cover surrounding the reinforcement. If the concrete confinement was enough to counterbalance the force generated by bond

action, a pull-out failure happens with shearing off the concrete at the top of the bar ribs.

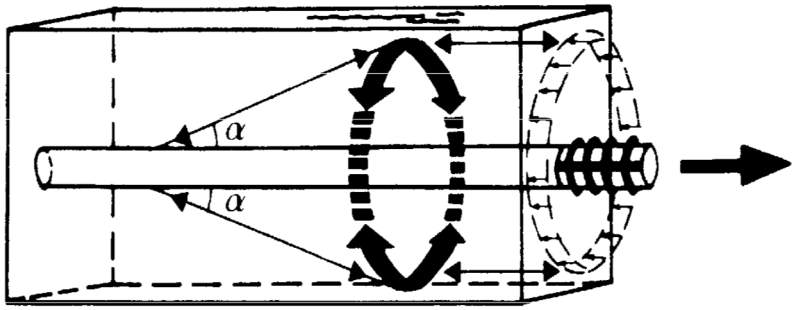

Figure 2.4: Schematic view of splitting forces generated by bond action of ribbed reinforcing bars (Cairns and Abdullah, 1996)

Based on Cairns and Plizzari (1995, 2003) studies, the bond force can be divided into two components. Bond stresses acting along the bar create a shear component of the bond force, while a normal component is created at right angle to the bar ribs as a result of the radial stresses. This normal component acts as an outward pressure on the concrete and is balanced by the hoop (tensile) stresses, (Tepfers and Olsson, 1992).

Joop and Bigaj (1996) published a report which includes a bond model for ribbed bars based on concrete confinement. Three stages have been reported in the study of Joop and Bigaj explaining the bond action between a ribbed steel bar subjected to pull-out force and the surrounding concrete. The model was based on the thick-walled cylinder theory. The internal pressure in this cylinder results from the radial component of the bond force which creates hoop stresses that in order will

perform a circumferential stresses in the concrete surrounding the bar. Those stages will be discussed and compared to Tepfers's study as similar stages in the State of Art report have been presented by Tepfers (2000).

After applying a pull-out force in the steel bar, a bond action will be activated between the two materials (steel and concrete). As stated earlier, this action can be explained by the following stages:

1. **Initial bond stage:** the initial contact between the steel bar and the concrete is developed by adhesion and interlocking. In this stage, the hoop stresses are below the tensile strength of the concrete and a linear-elastic state is performed without any cracks in the concrete section. Tepfers (2000) states that a certain displacement occurs in this stage, even though no bar slip is noticed. This displacement is due to the localized strains which are result of high localized stresses arising close to the interface. For that Tepfers reported that the relative displacement of a bar in this stage consists of the relative slip at the interface and the shear deformation in the concrete.
2. **Partly cracked stage:** this stage can be called an elastic-plastic stage as two sections with two different states, elastic and plastic, are developed in the concrete as shown in figure 2.5.

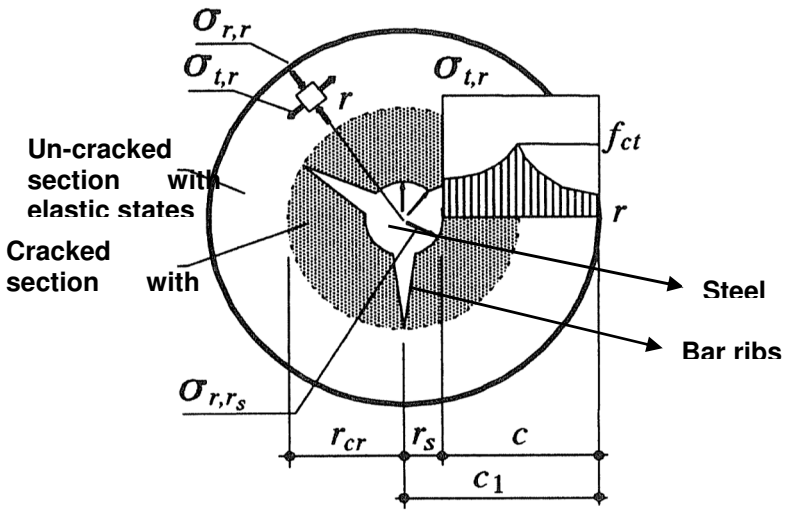

Figure 2.5: Partly cracked section in pull out based on thick walled cylinder theory (Joop and Bigaj, 1996)

Once the initial bond is broken, ribs exert a bearing action against the concrete resulting in a cone shape cracks starting at the edge of the ribs as indicated in figure 2.6, which is presented in a paper for Goto (1971). The bearing action which is exerted onto the concrete will be transferred through the concrete sections located in the space between each two adjacent ribs. It has been agreed to call this small concrete sections “corbels” as they have a similar shape to the real corbels that support beams in a structural building.

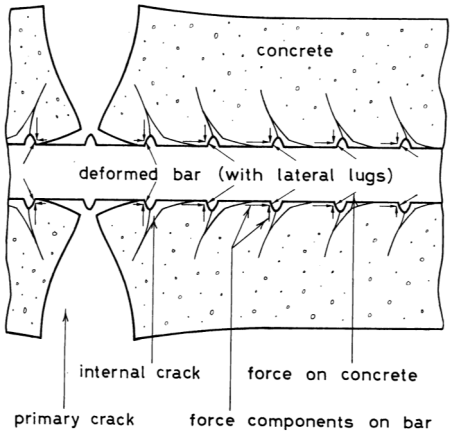

Figure 2.6: Schematic diagram of concrete deformation and crack development around reinforcing steel bar in pull out test (Goto, 1971)

Joop and Bigaj (1996) states that the displacement of the bar in respect to the concrete (slip) in this stage consists of bending of the corbels and movement due to crushing of the concrete in front of the ribs. Cracks start to appear once the circumferential stresses exceed the tensile forces of the confining action. According to the crack formation, the concrete cracked section surrounding the bar tends to be in a plastic state while the rest section of the un-cracked concrete remains in an elastic situation. The plastic region continues to extend radially as cracks are spreading.

It can be said that Tepfers (2000) divides the current stage which is being discussed at the moment into two sub-stages; first sub-stage represents the section when first cracking appears with bond stress values f_b > 0.2-0.8 f_{ct} while the second sub-stage starts when the bond stress exceed 0.8 f_{ct} and keep increasing up to 3 f_{ct}. At this point the outward component of the pressure, radial component of the bond force, is resisted by the hoop stresses in the surrounding concrete (Tepfers, 1979).

3. Entirely cracked section: Joop and Bigaj (1996) state that this stage follows the partly-cracked stage directly as the cracks become wider and the confining action diminishes as a consequence of the softening behavior. If the radial cracks reach the outer surface of the concrete a splitting failure is adopted and sudden drop of the bond stress happens. While when the shear resistance of the concrete corbels can be considered as a criterion for the force transfer mechanism, a new sliding plane will be created with reduction of bond stress until the bar is pulled out of the concrete and a pullout failure takes place.

In the State of Art Report, Tepfers (2000) was more critical in defining the last stage of the bond action as he reported that this stage can occur in three different modes:

1. In the case of plain bars, smooth reinforcing bars without ribs, bond is mainly provided by the adhesion between steel and concrete and partly by stirrups and concrete shrinkage. According to this, bond stress reduces once the adhesive bond is broken which will lead to a result that this stage follows directly the first un-cracked stage.
2. In case of deformed bars, bond tends to fail abruptly due to rib bearing action when the bars are confined by light to medium transverse reinforcement.
3. When deformed bars are heavily confined by transverse reinforcement, the force transfer mechanism changes from rib bearing to friction, as stated before in Joop and Bigaj stages, and the main criterion for the force transfer is the shear resistance of the bar longitudinal movement. Tepfers (2000) explained the reason behind decreasing the bond stress as the interface between steel and concrete gets smoother under continued loading due to wear and compaction leading to pull-out failure.

Another study from Tastani and Pantazopoulou (2013) has divided the behaviour of a reinforcing bar subjected to the pull-out force into four stages as shown in Figure 2.7. They have based on the elastic and plastic responses while applying the pull-out force on the bar. The bar remains in elastic phase in first stage as shown in Figure 2.7 (a). It then starts to enter the plastic region in the second stage as in Figure 2.7 (b) as the maximum bond stress may reach the characteristic

strength value. In Figure 2.7 (c), de-bonding starts and hence it limits the amount of load carried by the bar. The plastic bar response starts in the fourth stage as in Figure 2.7 (d), which lead to the sudden increase in slip with reduction of bond strength over the yielded bar length.

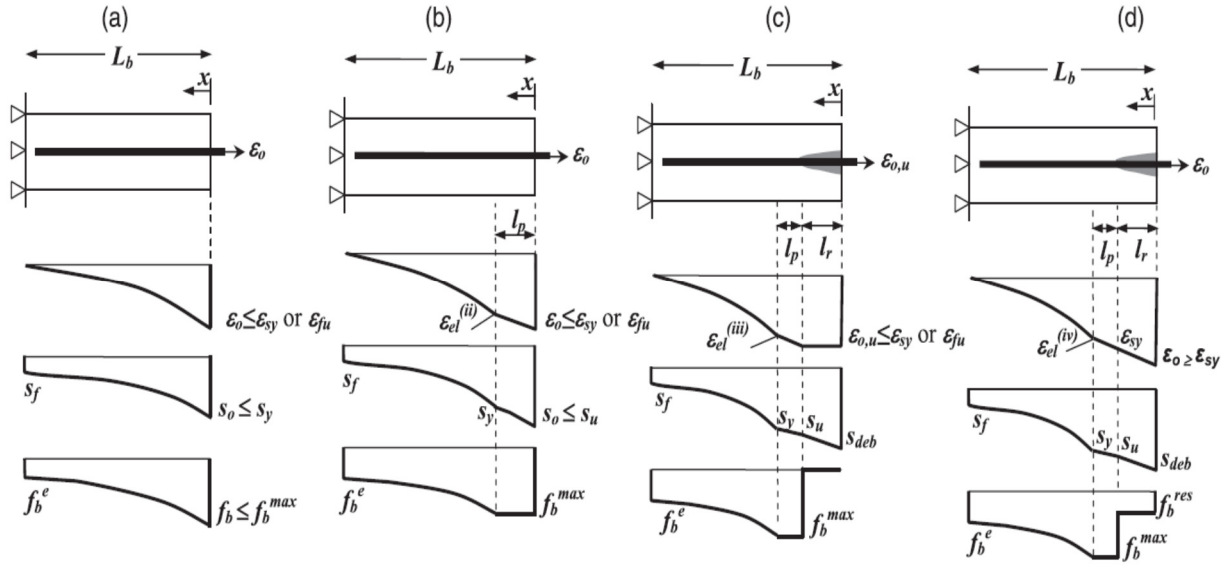

Figure 2.7: Elastic-plastic bar response while bond-slip law (Tastani and Pantazopoulou, 2013)

2.1.5 Bond failure types and cracks development

2.1.5.1 Bond failure types

To define the effect of different factors on the bond behaviour, it is necessary to exam the failure modes of each specimen and associated influence factors. Hamad (1995) defined the pull-out failure when steel is well confined by concrete cover or transverse steel, preventing a splitting failure. In this case, bond strength is controlled by the capacity of concrete in the direct shear. Roman and Robert (2005) reported that the mode of failure of bond is mainly dependent on the concrete

compressive strength, the shape (and composition) of the bar's surface, the cover thickness and the development length.

Based on the ring theory in figure 2.4, two types of failure were reported as follows:

- Concrete cover split: which occurs when the force generated by bond action exceeds the tensile capacity of the ring along with a concrete cover less than approximately three times bar diameter.
- Pull out failure: this occurs when the concrete cover is larger than three times bar diameter or if sufficient confining reinforcement or transverse pressure opposes the splitting force. This type of failure develops with the concrete being sheared on a surface across the tops of the ribs or in other words when the shear strength of concrete below the ribs is overcome.

Joop and Bigaj (1996) reported that the mode of failure is controlled by the confining action which is introduced by the circumferential tensile forces in the concrete and the additional confinement such as stirrups (transverse reinforcement) and external forces. This confining action will act against the radial components of the bond force, which radiate from the bar into the concrete, trying to make an equilibrium situation. In other words the previous statement by Joop and Bigaj can be represented in other words as follows:

- Bond pull-out failure happens if the tensile force represented by the concrete cover, stirrups or external confinement (i.e. external pressure) is greater than the radial component which is a result of the radial force that is transferred from the bar into concrete.

- Splitting failure happens if the confining action is smaller than the radial force.

In case that the confining action is just equilibrating with the radial force, the pull out failure might happen with splitting cracks being developed in the concrete surrounding the bar and tend to extend towards the outer surface of the concrete as the load increases.

The pull-out failure can be divided into two categories as Tepfers (2000) mentioned in the State of Art Report. The confining action represents the basis that Tepfers based on in order to define two different situations for the pull-out failure. When the confining action is large enough as in case of high confinement or large concrete cover; the pull-out failure occurs by shearing off the concrete keys without any visual splitting cracks or partial concrete splitting. On the other hand, the pull-out failure might be accompanied with the partial concrete splitting and visible splitting cracks in the case of limited concrete cover or moderate confinement. While the concrete cover is reduced to be very limited and the section is not confined by stirrups, the spalling-off of the concrete cover is noticed and splitting failure is observed.

2.1.5.2 Bond failure mechanism

Most of the work that has been performed regarding failure modes of the pull-out test specimens was concentrated on the splitting failure mode as it represented the weaker type. This weakness is due to the fact that the bond strengths are lower for splitting failures, which therefore tend to be more critical for design (Cairns and Plizzari, 2003). Cairns and Jones (1995) mentioned that Tepfers did his analysis, for his doctoral research thesis in the year of 1973 under the title “A theory of bond

applied to overlapped tensile reinforcement", based on the triangle model of forces for bond in which equilibrium conditions are considered as shown in figure 2.8a. F_{sp} represents the splitting resistance; F_b stands for bond strength where F_n is defined as the normal stress on the inclined failure surface beneath the bearing face of the rib. Cairns and Jones (1995) went further in their discussion for bond and suggests a non-splitting component of bond strength at zero confining stress. They introduced a fourth component F_v for the model of bond forces in the equilibrium conditions. They have said that the shear stress in the concrete on an inclined failure surface below the baring face of ribs will result in additional fourth F_v. Taking into account the new force the triangle that Tepfers (1973) developed in his thesis will take the shape of a quadrilateral in the equilibrium conditions as shown in figure 2.8b. Unlike Tepfers' analysis, Cairns and Jones reported that it's possible for the bond strength F_b to increase without any increase in the splitting resistance F_{sp} as shown in figure 2.8a.

By noticing Tepfer's model and the modified one by Cairns and Jones, it can be seen that an additional force, F'_v, should be included in the model to reach an equilibrium situation. That force can be defined as the friction interaction between the flat part of the rib and the surrounding concrete. F'_v and F_v are separated by an angle which is equal to the rib face angle. This will lead to a result that F_b can be increased without any increment in either splitting force or concrete cover or the rib face angle. That can be done by increasing the width of the ribs which will result in more friction between concrete and the flat part of the rib. Therefore, F'_v and F_b will be increased by equal increments.

Tepfers (2003) stated that the angle α of the bond forces in different stages of loading can be estimated by the use of “ring pullout test”. The ring pull-out test comprises a small cylindrical concrete body with the axially placed bar. The bond length is three bar diameters and the height of the concrete cylinder is equal to the bond length. A thin steel cylindrical tube with known section area surrounds the concrete cylinder. At loading, the radial and longitudinal bond force components are separated by a ring support with several Teflon sheet layers, which prevents radial forces being taken by supports. The circumferential bond force component is measured with strain gauges and force can be determined. The relation of the bond force components determines the angle α, which may change and increase when load increases.

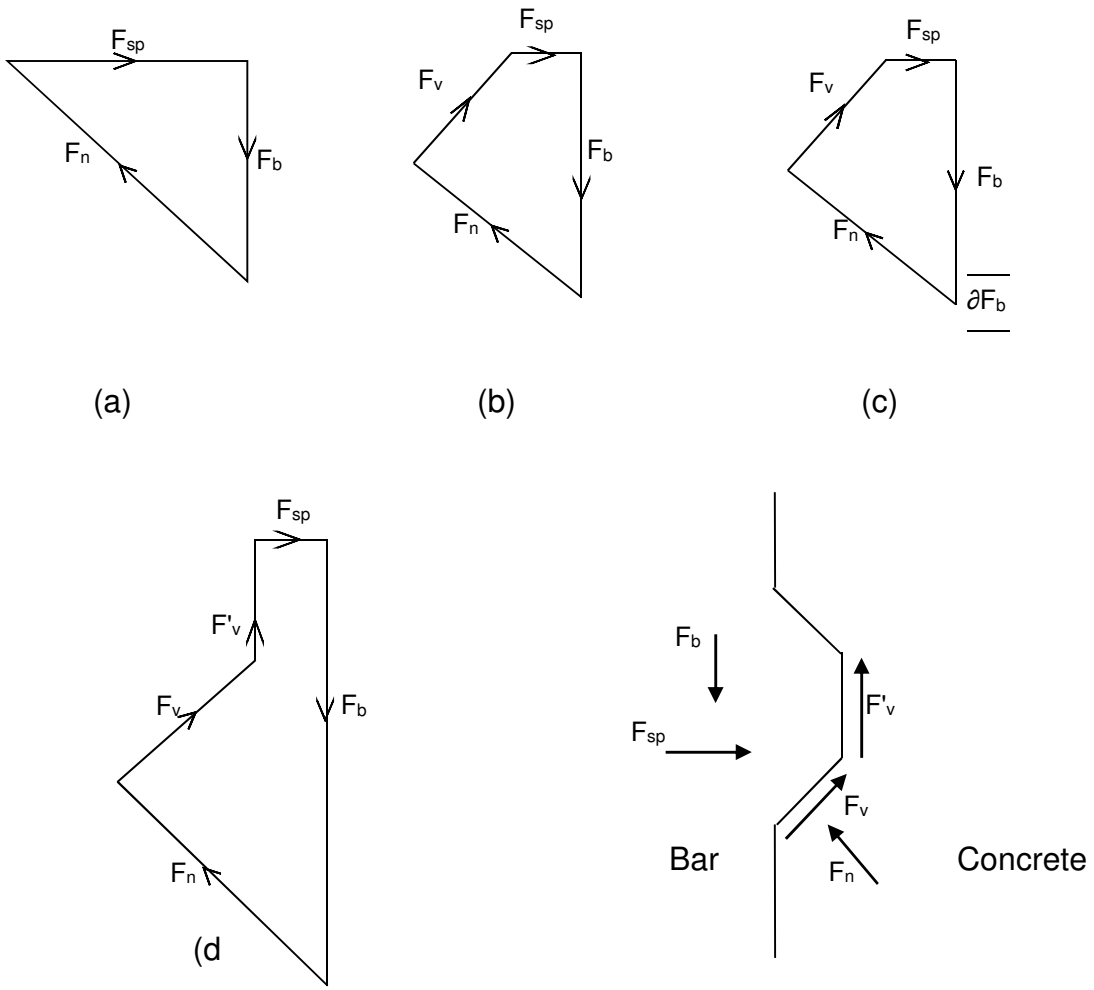

Figure 2.8: Forces associated with splitting bond behavior: (a) triangle of forces for equilibrium in Tepfers model (1973); (b) quadrilateral of forces for equilibrium in Cairns and Jones model (1995); (c) change in bond strength arising from increased cover, Cairns and Jones (1995); (d) bond forces in equilibrium condition associated with an additional force F'_v.

2.1.5.3 Cracks development according to the previous studies

Goto (1971) did a series of tests on axially loaded tensile specimens for the purpose of investigation the deformations in concrete around deformed tension bars by means of indicating ink. The method makes visible crack propagation and the existence of internal cracks when the specimen is split open after load test. Tracking the cracks development and crack types were the reasons for examining the specimens in Goto's study. By injecting ink into the tested block, Goto was able to track the development of the cracks after splitting the specimens longitudinally along the bar.

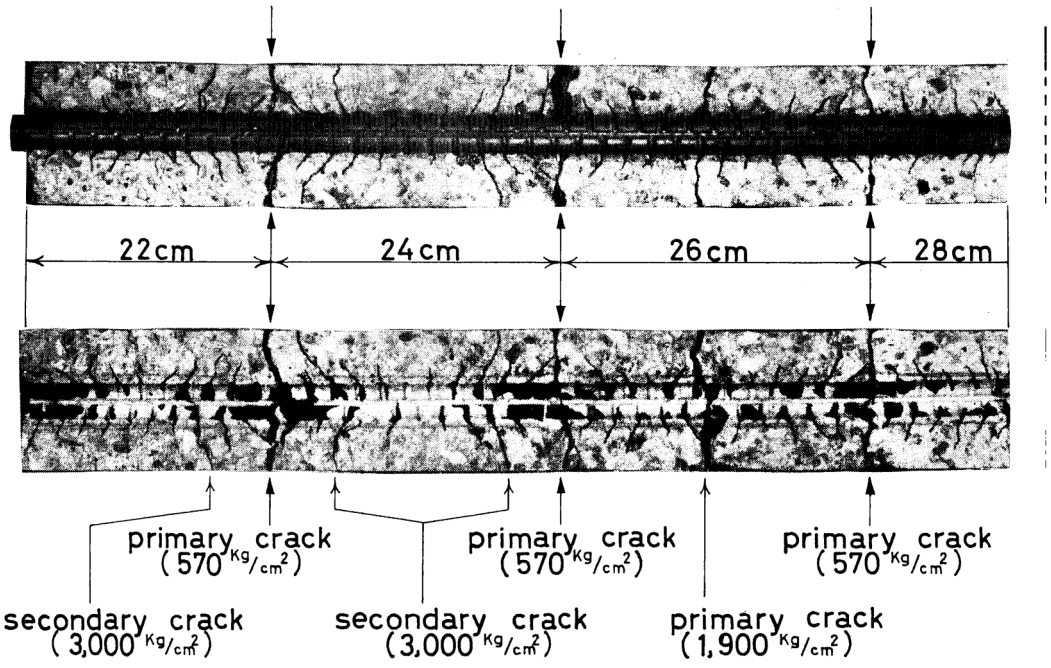

Figure 2.9: Internal cracks with (32 mm) bar (Goto, 1971)

Figure 2.9 shows that many internal cracks formed along the ribbed bar. Those internal cracks depend mainly on the ribs patterns. In the case of Goto's bars, internal cracks were more likely to occur in case of circular ribs more than diagonal

or wavy ribs. Figure 2.10 shows the difference between circular, diagonal and wavy ribs which have been used in the study of Goto (1971).

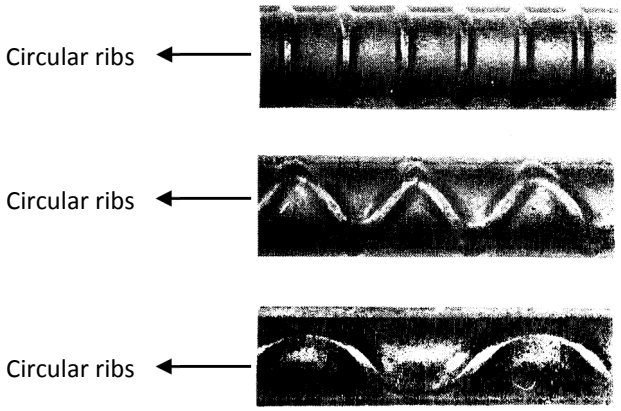

Figure 2.10: Different deformed bars Goto (1971)

From Goto's paper, it possible to say that internal cracks are more likely to happen in case of an angle of 90º is performed between the bar axis and the ribs. The reason for this can be explained as the ribs present a higher restraint on the concrete corbels which result in higher stresses at the interface between steel and concrete. According to this, higher localized strains will be induced at the concrete surface at the vicinity of the steel bar giving the permission for more internal cracks to be developed.

Internal cracks will extend to the outer surface of the specimen and produce vertical cracks as the steel stress increases resulting in the primary cracks as shown in Figures 2.9 & 2.11.

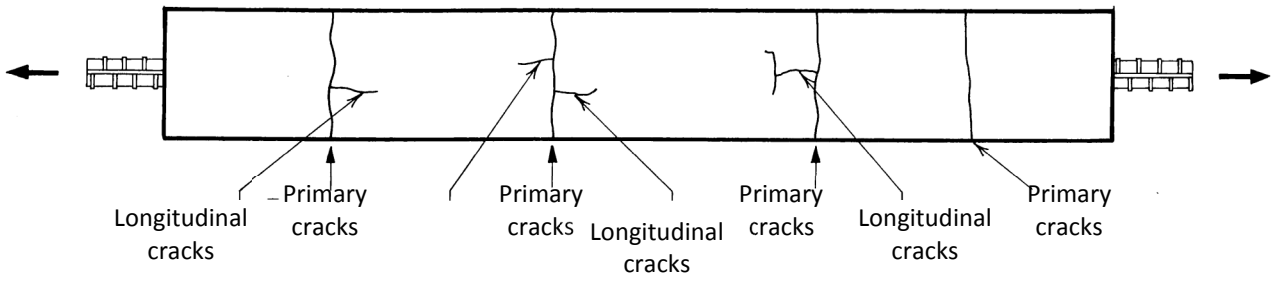

Figure 2.11: Formation of longitudinal cracks Goto (1971)

Starting from the primary cracks at the outer surface of the specimen in the same plane where the steel bar locates, longitudinal cracks initiate and grow horizontally as the steel stress becomes fairly high.

Plizzari et al. (2002) did a series of tests to examine the bond strength; they have done some preparations for their tests as follow:

- To avoid the reduction of the maximum pull-out load, a special heat treatment to the bars to increase the yield strength to about 1200 MPa without changing the other mechanical properties.
- The concrete was poured into wood forms with the principal bars in a vertical position; since the casting direction was opposite of the pull-out force, better bond characteristics were obtained.

As a result of Plizzari's et al. (2002) tests, it has been concluded that in case of using ribbed bars the splitting cracks are often present in the concrete surrounding the bar. These cracks start from the flexural cracks, as shown in figure 2.12, where the bar-to-concrete slip reaches its maximum, and propagate in the longitudinal planes along the reinforcement. Splitting cracks impair the bond mechanical

behaviour (stiffness and strength) and make bond sensitive to confinement. They also have particular relevance for structural durability owing to their longitudinal propagation that exposes a large area of the bar to the environment; this should make the corrosion resistance of members with splitting cracks lower than the resistance of members with flexural cracks.

Another conclusion form Plizzari et al. (2002) study is that the smaller the stirrups diameter is, the larger the splitting crack opening.

Wang (2009) has agreed that the bond between reinforcing steel and concrete can affect a structure's serviceability as it does affect the crack width, distribution and deflection. He has claimed that it is less likely to have splitting failure in wider beams as there is more concrete to prevent them from splitting. In other words, it is the effective beam width b_e that influences bond strength. b_e as shown in figure 2.13 is defined as the distance from centre to centre of the bar spacing or from the edge of the concrete to the centre of the bar spacing.

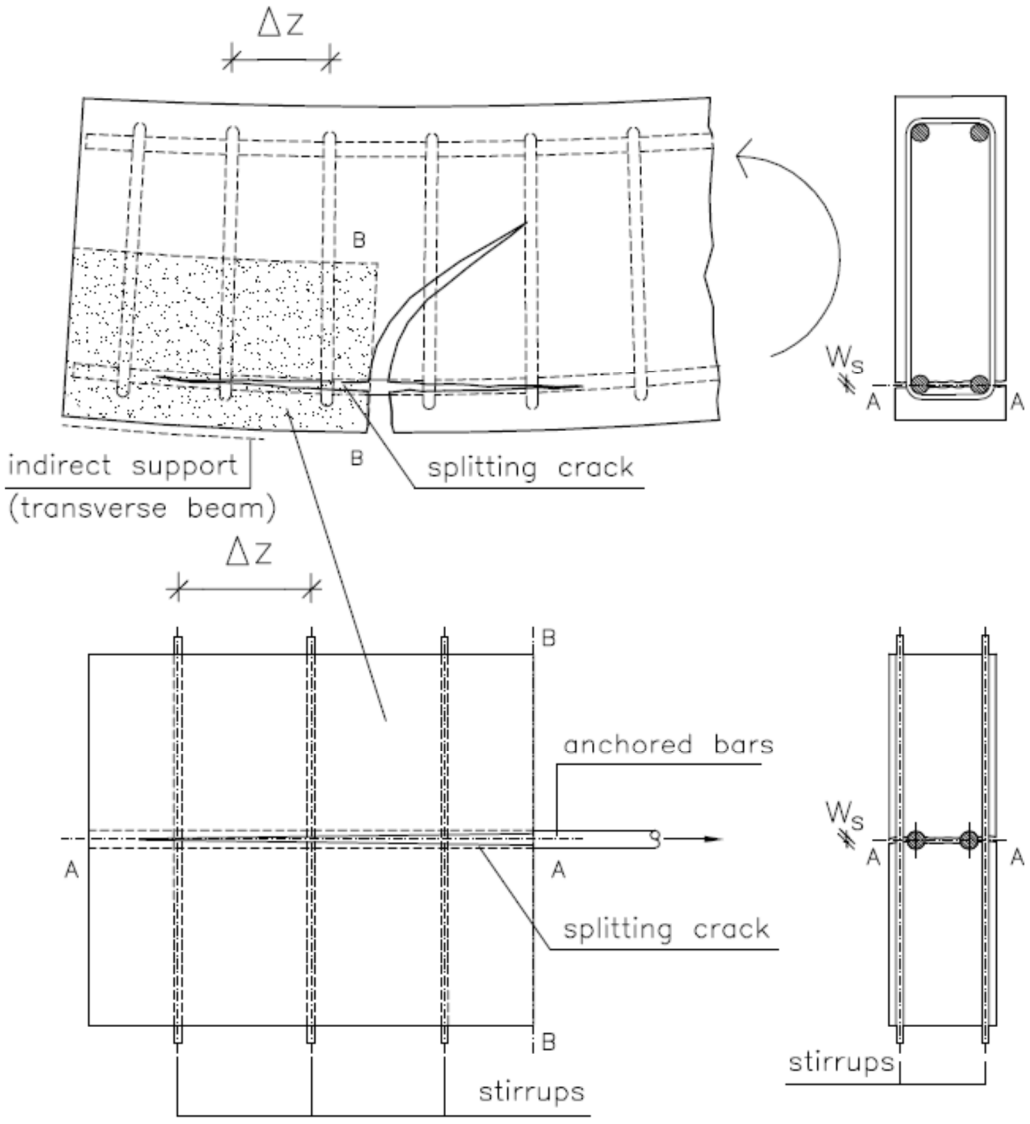

Figure 2.12: Splitting crack propagation Plizzari et al. (2002)

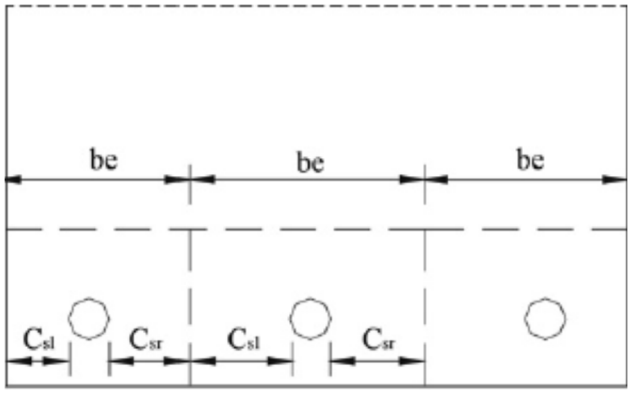

Figure 2.13: Effective beam width b_e (Wang, 2009)

2.1.6 Development length and the bond strength

It has been clear in the literature as Wang (2009) stated in his paper that bond strength is not linear along the development length and maximum bond stresses are developed near the loaded end.

A pull-out experiment of 151 steel specimens has been conducted by Okelo and Yuan (2005). They stated in their conclusion that pull-out force increases with increasing the development length, but the average bond strength decreases. Okelo and Yuan specified the reason for decreasing average bond strength as the pull-out load increase is not proportional to the increase in development length. This reason was one of the conclusions that Darwin et al. (1996) stated in their study. Darwin at al. (1996) pointed out that the relationship between bond force and development length ℓ_d is linear but not proportional. In addition to that Darwin and his colleagues have reported that:

- When the samples are confined with transverse reinforcement, high relative rib area bars require the development lengths that are 13 to 16 percent lower than required by conventional bars.
- If the development length is enough to cause yielding of the bar, the bond strength increases in case of bars reinforced by transverse reinforcement. This increment may result from a more uniform state of bond stress along the length of the bar due to greater slip that accompanies yielding. This greater slip mobilizes clamping stresses in the transverse reinforcement along a greater length of the bar.

Darwin et al (1992) stated that Orangun et al (1977) developed their famous equation for the bond strength of reinforcing bars relying on experimental results:

$$\frac{u}{\sqrt{f'_c}} = 1.22 + \frac{3.23C}{d_b} + \frac{53d_b}{l_d} \qquad (2.1)$$

Based on the same experiments that Orangun and his colleagues did (1977), they proposed a formula for the development length as follows:

$$l_d = \frac{\left(\frac{f_s}{4\sqrt{f'_c}} - 50\right)d_b}{3\left(\frac{C}{d_b}\right) + 1.2} \qquad (2.2)$$

Where:

u: bond strength

f'_c: concrete strength

d_b: steel bar diameter

l_d: developed or anchorage length

f_s: steel stress

C: the minimum of C_s or C_b, (see Figure 2.14) illustrates clearly C_s and C_b

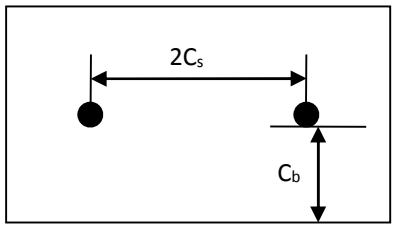

Figure 2.14: C_s and C_b (Darwin et al. 1992)

Orangun et al. (1977) have concluded that the bond force will be increased for an increase in the transverse reinforcement. However, the increment in bond strength will become less effective if an additional transverse reinforcement is provided. Orangun et al. (1977) have defined the additional transverse reinforcement as the amount above that needed to cause pull-out failure instead of splitting failure in case of non-confined concrete.

In light of the previous two equations and on the changes within the ACI Building Code (ACI 318-89), Darwin et al (1992) proposed a more accurate expression for the bond development length considering the effects of (bar size, concrete cover, bar spacing, concrete strength and steel stress):

$$\ell_d = \frac{0.15\left\{\frac{f_s}{\sqrt{f'_c}} - 300\right\}A_b}{(C + 0.5d_b)(0.92 + 0.08C_{max}/C_{min})} \qquad (2.3)$$

In which: C_{max}/C_{min} is the larger and smaller quantities of C_s and C_b, respectively.

A_b: Area of the cross sectional area of the steel bar.

They also presented a table containing modification ratios to modify the design provisions to produce ℓ_d from the previous equation above. The ratios were developed based on changes from the ACI 318-89 as shown in table (2.1).

Table 2.1: ℓ_d for f_y= 414 MPa and f_c=31 MPa, values greater than (1.0) in bold are un-conservative (Darwin et al, 1992)

Bar	No. 3	No. 4	No. 5	No. 6	No. 7	No. 8	No. 9	No. 10	No. 11	No. 14	No. 18
C-C spacing	¾ in. cover										
Minimum	**1.14**	**1.07**	0.98	0.91	0.85	**1.07**	0.96	0.86	0.78	—	—
2.50	1.00	**1.08**	**1.02**	0.97	0.93	0.89	0.88	0.87	—	—	—
3.00	1.00	**1.05**	1.00	0.95	0.90	0.86	0.83	0.79	0.76	—	—
4.00	1.00	1.00	0.95	0.90	0.86	0.82	0.79	0.75	0.72	—	—
5.00	1.00	0.95	0.90	0.86	0.82	0.78	0.75	0.71	0.68	—	—
6.00	1.00	0.91	0.86	0.82	0.78	0.75	0.71	0.68	0.65	—	—
8.00	1.00	**1.01**	0.99	0.94	0.90	0.86	0.82	0.78	0.75	—	—
12.00	1.00	0.89	0.85	0.81	0.77	0.74	0.70	0.67	0.64	—	—
	1½ in. cover										
Minimum	**1.02**	0.95	0.88	0.82	0.76	0.95	0.87	0.79	0.72	1.00	0.98
2.50	1.00	0.85	0.85	0.84	0.83	0.82	0.81	0.79	—	—	—
3.00	1.00	0.89	**1.08**	**1.08**	**1.07**	**1.07**	**1.06**	**1.04**	**1.03**	—	—
4.00	1.00	0.89	0.90	0.88	0.85	0.83	0.83	0.82	0.82	0.89	—
5.00	1.00	0.89	0.88	0.86	0.83	0.81	0.79	0.76	0.74	0.76	0.90
6.00	1.00	0.89	0.86	0.84	0.81	0.79	0.77	0.74	0.72	0.74	0.85
8.00	1.00	0.89	0.81	0.93	0.97	0.94	0.91	0.88	0.86	0.88	**1.01**
12.00	1.00	0.89	0.74	0.85	0.88	0.86	0.83	0.81	0.78	0.80	0.92
	3 in. cover										
Minimum	1.00	0.88	0.81	0.75	0.70	0.88	0.81	0.75	0.69	0.98	0.99
2.50	1.00	0.85	0.84	0.82	0.81	0.79	0.77	0.75	—	—	—
3.00	1.00	0.89	0.98	**1.09**	**1.07**	**1.06**	**1.05**	**1.02**	**1.01**	—	—
4.00	1.00	0.89	0.78	0.86	0.86	0.85	0.85	0.84	0.84	0.89	—
5.00	1.00	0.89	0.72	0.71	0.71	0.71	0.71	0.70	0.70	0.75	0.92
6.00	1.00	0.89	0.72	0.61	0.61	0.61	0.60	0.60	0.60	0.65	0.80
8.00	1.00	0.89	0.72	0.60	0.65	0.65	0.64	0.63	0.62	0.65	0.79
12.00	1.00	0.89	0.72	0.60	0.62	0.62	0.61	0.60	0.59	0.61	0.73

It is obvious from equations (2.2) and (2.3), that Darwin et al (1992) in equation (2.3) is more critical as both C_s & C_b are considered in equation (2.3) while only the minimum value between C_s & C_b has been taken into account in equation (2.2). Based on the previous difference, equation (2.3) tends to be more accurate from the practical point of view as it represents the exact values of bar spacing and concrete cover. Considering the design point of view, equation (2.2) is more conservative as it takes the minimum value between bar spacing and concrete cover which can be considered as the most prone part to fail in the section.

Darwin et al. (1996) conducted the bond tests on 133 splice and development specimens not confined by transverse reinforcement and containing bottom cast bars and 166 specimens, in which the bars are confined by transverse reinforcement. By comparing their results and applying different equations to characterise the bond strength and the development length, they arrived at the summary as follows:

- The square root of the concrete compressive strength f'_c does not accurately characterize the effect of concrete strength on bond strength for the full range of concrete strength in use today, where $f'_c{}^{1/4}$ provides a more accurate representation of the effect concrete of concrete strength on bond strength for concretes with compressive strengths between 17 and 110 Mpa.
- The yield stress of transverse reinforcement f_{yt} plays no measurable role in the contribution of confining steel to bond strength.

2.1.7 Previous studies of the effect of steel bar properties on the bond strength

Reinforcing steel bar properties that affect bond strength can be divided into five categories. Most of the recent studies have carried out on the bar geometry as one of the main factors affecting the bond strength. All factors are mentioned and explained widely below.

2.1.7.1 Bar Size

It has been stated in the State of Art Report (2000) that ribbed bars develop higher bursting forces than the smoothed bars due to the fact that they develop higher bond strength and not because they generate higher splitting forces.

Darwin et al. (1992) have stated that the bond force at failure is a function of bar area as well as being a function of the concrete cover, bar spacing and embedment length. In addition to that bar diameter plays a role in the effect of concrete cover on bond strength. Although there is a consensus that bond strength increases when concrete cover is increased but there is a limit for that increase depends on the ratio of concrete cover divided by bar diameter (c/d). Wu and Zhao (2013) have mentioned that there is a limit value for that increment of bond strength when c/d ≤ 3. So bond strength won't be affected by the concrete cover when c/d ratio is greater than 3.

2.1.7.2 Bar geometry

Skorobogatov and Edwards (1979) have agreed on what Lutz et al. (1966) have concluded regarding the effect of bar ribs on bond between steel and concrete. They have done a series of laboratory tests and showed that the differences in rib face angle doesn't affect the bond strength because ribs will crush the concrete on their way which result in flattening the high face angle of the rib.

Another study to examine the rib's geometry effect of deformed bars in reinforced concrete structures on bond slip characteristics was conducted by Hamad (1996). Fifty six bars were tested in rectangular eccentric pull-out specimens. Three variables were used in this test as follows: rib bar face angle, rib spacing and rib height. According to the results, Hamad noticed an increment of 24 percent in the ultimate load at failure as rib height increased from 5 percent d_b to 10 percent d_b with the rib height to rib spacing ration increased from 0.08 to 0.16. Hamad's results showed that a grade 60 bar (20.6 mm) with a rib face angle of 60 degrees, a rib

spacing of 50 percent d_b, and a rib height of 10 percent d_b was superior to all other bars and developed a greater bond strength during pull-out test.

Hamad defined the importance of bar rib as it plays a major role in developing bond strength by helping to prevent the concrete key (concrete between the bar ribs) from sliding, relative to the rib. Another conclusion from his paper is that the friction developed between reinforcing bars and surrounding concrete, which depends on the geometry of bar ribs, plays a less important role in pull-out failure.

Cairns and Abdullah did series of bond tests in 1990's (1994 & 1996). Two main rib geometric properties mentioned in Cairns and Abdullah studies which are the rib shape and relative rib area. Relative rib area is the ratio of the rib area of the bar above the core, projected on a plane perpendicular to the bar axis, to the nominal surface area of the bar.

Cairns and Abdullah stated that bars with steeper rib face slope tend to slip less than similar bars with less steep ribs, which could be explained as the increase in the rib face angle produces an increase in bond strength; rib face angle is detailed in figure 2.15.

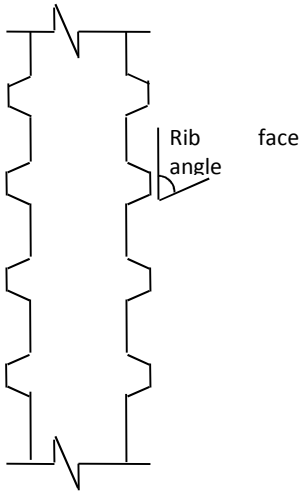

Figure 2.15: Rib bar angle (Leon, 1998)

It was clear from Cairns and Abdullah's study that steel bars with a rib face angle forty degrees or more have shown approximately the same bond behaviour; whereas those of angles below forty degree showed insufficient friction between ribs face and concrete to prevent slip on the rib face.

As a conclusion of the study, Cairns and Abdullah suggested that an increase in the rib face angles and more heavily ribbed deformation patterns would improve the bond strength. Same results were proposed by Darwin et al. (1996).

Darwin and Graham (1993) conducted many tests using beam-end specimens to study the effect of rib height and spacing on bond strength of reinforcing bars using specially machined bars together with standard deformation patterns for comparison. They have found that the relative rib area does affect the bond force-slip response of a bar. At the same time, they have showed that bond force-slip response will not be affected by the specific combination of rib height and spacing. In addition to rib height and rib spacing variation, they have also added confinement using transverse reinforcement in concrete. In all tests the failure mode was observed as a splitting failure. Based on their results and analysis, the bond force-slip response of reinforcing bars is a function of the relative rib area of the bars, independent of the specific combination of rib height and rib spacing. Another conclusion can be observed from their study is that the initial stiffness of the load-slip curve increases with an increase in the relative rib area, and the same trend applies to bond strength only if the bar is confined by transverse reinforcement or higher covers.

2.1.7.3 Steel stress and yield strength

It has been stated in the CEB-FIP state of art report (1990) that the influence of steel yielding is yet not well understood. Due to the contradiction of the steel bar at and beyond yielding, the outward component of the pressure (which is exerted by the bar ribs on the surrounding concrete) may decrease, resulting in a reduced contribution for macro friction. Furthermore, it is also possible that yielding in addition affects the geometry of the ribs, by reducing the area of the projection of the ribs and the relative rib area (bond index).

Also the CEB-FIP report or ribbed bars the influence of steel stress is small as long as the steel is in the elastic range. However, experimental results show that yielding has a drastic effect on the bond mechanism resulting in a non-linear descending branch in the bond-slip relationship at the very onset of the yielding. Hence, the bond stress-slip relationship can be influenced not only by the softening of the surrounding concrete, but also by the softening of the steel at yielding.

Zuo and Darwin (1998, 2000) found that bond stress of bars yield before bond failure are 2% lower than higher strength bars while same values differ by 10% when transverse reinforcement apply.

2.1.7.4 Bar cleanliness

ACI 318 suggests that reinforcement should be free of mud oil and other non-metallic coatings for a good bond condition between steel and concrete.

Pull-out tests performed by several researches (for example Carrera and Ghoddoussi, 1992) showed that bond strength increases with the corrosion rate up to a maximum, after which increasing corrosion causes a significant reduction of

bond strength. The initial increase has been attributed to the expansive nature of iron oxides, whilst the subsequent decrease is related to the build-u of a soft layer of loose corrosion products at the bar-concrete interface.

2.1.7.5 Epoxy-coated bars

The importance of epoxy coating is that it enhances the corrosion resistance of reinforcing bars. It has been noticed that bond strength will reduces when epoxy coating is applied.

2.1.8 Previous studies of the effect of concrete properties on the bond strength

ACI 408R-03 defined concrete properties which affect bond strength as follow:

- **Compressive strength**: it has been noticed that most of the studies and many codes normalize the bond strength by $\sqrt{f'_c}$ when using concrete of strength less than 55 MPa. Examples of the mentioned studies are: Tepfers (1973), Darwin et al. (1992), Esfahani and Rangan (1998a, b), ACI 318 and CEB-FIP. High strength concrete has more possibility for splitting failure comparing to normal strength concrete, this can be explained as there will be no crush for the concrete in front of concrete ribs due to the high bearing capacity. As a result the local slip is reduced and fewer ribs transfer load between steel and concrete which will help to increase the local tensile

stresses and initiate a splitting failure before achieving a uniform distribution of the bond force.

Yalciner et al. (2012) have conducted series of pull out tests using two different concrete mixes, three different concrete covers and different mass losses of reinforcement bars after corrosion. They have noticed that bond strength increases along with the compressive strength as long as the ratio of (concrete cover/bar diameter) is less than 3.2. Otherwise no significant change will be noticed in the bond strength.

They have concluded that increasing the compressive strength for bars with same concrete cover will result in higher bond strength than increasing the concrete cove for bars with same compressive strength.

- **Aggregate type and quantity**: Zuo and Darwin (1998, 2000) have concluded that high strength coarse aggregate can increase the bond strength by 13% in comparison with weaker coarse aggregate. They have also observed that strength and quantity of coarse aggregate can increase the bond strength for confined concrete by 45%.
- **Tensile strength and fracture energy**: the effect of compressive concrete strength and aggregate type and quantity can give an idea about the important role that tensile strength has on the bond strength. Braham and Darwin (1999) have observed that higher fracture energy has a positive effect on bond strength. Higher fracture energy can be provided by high-strength fibers.
- **Lightweight concrete**: bars casted in light weight concrete with or without confinement have lower bond strength values comparing with bars casted in

normal weight concrete. ACI 408R-03 has stated that lightweight concrete is expected to have lower tensile strength, fracture energy and bearing capacity than normal weight concrete which can be the reason behind the low values of bond strength in case of using lightweight concrete.

- **Concrete slump and workability admixtures**: high-slump concrete has a negative effect on bond strength and top and bottom-cast bars have reduced bond strength in case of using high-slump concrete compared with same bars and same conditions in case of using low-slump concrete as Zekany et al. (1981) observed from their study.
- **Mineral admixtures**: series of tests have been done by Gjorv, Monteiro and Mehta (1990) using the ASTM C 234 pull out test (ASTM 1991) to study the effect of silica fume on bond strength. They have concluded that adding silica fume can enhance the bond strength.
- **Fiber reinforcement**: adding fiber reinforcement to concrete can increase the tensile strength. It has been concluded by that a small increase in the modulus of rupture 10-20% can be resulted when using FRP.
- **Consolidation**: ACI 408R-03 defines consolidation as removing voids within concrete. Adequate consolidation can be obtained with high frequency vibration.

2.1.9 Analytical models and descriptive equations in literature, standards and codes of practice

2.1.9.1 Standards & codes of practice

Three codes are considered to be adapted and adopted in this study. Eurocode 2 has been chosen as it is the standard code in Europe in addition to two codes by the American Concrete institute (ACI 318-02 & ACI 408-01). In addition to the previous codes, Comite Euro-International du Beton and federation Internationale de la Precontraine (CEB-FIP) 1990 is considered as it covers in its report different types of structures as well as buildings.

The equation of each code is shown below along with each own variables.

- **Eurocode 2 (EC2):**

  Theoretical bond strength can be calculated based on BS EN 1992-1-1:2004. The ultimate bond strength is calculated by the equation:

$$f_{bd} = 2.25\eta_1\eta_2 f_{ct} \tag{2.4}$$

Where:

f_{bd} is the theoretical ultimate bond strength

f_{ct} is the concrete tensile strength according to section 3.1.6 (2) P in EC2

η_1 = 1.0 for good bond conditions and 0.7 for all other conditions, in this study η_1 is 1.0 for bottom bars as they are considered to be in good bond conditions, whereas η_1 is 0.7 for top bars

η_2 = 1.0 for bar diameter ≤ 32 mm and (132-Ø)/100 for bar diameter >32 mm

Equation (2.4) does not take into account the effect of steel confinement, so the theoretical bond strength prediction with equation (2.4) can be used to compare with test results without any shear links. However, the above equation can be modified by considering the development length calculation formula proposed in EC2, i.e.

$$l_{bd} = \alpha_1\alpha_2\alpha_3\alpha_4\alpha_5 . l_{b,rqd} \quad (2.5)$$

Where α coefficients have been included to allow for various influence factors. Since the bond length in this case is fixed, so we associated these coefficients with bond strength as follows

$$f_{bd} = \eta_1\eta_2 f_{ctd} / \alpha_1\alpha_2\alpha_3\alpha_4\alpha_5 \quad (2.6)$$

Where:

- α_1 is for the effect of the form of the bars assuming adequate cover.
- α_2 is for the effect of concrete minimum cover and calculated for straight bars as $\alpha_2 = 1 - 0.15\ (C_d - \varphi)/\varphi$ and $1.0 \leq \alpha_2 \geq 0.7$, in which C_d is the minimum of concrete cover and the clear distance between reinforcing bars.
- α_3 is for the effect of confinement by transverse reinforcement and given by the following equation:

  $$\alpha_3 = 1 - K\lambda \quad (2.7)$$

  Where $1.0 \geq \alpha_3 \geq 0.7$

  $\lambda = (\Sigma A_{st} - \Sigma A_{st,min})/ A_s$

ΣA_{st} cross-sectional area of the transverse reinforcement along the design anchorage length l_{bd}

$\Sigma A_{st,min}$ cross-sectional area of the minimum transverse reinforcement = 0.25 A_s for beams and 0 for slabs

A_s area of a single anchored bar with maximum bar diameter

K value is shown in figure 2.16

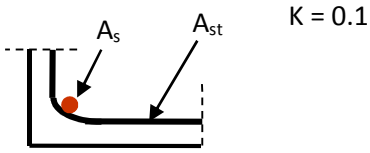

Figure 2.16: Values of K for beams and slabs

- α_4 is for the influence of one or more welded transverse bars ($\varphi_t > 0{,}6\varphi$) along the design anchorage length l_{bd}.
- α_5 is for the effect of the pressure transverse to the plane of splitting along the design anchorage length.

- **ACI 318-02**

For deformed bars or deformed wires, chapter 12 of ACI 318-02 presents in section 12.2 equation for the development length as shown in equation (2.8). Bond strength is calculated by considering yield force of the reinforcing bar as the pull-out force and using embedment length from equation (2.8).

$$l_d = \left[\frac{3}{40}\frac{f_y}{\sqrt{f_c'}}\frac{\alpha\beta\gamma\lambda}{\left(\frac{c+K_{tr}}{d_b}\right)}\right]d_b \qquad (2.8)$$

Where:

- c = spacing or concrete cover. The smaller of either distance from the centre of bar to the nearest concrete surface or one-half the centre-to-centre spacing or the bars (inch)
- d_b = nominal diameter of reinforcing bar
- f_y = yield strength of reinforcement (psi)
- K_{tr} = transverse reinforcement index = $\frac{A_{tr} f_{yt}}{1500sn}$ (psi) where:
  - A_{tr} = total-cross sectional area of all transverse reinforcement that is within the spacing s and that crosses the potential plane of splitting through the reinforcement being developed (inch^2)
  - f_{yt} = specified yield strength of transverse reinforcement (psi)
  - s = maximum centre-to-centre of transverse reinforcement within l_d (inch)
  - n = number of bars or wires being spliced or developed.
- f_c` = specified compressive strength of concrete (psi).
- l_d = development length of deformed bars and deformed wires in tension (inch)
- α = reinforcement location factor which is considered (1.3) in case more than 12 in (304.8 mm) of fresh concrete is casted below the reinforcing bar. Otherwise it should be has a value of (1.0) which is the case in all bars of this study
- β = coating factor that is considered to be (1.0) for uncoated reinforcement.

- γ = reinforcement size actor. Equals to (0.8) for all bars and deformed wires smaller than No. 6 (19.05 mm)
- λ = lightweight aggregate concrete factor.

- **ACI 408-01**

ACI committee 408 has updated the analytical equations for bond strength in the study of Zuo and Darwin (2000). Minor changes have been added by the ACI committee, only three numbers differ between Zuo and Dawrin (2000) and the ACI 408-01.

For the bars without any transverse reinforcement, the bond strength is given by equation (2.9) while equation (2.10) gives the bond strength for bars with transverse reinforcement. ACI 408-01 has adopted same restriction, equation (2.11) as in Zuo and Darwin (2000) to limit the applicability to cases in which a splitting failure governs. All equations are converted into SI system and presented as follow:

$$\frac{T_c}{f_c'^{1/4}} = \frac{A_b f_s}{f_c'^{1/4}} = \left[1.43 l_d \left(c_{\min} + 0.5 d_b\right) + 57.4 A_b\right]\left(0.1\frac{c_{\max}}{c_{\min}} + 0.90\right) \quad (2.9)$$

$$\frac{T_b}{f_c'^{1/4}} = \frac{T_c + T_s}{f_c'^{1/4}} = \frac{A_b f_s}{f_c'^{1/4}} = \left[1.43 l_d \left(c_{\min} + 0.5 d_b\right) + 57.4 A_b\right]\left(0.1\frac{c_{\max}}{c_{\min}} + 0.90\right) + \left(8.9 t_r t_d \frac{N A_{tr}}{n} + 558\right) f_c'^{1/2} \quad (2.10)$$

$$\frac{1}{d_b}\left[\left(c_{\min} + 0.5 d_b\right)\left(0.1\frac{c_{\max}}{c_{\min}} + 0.90\right) + \left(\frac{6.26 t_r t_d A_{tr}}{sn}\right) f_c'^{1/2}\right] \le 4.0 \quad (2.11)$$

where:

A_b = area of bar being developed

A_{tr} = area of each stirrup or tie crossing the potential plane of splitting

adjacent to the reinforcement being developed

c_{max} = maximum of bottom concrete cover of the reinforcing bar, side concrete cover of reinforcing bar or half of the clear spacing between bars

c_{min} = minimum of bottom concrete cover of the reinforcing bar, side concrete cover of reinforcing bar or half of the clear spacing between bars

d_b = diameter of bar

f_c` = concrete compressive strength based on (150 X 300 mm) cylinders

f_s = stress in reinforcing bar

l_d = development length

M = ratio of the average yield strength to the design yield strength if the developed bar

N = number of transverse stirrups within the development length

N = number of bars being developed

T_c = concrete contribution to total bond force, the bond force that would be developed without transverse reinforcement

T_b = total bond force of a developed or spliced bar

T_s = steel contribution to total bond force, the additional bond strength provided by the transverse steel

t_r = term representing the effect of relative rib area on T_s

= $9.6R_r + 0.28$

t_d = term representing the effect of bar size on T_s

$= 0.03d_b + 0.22$

R_r = bearing area / shearing area = h_r / s_r, see figure 1.17.

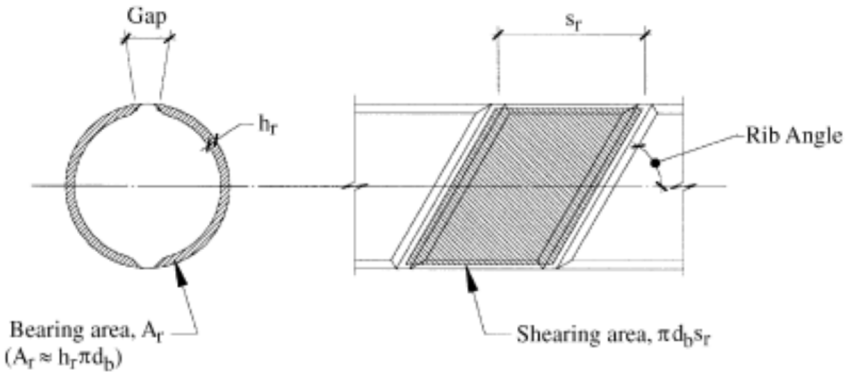

Figure 2.17: Definition of R_r (ACI 408.3R)

- **CEB-FIP Model code**

  The Comite Euro-International du Beton and federation Internationale de la Precontraine (CEB-FIP) 1990 has presented an expression for the development length of straight reinforcing bars ad splice lengths. The SI version of the development length is:

$$\frac{l_b}{d_b} = \frac{1}{6.55}\left(1.15 + 0.15\frac{c_{\min}}{d_b}\right)\left(1 - K\frac{\sum A_{tr} - \sum A_{tr,\min}}{A_b}\right) + \frac{Mf_y}{\left(\frac{f_c' - 2.75}{10}\right)^{2/3}} \qquad (2.12)$$

The bond strength can be calculated using the development length from equation (2.12) and considering the maximum pull-out force equals to the yield force of the reinforcing bar:

where:

A_b = area of largest bar being developed

A_{tr} = area of each stirrup or tie crossing the potential plane of splitting adjacent to the reinforcement being developed

$\sum A_{tr}$ = $0.25A_b$ for beams and 0 for slabs

c_{min} = minimum of bottom concrete cover of the reinforcing bar, side concrete cover of reinforcing bar or half of the clear spacing between bars

d_b = diameter of bar

f_c` = concrete compressive strength based on (150 X 300 mm) cylinders

f_y = yield strength of steel being developed

K = 0.10 for a bar confined at a corner bend of a stirrup or tie

= 0.05 for a bar confined by a single leg of a stirrup or tie

= 0 for a bar that is not confined

l_d = development length

M = ratio of the average yield strength to the designed yield strength of the developed bar

2.1.9.2 Analytical models expressions

Four models are shown in this study as follow:

- **Zuo and Darwin (1998,2000)**

  Zuo and Darwin (1998, 2000) have extended the work of Darwin et al. (1996). They have done a wide range of tests, more than 300 specimens, in order to examine the bond interaction between concrete and reinforcing steel.

The study of Zuo and Darwin (1998, 2000) came out with two expressions for bond strength based on that $f_c`^{1/4}$ is the most realistic value to represent the contribution of concrete to the bond strength

$$\frac{T_c}{f_c'^{1/4}} = \frac{A_b f_s}{f_c'^{1/4}} = \left[1.43 l_d \left(c_{\min} + 0.5 d_b\right) + 56.2 A_b\right]\left(0.1\frac{c_{\max}}{c_{\min}} + 0.90\right) \tag{2.13}$$

$$\frac{T_b}{f_c'^{1/4}} = \frac{T_c + T_s}{f_c'^{1/4}} = \frac{A_b f_s}{f_c'^{1/4}} = \left[1.43 l_d \left(c_{\min} + 0.5 d_b\right) + 56.2 A_b\right]\left(0.1\frac{c_{\max}}{c_{\min}} + 0.90\right) + \left(9 t_r t_d \frac{N A_{tr}}{n} + 744\right) f_c'^{1/2} \tag{2.14}$$

Both equations (2.13&2.14) are limited to splitting failure mode so equation (2.15) is presented with Zuo and Darwin (1998, 2000) study to limit the applicability of their expressions.

$$\frac{1}{d_b}\left[\left(c_{\min} + 0.5 d_b\right)\left(0.1\frac{c_{\max}}{c_{\min}} + 0.90\right) + \left(\frac{6.26 t_r t_d A_{tr}}{sn}\right) f_c'^{1/2}\right] \le 4.0 \tag{2.15}$$

Where:

A_b = area of bar being developed

A_{tr} = area of each stirrup or tie crossing the potential plane of splitting adjacent to the reinforcement being developed

c_{max} = maximum of bottom concrete cover of the reinforcing bar, side concrete cover of reinforcing bar or half of the clear spacing between bars

c_{min} = minimum of bottom concrete cover of the reinforcing bar, side

concrete cover of reinforcing bar or half of the clear spacing between bars

d_b = diameter of bar

f_c` = concrete compressive strength based on (150 X 300 mm) cylinders

f_s = stress in reinforcing bar

l_d = development length

N = number of transverse stirrups within the development length

n = number of bars being developed

T_c = concrete contribution to total bond force, the bond force that would be developed without transverse reinforcement

T_b = total bond force of a developed or spliced bar

T_s = steel contribution to total bond force, the additional bond strength provided by the transverse steel

t_r = term representing the effect of relative rib area on T_s

$= 9.6R_r + 0.28$

t_d = term representing the effect of bar size on T_s

$= 0.03d_b + 0.22$

R_r = bearing area / shearing area = h_r / s_r

Figure 22 shows a drawing for R_r as it is defined by ACI 408.3R

- **Orangun, Jirsa and Breen (1975, 1977)**

Orangun, Jirsa and Breen (1975, 1977) have done a number of experimental tests and used regression analysis in order to develop two expressions for calculating bond strength of a reinforcing steel bar with and

without confinement. Equations (2.16 & 2.17) represent bond strength for non-confined and confined bars respectively.

$$\frac{u_c}{\sqrt{f_c'}} = 0.10 + 0.25\frac{c_{\min}}{d_b} + 4.15\frac{d_b}{l_d} \tag{2.16}$$

$$\frac{u_b}{\sqrt{f_c'}} = \frac{u_c + u_s}{\sqrt{f_c'}} = 0.10 + 0.25\frac{c_{\min}}{d_b} + 4.15\frac{d_b}{l_d} + \frac{A_{tr} f_{yt}}{41.5 s n d_b} \tag{2.17}$$

$$\frac{1}{d_b}\left(c_{\min} + 0.4 d_b + \frac{A_{tr} f_{yt}}{10.34 s n}\right) \le 2.5 \tag{2.18}$$

Where:

A_{tr} = area of each stirrup or tie crossing the potential plane of splitting adjacent to the reinforcement being developed

c_{min} = minimum of bottom concrete cover of the reinforcing bar, side concrete cover of reinforcing bar or half of the clear spacing between bars

d_b = diameter of bar

f_c` = concrete compressive strength based on (150 X 300 mm) cylinders

f_{yt} = yield strength of transverse reinforcement

l_d = development length

n = number of bars being developed

s = spacing of transverse reinforcement

u_b = bond strength of a bar confined by transverse reinforcement

u_c = average bond strength at failure of bar nor confined by transverse reinforcement

u_s = bond strength of a bar attributed to the confinement provided by the transverse reinforcement

- **Darwin et al. (1996)**

Dawrin et al. (1996) have used the data provided by Orangun, Jirsa and Breen to and came out with two equations (2.19 & 2.20) to calculate bond strength of non-confined and confined reinforcing bars respectively. Darwin et al. (1996) have done more laboratories tests and extended their equation to include the effect of relative rib area R_r as they have found out that it has a major contribution to the bond strength of reinforcement.

Dawrin et al. have also limit the applicability of their equations to cases in which splitting failure occurs as presented in equation (1.21).

$$\frac{T_c}{f_c'^{1/4}} = \frac{A_b f_s}{f_c'^{1/4}} = \left[1.5 l_d \left(c_{\min} + 0.5 d_b\right) + 51 A_b\right]\left(0.1\frac{c_{\max}}{c_{\min}} + 0.90\right) \quad (2.19)$$

Where $\left(0.1\frac{c_{max}}{c_{min}} + 0.9\right) \leq 1.25$

$$\frac{T_b}{f_c'^{1/4}} = \frac{T_c + T_s}{f_c'^{1/4}} = \frac{A_b f_s}{f_c'^{1/4}} = \left[1.5 l_d \left(c_{\min} + 0.5 d_b\right) + 51 A_b\right]\left(0.1\frac{c_{\max}}{c_{\min}} + 0.90\right) + 53.3 t_r t_d \frac{N A_{tr}}{n} + 1019 \quad (2.20)$$

$$\frac{1}{d_b}\left[\left(c_{\min} + 0.5 d_b\right)\left(0.1\frac{c_{\max}}{c_{\min}} + 0.90\right) + \left(\frac{35.3 t_r t_d A_{tr}}{sn}\right)\right] \leq 4.0 \quad (2.21)$$

Where:

A_b = area of bar being developed

A_{tr} = area of each stirrup or tie crossing the potential plane of splitting adjacent to the reinforcement being developed

c_{max} = maximum of bottom concrete cover of the reinforcing bar, side concrete cover of reinforcing bar or half of the clear spacing between bars

c_{min} = minimum of bottom concrete cover of the reinforcing bar, side concrete cover of reinforcing bar or half of the clear spacing between bars

d_b = diameter of bar

f_c` = concrete compressive strength based on (150 X 300 mm) cylinders

f_s = stress in reinforcing bar

l_d = development length

N = number of transverse stirrups within the development length

n = number of bars being developed

T_c = concrete contribution to total bond force, the bond force that would be developed without transverse reinforcement

T_b = total bond force of a developed or spliced bar

T_s = steel contribution to total bond force, the additional bond strength provided by the transverse steel

t_r = term representing the effect of relative rib area on T_s

$= 9.6R_r + 0.28$

t_d = term representing the effect of bar size on T_s

$= 0.03d_b + 0.22$

R_r = bearing area / shearing area = h_r / s_r

Figure 22 shows a drawing for R_r as it is defined by ACI 408.3R

- **Esfahani and Rangan (1998)**

Esfahani and rangan (1998) have done a series of tests and developed an analytical model for reinforcing bars not confined with stirrups based on Tepfers (1973). They have come out with two expressions based on the specified compressive strength of concrete. They have specified (50 MPa) as a limit for using the expressions

For f_c`< 50 MPa:

$$\frac{T_c}{\sqrt{f_c'}} = \frac{A_b f_s}{\sqrt{f_c'}} = 2.7\pi l_d \frac{(c_{\min} + 0.5d_b)\left(1+\frac{1}{M}\right)}{\left(\frac{c_{\min}}{d_b}+3.6\right)\left(1.85+0.024\sqrt{M}\right)}\left(0.12\frac{c_{med}}{c_{\min}}+0.88\right) \qquad (2.22)$$

Where:

A_b = area of bar being developed

c_{min} = minimum of bottom concrete cover of the reinforcing bar, side concrete cover of reinforcing bar or (half of the clear spacing between bars + bar radius)

c_{med} = median of bottom concrete cover of the reinforcing bar, side concrete cover of reinforcing bar or (half of the clear spacing between bars + bar radius)

d_b = diameter of bar

f_c` = concrete compressive strength based on (150 X 300 mm) cylinders

f_s = stress in reinforcing bar

l_d = development length

T_c = concrete contribution to total bond force, the bond force that would be developed without transverse reinforcement

2.2 Ductility literature review

2.2.1 Introduction

Concrete ductility is the ability to absorb energy by developing large deformation while retaining the integrity of the structure. It plays an important role in developing alternative loading path upon overloading, withstanding seismic and impact loadings and providing adequate robustness without causing disproportional failure (Kwan et al, 2002).

2.2.2 Definition of ductility

Ductility can be broadly defined as the ability of the member/structure to withstand load while incurring additional deformation beyond the maximum point, Ahmad et al (1995). Another definition for ductility was given by NIST (2007) as an ability of the members and their connections to maintain their strength through large deformation and load distribution associated with the loss of key structural elements.

Beeby (1997) reported that ductility is a property which has been valued in reinforced concrete design from an early stage in the development of the material. In some areas the requirements for ductility and the means of providing it have been extensively researched while, in others, understanding does not extend beyond a qualitative feel for its benefits. The reasons generally given for requiring ductility are:

- Provide ‘robustness’ which is an ability to withstand unforeseen local accidents without progressive collapse.
- Give warning of incipient collapse by the development of large deformations prior to collapse.

- Enable moments in indeterminate structures to redistribute themselves near ultimate so that intentional and unintentional deviations from the 'true' bending moment distribution can be accommodated;
- Enable major distortions to be accommodated and energy to be absorbed without collapse during an earthquake in seismic regions.

A coordinate research program set by Commission of the Committee European de Beton (CEB) in 1967 in order to establish rules governing the ductility of reinforced concrete. The research took place in many countries and laboratories and the results were brought together as one report. CEB results have characterized ductility by the plastic rotational capacity (θ_p) which was given by the equation:

$$\theta_b = 0.004(d/x) \tag{2.23}$$

A typical moment-rotation relationship for simply supported double reinforced concrete subjected to a concentrated load at the mid-span is shown in figure 2.18. In the initial stage of the curve, the beam is under elastic behaviour and no cracks` will be observed. Concrete starts to crack and loose stiffness at point B, but still both steel and concrete considered to be elastic. Moving to point C one of the two materials, either steel or concrete or both of them, will become inelastic, depending where the section is under or over reinforced. At point D maximum moment is obtained and starts to decrease after D with a rate that depends on the amount of reinforcement in the section.

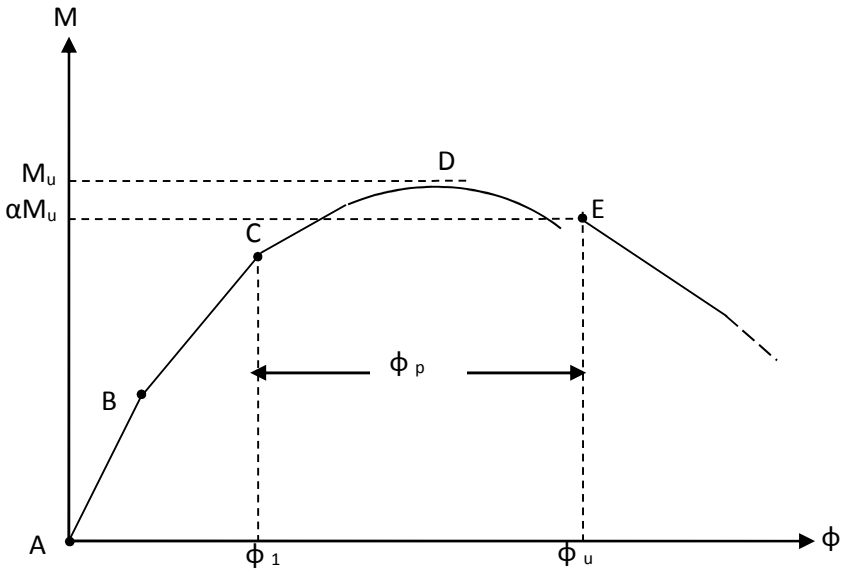

Figure 2.18: Typical curve for moment-curvature relationship (Rudi, 2007)

Park and paulay (1975) proposed an expression for the curvature:

$$\varphi = \frac{\varepsilon_i}{x_i} \tag{2.24}$$

where:

ε: is the steel strain at central point i.

x: is the depth of the neutral axis at central position i.

They also stated that, at the ultimate moment capacity, point D in figure 2.18, a plastic hinge forms in the beam. The hinge does not form at the loaded cross section; instead, a length (L_p) of the beam becomes plastic. Hence, θ_p (the rotational capacity) will be given as:

$$\theta_p = \int_0^L \varphi_p . da = \int_0^L \left(\frac{\varepsilon_u}{x_u} - \frac{\varepsilon_1}{x_1} \right) da \tag{2.25}$$

where:

ε_1 & ε_u: the steel strain at points C & D, respectively, in figure 1.

x_1 & x_u: the neutral axis depth at points C & D, respectively, in figure 1.

Commonly two failure modes have been addressed by Beeby (1994) for simply supported reinforced concrete beams subjected to concentrated load at the mid span:

- Ductile failure with cracking over a large length on each side of the critical sections
- Non-ductile failure with one major crack at the critical section.

As a conclusion, ductility can be defined as an added property to the structure and presented by the large deformations at certain level of load. Therefore, it gives more time to the building to survive and provides notations before failure. Based on that, ductility should be deemed as important as strength; there is no point of designing structures which sustain high loads and then fail suddenly when load reaches the maximum strength of the structure. It is efficient to have ductility especially in regions where the possibility of unexpected impacts is high so more time will be given to the structure to be evacuated before failure or it will not fail abruptly due to sudden raise in the applied load.

2.2.3 Definition of ductility factor μ

There is no simple method for direct evaluation of the flexural ductility of reinforced concrete structures. Most of the previous studies have chosen the symbol μ to represent ductility as in the researches of Beeby (1997), Kwan (2002), Park (1988), etc., and have commonly defined it as ductility factor. This factor can be represented by the use of deformation, where the deformations employed to evaluate the ductility factor may be strain, curvature, displacement, deflection or

rotation. Within these quantities, many definitions for each of them can be found in existing literatures.

Knoll et al (2003) defined ductility by the general ratio as follows:

Ductility = maximum deformation / maximum elastic deformation.,

where the term maximum elastic deformation may sometime be a matter of debate, especially for materials or situations where there is gradual decay of stiffness which is defined as the ratio of load increment to the deformation increment.

Curvature has been chosen to define the ductility factor μ in the technical paper that has been published by Park and Ruitong (1988). According to their study, the ductility of a section is normally expressed as the curvature ductility factor:

$$\mu = \Phi_u / \Phi_y \tag{2.26}$$

where Φ_y is the curvature when the tension reinforcement first reaches the yield strength and Φ_u is the ultimate curvature normally defined for unconfined concrete as when the concrete compression strain reaches a specified limiting value. The suggested value by Park and Ruitong (1988) for the limiting concrete compression strain in the extreme fibre at ultimate curvature was assumed to be ε_{cu} = 0.004. As explained in the paper, that assumption was based on the fact that this value can be regarded as a conservative value for the strain at the extreme compression fibre when concrete begins to spall. By reviewing the code quoted in that paper, i.e. ACI code, it can be noticed that a strain value of 0.004 is the maximum value which is allowed by the code for the strain in the compression fibre.

Park and Ruitong (1988) did their analysis on doubly reinforced beams and therefore Φ_u and Φ_y can be expressed by the following equations based on figure 2.19:

$$\phi_y = \frac{f_y / E_s}{d(1-k)} \tag{2.27}$$

$$\phi_u = \frac{\varepsilon_{cu}}{c} \tag{2.28}$$

Where: f_y: yield strength of steel

E_s: modulus of elasticity of steel

d: the depth from extreme compression fibre to the centred of the tension reinforcement

k: neutral axis depth factor

ε_{cu}: specified limiting value that the concrete strain reaches at the extreme compression fibre

c: neutral axis depth

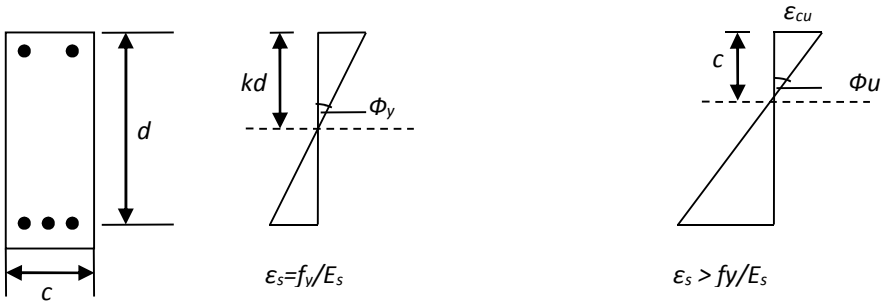

(a) At first yield curvature (b) At ultimate curvature

Figure 2.19: Doubly reinforced concrete beam section with flexure (Park and Ruitong, 1988)

It is clear from equation 4 that the ductility factor is related to the neutral axis depth which is presented by the factor K.

Beeby (1997) has also agreed that the plastic rotation capacity is proportional to the ratio of the neutral axis depth to the effective depth (x/d) to a certain point and starts to decrease as x/d starts to increase beyond that point. By considering d as a constant it can be said that plastic rotational capacity is proportional to the neutral axis depth. That will lead to conclude a relation between reinforcement ratio (RR) and ductility as neutral axis depth is proportional to the reinforcement ratio (RR). Figure 2.20 illustrates the relationship between the plastic rotational capacity and x/d ratio.

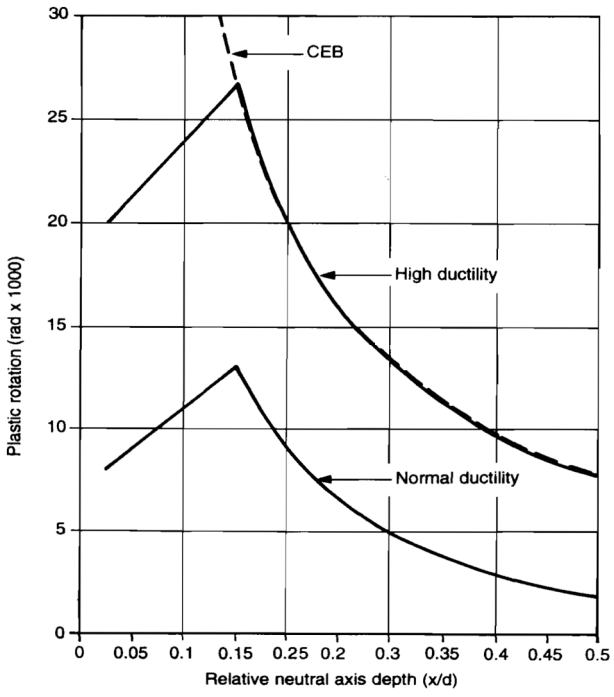

Figure 2.20: Relative neutral axis depth x/d versus rotational capacity (Beeby, 1997)

Deflection has been used in the paper that was published by Pam et al (2001) for the purpose of defining the ductility factor μ. Pam and her colleagues have chosen deflection to represent ductility as it is easy to be measured. The ductility factor was given by Pam et al (2001) as follows:

$$\mu = \frac{\Delta_{max}}{\Delta_y} \tag{2.29}$$

Δ_{max} is the maximum deflection at which the load has been dropped to 85% of the maximum applied load in the descending part of the load-deflection curve. The researchers have stated that this definition has the advantages that it can be applied to basically all kinds of structures and is relatively easy to determine either analytically or experimentally; having taken into account the ability of the material to deform beyond the peak load.

Δ_y is the deflection at an equivalent elastic-plastic system with its equivalent elastic stiffness taken as the secant stiffness at 75% of the ultimate load at the real system.

Figure 2.21 shows the location of both Δ_{max} and Δ_y. It can be seen that the value of Δ_y is actually equal to 4/3 time the value of Δ at 75% of the ultimate load.

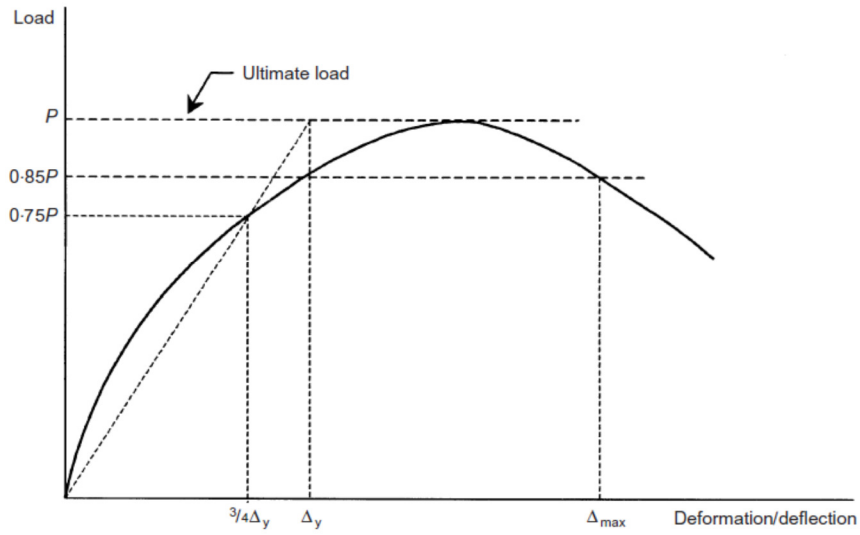

Figure 2.21: Definitions of Δ_{max} and Δ_y (Pam et al, 2001)

In another study, Kwan et al (2002) published a paper which carried out a similar definition for ductility as in the research of Park and Ruitong (1988) which was given in equation 2.26. Kwan et al (2002) defined both curvatures Φ_u and Φ_y in a different way as follows:

Φ_u is the ultimate curvature at which the resisting moment has dropped to 80% of the peak moment in the descending part.

Φ_y is the yield curvature and defined as the curvature at the hypothetical yield point of an equivalent elastic-plastic system whose equivalent elastic stiffness is taken as the secant stiffness at 0.75 of the peak moment before the peak moment is reached and yield strength is taken as the peak moment; the yield curvature is then defined as the curvature at 0.75 of the peak moment divided by 0.75. It can be noticed that Φ_y in Kwan's study has a similar definition as Δ_y which was mentioned previously in Pam at al's (2001) paper.

Load-deflection curve was employed to represent the ductility in the study of Ahmad et al (1995). In the research of Ahmad and his colleagues, the ductility factor was referred to as shear ductility factor as the load-deflection curve was strictly representing the deflection ductility of shear-critical beams. This is because the study has been used a total of 15 shear-critical reinforced concrete beams with and without shear reinforcement.

Ahmad et al (1995) have reported that the shear ductility ratio μ can be expressed as the ratio of the area of the load-deflection response up to $3\Delta_0$ to the area up to Δ_0.

Δ_0 can be defined as the deflection corresponding to the maximum load P_{max}. Figure 5 represents a load-deflection diagram for reinforced concrete beam, relying on the definition that was given by Ahmad et al (1995) and noticing the areas under curve in figure 2.22; the shear ductility ratio can be defined using the following formula:

$$\mu = \frac{A_1 + A_2}{A_1} \tag{2.30}$$

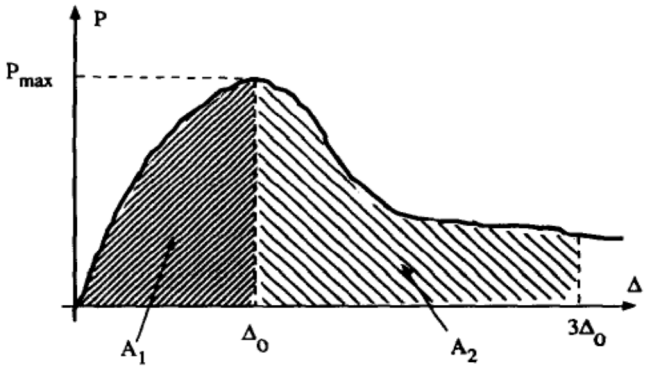

Figure 2.22: Load-deflection diagram for definition of shear ductility ratio (Ahmad et al, 1995)

Pam et al (2001) did an experimental investigation for twenty rectangular singly reinforced concrete beams. The beams were casted using normal and high strength concrete and loaded as simply supported beams, figure 2.23 shows the tested beams cross section and the loading arrangement.

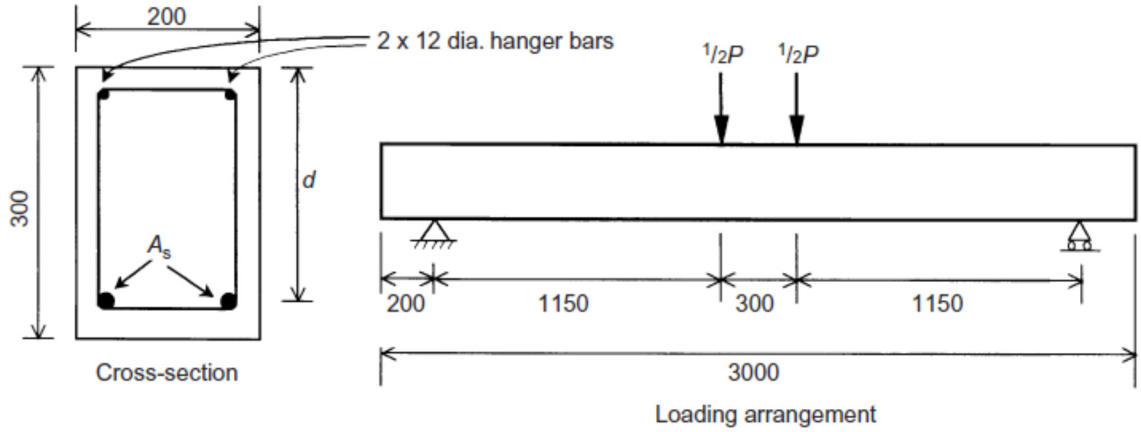

Figure 2.23: Beam cross section and loading arrangement (Pam et al, 2001)

Pam and her colleagues discussed the results that were found by the experimental work and used the regression analysis to develop a simple formula for estimating the flexural ductility of normal and high strength concrete. The parameters that were used in the developed formula are tension and balanced steel ratios (ρ and ρ_b, respectively) and the concrete cube compressive strength was adopted as follows:

$$\mu = 9.5(f_{cu})^{-0.3}(\rho / \ \rho_b)^{-0.75} \qquad (2.31)$$

The later formula is not expected to be very accurate, but at least can give a guideline for ductility evaluation and control.

The formula that was presented by Pam et al (2001) is for singly reinforced beams. Kwan et al (2002) performed an analysis for doubly reinforced beams and therefore it was necessary to add the compression reinforcement ratio (ρ_c) to equation 2.31. The new formula that Kwan et al (2002) developed is:

$$\mu = 10.7(f_{co})^{-0.45}[(\rho_t - \rho_c)/\rho_{bo}]^{-1.25} \quad (2.32)$$

It can be noticed that the balanced steel ratio in Kwan's formula is expressed by the term (ρ_{bo}) and was defined as the balanced steel ratio of the same beam section with no compression steel, while in Pam's study the balanced steel ratio (ρ_b) was defined as the balanced steel ratio of the actual beam section, already Pam's beams were singly reinforced, and expressed by the term (ρ_b). For that reason we can attribute the difference in defining the balanced steel ratio between equations 2.31 & 2.32, as if Kwan kept the term (ρ_b) that will represent the balanced steel ratio of the beam section and will be considered to take the compression reinforcement into account while equation 2.32 was based on the balanced steel ratio for the beam section with no compression steel.

Comparing all the ductility factor definitions which have been mentioned, it is clear that Pam et al (2001) adopted the most conservative definition. Pam defined the ultimate deformation as when load drops down to 85% of the peak load, which is the smallest value for deformation among all other studies. This will lead to a smaller ductility factor μ and therefore being more conservative in defining the level of ductility of a structure.

As Ahmad et al (1995) have defined the ductility factor in a different way as the area under Load-displacement curve was used to define the ductility factor. It also can be said that Pam et al (2000) is more conservative than Ahmad's study. Figure 2.22 shows that Ahmad has defined the ultimate deformation at a load value less than 50% of the maximum load, which is less than Pam's one of 85%.

As a conclusion, it can be said that equation 2.31, which is presented by Pam et al (2000), is safer than equation 2.32 from design point of view. This is due to the fact that equation 2.31 was developed based on the most conservative definition for ductility factor.

2.2.4 Factors affecting ductility

In order to evaluate the ductility of a concrete member, most of the researchers use a non-linear analysis extended well into the post-peak range, so that the complete load-deflection or moment-curvature curve may be obtained. In such an analysis the following assumptions should be made as stated in the paper of HO et al (2003):

1. Plane sections before bending remain plane after bending: this implies that the bending strain in the section is proportional to the distance from the neutral axis.
2. The tensile strength of the concrete may be neglected: any tensile stress that exists in the concrete near the neutral axis is small and has a small lever arm leading to negligible contribution to the moment resistance.
3. There is no bond-slip between the reinforcement bars and the concrete: this assumption implies that the strain in the reinforcement is equal to that of the

concrete. The assumption is accurate except near cracks where there tends to be some bond-slip.

Beeby (1997) has stated the following three aspects, as shown in figure 2.24, which ductility can be affected:

- Ductility reduces with reducing reinforcement ratio where failure is due to rupture of the reinforcement.
- The ductility is markedly affected by the ductility properties of the reinforcement.
- Ductility reduces with increasing section depth and increases with increasing span/effective depth ratio.

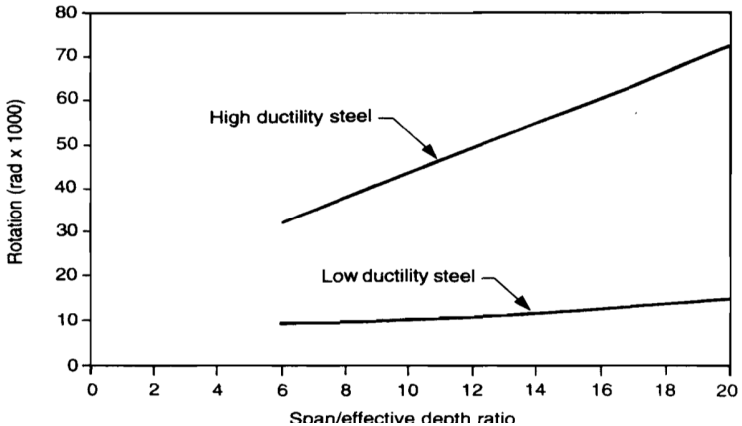

(a) Span/depth ratio versus rotation capacity

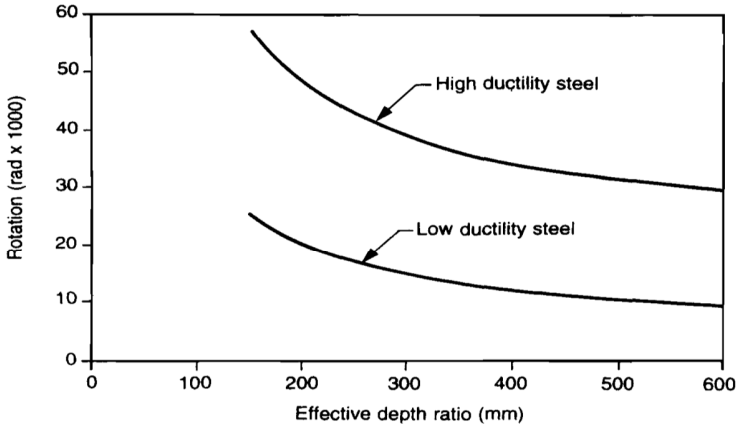

(b) Effective depth d versus rotational capacity

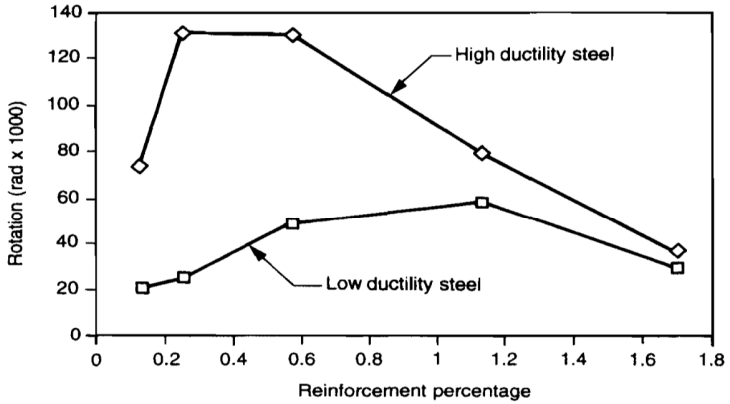

(c) Influence of reinforcement percentage on rotational capacity

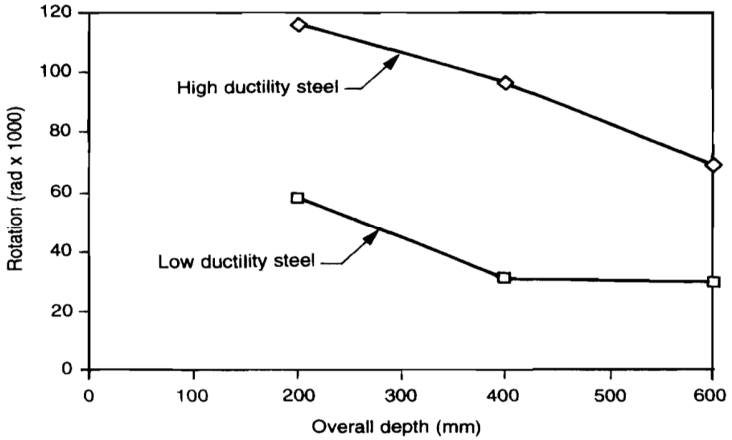

(d) Influence of beam's depth on the rotational capacity

Figure 2.24: Effects of many aspects on ductility (Beeby, 1997)

As a conclusion of the parameters that ductility can be affected with, it can be said that the major factors affecting ductility in reinforced concrete structures are:

- Tension steel ratio ρ and tension to balanced steel ratio ρ/ρ_b
- Concrete strength.
- Presence and ratio of concrete confinement.
- Yield strength and ductility of reinforcing steel.

The effect of these parameters will be discussed and compared as presented in relevant researches and studies, i.e. Pam et al (2000), Ahmad et al (1995), Kwan et al (2002), etc

Park and Ruitong (1988) have done a curvature analysis for doubly reinforced beams sections. They have tried different values for the concrete compressive strain in the top fiber ,ε_{ce}, and calculated the tension steel ration ρ and associated Φ_u/Φ_y based on a given ρ'/ρ, f_y and f'_c. Equations 2.26, 2.27 & 2.28 were used to calculate the ductility factor μ in Park and Ruitong analysis. The found values enabled the curves of Φ_u/Φ_y versus ρ to be traced as shown in figure 2.25.

ehere: $\rho=A_s/bd$; $\rho'=A'_s/bd$

As mentioned in the preceding section of this review, Kwan et al (2002) adopted the same definition for ductility factor as Park and Ruitong (1988) with different definitions for Φ_u and Φ_y. Based on that an analysis has been carried out again for the ductility of a doubly reinforced beam section and the values of the ductility factor μ were plotted against the tension steel ratio ρ_t, as shown in figure 2.26. Different concrete grades and tension and compression steel ratios were used in Kwan et al (2002) analysis as in park and Ruitong one.

Relying on Figures 2.25 & 2.26, it can be noticed that with other variables held constant the ductility of a section will increase if the tension steel ratio ρ is decreased, compression steel ratio ρ_c or ρ' is increased, concrete strength and reinforcement yield strength in decreased. More detailed discussion and reasons behind each of the previous correlations will be discussed individually.

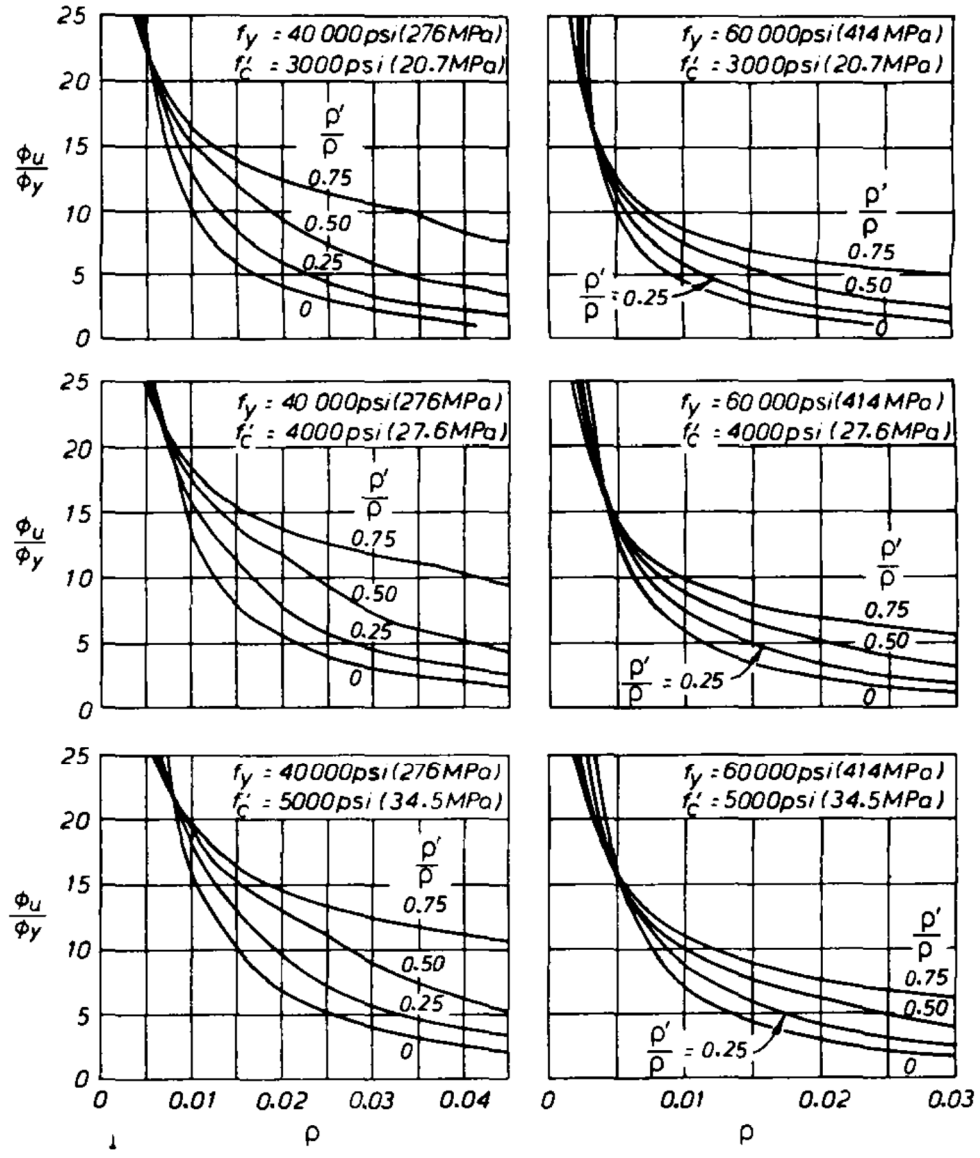

Figure 2.25: Variation of curvature ductility factor Φ_u/Φ_y for reinforced concrete beams with unconfined concrete (Park and Ruitong, 1988)

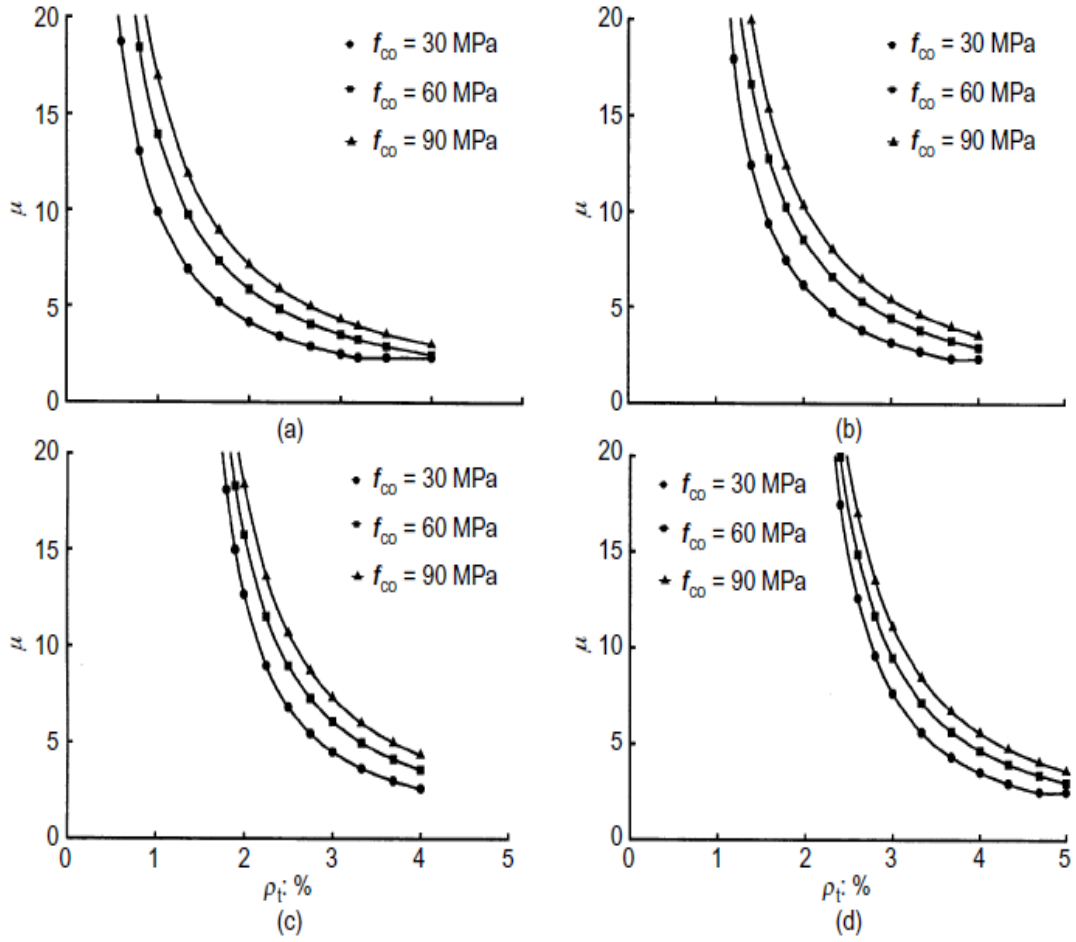

Figure 2.26: Ductility factor plotted against tension steel ratio ρ_t (Kwan, et al, 2002)

(a) ρ_c=0% (b) ρ_c=0.5% (c) ρ_c=1% (d) ρ_c=1.5%

2.2.4.1 Effect of concrete strength f_c`

At a given tension steel ratio, the ductility increases in parallel with concrete grade. Kwan et al (2002) stated that the increase in ductility seems not to be accurate as the high strength concrete is a brittle material, but in fact the major factor affecting the ductility in a beam is the degree of the beam being under or over reinforced. Actually the increase in the ductility due to the reduction in the ρ_t/ρ_b ratio

has overweighed the decrease in the ductility due to the reduction of the ductility of the concrete itself. The reduction in the ρ_t/ρ_b ratio is due to the lower values that ρ_b will obtain as the concrete grade goes higher. In another research by Kwan et al (2006), it has been found that at a given steel ratio, the flexural ductility increases with the concrete grade but at the same tension steel to balanced steel ratio (i.e. at the same degree of under or over reinforcement), the flexural ductility decreases with the concrete grade. Hence, if reinforced to the same degree of under/over-reinforcement, an RC beam cast of high strength concrete HSC would have a significantly lower flexural ductility than that of a similar beam cast of normal concrete.

2.2.4.2 Effect of tension steel ratio ρ & tension to balanced steel ratio ρ/ρ_b

Ductility will decrease at a fixed concrete grade while increasing the tension steel ratio. It has been mentioned in the study of Pam et al (2001) that if the amount of reinforcement is small, the tension reinforcement will yield before the concrete is crushed and the beam will fail in a ductile manner. Where if the amount of tension reinforcement is large, the concrete will be crushed without prior yielding of the tension reinforcement and the beam will fail in a brittle manner. That can explain the reason behind decreasing the ductility while increasing the tension steel ratio, as when the tension steel amount increases the beam section will tend to be more as an over reinforced section and less as an under reinforced section.

Kwan et al (2002) proposed the following equation based on figure 2.27:

$$\varepsilon = \phi x \tag{2.33}$$

Equation 2.33 represents the strain developed in a beam section ε in terms of the curvature Φ and the distance from the neutral axis x. Based on equation 2.33, moment-curvature analysis for the beam section have been carried out as explained in figure 2.28. After getting all the results, a moment-curvature graph was plotted and shown in figure 2.29.

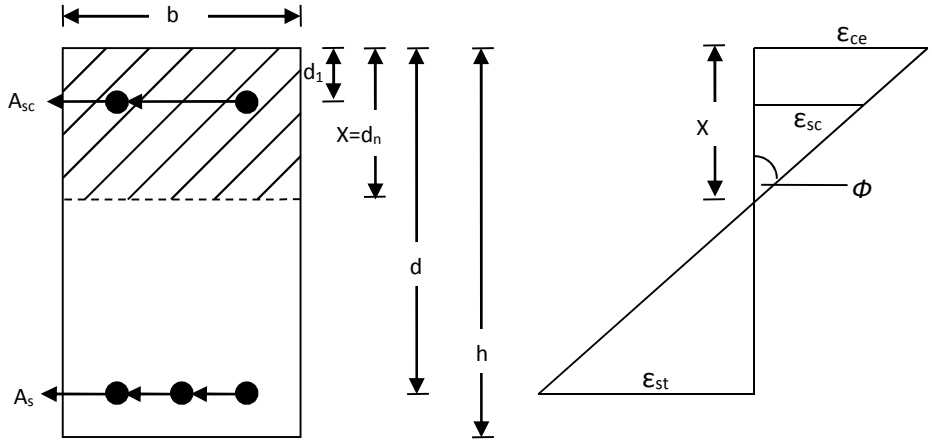

Figure 2.27: Double reinforced beam section subjected to bending moment (Kwan et al, 2002)

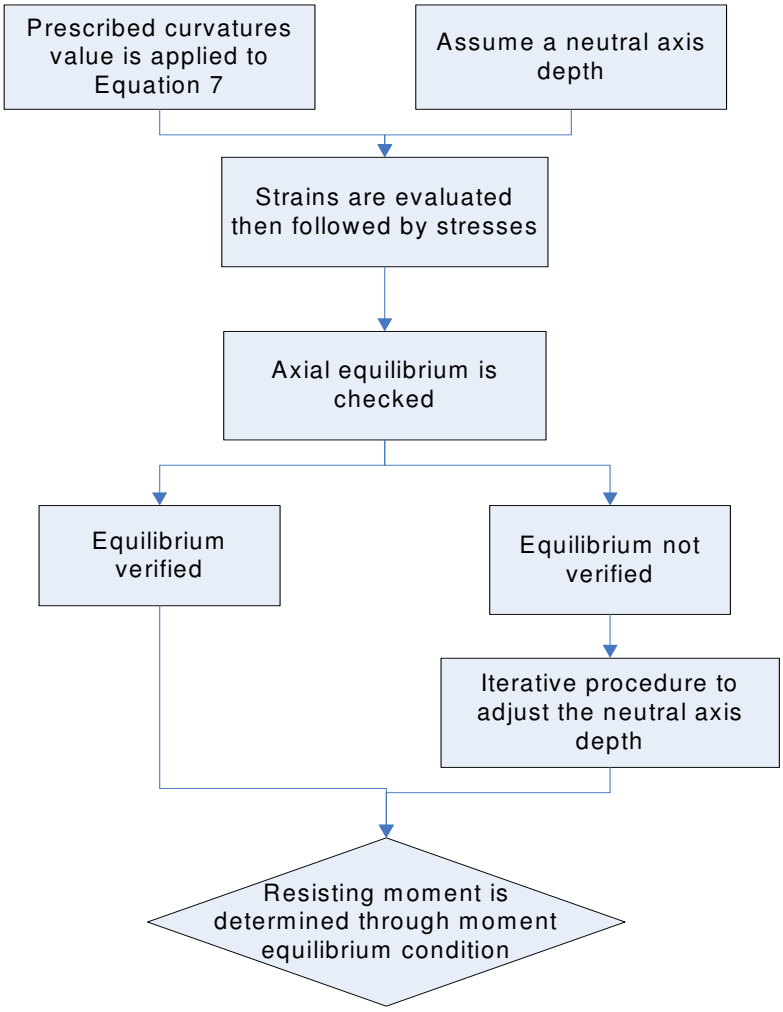

Figure 2.28: Moment-curvature analysis for reinforced beam sections.

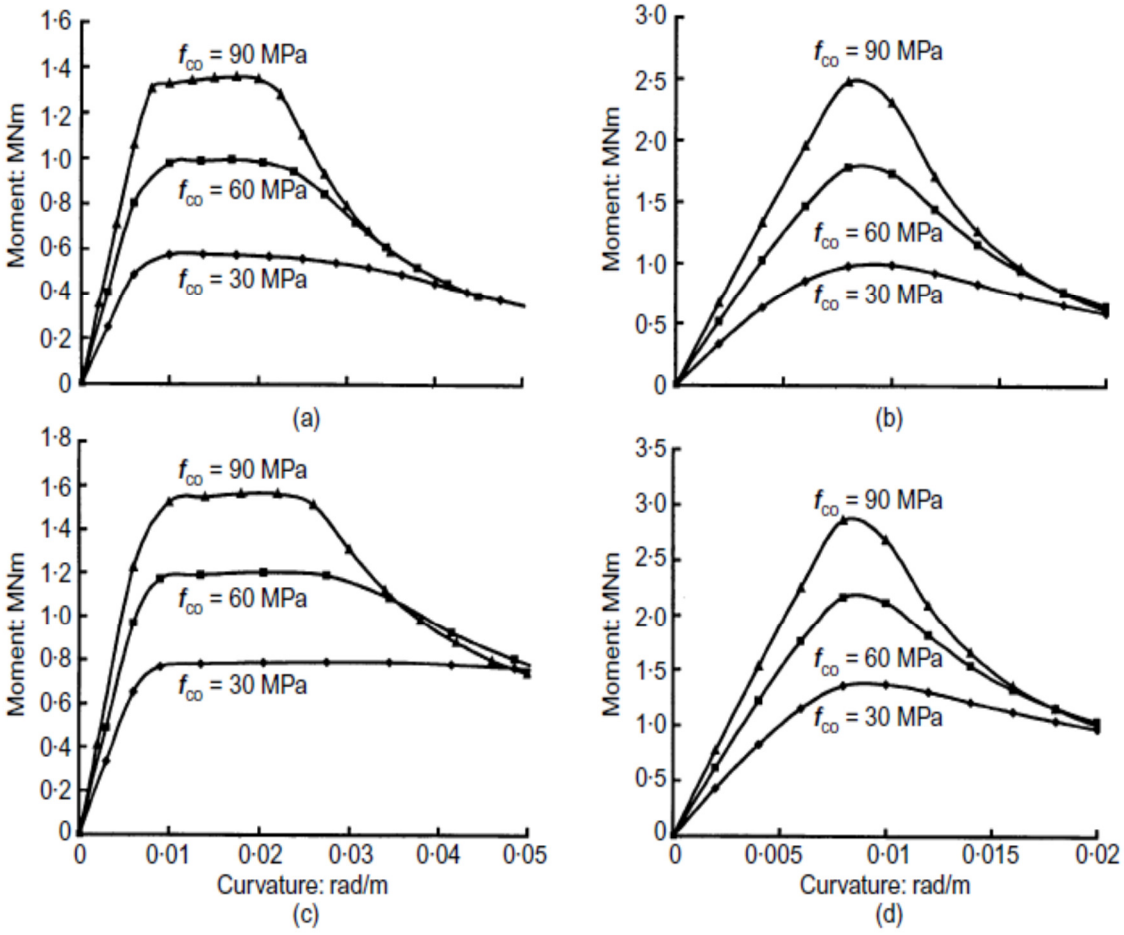

Figure 2.29: Complete moment curvature curves (Kwan et al, 2002)

(a) ρ_t/ρ_b=0.5, ρc=0%

(b) ρ_t/ρ_b =1.5, ρc=0%

(c) ρ_t/ρ_b =0.5, ρc=1%

(d) ρ_t/ρ_b =1.5, ρc=1%

It is clear from figure 2.29 that both charts a & c are under-reinforced as ρ_t/ρ_b is less than one, on the other hand b & d are over-reinforced as ρ_t/ρ_b is greater than one. From the same figure a major difference in the moment-curvature curves between under and over reinforced sections can be adopted. In the under-reinforced sections the curve is linear before reaching the peak moment, and then a long yield

plateau is performed which is followed by a drop in the resisting moment more rapidly until complete failure. In the case of over-reinforced sections the moment-curvature curve is more likely taking the shape of a single smooth curve with a sharp peak indicating a brittle mode of failure. Comparing the behaviour of both under and over reinforced sections, it is obvious that under-reinforced beams showed more ductility in the post-peak and failure stages.

2.2.4.3 Effect of compression steel ratio ρ_c or ρ'

It is evident in figures 2.25 & 2.26 that ductility will increase when compression steel ratio increases with other variables held constant. Chau et al (2004) discussed the effect of compression steel ratio on ductility and agreed that the provision of confinement would always increase the flexural ductility. It does this in two ways: first, it increases the balanced steel ratio so that, at the same tension steel ratio, the tension to balanced steel ratio is decreased; and second, it increases the residual strength and ductility of the concrete so that, at the same tension to balanced steel ratio, the flexural ductility of the beam section is increased.

2.2.4.4 Effect of the yield strength and ductility of reinforcing steel

No work has been noticed to be done regarding the direct effect of steel ductility on the ductility of a beam or a structure. Generally, it can be said that ductile steel should has a positive effect on the behaviour of a reinforced beam as it allow the beam to suffer a large deformation before failure. The most important factor of steel properties is the length of the yield plateau. If steel with long yield plateau is used, then the tension bars in a beam will experience quite a large deformation

(strain) on the same level of load, yield load. This will affect the flexural resistance of the beam negatively and shear failure will be more probable to occur.

2.2.5 Ductility recommendations by Standards and other researches

Generally, it is a good practice to design the beam section under reinforced from the ductility point of view as that will ensure the yielding of tension steel before the failure of concrete. This kind of failure is called tension failure and it is more ductile than the other type of failure such as compression or shear failure. Compression failure happens when the tension steel does not yield even when concrete fails which results in a brittle mode of failure. This kind of strategy is usually suggested to normal strength concrete as was pointed out in the study of Pam et al (2001). For the later reason, Pam et al (2001) reported that based on the testing results it is more useful to use the provision of confinement for high-strength concrete. Confinement will increase the strength of the concrete in the compression fibre resulting in a higher strength which allows the steel to yield at an earlier stage compared with the same section without confinement. This option will help in introducing the failure mode of the beam to be more ductile as the beam section will tend to be more likely as an under-reinforced and less as an over-reinforced section.

Chau et al (2004) also suggested that high strength concrete needs to be controlled for the ductility enhancement by reducing the tension at the f balanced steel ratio. Thus for a section cast with high-strength concrete, it may be necessary to limit the tension at the balanced steel ratio to a relatively lower value than that that is used with normal concrete. In the study of Chau et al (2006), same suggestions have been presented as Pam et al (2001) did, which is adding confinement to the concrete. Chau assumes that adding confinement can make up the reduction in

flexural ductility which is caused due to the increase in the concrete strength. The provision of confinement would always increase the flexural ductility. It does this in two ways: firstly, it increases the balanced steel ratio so that, at the same tension steel ratio, the tension at the balances steel ratio is decreased; and secondly, it increases the residual strength and ductility of the concrete so that, at the same tension at the balanced steel ratio, the flexural ductility of the beam section is increased. In other words, it can be said that the resulting confining stress would subject the concrete to tri-axial stress condition, under which it should behave in a more ductile manner.

Standards and codes of practice vary in applying limitations to the designed section for the purpose of meeting its ductility requirement. Table 2.2 contains the specified limitations which are provided by various codes regarding ductile requirements.

Table 2.2: Code limitations regarding ductility of reinforced concrete beams

Standard name	**Suggested limitation**
ACI-318, 1999	$\rho / \rho_b \leq 0.75$
ACI-318, 2002	Tension steel strain ≥ 0.004 when concrete fails
BS-8110	Neutral axis depth /d ≤ 0.5
NZS-3101, 1995 (New Zealand code)	Neutral axis depth / Neutral axis depth of the balanced section < 0.75
EC2	Neutral axis depth / d ≤ 0.45 if f_{cu} < 50 MPa Neutral axis depth / d ≤ 0.35 if f_{cu} ≥ 50 MPa

As noticed from table 2.2, EC2 is the only code that specifies different restrictions associated with different concrete strength while the restrictions in other codes are applied for all grades of concrete.

Based on the ACI-318 code published in 1999, Kwan et al (2002) suggested that it is a good practice in the conventional RC design to limit the tension steel ratio in a singly reinforced beam section to be not more than 75% of the balanced steel ratio. This ratio will give a minimum ductility factor of 3.32 for beams made of normal-strength concrete with compressive strength equal to 30 MPa. So it has been suggested in their study that the value of 3.32 should be regarded as an absolute minimum ductility value to be provided in all reinforced concrete beams. Kwan and his colleagues used the value of 3.32 as it was the ductility value provided by ACI and New Zealand codes of practice for singly reinforced beams.

Another research for Kwan et al (2006) has concluded that in the ACI 318-1999, the tension to balanced steel ratio is limited to a maximum of 0.75. At a concrete grade f_c of 30MPa, this would provide a minimum ductility factor μ of 3.32. In BS 8110, the neutral axis to effective depth ratio is limited to 0.5. At a concrete grade f_c of 30MPa, this would provide a minimum ductility factor μ of 3.22. In order to maintain a consistent level of minimum flexural ductility, it is proposed to set a minimum fixed value of 3.32 or 3.22 for the ductility factor μ. In the same research the researchers use the trial-and-error numerical process to relate the amounts of compression and/or confining reinforcement, needed to maintain a minimum ductility factor of μ =3.32 or μ=3.22 regardless of the concrete grade, have been determined and expressed in terms of the concrete strength in two formulas as follows:

$3350\rho_c + 54f_r = f_c - 30$ According to ACI 318-99 (μ =3.32)

$2570\rho_c + 39f_r = f_c - 30$ According to BS 8110 (μ =3.22)

Using the previous two formulas the designer has the flexibility of putting in more compression reinforcement and less confining reinforcement, or vice versa, depending on the situation and the relative cost-effectiveness of the two different types of reinforcement.

2.3 Knowledge gap and summary

The literature review presented the critical and up-to-date studies and researches regarding the bond and ductility performance of RC members. The literature review also presented the key findings from different researchers and it can be divided into the following categories:

- Experimental testing methods for examining bond interaction between concrete and reinforcing steel.
- Analytical models and codes of practice suggestions to investigate the bond strength of RC members.
- Different experimental methods of flexural testing to evaluate the flexural behavior and ductility of RC beams.
- Effects of steel and concrete properties on the bond interaction and flexural behavior of RC members.

The literature review also addressed the properties and factors affecting bond and ductility in reinforced concrete structure. The following knowledge gaps were found and addressed in this work:

- All studies which have been conducted in the past examined only the traditional steel classes A, B and C and did not examine any other type of steel. in this study a new type of steel C', which is identified to be close to C class from ductility point of view is examined to see how it can affect the bond and ductility performance of RC structures.
- Different reinforcing steel elements are used in this study, i.e. single steel bars and steel welded meshes while in previous studies, the same style of reinforcing steel elements were used in an experimental work to investigate the bond or flexural behavior of reinforced concrete.
- Previous studies concerned steel bars of the different rib specifications but all steel bars had two longitudinal ribs running along the bar. No investigations have been performed to check the effect of having more than two longitudinal ribs in the reinforcing steel. In this work, one type of the reinforcing steel has four longitudinal ribs running along the steel. Investigations and laboratory work has also been carried out to discover the effect of the presence of more longitudinal ribs on the bond and ductility of the RC member.

2.4 Research methodology

The aim and objectives will be achieved through experimental and analytical methods as it is documented in the thesis. The experimental and analytical work is as follow:

- Conducting a series of pull-out and ductility tests to investigate the bond strength and ductility of reinforced concrete slabs and beams using different types of steel bars and meshes. Evaluating the

influence of reinforcement types and different spacing values on the ductility and bond strength. This part of experimental work consists of two phases:

  - *Phase 1*: bond strength or pull-out test of RC beams and slabs will be conducted to study the effects of variables on bond performance, such as the steel bars surface rib pattern, steel mesh size, shear links spacing and the presence of steel mesh.
  - *Phase 2*: RC beams and slab ductility tests to investigate how the reinforcement ductility influences beam or slab ductility.

- Carrying out parametric studies to propose general design information. The behaviour and results for bond and ductility tests will be calculated by using design models and results will be compared with test data.

Chapter 3: Material Tests and Preparation

3.1 Introduction

Prior to the commencement of the full test program, several initial preparations and materials tests were carried out. Materials tests follow the standard test methods stipulated in the Codes of Practice, e.g. British standards. One of the reasons that those tests are to be conducted prior to main test program is to make sure that materials which are used in main tests meet the standards' requirements. Materials tests also produce more accurate data which can be used in the following calculations and model verifications.

This chapter covers the material tests for concrete and reinforcing steel which are used in both bond and ductility tests. All used steel classes with different diameters were subjected to tensile tests and the stress-strain curves are recorded for each sample. Some of the RC beams which have been casted for the purpose of ductility tests are reinforced with welded steel meshes.

Since concrete may have different strength depending on curing age at the testing day, when casting each group of RC beams, the following concrete specimens were also casted: nine cubes, nine cylinders and eight prisms in order to determine the compressive strength, indirect tensile strength and modulus of rupture, respectively, on the testing day.

In terms of concrete preparation, all the raw materials are prepared and documented later in this chapter.

3.2 Steel bars and meshes

3.2.1 Longitudinal Steel and shear reinforcements

Standard C and C' steel were provided by Celsa Steel UK Ltd in addition to normal steel classes A and B from the market. Bar diameters of 8, 10 and 12 mm bars with a nominal characteristic strength of 500 N/mm^2 were chosen for longitudinal bars. 8 mm standard class A bar was used for the shear links or for the cross bars in welded meshes. Five or four samples of each group were tested using a Denison Testing Machine as shown in Figure 3.1. The results are presented in Figures 3.3 -3.10 from which material properties were determined. It can be observed that B & C' bars do not have an obvious yield plateau in the stress-strain curve; therefore, a 0.2% proof stress, as suggested by the British standards (BS EN 1992-1-1: 2004) and shown in Figure 3.2, was determined as the equivalence of the yield stress.

Results of material properties are summarised in Table 3.1, it can be seen that all bars have achieved yield/proof stress higher than 500 N/mm^2. Table 3.1 shows that bar C' has an 8% higher value of proof stress than that of the yield stress for bar C. In contrast, bar C has a slightly higher (6%) ultimate strain than bar C'. Both bars have the similar ratio of yield/proof stress to ultimate strength.

It is obvious that C and C' bars are close in terms of ductility to B class but can withstand higher loads so the ultimate load of C and C' bars higher than that of B bars. It is noticeable from Figures 3.3-3.10 that A class bars are less ductile than C, C' and B bars.

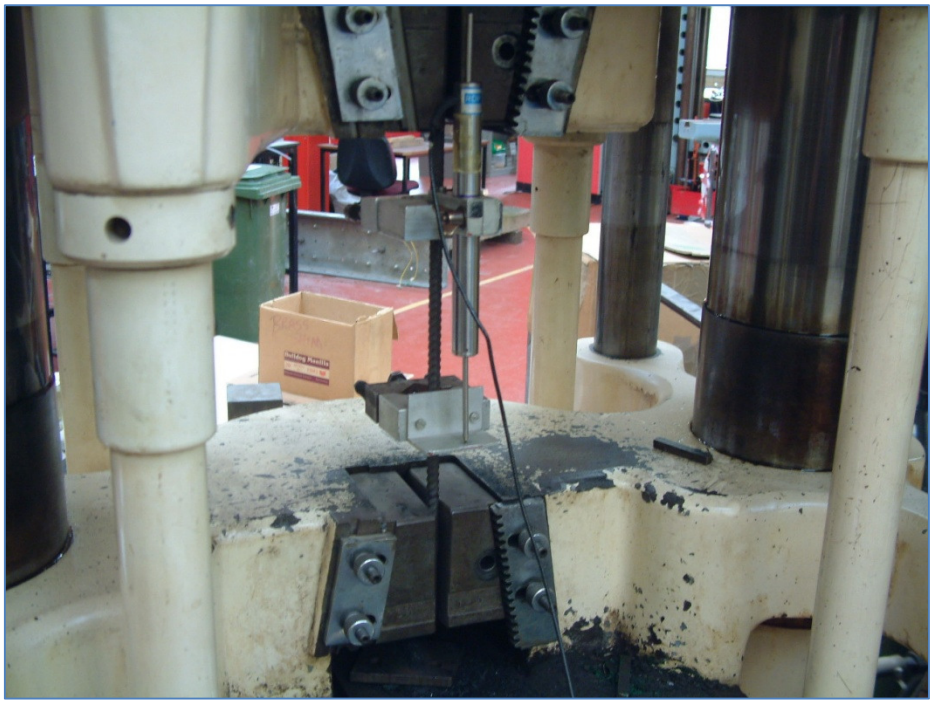

Figure 3.1: Denison machine used for steel bars tensile test

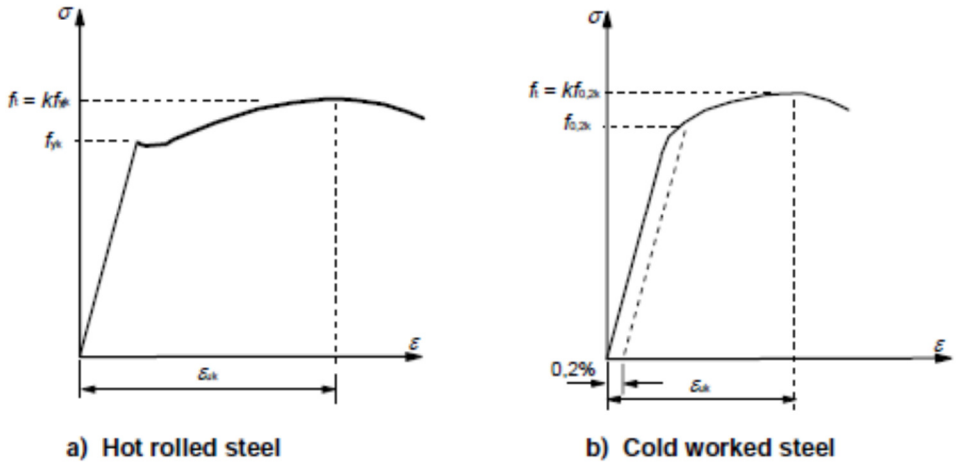

Figure 3.2: Stress-strain diagrams of typical reinforcing steel BS EN 1992-1-1:2004

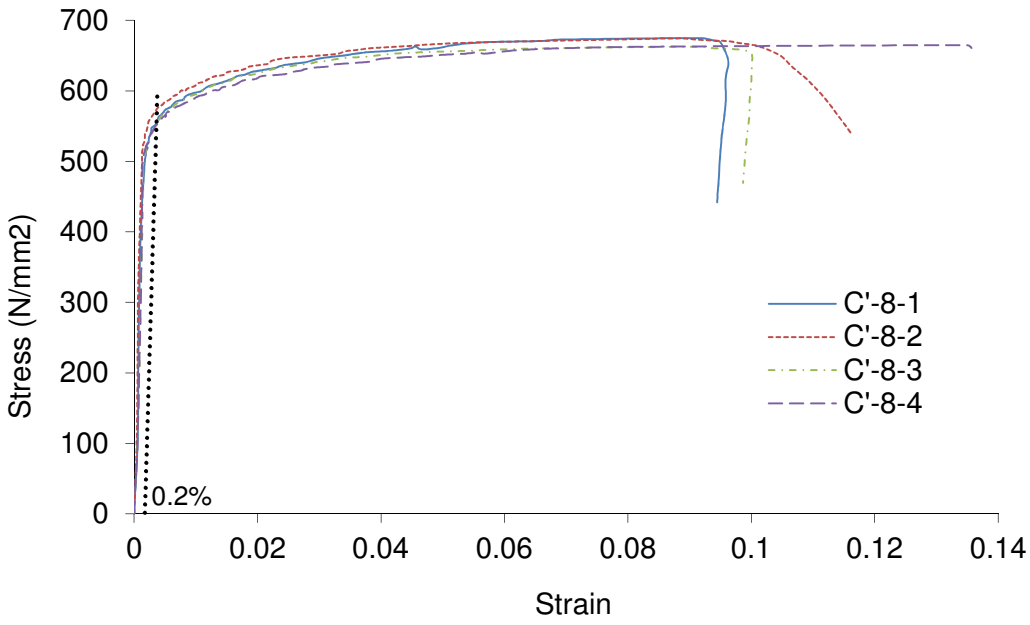

Figure 3.3: Stress-strain curves for C' bars size 8 mm

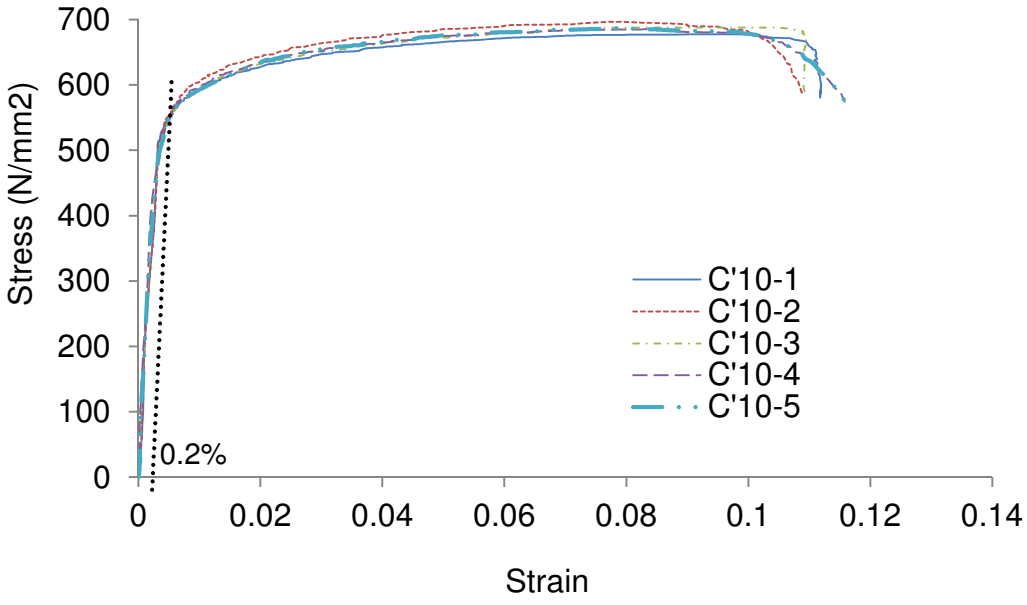

Figure 3.4: Stress-strain curves for C' bars size 10 mm

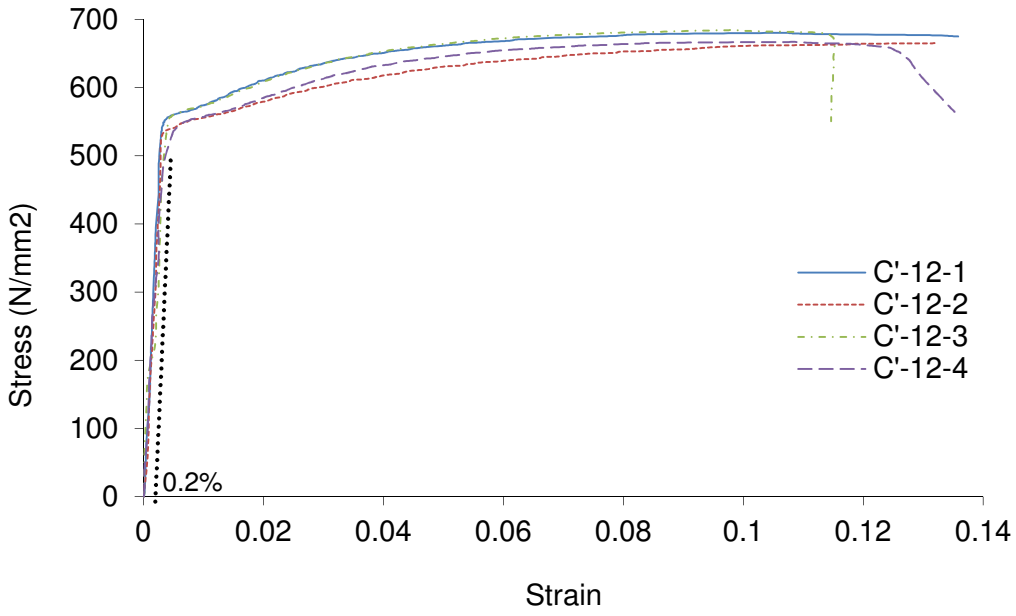

Figure 3.5: Stress-strain curves for C' bars size 12 mm

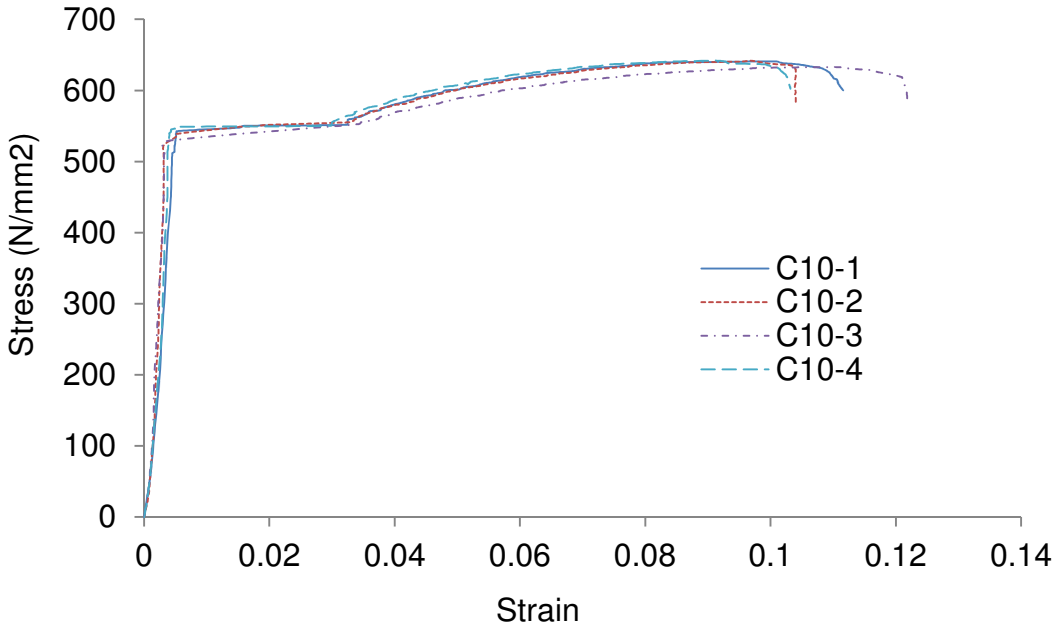

Figure 3.6: Stress-strain curves for C bars size 10 mm

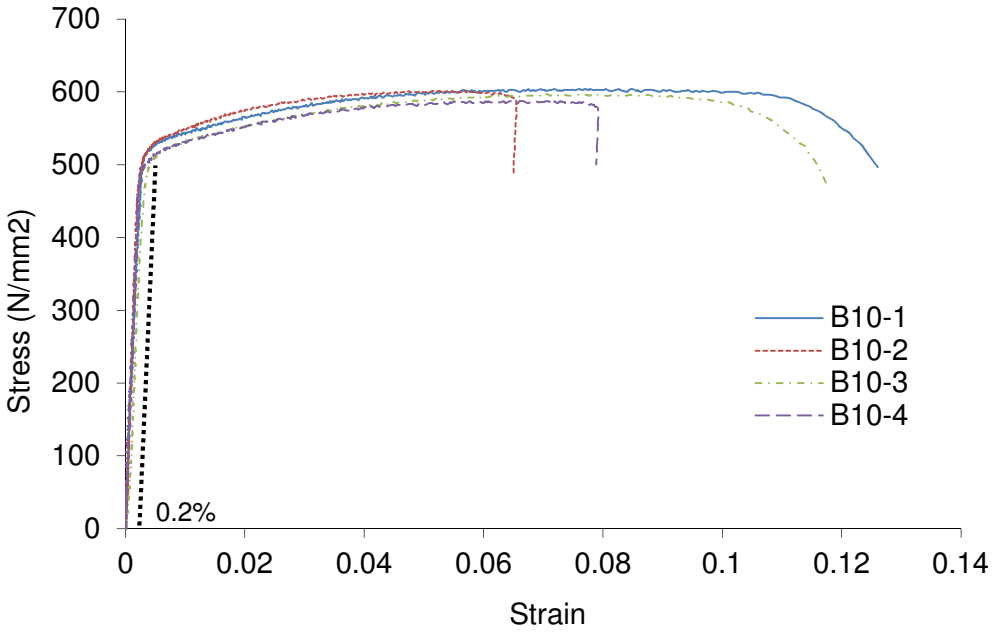

Figure 3.7: Stress-strain curves for B bars size 10 mm

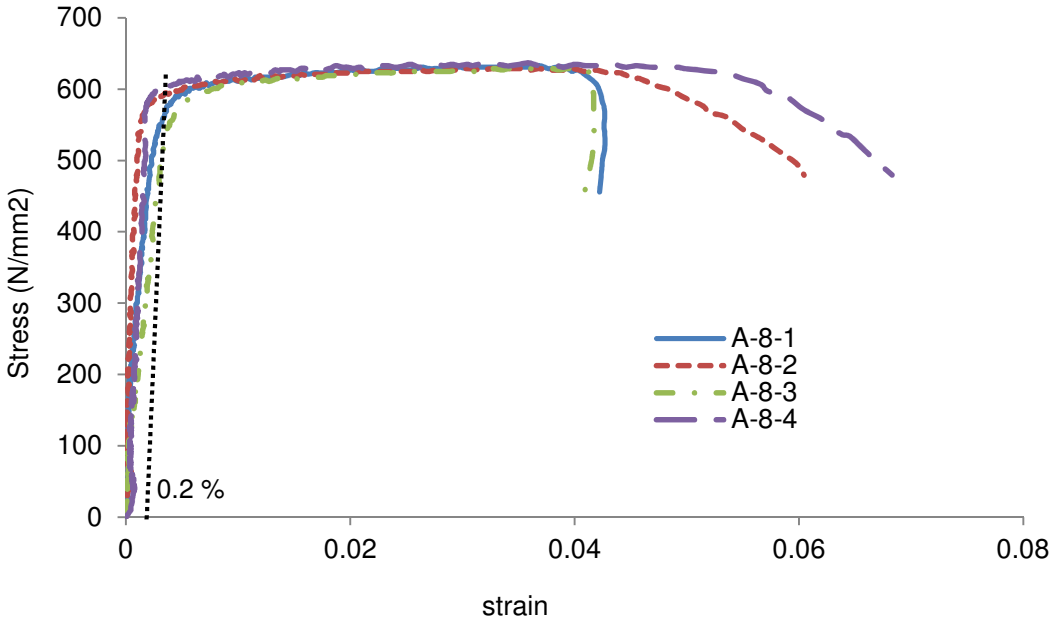

Figure 3.8: stress-strain curves for A bars of 8 mm diameter

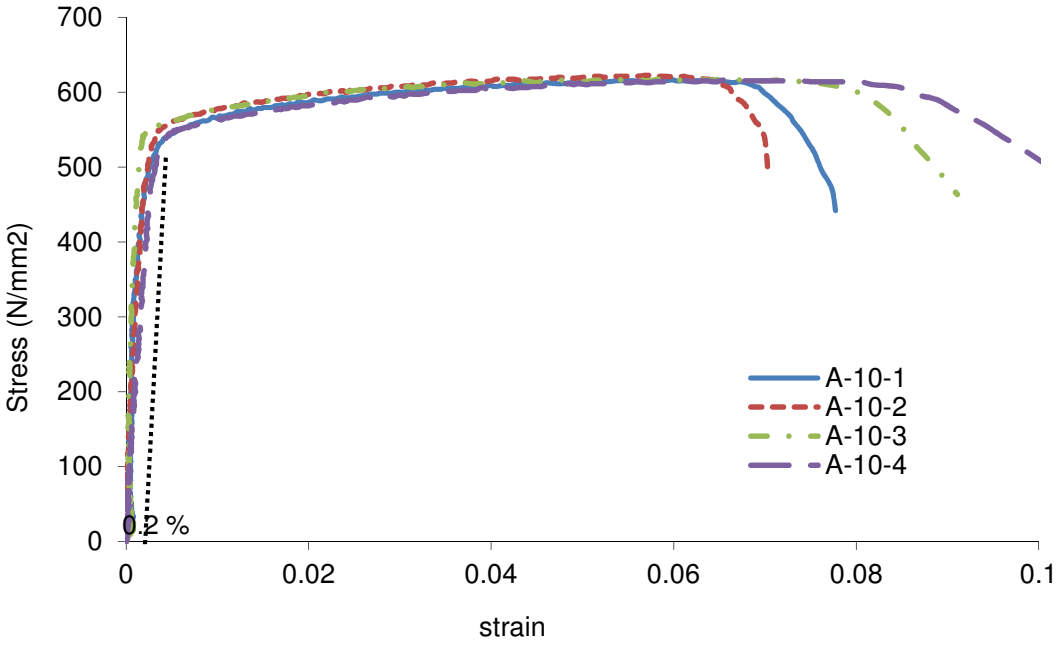

Figure 3.9: stress-strain curves for A bars of 10 mm diameter

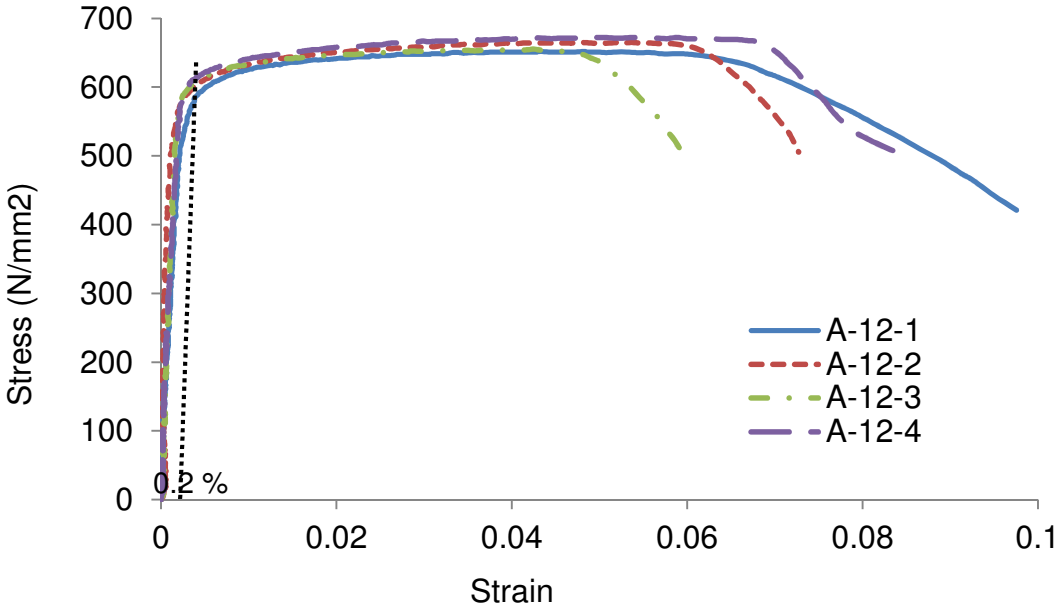

Figure 3.10: stress-strain curves for A bars of 12 mm diameter

Table 3.1: Properties of longitudinal bars tensile test

Steel class & size	Specimen	Yield stress (f_y)/ 0.2 proof stress ($f_{0.2\%}$) (N/mm^2)	Ultimate strength(f_t) (N/mm^2)	f_t/f_y	Strain at ultimate strength (%)
C'-8	1	575	674.7	1.17	9.23
	2	593	674.7	1.14	8.90
	3	570	662.8	1.16	9.38
	4	565	664.8	1.17	13.69
	Average	**575**	**669.3**	**1.16**	**10.30**
C'-10	1	579	677.7	1.17	8.25
	2	583	695.5	1.19	9.19
	3	580	687.9	1.19	10.54
	4	585	685.4	1.17	9.23
	5	585	690.5	1.18	9.30
	Average	**582**	**687.0**	**1.18**	**9.10**
C'-12	1	562	680.3	1.21	11.05
	2	550	666.1	1.21	14.95
	3	562	684.7	1.21	10.03
	4	555	667.0	1.20	11.12
	Average	**557**	**674.5**	**1.21**	**11.78**
C-10	1	542	642.0	1.18	9.98
	2	541	640.7	1.18	9.78
	3	531	630.6	1.19	9.47
	4	532	633.1	1.19	11.01
	5	546	642.0	1.17	9.10
	Average	**538**	**638.0**	**1.18**	**9.90**
B-10	**1**	511	603.8	1.18	6.75
	2	510	602.5	1.18	6.69
	3	508	597.5	1.17	7.80
	4	502	587.3	1.17	7.10
	Average	**508**	**597.7**	**1.17**	**7.09**
A-8	1	580	632.9	1.09	3.69
	2	595	628.9	1.06	3.68
	3	545	628.9	1.15	3.8
	4	608	636.9	1.05	3.59
	Average	**582**	**631.7**	**1.08**	**3.69**
A-10	1	548	616.6	1.12	5.98
	2	564	622.9	1.10	5.74
	3	564	617.8	1.09	5.84
	4	548	614.0	1.12	5.83
	Average	**556**	**617.8**	**1.11**	**5.85**
A-12	1	612	651.1	1.06	4.98
	2	625	665.3	1.06	5.36
	3	625	655.5	1.05	4.25
	4	631	672.3	1.06	5.87
	Average	**622**	**661.1**	**1.06**	**5.11**

All the tested bars in Table 3.1 meet the requirements of classes A, B & C that are shown in Table 3.2.

Table 3.2: requirements for reinforcing steel bars BS EN 1992-1-1: 2004

Class	A	B	C
Characteristic yield strength f_{yk} or $f_{0.2\%,k}$	400-600	400-600	400-600
Minimum value of $(f_t/f_y)_k$	≥1.05	≥1.08	≥1.15 and <1.35
Characteristic strain of reinforcement at maximum load ε_{uk} (%)	≥2.5	≥5.0	≥7.5

Since all steel classes delivered by Celsamax are cold worked steel, this can explain the absence of yield plateau in most of the tested C' bars as they will be strained beyond the yield plateau during cold working because of stretching and then unloading, which will lead to a strain hardening effects a result of that work, higher yield stresses can be attained with reduced level of strains and the hardening of strain commences immediately after the onset of yielding which will lower the ductility of the steel as bars will reach the ultimate strength at a lower strain values which may hence decrease the ductility of the concrete members reinforced with these types of bars.

3.2.2 Tension test for welded mesh

Tension test was carried out for welded meshes to make sure that they agree with Section 3.2.5 of EC2 that specifies a joint of welded fabric to be adequate, i.e., it should withstand a shearing force equal to a minimum of 25 % of the specified characteristic yield stress times the nominal cross sectional area. The later force should be based on the larger sized bar.

The steel weld for the mesh was tested by applying a load to the longitudinal bar for each grade as shown in Figure 3.11. The cross bar was welded in place to two other longitudinal bars to enable the central weld strength to be tested. Load was applied to the bars and all grades proved to have the weld sufficiently strong and satisfying the code requirements

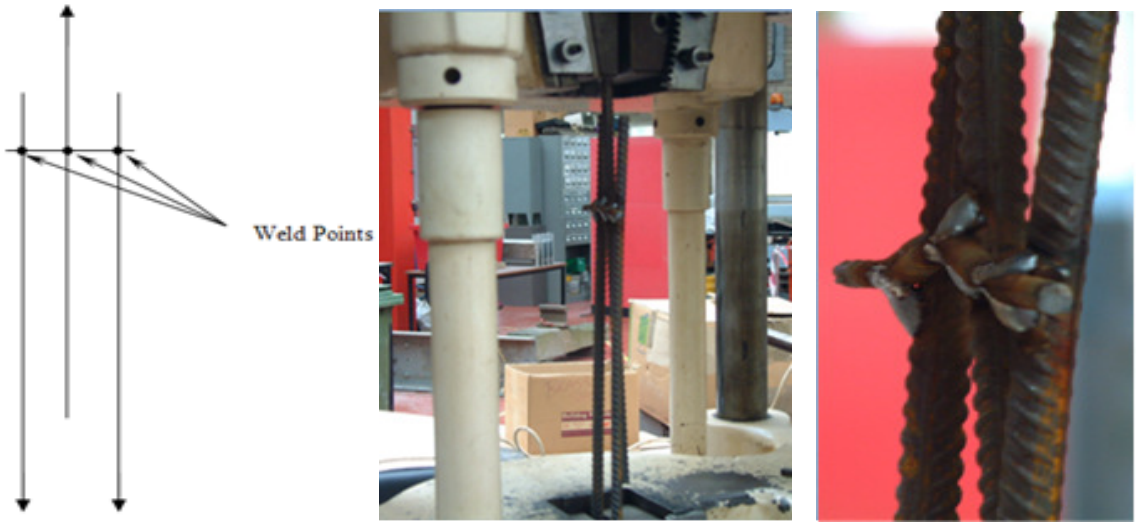

(a) Welded steel mesh (b) Test set up (c) Steel mesh after test

Figure 3.11: Steel Mesh Weld Testing

3.3 Concrete preparation & mix design

3.3.1 Cement

Ordinary Portland Cement (OPC) supplied by Rugby Cement plc was used for the concrete mix. Its chemical composition as provided by the manufacturer is given in Table 3.3.

Table 3.3: Cement chemical compositions

Oxide	CaO	SiO_2	Al_2O_3	Fe_2O_3	MgO	SO_3	Cl
%	64.4	20.3	5.7	2.3	1.4	2.9	< 0.02

3.3.2 Fine and coarse aggregate

Gravel of size 10 mm from Edwin Richards Quarry and sand from Weeford Pit were used as the coarse and fine aggregate, respectively. The grading is shown in Figure 3.12.

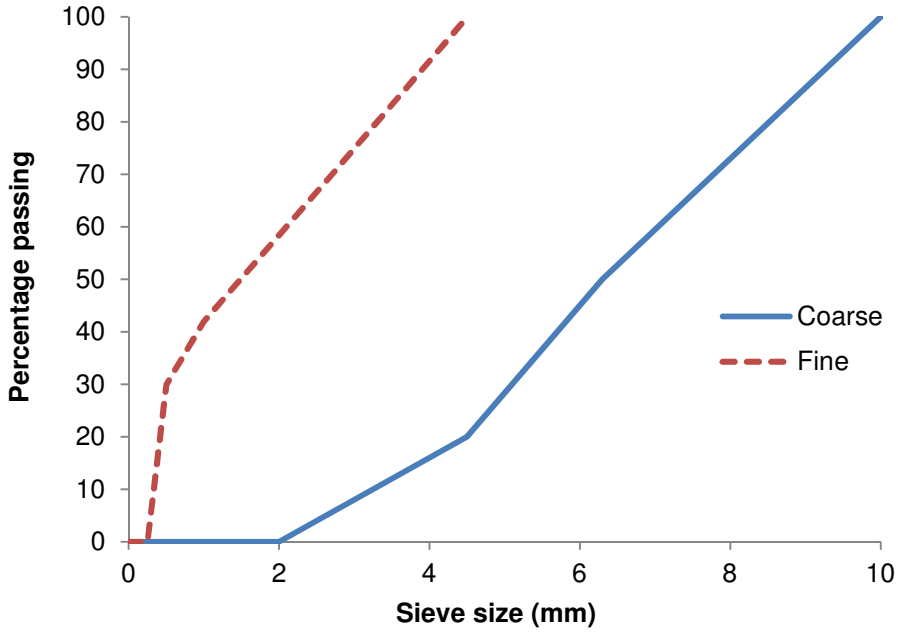

Figure 3.12: Aggregate grading curves

3.3.3 Concrete mix design

The concrete mix used for all batches was proportioned for a 28 days compressive strength of 43 N/mm^2 and a slump of 30~60 mm. The mix proportions for each test are presented in Table 3.4. The quantities were based on oven dry aggregate materials; moisture content was determined for the used aggregate when each batch was cast and due adjustment was made.

- In each set of two identical concrete blocks, the following concrete standard specimens were cast: three cubes, three cylinders and three prisms to determine the compressive strength, cylinder split tensile strength and modulus of rupture, respectively (see Figure 3.14). As BS EN 206-2013 recommends to use cylinders for the purpose of determining compressive strength, the mean cube strength has been converted into the equivalent cylinder strength f_{cm} by following EC2 (BS EN:1992-1-1:2004) as will be shown later in part 4.4 of chapter 4. The reason of testing cubes and then converting to cylinders is due to the fact the compressive testing machine in the laboratory of the University of Birmingham is not fit for the standard size of the cylinders which are used to determine the compressive strength.

All standard specimens were tested and strengths were calculated based on BS EN 1992-1-1:2004 by applying the following equations:

$$\text{Compressive strength of a cube} = \frac{P}{A_s} \tag{3.1}$$

$$\text{Cylinder split tensile strength} = \frac{2 \times P}{\pi \times H \times D} \tag{3.2}$$

Modulus of rupture of a prism= $\frac{P \times L}{b \times d^2}$ (3.3)

where:

P: maximum load applied (N). D: diameter of the cylinder (mm).

H: length of the cylinder (mm). A_s: cross sectional area of the cube (mm^2).

L: length of the prism (mm). b, d: cross sectional area of the prism (mm).

Table 3.4: Concrete mix design (based on oven dry condition)

Constituent	**Quantities (kg/m^3)**	**Description**
Cement	426	Ordinary Portland Cement
Water	200	Tap Water
Coarse Aggregate	583	10mm maximum size gravel from Weeford Quarry, Sutton Coldfield
Fine Aggregate	1132	Sand from Weeford Quarry, Sutton Coldfield

(a) Cube test for compressive strength

(b) Prism test for modulus of rupture

(c) Cylinder test for indirect tensile strength

Figure 3.13: Control specimen tests

Chapter 4: Bond Tests & Results

4.1 Introduction

It has been noticed that a relatively less attention has been paid to the influence of rib pattern of reinforcement on the bond strength among most of the previous studies regarding the bond issues. Recently, since the start of this century, researchers started to focus on the bar ribbing patterns and its relation to bond strength and failure mechanism. This study is one of the studies which considers bar ribbing patterns as one of the variables during a pull-out test. Apart from the bar rib pattern, two other variables will be studied in this experimental study, which are the amount of shear link and the material property of steel bars. Celsa Steel Ltd. provided three types of steel, standard C & B classes and steel C', which were produced with different rib patterns as will be illustrated later in this chapter.

Bar C and C' both being classified as Class C steel, the major differences between these two groups is the rib pattern (see Figure 4.1) and the materials properties as illustrated in Chapter 3. However, it is believed the later difference has less significant effect on the bond behaviour. On the surface of both bars, two longitudinal ribs split the surface into two equal halves. Transverse ribs run in the same direction with an equal rib height and spacing, i.e. 0.8mm and 13 mm, respectively; Two additional longitudinal ribs were introduced for C' going through the peak of the transverse ribs.

Pull-out tests were conducted on bar B, C and C' to investigate the effect of shear link spacing, bar location, concrete cover, steel class, embedment length and bar size on the bond strength of the reinforcement.

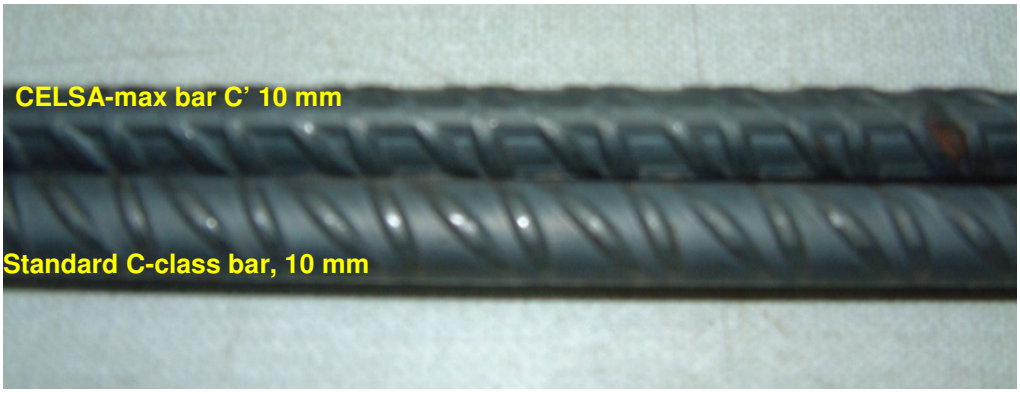

(a) Bar C& C' and B & A

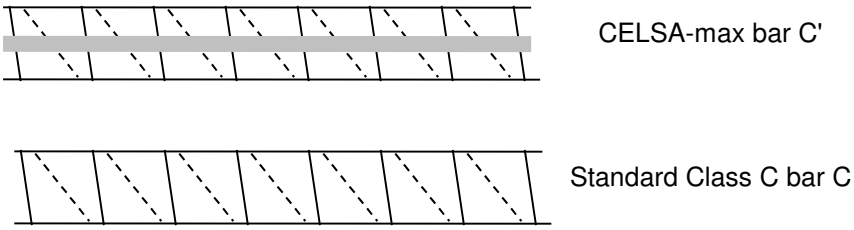

(b) Illustrative diagram of the rib pattern

Figure 4.1: Rib pattern for Classes A, B, C & C' reinforcing bars

4.2 Test specimens

50 pull-out tests have been conducted to study the above-mentioned influence factors divided into four groups with different block sizes, steel bar locations, concrete covers, embedment lengths and different amount of shear links. Tests are divided into four groups based on the location of the reinforcing steel.

Test I: Test specimens (see Figure 4.2) are 250 mm long concrete blocks with a nominal width and depth of 150 mm. Each concrete block contained four bars located at the top and bottom of the specimen with a 20 mm concrete cover to shear links (or longitudinal bars in the absence of shear links) at all sides. Top and bottom bars were placed in opposite directions so that the effect of the concrete cracks caused by the bars at one side will be minimized on the other side during testing.

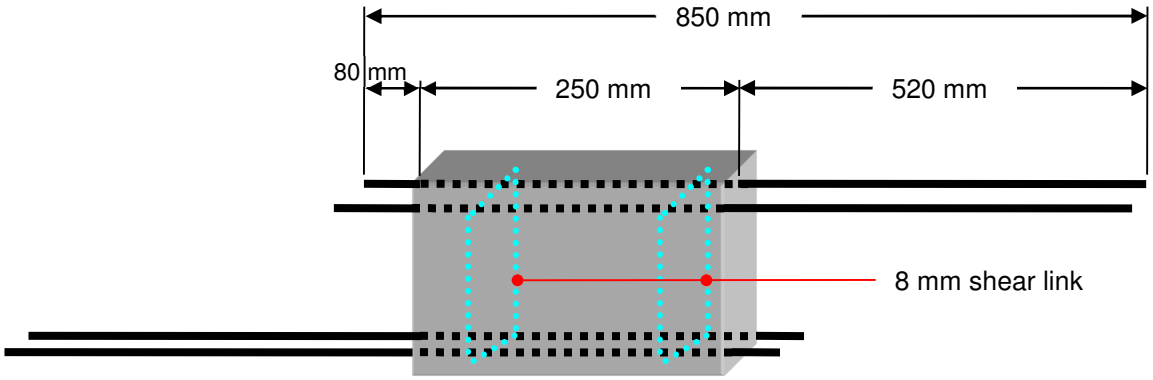

(a) Concrete pull-out test block (250 X 150 X 150 mm)

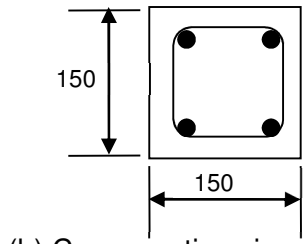

20 mm cover all sides

10 mm main steel bars
& 8 mm shear links

(b) Cross-section view

(c) Specimen for Test I

Figure 4.2: Typical pull-out test specimen for Test I

2. **Test II:** Test specimens (see Figure 4.3) are 250 mm long concrete blocks with a nominal width and depth of 100 mm. Each concrete block contained two bars located at the bottom and top of the specimen with a 45 mm concrete cover to sides and 20 mm to top and bottom face.

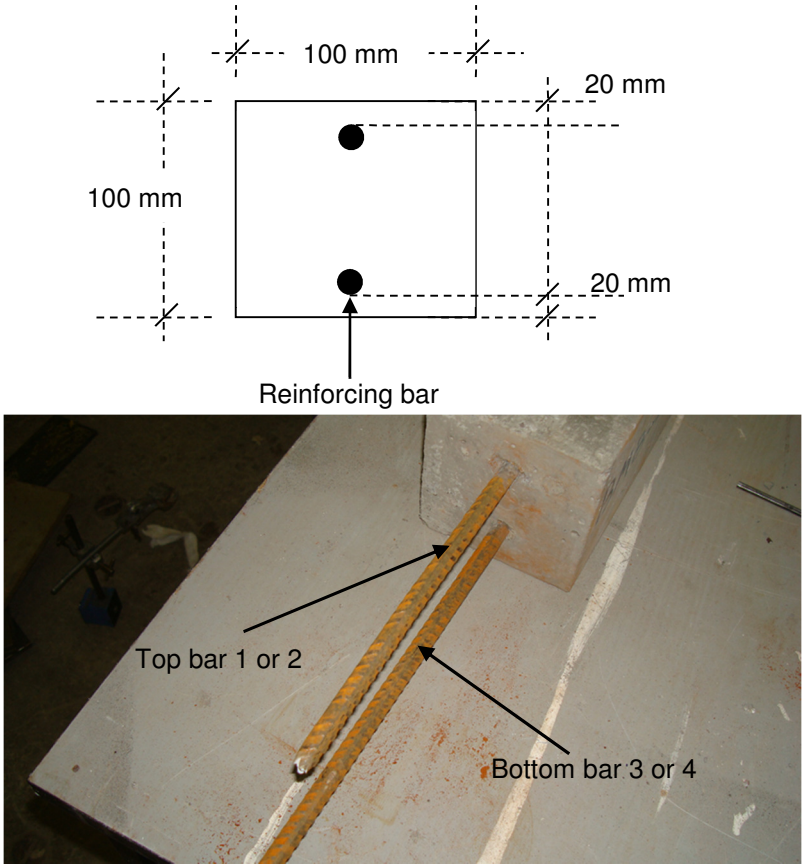

Figure 4.3: Specimen cross section for Test II

3. **Test III:**

Test specimens (see Figure 4.4) are 250 or 300 mm long concrete blocks with a nominal width and depth of 100 mm. Each concrete block contained two bars located at the top of the specimen with a 20 mm concrete cover to sides and top face.

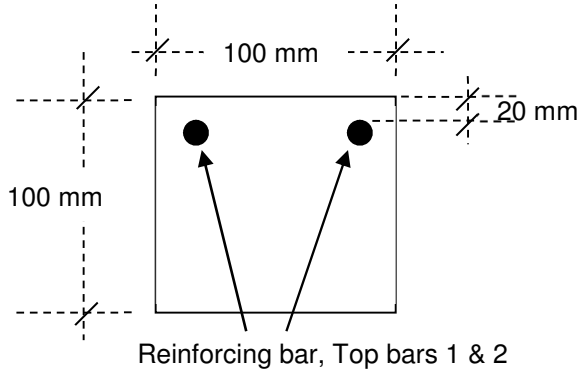

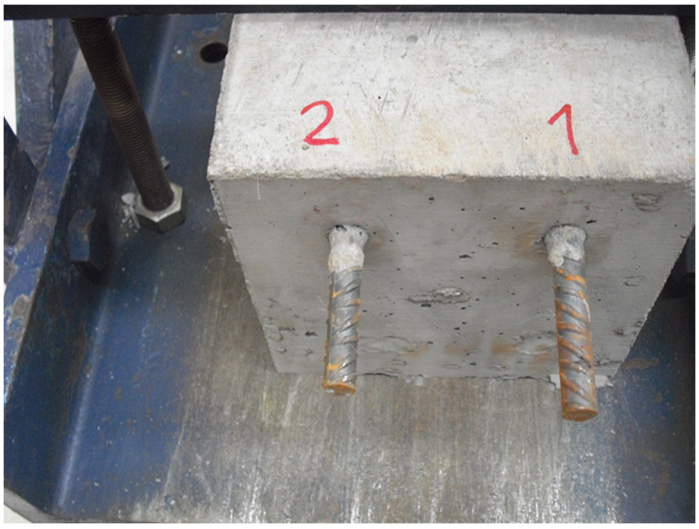

Figure 4.4: Specimen for Test III

4. Test IV

An example of specimen of this group is shown in Figure 4.5. Each block is 150, 250, 300 or 350 mm long with a nominal width and height of 100 mm, reinforced with single bar in middle of the specimen with ≈ 40 mm concrete cover to bottom and ≈ 45 mm to both sides. Six specimens have plastic sleeves of 25 mm length inserted at each end of the reinforced bar as shown in Figure 4.6.

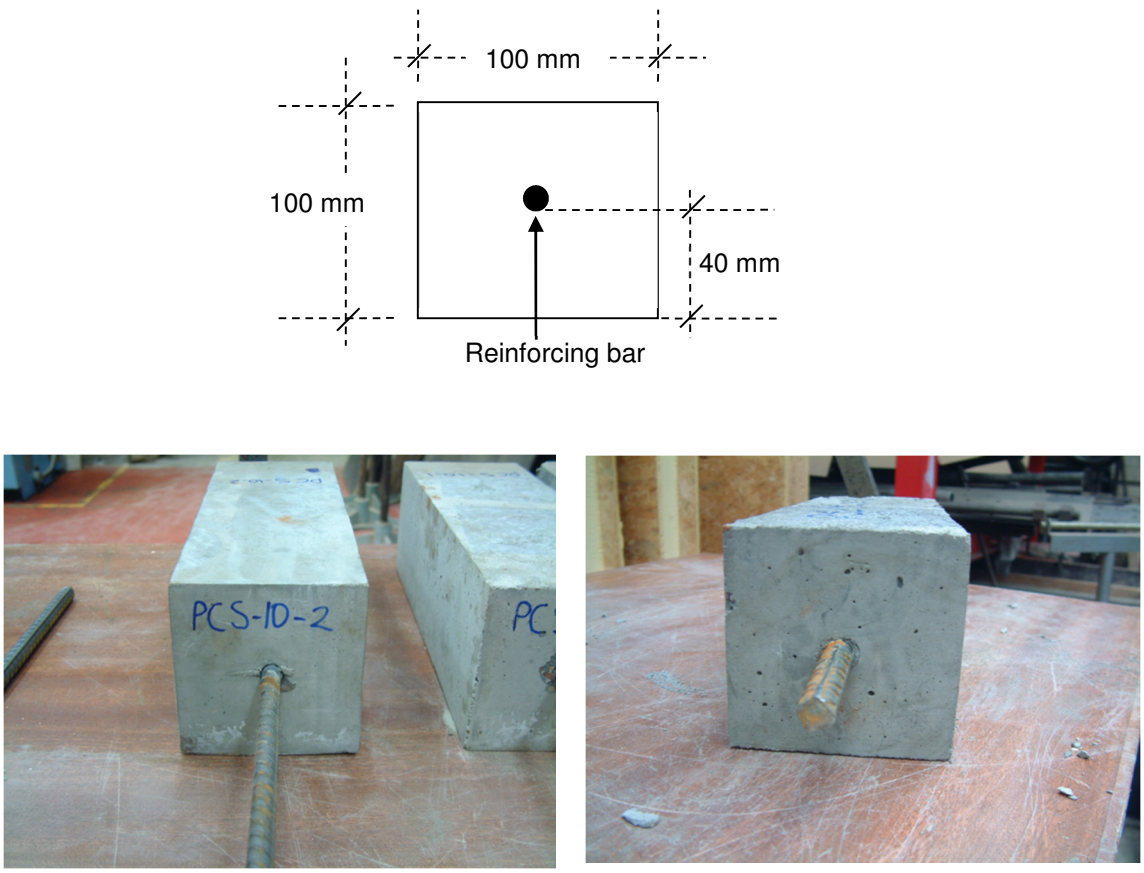

Figure 4.5: Specimen picture & cross section for Test IV

Figure 4.6: Reinforcing bars with sleeves at both ends, fitted into moulds prior to concrete casting

A designation system was used to identify each bar in the pull-out test. The first letter P indicated pull out test, followed by another two letters (S or M), for single bar or mesh, and (A, B, C or C`) indicating the bar type. Six numbers follow the two letters indicating the block length depth and width. Shear link spacing (zero represents no shear link), the number of the two identical concrete blocks and the number of the tested bar in the block. Bar 1 and 2 are for top bars and bar 3 and 4 are for bottom ones. An example of the designation is shown in Figure 4.7.

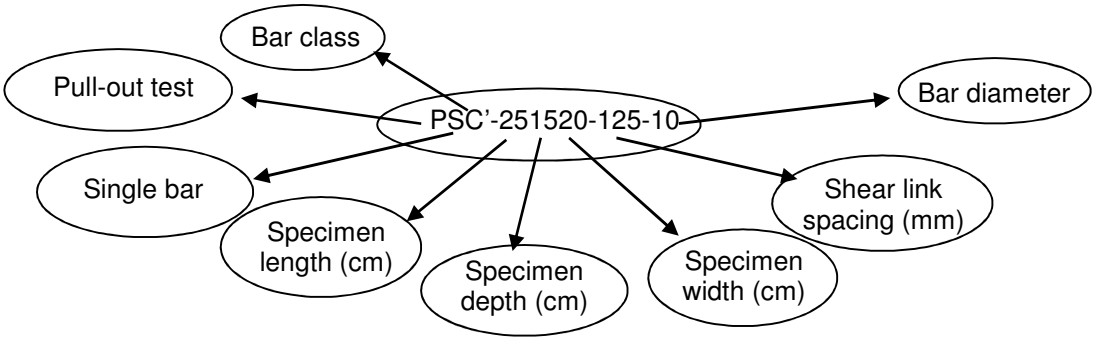

Figure 4.7: Example of specimen designation

4.3 Test setup

4.3.1 Instrumentation

The testing rig utilized is shown in Figure 4.8. Three LVDTs and one load cell, each connected to a data logger, were utilized to measure the movement and load simultaneously. These instruments, together with some others, are labelled in figure 4.8 and explained as follow:

- **A:** LVDT sensors to record the movement of the steel bar.

- **B**: G- clamps were fixed at the steel bar to provide the measuring points for LVDT sensors.

- **C**: hydraulic jack to apply horizontal force on the tested bar.

- **D**: steel plates to transfer load from jack to the load cell.

- **E**: load cell to read the applied load and send it to be recorded by the data logger.

- **F**: anchorage unit to be placed over the bar using its four screws.

- **G**: Squirrel data logger, an electronic device connected with LVDT sensors and load cell. Displacement readings from LVDT sensors and the load cell were stored in a memory card and downloaded into an excel sheet using a special software.

Two LVDT sensors were used to get front slip of the steel bar. The differential reading from these two sensors can be used to calculate the strain of the reinforcing steel bar. The detailed calculation is as follows

$$s = d_1 - e \tag{4.1}$$

$$e = \varepsilon \times L_{1,0} \tag{4.2}$$

Based on the strain definition which can be described as the change of the length divided by the original length then:

$$\varepsilon = \frac{d_1 - d_2}{L_{1,0} - L_{2,0}} \tag{4.3}$$

By substitution we can get the following formula:

$$s = d_1 - \left(\frac{d_1 - d_2}{L_{1,0} - L_{2,0}} \right) \times L_{1,0} \qquad (4.4)$$

where:

s: slip of the steel bar out of the concrete;

e: elongation of the bar;

d_1 & d_2: movement of G-gauge 1 and 2, respectively;

$L_{1,0}$ & $L_{2,0}$: the initial location of G-gauge 1 and 2 in relation to the concrete front surface;

ε : strain of the steel bar.

At the rear side of the concrete block, the LVDT was held by using a steel clamp fixed at the tested steel bar. The reason for attaching the LVDT to the steel bar in this way is to minimise any error which can be caused due to the movement of the block itself during the test.

Load was applied using the hydraulic jack. Force exerted on the steel bar was increased in an increment of 1 or 1.5 KN at the beginning, reduced to 0.5 KN prior to the maximum load until it reaches its ultimate failure load. The results obtained were used to calculate and compare the bond strength for each bar and then study the influence of ribs geometry, shear link spacing and the location of the reinforcing bar on the bond strength.

(a) Overview of the test rig and instruments

(b) Overview of the data acquisition system

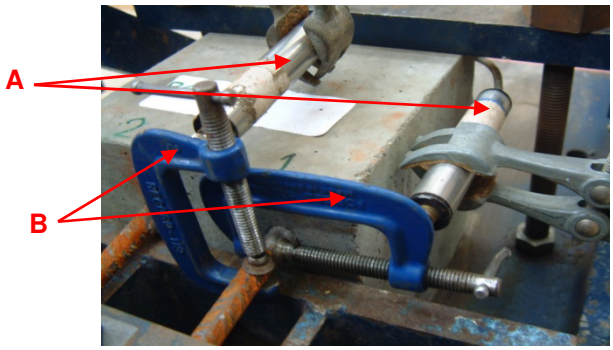

(c) Front slip measurement

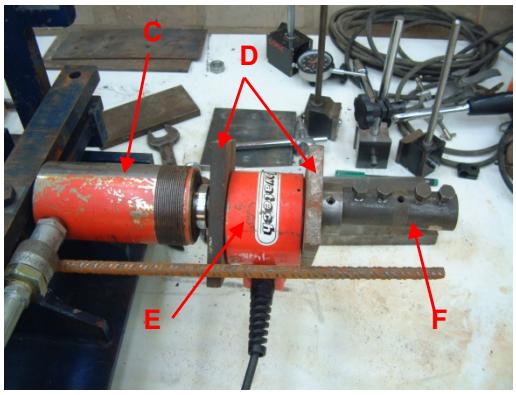

(d) Applying and recording loads

(e) Rear slip measurement

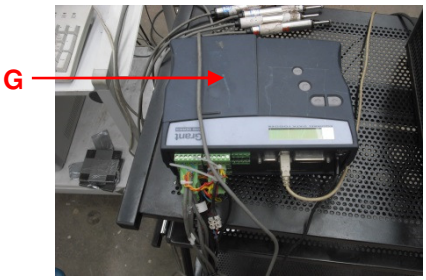

(f) Data logger

Figure 4.8: Pull-out testing rig and instruments used

4.3.2 Equipment calibration

- **Load cell calibration**

Cube testing machine was used to calibrate the load cell to ensure correct load readings during experiments. The load cell has been located centrally between two loading steel plates to insure that load is equally distributed on the load cell.

After cleaning loading area of the cube testing machine to ensure accurate measurements as it can be, load was applied on the load cell with 5 KN increments. The process was repeated up to a load of 75 KN which is greater than the maximum tensile force of a bar size of 12 mm diameter that is the biggest bar diameter used in all tests.

- **Linear Variable Displacement Transducer (LVDT) calibration**

The LVDT produces an output of a measurement of slip which is accurate to 0.01 mm, designed for a maximum displacement of 50mm; the LVDT setup is shown in Figure 4.9

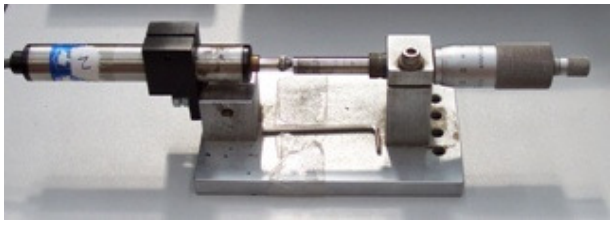

Figure 4.9: Transducer with micrometre

Firstly the tip of the micrometer and transducers were cleaned before locking the transducer into position. This was done to ensure the transducers moved smoothly providing accurate readings for subsequent tests. A 0.2 mm for up to 1.0 mm and 0.5 mm for up to 3.0 mm displacement increments were made on the micrometer to allow the transducer to measure it, starting at zero millimeters. Meanwhile for periods of more than 10 seconds of stability the output from the transducer was measured by the data logger. These steps were repeated until the displacement reached 3.0 mm. The slip of the reinforcing bar when maximum pull load achieved was estimated to be less than 1.0mm, thus every 0.2 mm displacement was measured in order to achieve more accurate readings. While higher slip was estimated to occur at its residual bond strength, and thus only every 0.5 mm displacements were measured.

4.4 Testing results analysis and discussion

Table 4.1 summarise results for all pull-out tests that have been done in this study, which contains:

- The maximum applied load for each steel bar, i.e. ultimate failure load P_{max};
- Experimental bond strength (f_b) which was calculated based on the formula (Clark and Gorst, 2003):

$$f_b = \frac{P_{\max}}{\pi \times D \times L} \tag{4.5}$$

Where:

P_{max}: ultimate failure load.

D: diameter of the tested bar.

L: length of the embedment part of the tested bar.

- Mean values for top & bottom bars for each tested concrete block.

- f_{cum}: the mean cube strength which has been converted into the equivalent cylinder strength f_{cm} by following EC2 (BS EN:1992-1-1:2004)

In the last column of Table 4.1, the bond strength is normalized by $(f_{ck})^{2/3}$ to eliminate the effect of concrete strength.

Table 4.1 Pull-out test results

Specimen	Bar location	Link spacing (mm)	Concrete strength (N/mm^2) $f_{ck,cube}/f_{ck}$	Max load (P_{max}) (KN)	Bond strength (f_b) (N/mm^2)	$f_b/(f_{cm})^{2/3}$
Bar Size						
PSC'-301040-8			19.43/15.54	32.14	4.265	0.684
PSC'-301040-10			19.43/15.54	50	5.308	0.852
PSC'-301040-12			19.43/15.54	54.52	4.82	0.773
Concrete Cover						
PSC'-251040-10			22.6/18.08	38.9	4.955	0.719
PSC'-251020-10			25.55/20.55	29.3	3.732	0.497
PSC'-301020-10			22.6/18.08	33.7	3.577	0.519
PSC'-301020-10			22.6/18.08	30.5	3.238	0.469
PSC'-301040-10			19.43/15.54	50	5.308	0.852
Bar Location						
PSC'-301020-10	Top		22.6/18.08	26.2	2.781	0.403
PSC'-301020-10	Top		22.6/18.08	24	2.548	0.369
PSC'-301020-10	Bottom		22.6/18.08	30.51	3.239	0.470
PSC'-301020-10	Bottom		22.6/18.08	33.7	3.577	0.519

Table 4.1 continued

PSB-251020-10	Top		25.55/20.55	29.2	3.72	0.495
PSB-251020-10	Bottom		25.55/20.55	31.6	4.025	0.536
PSC-251020-10	Top		27/22	42.9	5.464	0.695
PSC-251020-10	Bottom		27/22	44.1	5.618	0.715
Bar Type						
PSB-251020-10			25.55/20.55	29.2	3.720	0.495
PSC'-251020-10			25.55/20.55	29.25	3.725	0.496
PSC-151020-10			20.37/16.3	22.42	4.760	0.740
PSC'-151020-10			28.13/23.13	23.74	5.040	0.620
Embedment Length						
PSC'-151020-10			23.17/18.54	17.85	3.790	0.540
PSC'-251020-10			23.17/18.54	41.43	5.278	0.753
PSC'-351020-10			23.17/18.54	43	3.913	0.558
PSC'-151020-10			25.55/20.55	41.8	6.657	0.886
PSC'-151020-10			22.6/18.08	40.22	5.123	0.436
Shear Link						
PSC'-251020-10		None	29.2/25	34.01	4.332	0.506
PSC'-251020-10		80	23.3/18.64	41.45	5.280	0.750
PSC'-251020-10		125	31/25.7	49.65	6.325	0.725
PSC-251020-10		None	26.2/21.2	28.43	3.622	0.472
PSC-251020-10		80	26.6/21.6	39.98	5.093	0.660
PSC-251020-10		125	27/22	44.08	5.615	0.714

4.4.1 Comparisons and discussions of bond behaviour and strength

Comparisons were made based on the results presented in Table 4.1 and Figures 4.10 to 4.27. Data are presented and studied by considering factors in six categories: reinforcing bar location, shear link spacing, steel bar class, bar size, embedment length and concrete cover.

Figures 4.10 to 4.27 present the force vs. slip relationship of each test specimen. For comparison reason, various results are grouped together and presented in a same graph. In general, four types of results were observed: (1) bar yields before the pull-out failure occurs (e.g. size 8 in Figures 4.10 and 11); (2) bar fractures before the pull-out failure occurs (e.g. size 10 in Figure 4.10); (3) bar experiences pull-out failure with the inadequate embedment as evidenced by a rapid drop in pull-out force following the peak point (e.g. sizes 10 and 12 in Figure 4.11); (4) bar experiences pull-out failure with adequate embedment as evidenced by a slow reduction in pull-out force is indicate a less steep declining section in the curve (e.g. size 12 in Figure 4.10).

4.4.1.1 Influence of bar size

Figures 4.10 & 4.11 present the force vs. slip relationship of bar C' of sizes 8, 10 and 12 respectively. Figure 4.10 shows the results of specimens without any sleeve, i.e. the embedment length being 300mm; while in Figure 4.11, the embedment length was reduced to 250mm due to the use of plastic sleeves at both ends. Both figures show similar trends relative to the effect of bar size. As expected, larger bar size will lead to higher ultimate force. However, the normalized bond strength by the concrete strength does not show obvious correlation with the bar size, as illustrated in the last column of Table 4.1.

Figures 4.10 and 4.11 also reveal that size 8mm bars yielded before they were pulled out of the concrete and hence the peak forces in the curves are governed by the yield force of the steel bars rather than the ultimate bond force. This happens when the ultimate bond force is greater than the yield force of the bar and the embedment length is adequate. Tests with 8 mm bars stopped when bars start to yield and develop excessive elongation.

In Figure 4.10, the size 10mm C' bar fractured as the pull-out force has yet reached the maximum value. That happens when the ultimate force of the bar is greater than the ultimate bond force and the actual embedment length is adequate. However, in Figure 4.11, the same bar did not fracture with the presence of plastic sleeves which reduced the embedment length to 250mm. This bar experienced the pull-out failure but with a sudden drop in the post-bond-failure strength. This has suggested the embedment length is not adequate, so the required bond length must be greater than 250mm. Size 12mm C' bars experience pull-out failure in both cases, both failed at a similar level of pull-out force.

12mm bars experience the pull-out failure with the inadequate embedment as evidenced by a rapid drop in pull-out force following the peak point as shown in Figure 4.11. That can explain the reason of not having bond strength greater than that in the 10mm bar case as embedment length of 300mm is adequate for 10mm bar but not for 12mm. The bar with 12mm diameter cannot achieve its maximum bond strength with inadequate embedment length of 300 and attained a lower bond strength.

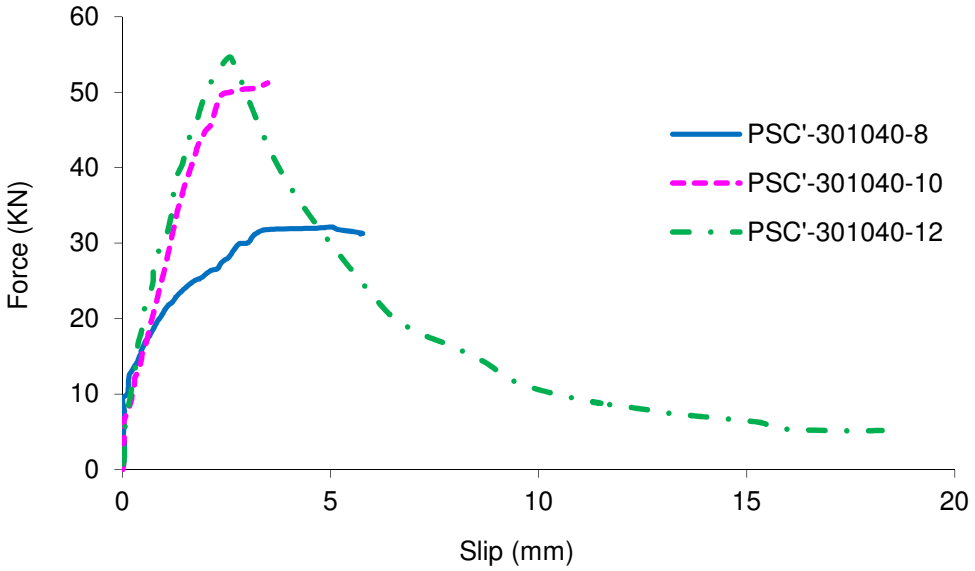

Figure 4.10: Bond force versus bar size without plastic sleeves

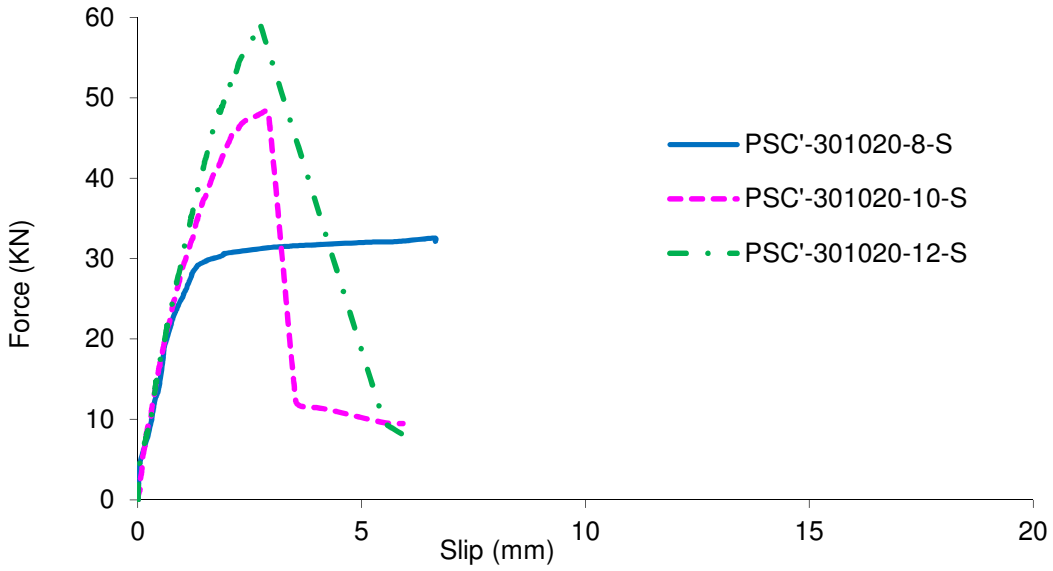

Figure 4.11: Bond force versus bar size with 25 mm sleeves at both ends

4.4.1.2 Influence of shear links

As expected, Table 4.1 shows that the normalized bond strength increased when having shear links and when reducing the shear link spacing as indicated by PSC-251520-n/80/125-10 series. However, In the PSC'-251520-n/80/125-10 series, the normalized bond strength of C' with 80 mm shear link spacing was found to be slightly lower than that with 125 mm spacing. This anomaly is probably attributed to some unpredicted testing errors. Figures 4.13 and 4.14 both show that 125 mm shear link spacing rendered highest ultimate bond force. This is because in both cases, the concrete strength was highest within the group.

It was found that the shear link free blocks experienced splitting failure as shown in Figure 4.12, and while those with shear links mainly showed the pull-out failure mode as shown in Figures 4.13 and 4.14. The reason behind the occurrence of a pull-out failure in presence of confinement with shear links is due to the fact that the shear links have exerted a confining action for concrete surrounding the steel bars. Due to this confining action, concrete was able to resist high hoop stresses which are resulted from the radial component of the bond force. Therefore, bond strength will be increased and the specimens are more prone to pull-out failure. The longitudinal component will shear off the concrete along the interfacial zone which leads to pull-out failure when the load is increased.

Figure 4.12: Splitting failure mode of concrete block with no shear link reinforcement

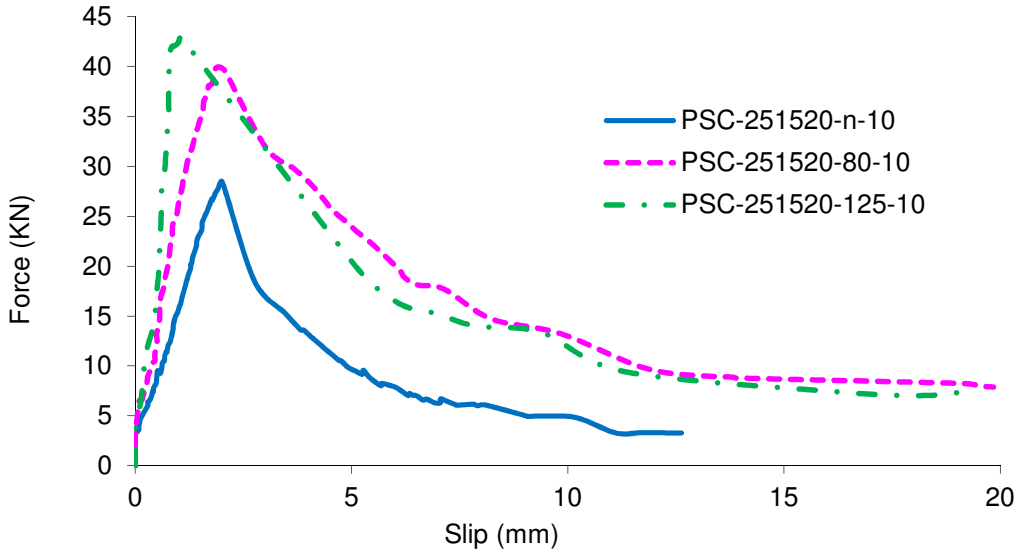

Figure 4.13: Bond force versus Shear link spacing

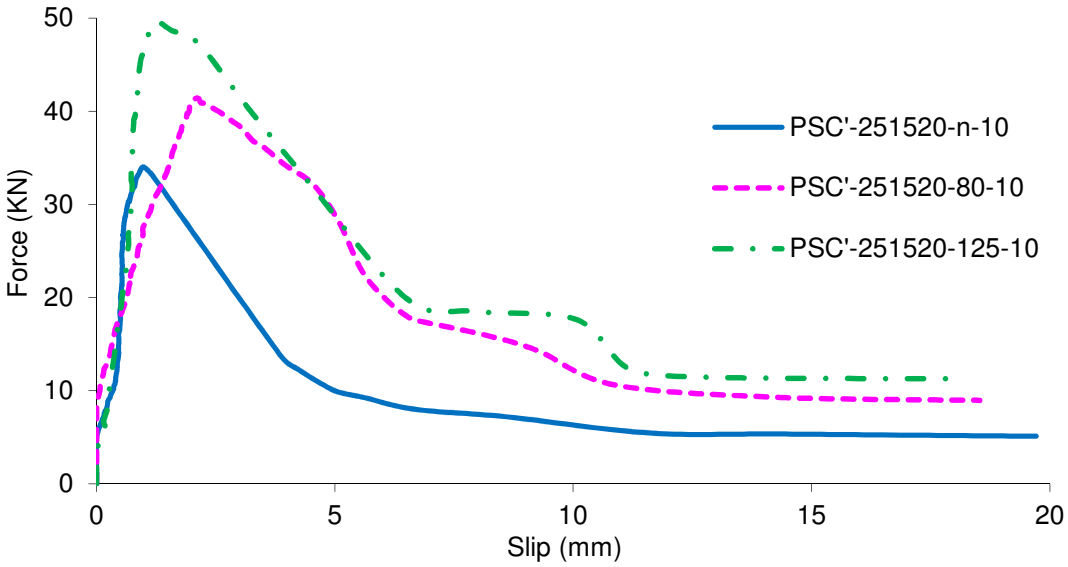

Figure 4.14: Bond force versus Shear link spacing

4.4.1.3 Influence of steel type & surface pattern

In Figure 4.15 both tested bars are considered C class bars but the difference is on the surface pattern. The surface pattern of steel bars appears to affect the bond strength. The normalized bond strength of bar C is only about 6 % higher than that for bar C' as shown in Table 4.11; this modest increase is due to the additional longitudinal ribs in C' bars, which reduces the rib projection surface area and hence reduces the friction and interlocking actions leading to the reduction in bond. Furthermore, the longitudinal rigs in bar C' can provide more restraint for the surrounding concrete in the circumferential direction so that the tendency of splitting has been alleviated. This agrees with the observation of crack patterns of the failed specimens as shown in Figures 4.15 and 16. The specimen containing C bar in Figure 4.15 shows wider and longer crack than C' bar in Figure 4.16.

It is clear in Figure 4.18 that both bars B & C' show similar bond behaviour; which can be due to the fact that the material properties, e.g. the ductility of bars, have negligible impact on the bond behaviour.

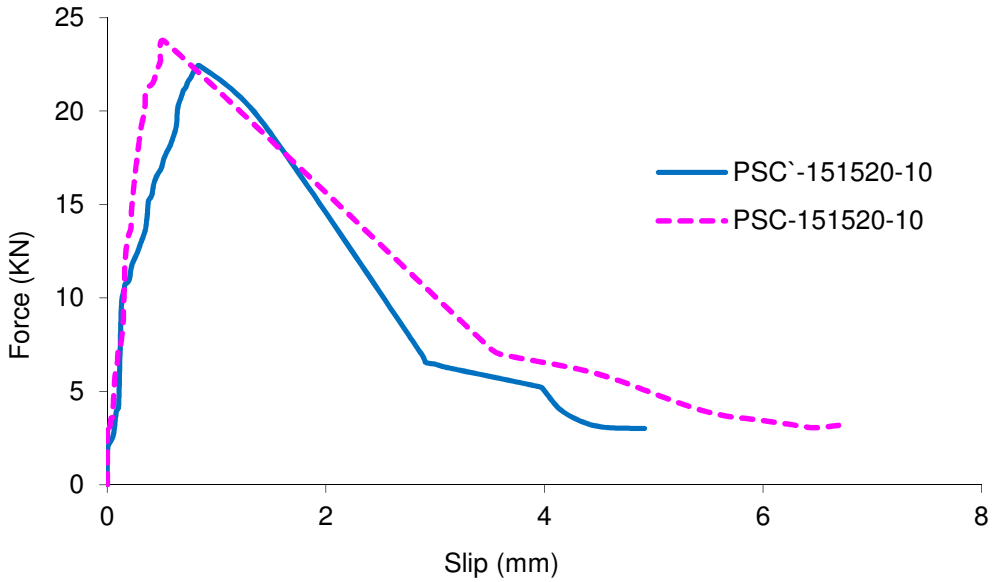

Figure 4.15: Bond force versus surface pattern

Figure 4.16: Failure mode with C` bar reinforcement

Figure 4.17: Failure mode with C bar reinforcement

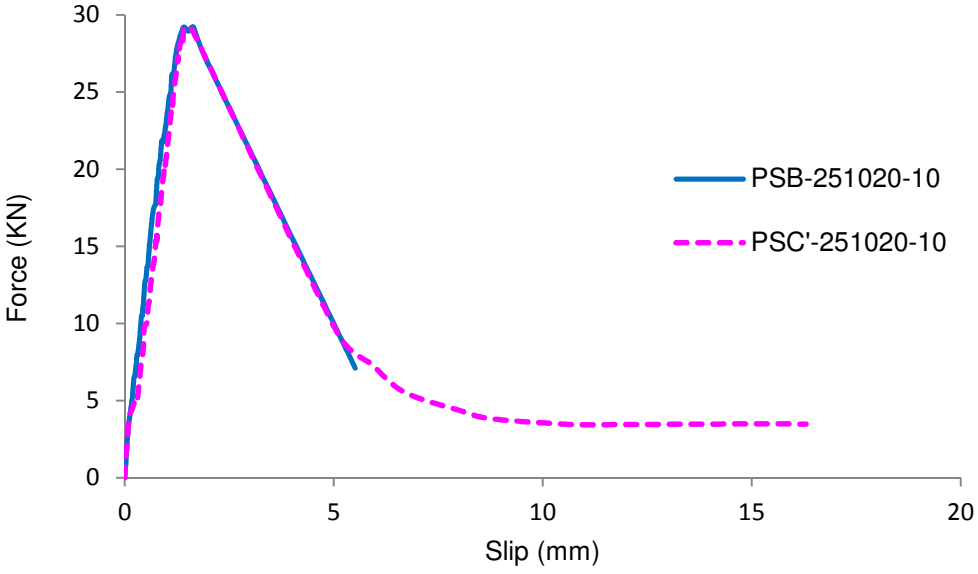

Figure 4.18: Bond force versus steel classes

4.4.1.4 Influence of reinforcement location

Results from Table 4.1 indicate that bottom bars have higher bond strength (10-20%) than top bars in all tests. This conclusion concurs with the trend found in Figures 4.19 and 4.20, where for both C' and B bars, the bottom bars always exhibited a better bond performance. This is mainly related to the autogenously shrinkage cracking, porosity, compactness and bleeding effect during the test. It has been observed that there were some autogenously shrinkage cracks developed on the top surface of the concrete block. No cracks were noticed at the bottom surface. Those cracks can reduce the concrete strength and concrete confinement to the top reinforcement. The concrete surrounding bottom bars was compacted twice during casting while the concrete surrounding top bars was compacted only once. The vibrating table during pouring was activated after the first half of moulds were filled and then activated again after moulds were fully filled. Another reason is the bleeding and settlement of fluid concrete as well as the evaporating of constrained air that formed a weak layer containing more voids at the top part of the concrete.

Failure modes for both top and bottom bars are shown in Figure 4.21, it can be noticed that more cracks exist in the top bar failure mode as well as more damages in the concrete appearing at the top surface than the bottom.

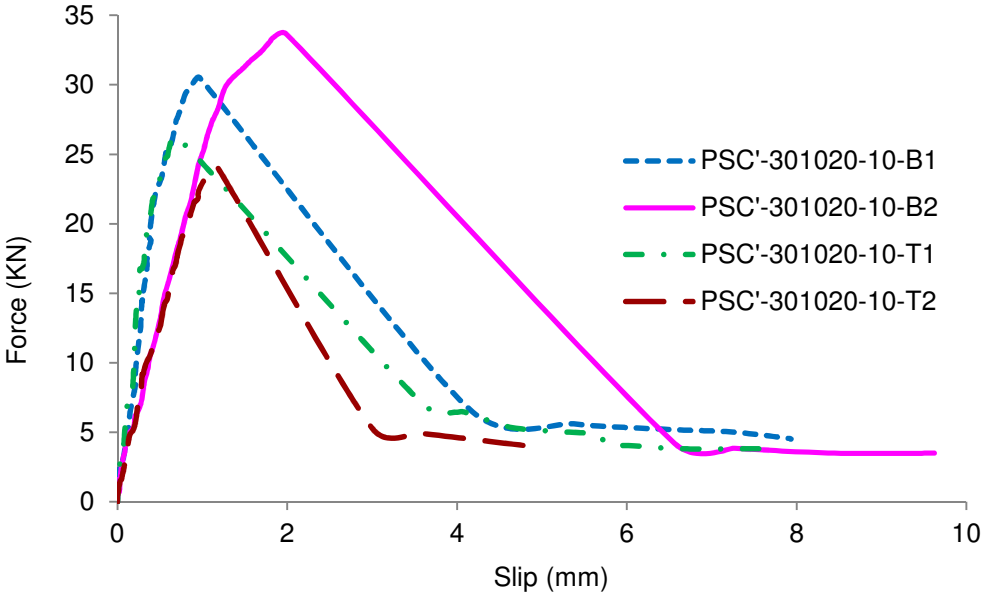

Figure 4.19: Bond force versus bar location

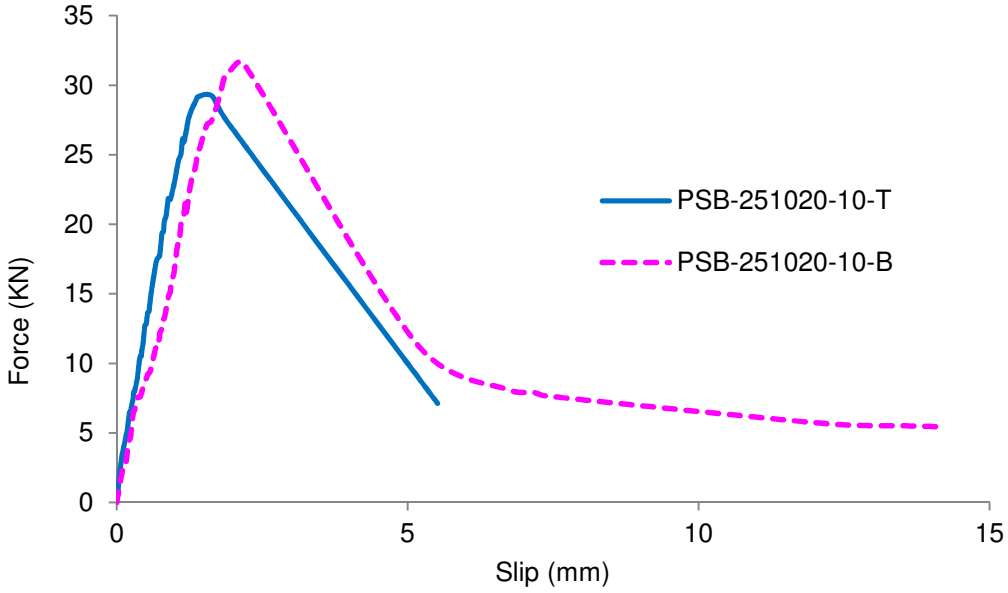

Figure 4.20: Bond force versus bar location

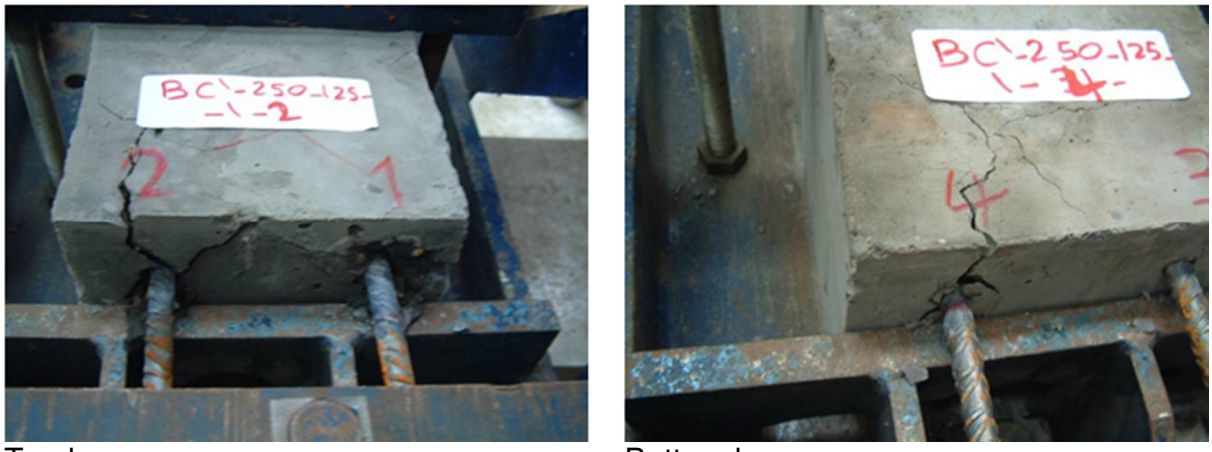

Top bars Bottom bars

Figure 4.21: Failure modes for bottom and top bars

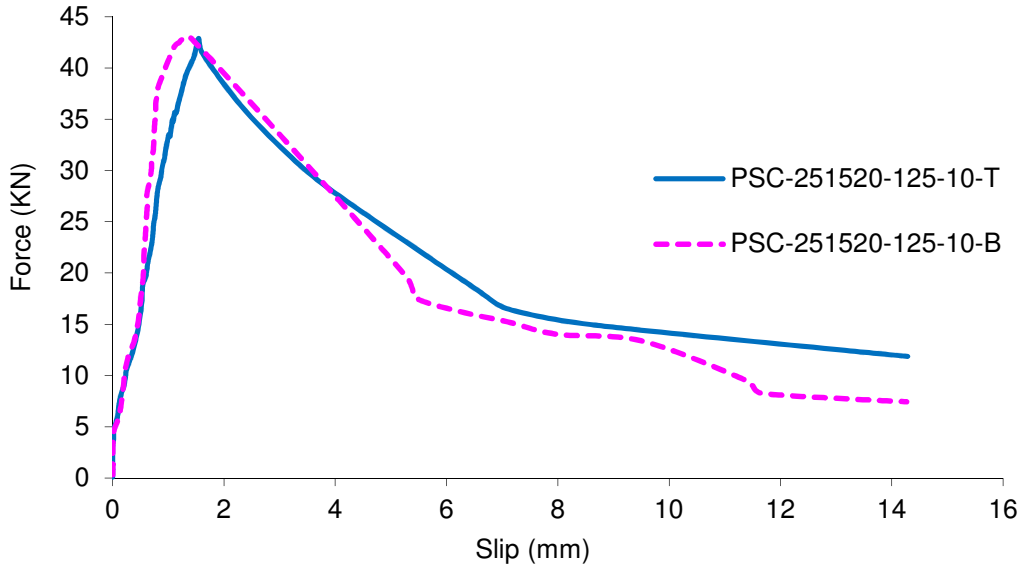

Figure 4.22: Bond force versus bar location with shear link spacing of 125 mm

Figure 4.22 shows that both the top and bottom bars exhibit very similar bond behaviour in the specimen with 125mm shear link spacing. As mentioned previously, the shear link will generate constraining effect on the concrete strength and hence enhance bond. The constraining effect of the shear link in this case overweighed the detrimental effect caused by the casting condition at the top location. So the effect of bar locations will be negligible.

4.4.1.5 Influence of the embedment length

It is envisaged that the increase in bond length up to a certain value will lead to an increase in bond force. If the embedment length exceeds the required bond length, the bond force will stop growing while increasing the embedment length. In Figure 4.23 longer embedment length results in higher ultimate bond force when the embedment length was increased from 150mm to 250mm; but when the embedment length was further increased to 350mm, the ultimate bond force tended to increase more and exceeded the ultimate force of the bar, leading the fracture of bar (see Figure 4.24). Figure 4.25 shows that both bars have similar behaviour as the embedment lengths increase from 200 to 250 mm, which suggests that any increase in embedment length beyond 200mm will not contribute to the increase in the bond force.

It is noticed that the increase in the bond strength stops at certain value of the bond length. That can be explained as the bond stress is not uniformly distributed along the bar-concrete interface. The bond force has its maximum value near the loaded end and decays very rapidly away from that surface. Beyond a certain distance, the bond stress will reach a neglected value close to zero, and hence the further increase in the bond length beyond that point will not always increase the pull-out force.

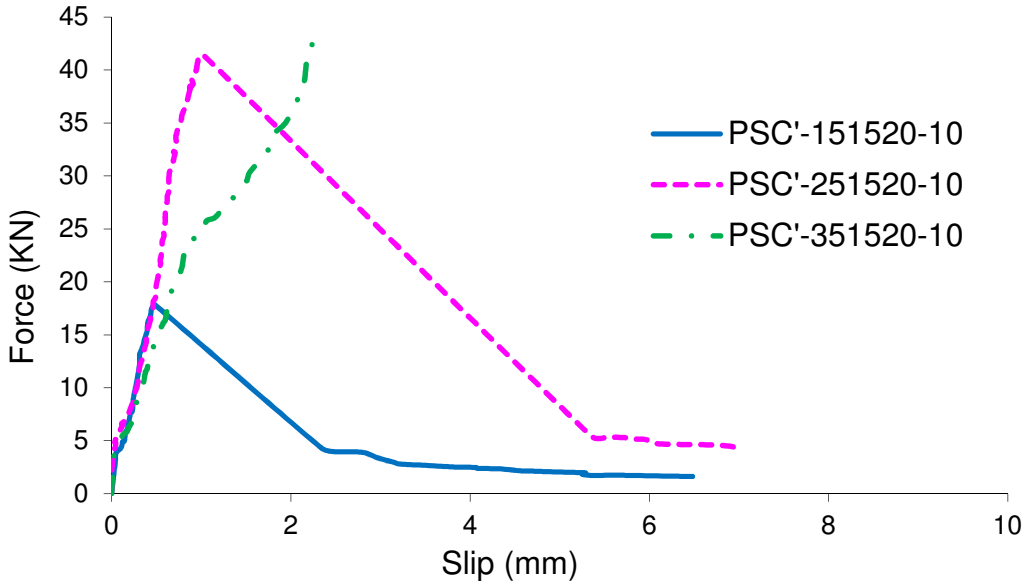

Figure 4.23: Bond force versus embedment length

Figure 4.24: Fractured bar after pull-out test with 350 mm embedment length

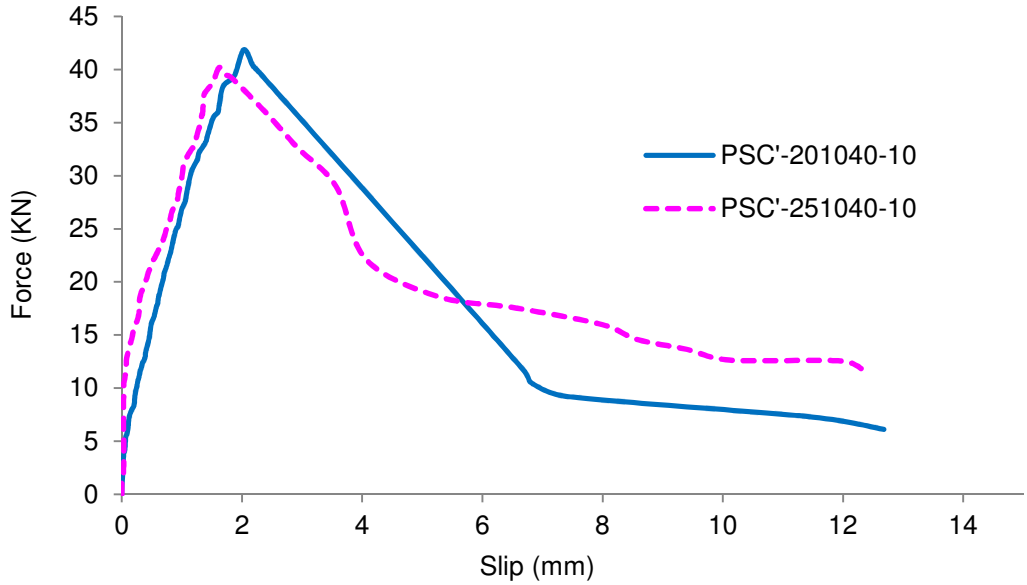

Figure 4.25: Bond force versus embedment length

4.4.1.6 Influence of concrete cover

Figures 4.26 and 4.27 show an increase in bond strength as the increase in cover.

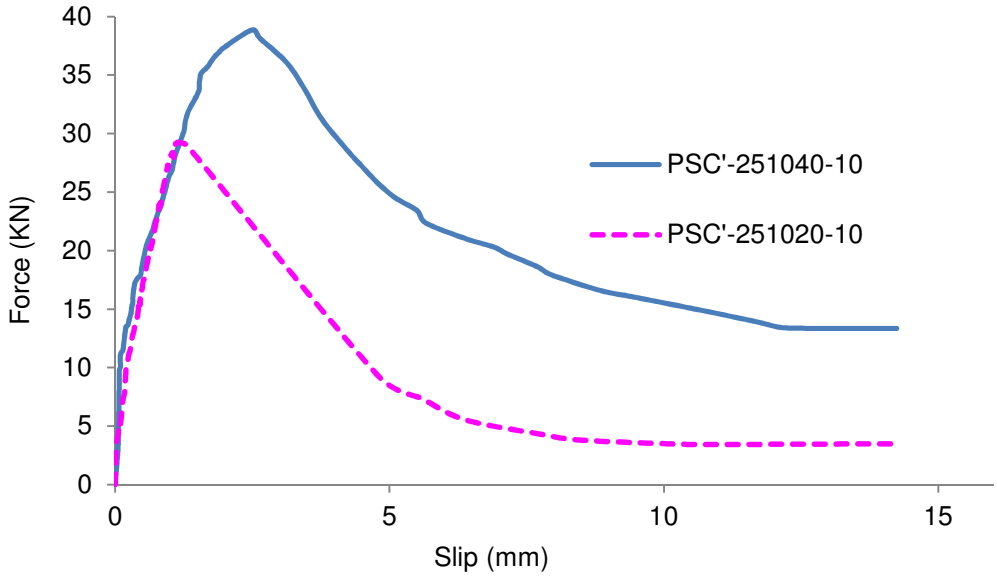

Figure 4.26: Bond force versus concrete cover

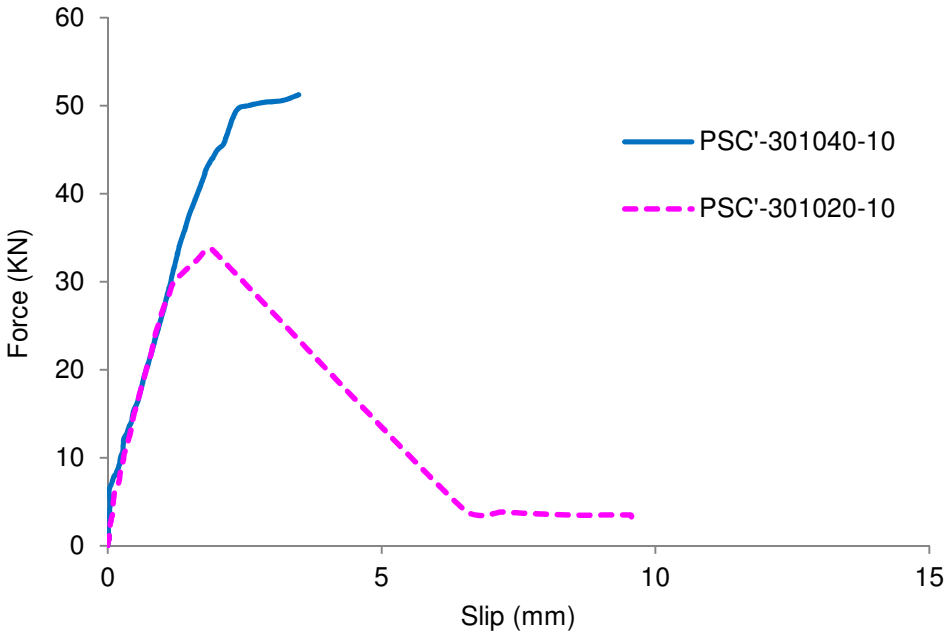

Figure 4.27: Bond force versus concrete cover

Figure 4.28: Failure modes for 20 & 40 mm concrete cover respectively pictures

As mentioned earlier in the literature review in chapter 2 regarding Cairns and Plizzari (1995, 2003) work about the bond theory, the stress field in the transition zone between the steel bar and surrounding concrete follows a cone shape. A greater cover layer can provide better mechanism by dispersing the stress field into a larger zone and hence reduce the stress concentration effect. The second reason is that the greater cover, in particular, the zone far away from the bar, will provide a better constraining effect on the stressed concrete near the bar and hence reduce

the tendency of splitting failure as indicated by Figure 4.28. These are the reasons why the bond performance will be improved with a greater cover. But it is envisaged that the increase in the bond strength is not proportional to the cover thickness and an overly specified cover thickness will not yield best effect from economy perspective. This is why minimum covers are always specified in most concrete design codes, which are often relative to the bar size.

4.5 Summery

Experimental work has been carried out to investigate the effect of steel properties on the bond interaction between reinforcing steel and concrete. The results can be summarized as follows:

- For bars of 8mm diameters the bond in governed by the yield force of the bar as in case of adequate bond length, bars of ultimate force less than the ultimate bond force, i.e. 8mm bars, will yield before pull-out occurs. In other larger bar diameters can provide higher bond in case of adequate bond length.
- Presence of shear links can positively affect the bond strength in reinforced concrete.
- C` bars have less bond strength comparing with C bars with a tendency to fail in pull-out rather than splitting due to the additional longitudinal ribs on the surface of C` bars.
- It was observed that bottom bars, from casting point of view, show better bond performance comparing to top bars.

- Increment in the embedment length can affect positively until the required bond length is approached. After the required bond length is approached, the larger embedment length will have no effect on the bond performance.
- Larger concrete cover can provide better bond performance and decrease the tendency of experiencing a splitting failure.
- The presences of plastic sleeves at both ends of the reinforcing bar allow elevating the splitting failure. Plastic sleeves can be used to reduce the embedment length in case it is larger than the required bond length.

Chapter 5: Comparison between experimental test data & predictions by codes and analytical models

5.1 Introduction

There is no absolutely accurate model to predict an exact value of the bond strength between concrete and reinforcing steel. Codes of practice usually predict failure loads or strengths in a conservative manner. Codes and analytical models do not consider all factors affecting the bond strength. Examples of factors not being considered are steel bar ribs profiles, bar surface conditions, aggregate size and shape and use of concrete mixtures. Some of the previous factors have been studies in the literature but there is a consensus that more systematic work is needed to develop a standard equation for bond strength containing all factors that affect the interaction between concrete and steel bars.

5.2 Comparison amongst various building codes and standards

Pull-out tests results will be compared to the prediction results by using EC2, ACI 318-02, ACI 408-01 and CEB-FIP 1990 using equations mentioned earlier in the literature. All partial factors are applied based on the condition of each test. Table 5.1 shows the tests results along with codes' predictions. Each value for bond strength is normalized by $f_{cm}{}^{2/3}$ and showed in the same cell in table 5.1.

It is obvious from table 5.1 that all bond strength values based on codes are smaller than experimental codes as it is supposed to be so. The reason that experimental values should be greater is that all codes are designed to be conservative and for the worst-case scenario. In case that a tested bar showed a

lower bond strength value than the codes' prediction, this may be due to the fact that the interaction between concrete and reinforcing steel does not develop the required bond that the codified method assumed to be. For instance, there may be pre-existing debonding or local weakness along the interface.

Table 5.1: Comparison of pull-out test results with codes

Specimen	$f_{cm,cube}$ / f_{ctm} / f_{cm}	Experimental bond strength & $f_{b,exp}$ (N/mm^2)/ f_{cm} `$^{2/3}$		EC2 (N/mm^2)		ACI 318-02 (N/mm^2)		ACI 408-01 (N/mm^2)		CEB-FIP model Code (1990)	
Bar Size											
PSC'-301040-8	19.4/1.2/15.5	4.26	0.70	2.67	0.44	3.40	0.56	2.41	0.39	1.62	0.27
PSC'-301040-10	19.4/1.2/15.5	5.30	0.87	2.67	0.44	3.40	0.56	2.47	0.40	1.57	0.26
PSC'-301040-12	19.4/1.2/15.5	4.82	0.79	2.13	0.35	2.95	0.48	2.59	0.42	1.61	0.26
PSC'-301020-8-S	15.9/0.8/12.7	5.10	0.95	2.13	0.40	3.08	0.58	2.40	0.45	1.42	0.27
PSC'-301020-10-S	19/1.1/15.2	6.12	1.02	2.16	0.36	3.37	0.56	2.62	0.43	1.54	0.26
PSC'-301020-12-S	18.5/1.1/14.8	6.36	1.07	2.00	0.34	2.88	0.49	2.76	0.47	1.55	0.26
Concrete Cover											
PSC'-251040-10	22.6/1.4/18.1	4.96	0.73	2.94	0.43	3.68	0.54	2.81	0.42	1.77	0.26
PSC'-251020-10	25.6/1.6/20.6	3.73	0.51	2.64	0.36	3.92	0.53	2.82	0.38	1.77	0.24

Table 5.1 continued

PSC'-301020-10	22.6/1.4/18.1	3.58	0.53	2.41	0.36	3.68	0.54	2.49	0.37	1.77	0.26
PSC'-301020-10	22.6/1.4/18.1	3.24	0.48	2.41	0.36	3.68	0.54	2.49	0.37	1.77	0.26
PSC'-301040-10	19.4/1.2/15.5	5.31	0.87	2.67	0.44	3.40	0.56	2.47	0.40	1.57	0.26
Bar Location											
PSC'-301020-10 top	22.6/1.4/18.1	2.78	0.41	2.41	0.36	3.68	0.54	2.49	0.37	1.77	0.26
PSC'-301020-10 top	22.6/1.4/18.1	2.55	0.38	2.41	0.36	3.68	0.54	2.49	0.37	1.77	0.26
PSC'-301020-10 Bottom	22.6/1.4/18.1	3.24	0.48	2.41	0.36	3.68	0.54	2.49	0.37	1.77	0.26
PSC'-301020-10 Bottom	22.6/1.4/18.1	3.58	0.53	2.41	0.36	3.68	0.54	2.49	0.37	1.77	0.26
PSB-251020-10 top	25.6/1.6/20.6	3.72	0.51	2.64	0.36	3.92	0.53	2.82	0.38	2.12	0.29
PSB-251020-10 Bottom	25.6/1.6/20.6	4.02	0.55	2.64	0.36	3.92	0.53	2.82	0.38	2.12	.029
PSC-251020-10 top	27/1.7/22	5.46	0.71	2.78	0.36	4.05	0.53	2.87	0.37	2.23	0.29
PSC-251020-10 bottom	27/1.7/22	5.62	0.73	2.78	0.36	4.05	0.53	2.87	0.37	2.23	.029
Bar Type											
PSB-251020-10	25.6/1.6/20.6	3.72	0.51	2.64	0.36	3.92	0.53	2.82	0.38	2.12	0.29
PSC'-251020-10	25.6/1.6/20.6	3.72	0.51	2.64	0.36	3.92	0.53	2.82	0.38	1.96	0.27

Table 5.1 continued

PSC-151020-10	20.4/1.2/16.3	4.76	0.75	2.26	0.36	3.49	0.55	3.60	.057	1.77	0.28
PSC'-151020-10	28.1/1.8/23.1	5.04	0.63	2.88	0.36	4.15	0.52	3.92	0.49	2.14	0.27
Embedment Length											
PSC'-151020-10	23.2/1.4/18.5	3.79	0.55	2.46	0.36	3.72	0.54	3.71	0.54	1.80	0.26
PSC'-251020-10	23.2/1.4/18.5	5.28	0.77	2.46	0.36	3.72	0.54	2.75	0.40	1.80	0.26
PSC'-351020-10	23.2/1.4/18.5	3.91	0.57	2.46	0.36	3.72	.054	2.34	0.34	1.80	.026
PSC'-201020-10	25.6/1.6/20.6	6.66	0.90	2.64	0.36	3.92	0.53	3.19	0.43	1.96	0.27
PSC'-251020-10	22.6/1.4/18.1	5.12	0.76	2.41	0.36	3.68	0.54	2.82	0.42	1.77	0.26
Shear Link											
PSC'-251520-10	29.2/1.9/25	4.33	0.52	2.98	0.36	4.32	0.52	2.96	0.35	2.27	0.27
PSC'-251520-10	23.3/1.5/23.3	5.28	0.66	2.96	0.37	4.17	0.52	N.A restriction ≥ 4		2.92	0.37
PSC'-251520-10	31/2/25.7	6.32	0.74	3.47	0.41	4.38	0.51	6.23	0.73	3.02	0.35
PSC-251520-10	26.2/1.7/21.2	3.62	0.48	2.70	0.36	3.06	0.41	2.84	0.38	2.01	0.27
PSC-251520-10	26.6/1.7/21.6	5.09	0.67	3.29	0.43	4.02	0.53	N.A restriction ≥ 4		2.75	0.36
PSC-251520-10	27/1.7/22	5.61	0.73	3.10	0.40	4.05	0.53	5.82	0.76	2.69	0.35

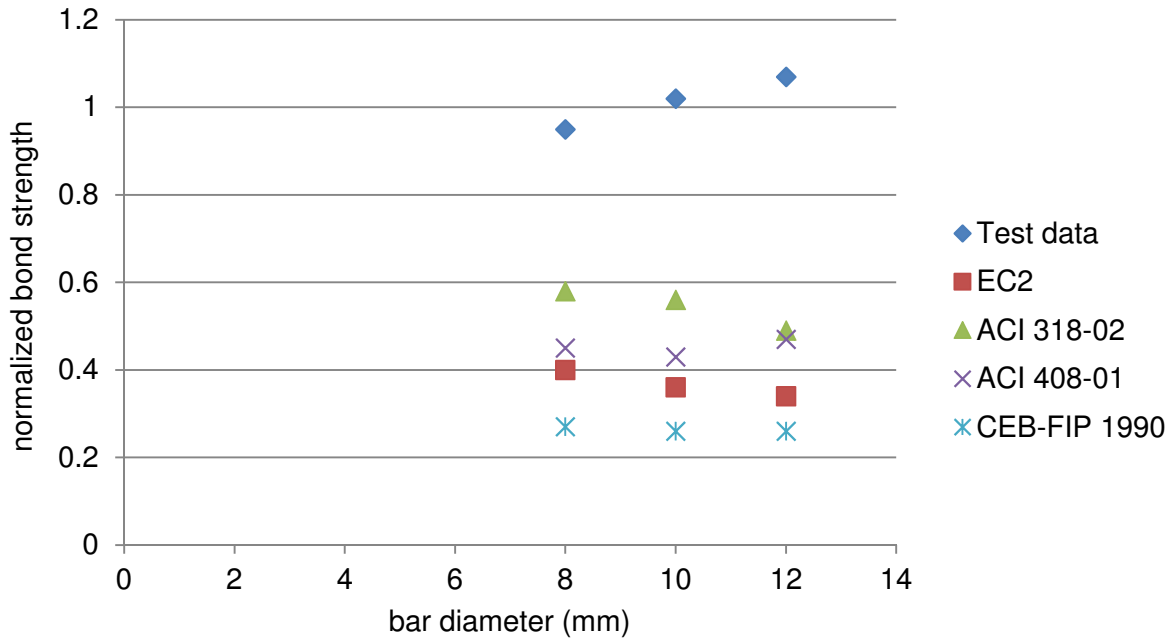

Figure 5.1: Comparison between test data and codified predictions for different bar diameters

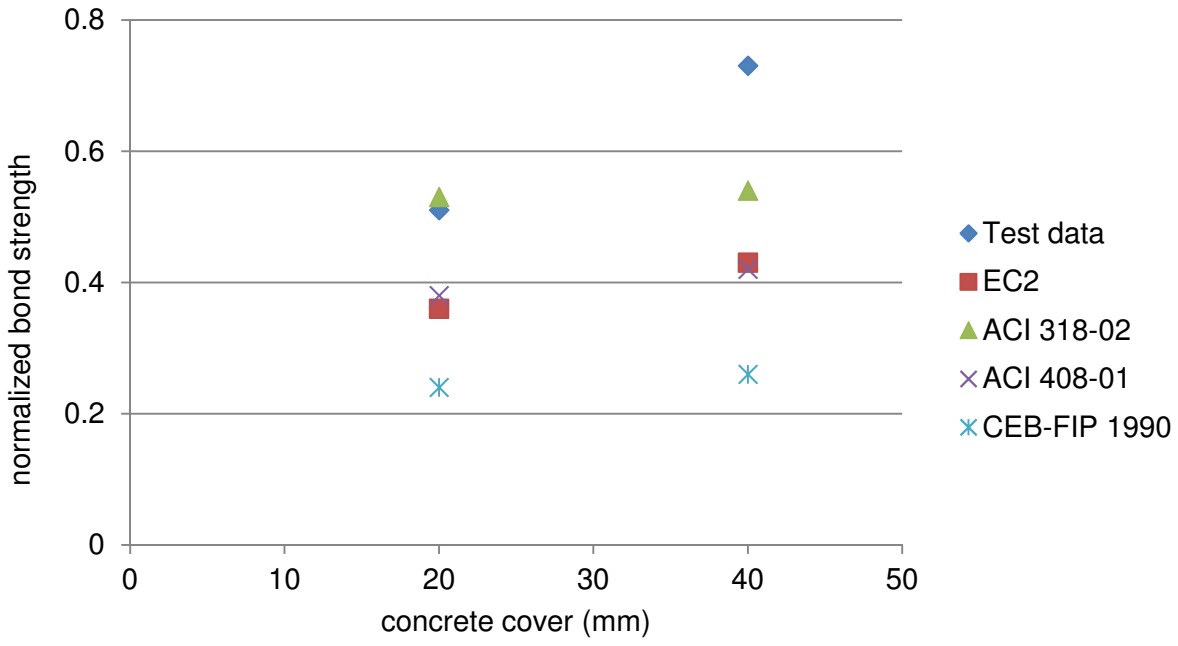

Figure 5.2: Comparison between test data and codified predictions for different concrete covers

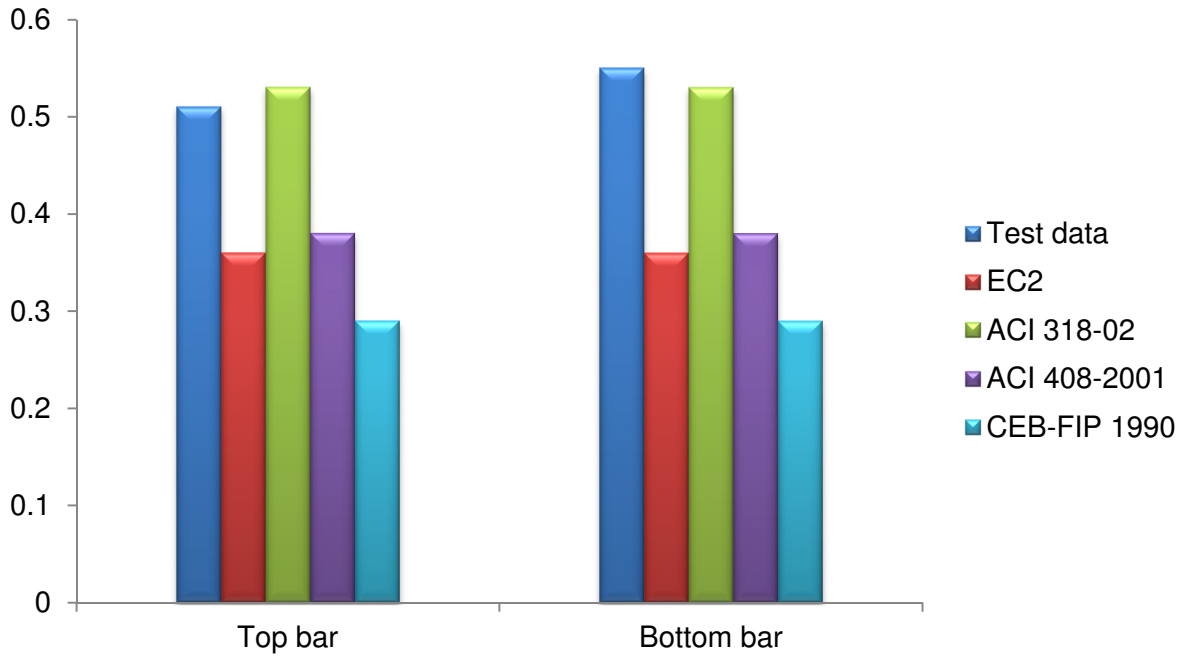

Figure 5.3: Comparison between test data and codified predictions for different bar locations

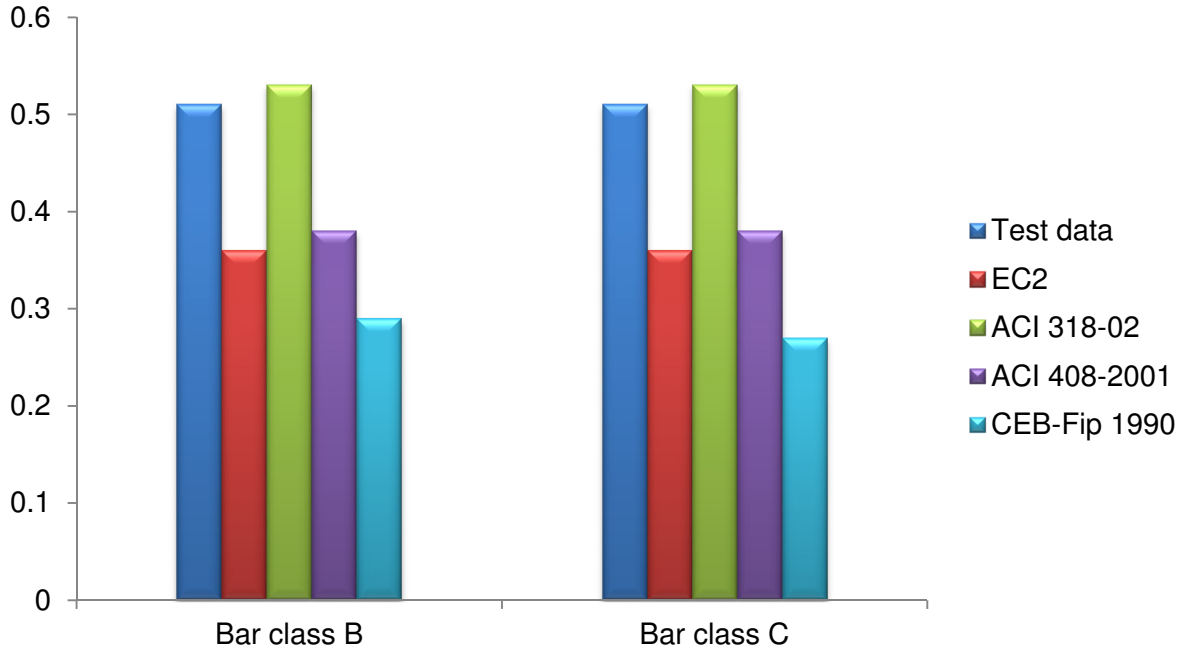

Figure 5.4: Comparison between test data and codified predictions for different classes

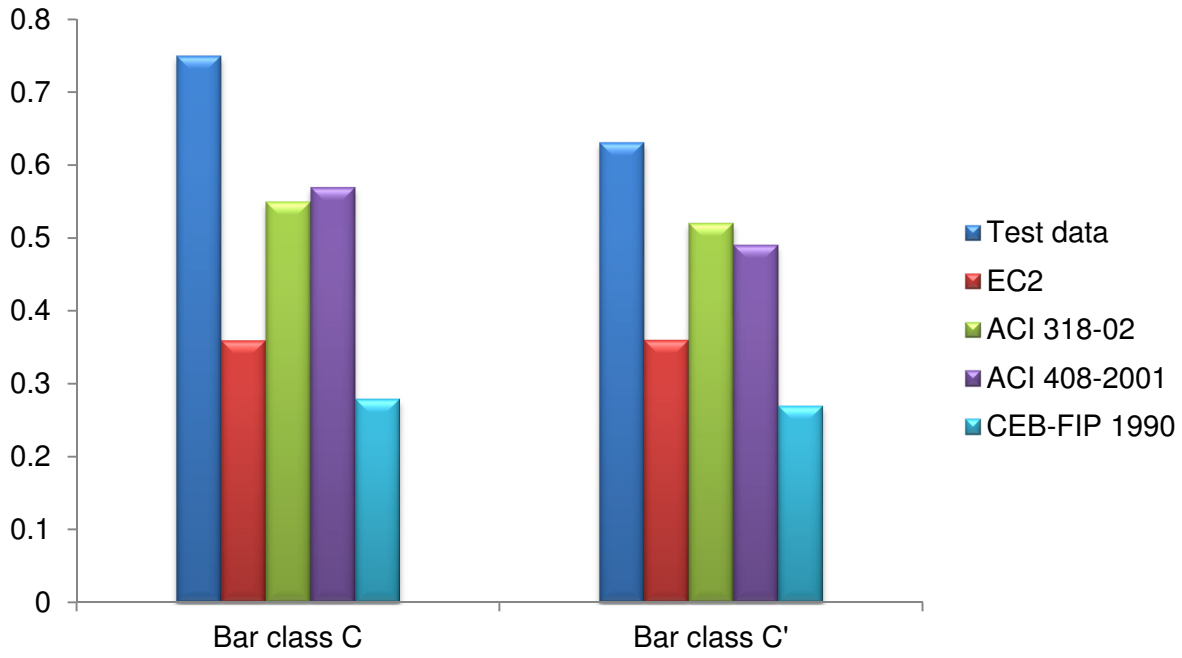

Figure 5.5: Comparison between test data and codified predictions for different bar deformation patterns

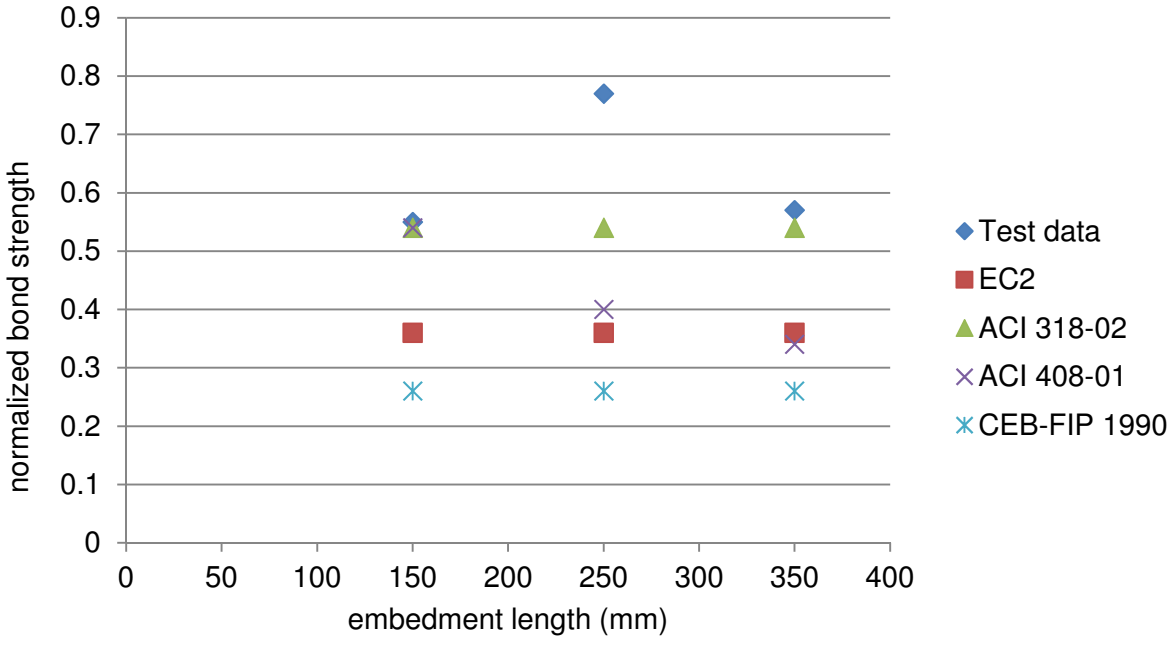

Figure 5.6: Comparison between test data and codified predictions for different embedment lengths

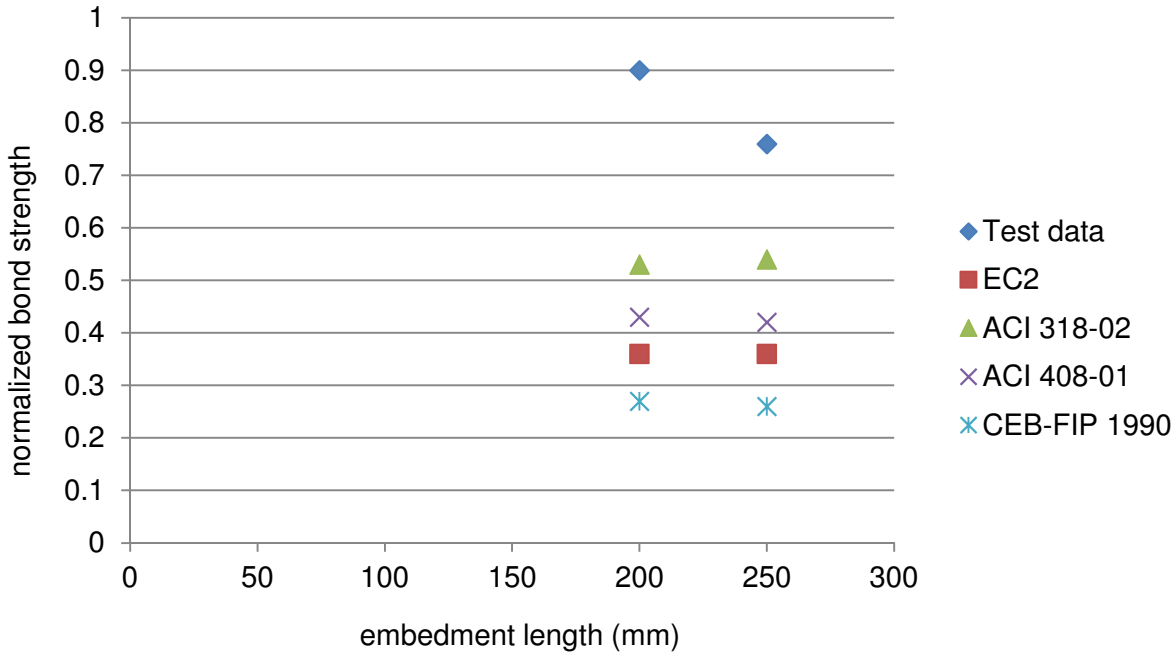

Figure 5.7: Comparison between test data and codes for different embedment lengths

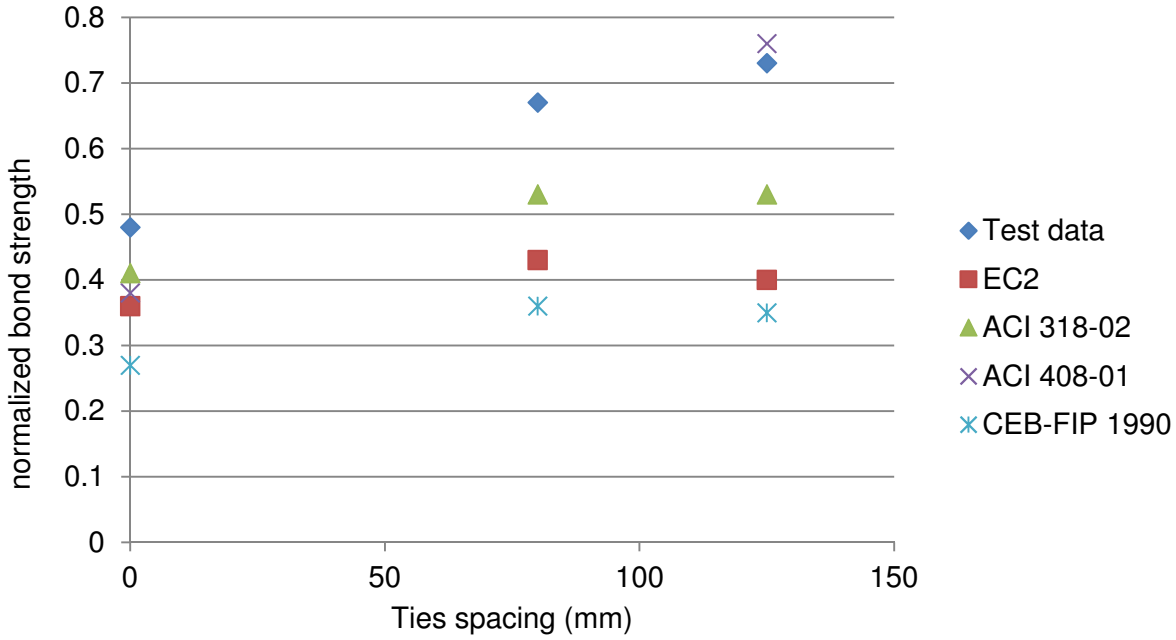

Figure 5.8: Comparison between test data and codes for different values of confinement spacing

5.3 Comparison with analytical models

All pull-out test results are compared with the four models mentioned in section 1.1.9.2 of the literature review. Same as in Table 5.1, all bond strength values are normalized by $f_{cm}{}^{`2/3}$ in table 5.2. Most of the analytical models limit the applicability of their expressions as they have been derived based on certain test data. For that reason, few cases in this study cannot be predicted using the models equations due to limitations. All the expressions for limiting the applicability of the models have been mentioned in the literature along with the bond strength or development length equation.

Each model is represented by its own alphabetical term as follows:

- ORA: Orangun, Jirsa, Breen (1975, 1977)
- DAR: Darwin et al. (1996a)
- ZUD: Zuo & Darwin (1998, 2000)
- ESRA: Esfahani & Rangan (1998a, b)

Table 5.2: Comparison of pull-out test results with models

Specimen	$f_{ck,cube}$ / f_{ctm} / f_{ck}	Experimental bond strength $f_{b,exp}$ (N/mm²)/ normalized strength		Orangun, Jirsa, Breen (1975,1977)		Darwin et al. (1996a)		Zuo & Darwin (1998,2000)		Esfahani & Rangan (1998a,b)	
Bar Size											
PSC'-301040-8	19.4/1.2/15.5	4.26	0.70	1.61	0.26	2.38	0.39	2.39	0.39	3.97	0.65
PSC'-301040-10	19.4/1.2/15.5	5.30	0.87	1.56	0.26	2.40	0.39	2.44	0.40	3.68	0.60
PSC'-301040-12	19.4/1.2/15.5	4.82	0.79	1.57	0.26	2.48	0.41	2.56	0.42	3.49	0.57
PSC'-301020-8-S	15.9/0.8/12.7	5.10	0.95	1.54	0.29	2.35	0.44	2.38	0.44	2.86	0.53
PSC'-301020-10-S	19/1.1/15.2	6.12	1.02	1.66	0.28	2.52	0.42	2.59	0.43	2.90	0.48
PSC'-301020-12-S	18.5/1.1/14.8	6.36	1.07	1.66	0.28	2.63	0.44	2.74	0.46	2.79	0.47
Concrete Cover											
PSC'-251040-10	22.6/1.4/18.1	4.96	0.73	1.81	0.27	2.71	0.40	2.78	0.41	4.15	0.61
PSC'-251020-10	25.6/1.6/20.6	3.73	0.51	1.93	0.26	2.72	0.37	2.79	0.38	3.19	0.43

Table 5.2 continued

PSC'-301020-10	22.6/1.4/18.1	3.58	0.53	1.69	0.25	2.42	0.36	2.47	0.37	2.85	0.42
PSC'-301020-10	22.6/1.4/18.1	3.24	0.48	1.69	0.25	2.42	0.36	2.47	0.37	2.85	0.42
PSC'-301040-10	19.4/1.2/15.5	5.31	0.87	1.56	0.26	2.49	0.41	2.44	0.40	3.85	0.63
Bar Location											
PSC'-301020-10	22.6/1.4/18.1	2.78	0.41	1.69	0.25	2.42	0.36	2.47	0.37	2.85	0.42
PSC'-301020-10	22.6/1.4/18.1	2.55	0.38	1.69	0.25	2.42	0.36	2.47	0.37	2.85	0.42
PSC'-301020-10	22.6/1.4/18.1	3.24	0.48	1.69	0.25	2.42	0.36	2.47	0.37	2.85	0.42
PSC'-301020-10	22.6/1.4/18.1	3.58	0.53	1.69	0.25	2.42	0.36	2.47	0.37	2.85	0.42
PSB-251020-10	25.6/1.6/20.6	3.72	0.51	1.93	0.26	2.72	0.37	2.79	0.38	3.19	0.43
PSB-251020-10	25.6/1.6/20.6	4.02	0.55	1.93	0.26	2.72	0.37	2.79	0.38	3.19	0.43
PSC-251020-10	27/1.7/22	5.46	0.71	1.99	0.26	2.77	0.36	2.84	0.37	3.25	0.42
PSC-251020-10	27/1.7/22	5.62	0.73	1.99	0.26	2.77	0.36	2.84	0.37	3.25	0.42
Bar Type											
PSB-251020-10	25.6/1.6/20.6	3.72	0.51	1.93	0.26	2.72	0.37	2.79	0.38	3.19	0.43
PSC'-251020-10	25.6/1.6/20.6	3.72	0.51	1.93	0.26	2.72	0.37	2.79	0.38	3.19	0.43

Table 5.2 continued

PSC-151020-10	20.4/1.2/16.3	4.76	0.75	2.16	0.34	3.40	0.54	3.55	0.56	3.43	0.54
PSC'-151020-10	28.1/1.8/23.1	5.04	0.63	2.57	0.32	3.71	0.47	3.87	0.49	3.93	0.49
Embedment Length											
PSC'-151020-10	23.2/1.4/18.5	3.79	0.55	2.30	0.34	3.51	0.51	3.66	0.53	3.61	0.53
PSC'-251020-10	23.2/1.4/18.5	5.28	0.77	1.83	0.27	2.65	0.39	2.72	0.40	3.09	0.45
PSC'-351020-10	23.2/1.4/18.5	3.91	0.57	1.71	0.25	2.28	0.33	2.31	0.34	2.68	0.39
PSC'-201020-10	25.6/1.6/20.6	6.66	0.90	2.12	0.29	3.05	0.41	3.16	0.43	3.46	0.47
PSC'-251020-10	22.6/1.4/18.1	5.12	0.76	1.81	0.27	2.64	0.39	2.70	0.40	3.07	0.45
Shear Link											
PSC'-251520-10	29.2/1.9/25	4.33	0.52	2.12	0.25	2.86	0.34	2.93	0.35	3.38	0.40
PSC'-251520-10	23.3/1.5/23.3	5.28	0.66	N.A restriction ≥ 2.5		5.28	0.66	N.A restriction ≥ 4		4.45	0.56
PSC'-251520-10	31/2/25.7	6.32	0.74	N.A restriction ≥ 2.5		4.16	0.49	N.A restriction ≥ 4		4.58	0.54
PSC-251520-10	26.2/1.7/21.2	3.62	0.48	1.96	0.26	2.74	0.37	2.81	0.37	3.22	0.43
PSC-251520-10	26.6/1.7/21.6	5.09	0.67	N.A restriction ≥ 2.5			0.68	N.A restriction ≥ 4		4.35	0.57
PSC-251520-10	27/1.7/22	5.61	0.73	N.A restriction ≥ 2.5		4.01—0.52		N.A restriction ≥ 4		4.38	0.57

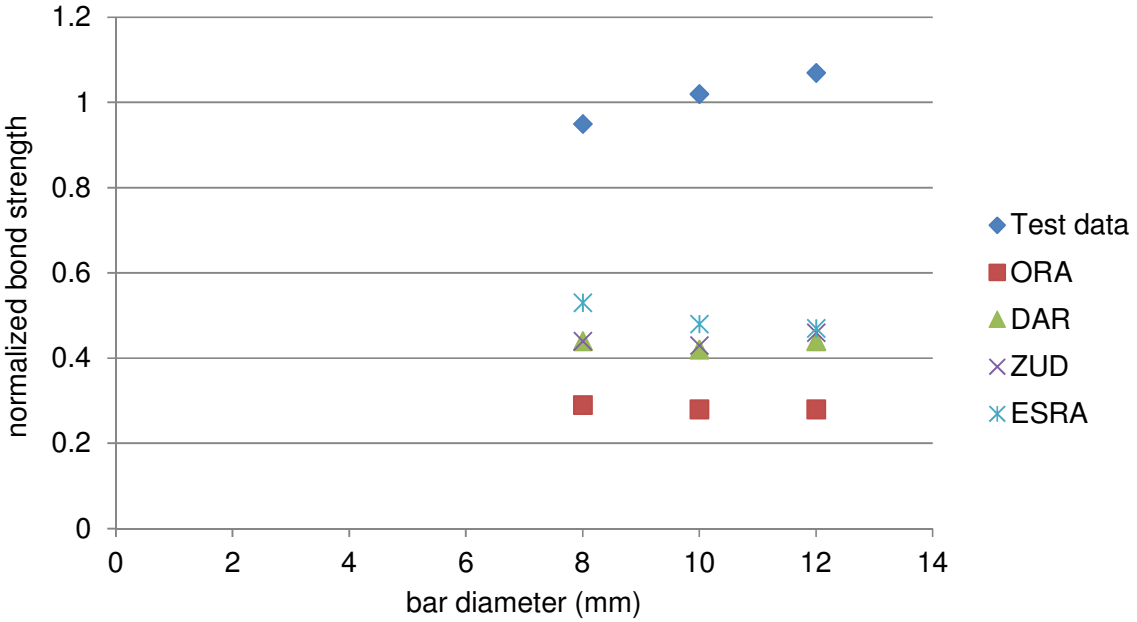

Figure 5.9: Comparison between test data and analytical models as variable is bar diameter

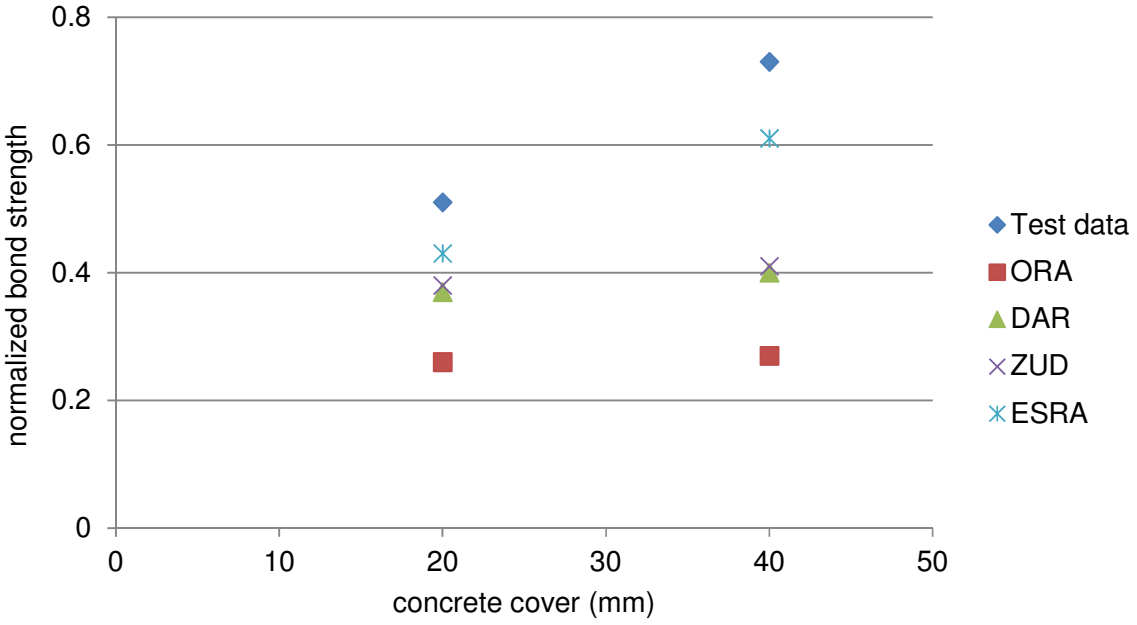

Figure 5.10: Comparison between test data and analytical models as variable is concrete cover

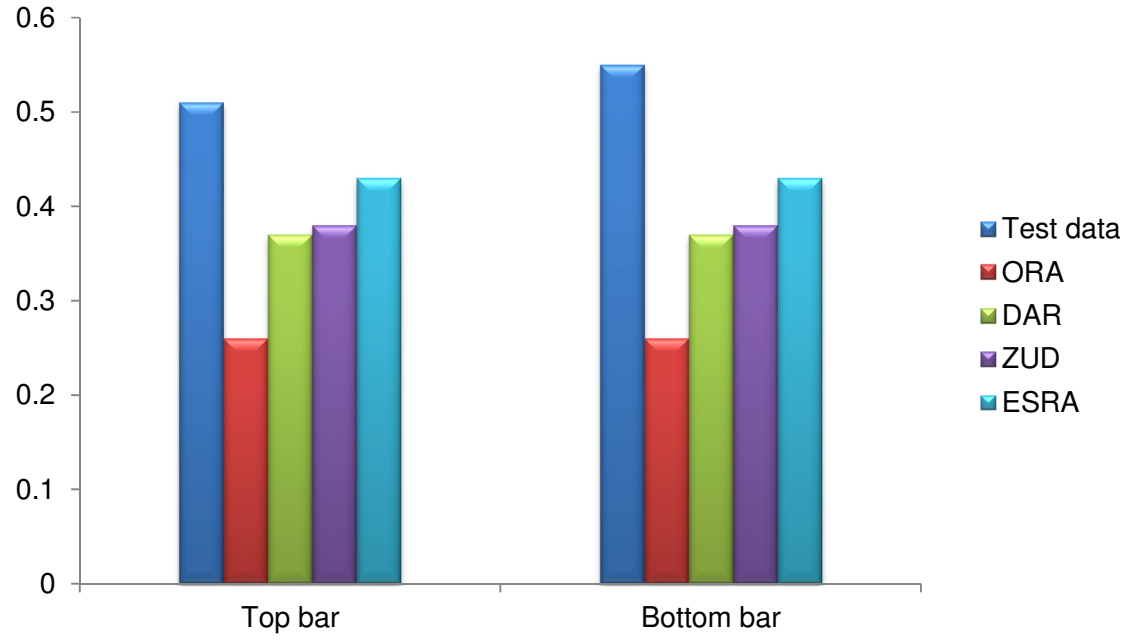

Figure 5.11: Comparison between test data and analytical models as variable is bar location

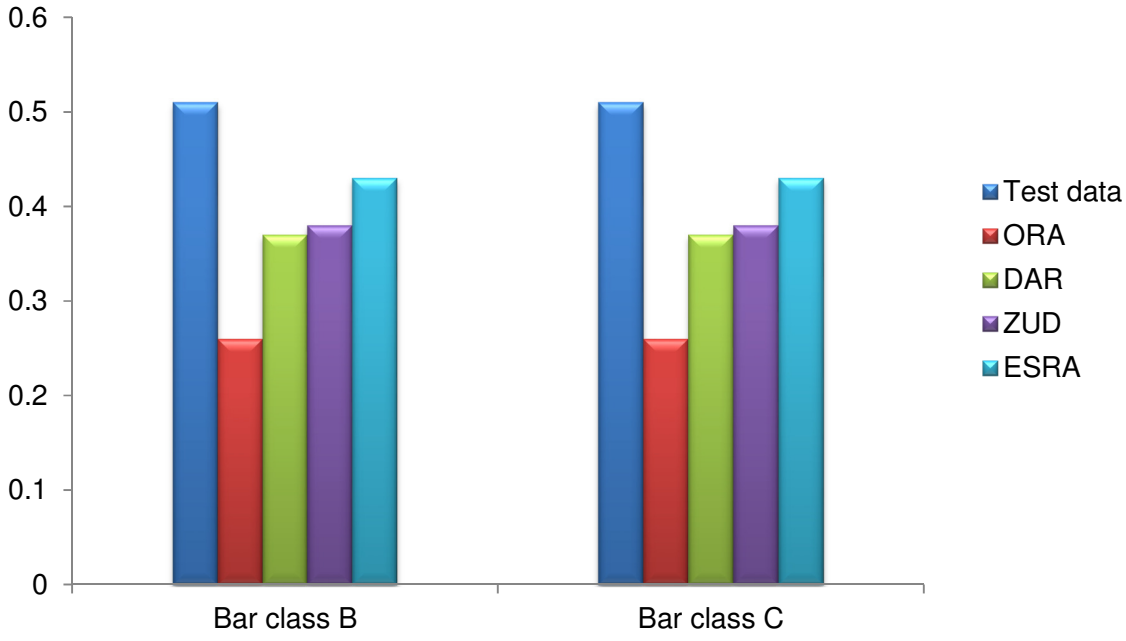

Figure 5.12: Comparison between test data and analytical models as variable is bar grade

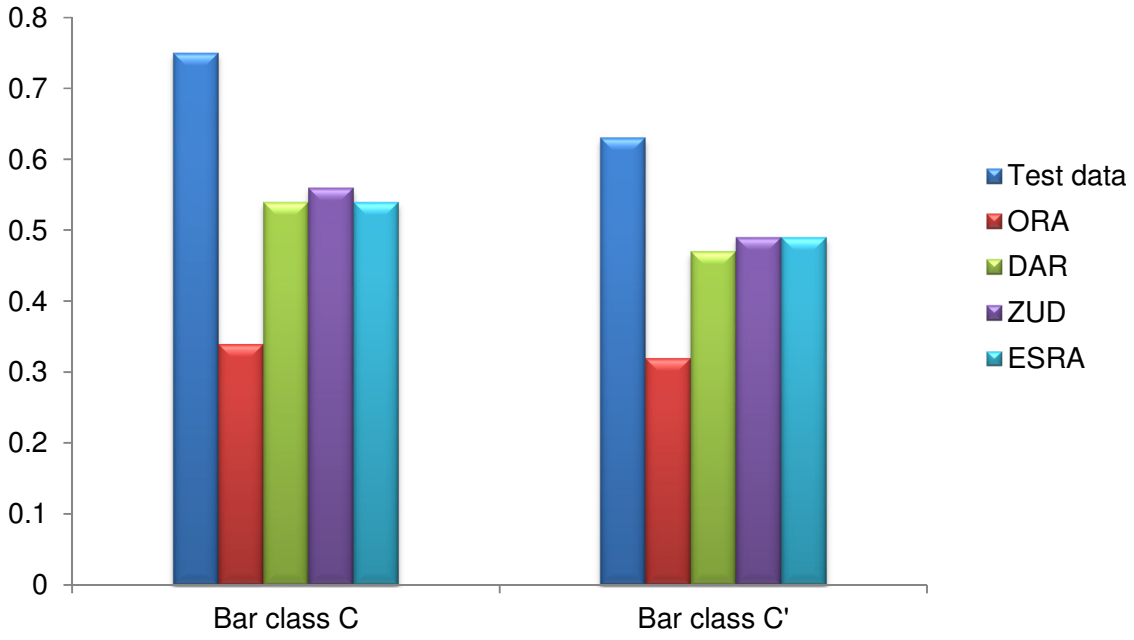

Figure 5.13: Comparison between test data and analytical models as variable is bar grade

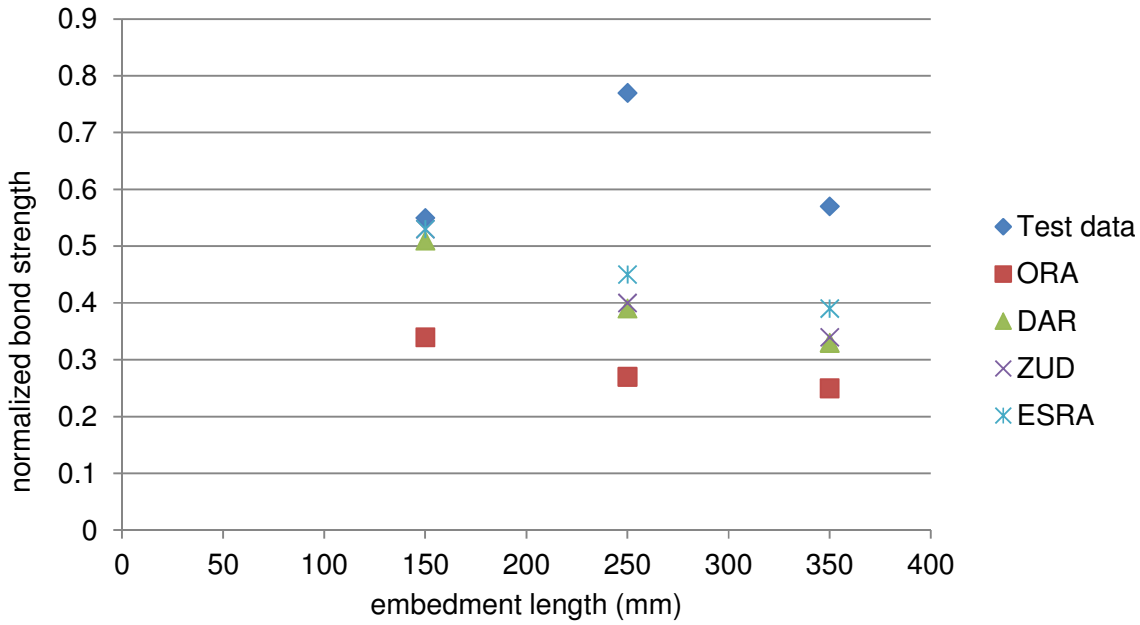

Figure 5.14: Comparison between test data and analytical models as variable is embedment length

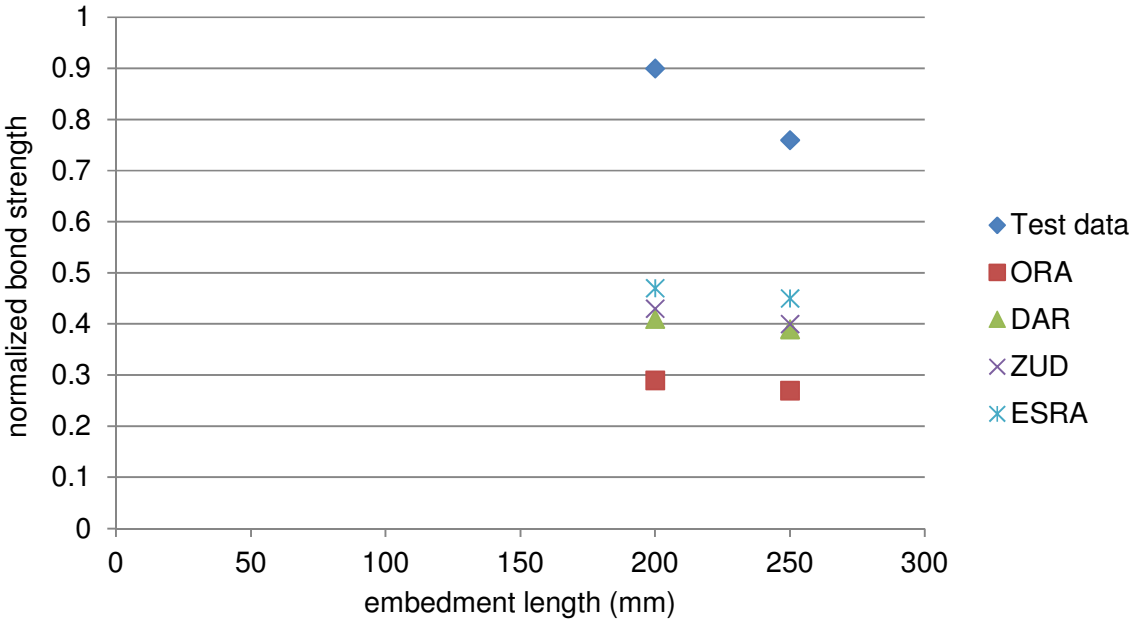

Figure 5.15: Comparison between test data and analytical models as variable is embedment length

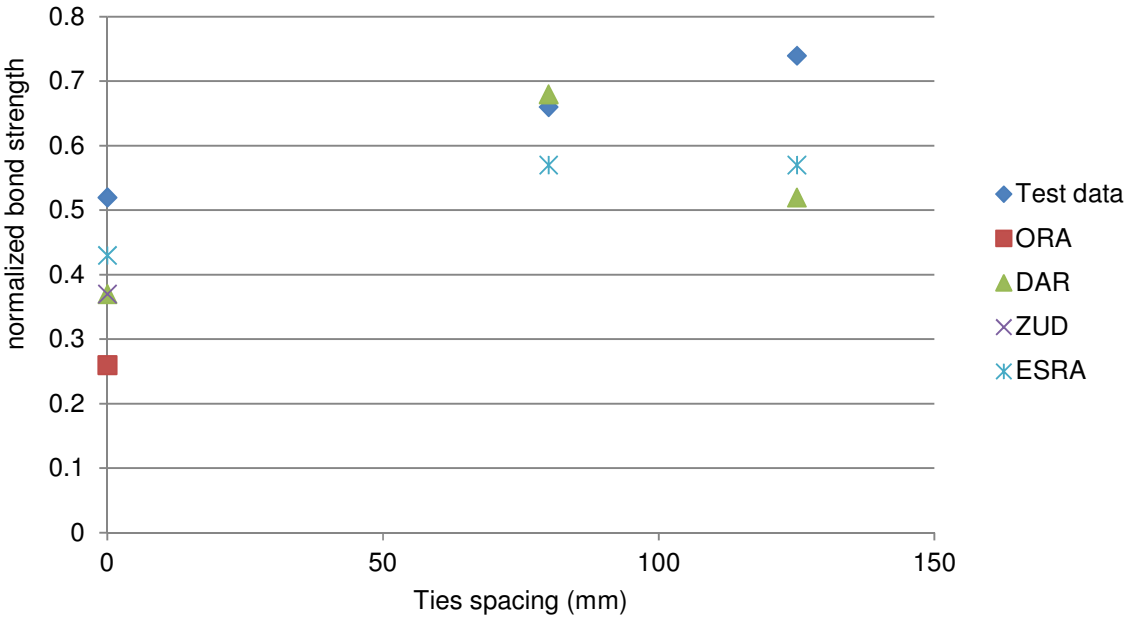

Figure 5.16: Comparison between test data and analytical models as variable is concrete confinement spacing

5.4 Summery

It is noticed from all graphs in this chapter that most of the laboratory tests that have been conducted for the aim of this research are higher than all the predictions. That applies to the predicted bond strength using equations from both codes and the considered models from the literature.

In other words, the results from pull-out tests which have been conducted have definitely achieved bond strength values that are recommended by standards and codes or published models from the literature.

As a result of comparison, it is clear that the pull-outs tests' results match with the codes from different countries and the models which have been developed by different researchers. That can be considered a good support for all the extracted arguments and analysis that are made on the basis of the work done in this research.

It can be see that based on the results in this chapter the standard reinforcement classes of B & C meet the standards in terms of the bond strength. It can also be seen that the new type of reinforcing steel Celsa max (C`) has met the standards for the bond strength. That proves the success of the new rib patter which is introduced in the Celsa max bars in developing good bond interaction between the reinforcement and the surrounding concrete.

Chapter 6: Ductility Tests and Results

6.1 Introduction

Tests were conducted for simply supported reinforced concrete beams subjected to a concentrated point load at the mid span to study the ductility behaviour of RC beams reinforced with two types of reinforcement. The first set of beams consists of 12 specimens reinforced with single bars and shear links to examine the behaviour of two steel classes C and C' and two shear links spacing 100 and 150 mm. The tested beams are categorised in four groups, each group consists of 3 identical samples. The second sets of test consist of 13 beams to examine two different steel classes C` and A in the form of the mesh reinforcement with various main bars diameters.

6.2 Steel bars confined with shear links

All beams are designed with the same size, i.e., 150 mm wide, 225 mm deep and 1500 mm long. Longitudinal steel reinforcement arrangement was identical in all beams as shown in Figure 6.1, i.e. five 10 mm bars were utilized to reinforce beams, three at the bottom and two at the top. Shear links were 8 mm Class A bars with the spacing of either 100 or 150 mm with the concrete cover of 20 mm to the bottom face of specimen. Beams were cast on a vibration table in two layers and vibrated after placing each. The new cast beam was covered with polythene sheeting, de-moulded after 48 hours and cured in a curing tank until being removed for testing.

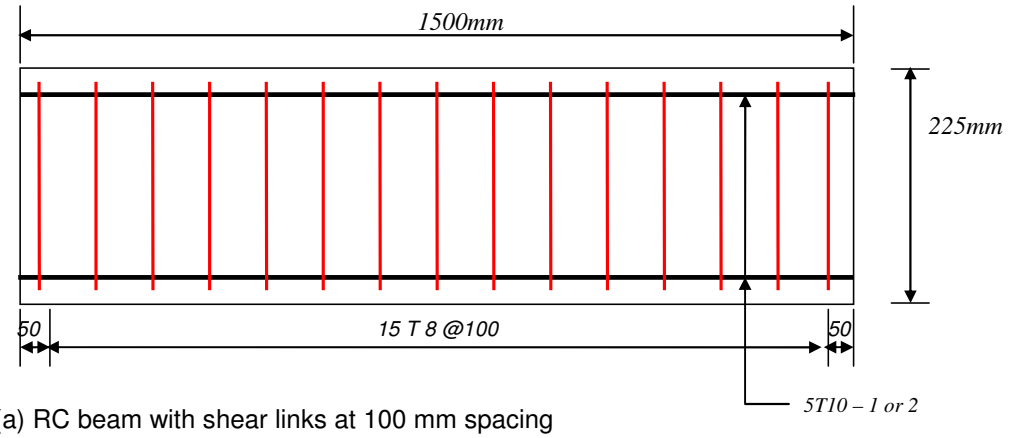

(a) RC beam with shear links at 100 mm spacing

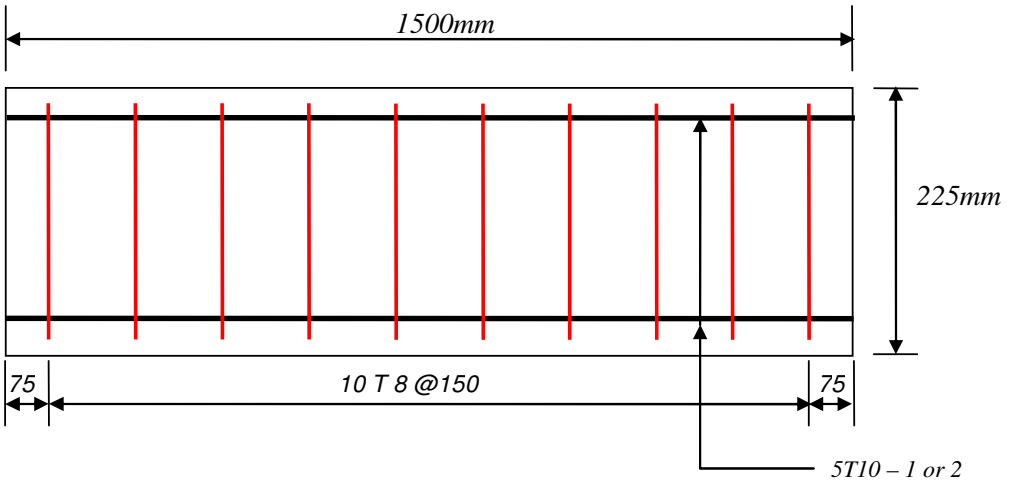

(b) RC beam shear links at 150 mm spacing

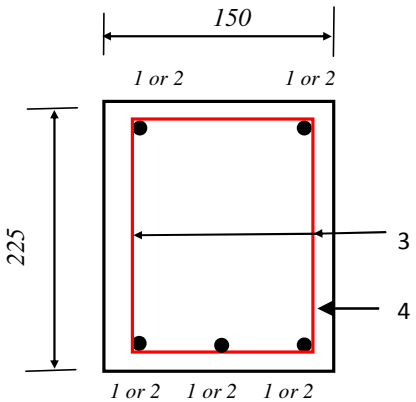

(c) Typical cross section

1: Bar C

2: Bar C'

3: Class A steel used for shear links

Figure 6.1: Test beam details

Table 6.1: Beam details and reinforcement

Test	Number of tested beams	Longitudinal steel type & size	Shear link type & size	Shear link spacing (mm)	Number of shear links in each sample
DC-100	3	Bar C, 10 mm	Class A, 8 mm	100	15
DC-150	3	Bar C, 10 mm	Class A, 8 mm	150	10
DC`-100	3	Bar C', 10 mm	Class A, 8 mm	100	15
DC`-150	3	Bar C', 10 mm	Class A, 8 mm	150	10

An alpha numeric designation was used to identify each beam sample in the test. The first letter D indicates the ductility test, followed by another alphabet C or C' indicating the bar type. Two numbers follow the alphabets indicating the shear link spacing and the number of the concrete beam in each group. Beam details and reinforcement are shown in Table 6.1.

6.2.1 Materials

The steel which was used this experiment was tested and their properties are reported in chapter 3. Concrete may have different strength depending on the curing age at the testing day. When casting each group of RC beams, the

following concrete specimens were also casted: nine cubes, nine cylinders and eight prisms in order to determine the compressive strength, cylinder splitting strength and the modulus of rupture, respectively, on the testing day. Properties of the concrete standard specimens are presented in Table 6.2.

Table 6.2: Concrete control specimens results

Beam group	**Test beam**	**Cube strength $f_{m,cube}$ (N/mm^2)**	**Equivalent cylinder strength f_{ck} (N/mm^2)**	**Cylinder splitting strength (N/mm^2)**	**Modulus of rupture (N/mm^2)**
DC`-100	DC-100-1	33.2	27.3	3.4	4.8
	DC-100-2	36.0	29.3	3.0	4.6
	DC-100-3	36.4	29.6	2.8	4.6
DC`-150	DC-150-1	40.3	32.1	3.3	4.3
	DC-150-2	39.5	31.6	3.4	4.6
	DC-150-3	37.5	30.3	3.3	4.7
DC-100	DC'-100-1	33.2	27.3	2.7	4.3
	DC'-100-2	37.9	30.6	3.0	4.7
	DC'-100-3	39.9	31.8	3.5	4.5
DC-150	DC'-150-1	44.3	34.6	3.1	4.5
	DC'-150-2	45.3	35.3	3.4	4.5
	DC'-150-3	45.3	35.3	3.8	4.7

6.2.2 Test setup and instrumentation

Instruments are illustrated as in Figure 6.4 and their respective uses are explained as follows:

- Mand testing machine: to apply and record the loading.
- Mechanical dial gauge: to measure the beam deflection at the mid-span loading point.
- LVDTs (linear variable differential transducer): sensors to measure the beam deflection at mid & quarter-spans and send it to be recorded in a data logger.
- Micrometre rotation gauge: measure the beam rotation at each support.
- Mechanical Demec Gauge: Figure 6.2 shows a 50 mm length gauge that was used to measure the concrete strains. Four measurements were taken in the compression zone, i.e., 20 mm from the beam's top surface and four measurements at the level of bottom reinforcement, i.e., 33 mm from the beam's bottom surface.
- Crack comparator: to measure crack widths at every load stage, Figure 6.3 shows a clear photo for the crack comparator.
- Load cell: to detect the applied load and send it to a data logger to be recorded.

LVDTs and load cell, each connected to a data logger, were utilized to measure the movement and load simultaneously.

Figure 6.2: 50 mm length Demec gauge for measuring concrete strain

Figure 6.3: Crack comparator for measuring cracks widths during tests

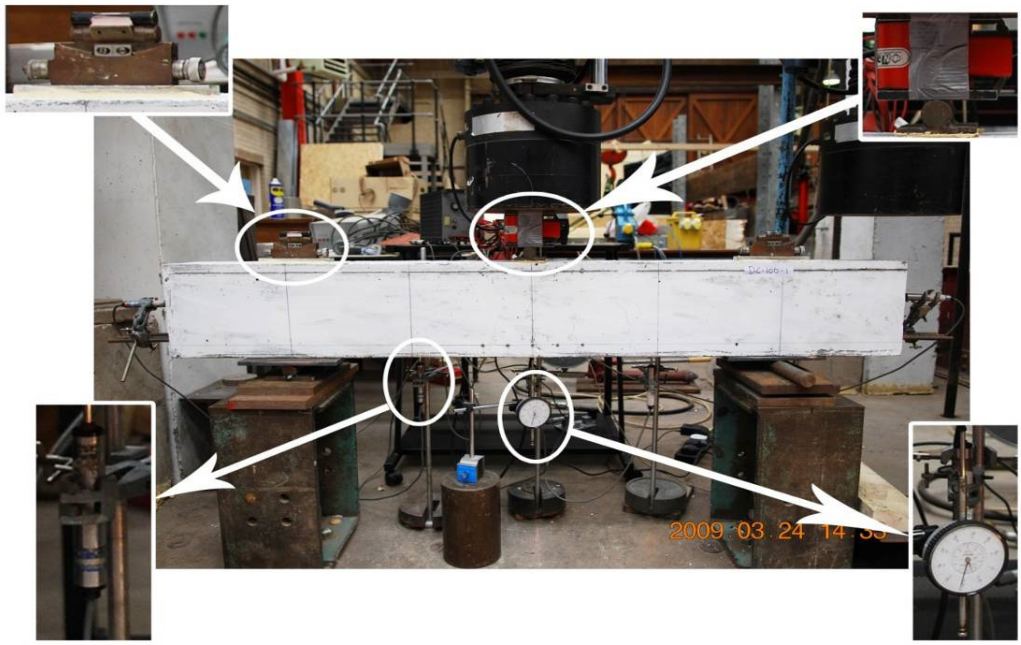

Figure 6.4: Testing instruments

6.2.3 Testing method

All beams were subjected to a central concentrated load as shown in Figure 6.5. Supports did not provide any fixity from friction. Thus, the beams could be analysed as simply-supported beams. All beams were supported over a span of 1000 mm. A Mand Hydraulic Jack with load cell connected was used to load the specimens through a 100mm wide steel plate. After taking initial readings of all gauges, load was applied under load control mode with increment of 10 KN until reaching a value of 40 KN where an increment of 5 KN was

applied instead. Once the applied load approached the yield load, the displacement control loading mode was employed with the deflection increments of 2.0, 3.0, 5.0 and 10.0 mm, respectively. The deflection increments were continued past the maximum load until either the tensile steel fractured or the load decreased to about 40-60 % of the maximum load. Deflection and gauge readings were taken at each increment. After the load reached 40 KN, both callipers and Demec readings were taken. Prior to Demec gauge reaching its capacity, only callipers reading was taken subsequently and was continued until the test ended. Deflection data were collected from three locations, i.e. mid & quarter-span points using LVDTs. A dial gauge was placed at the mid-span point as well to verify the reading from one of the LVDTs.

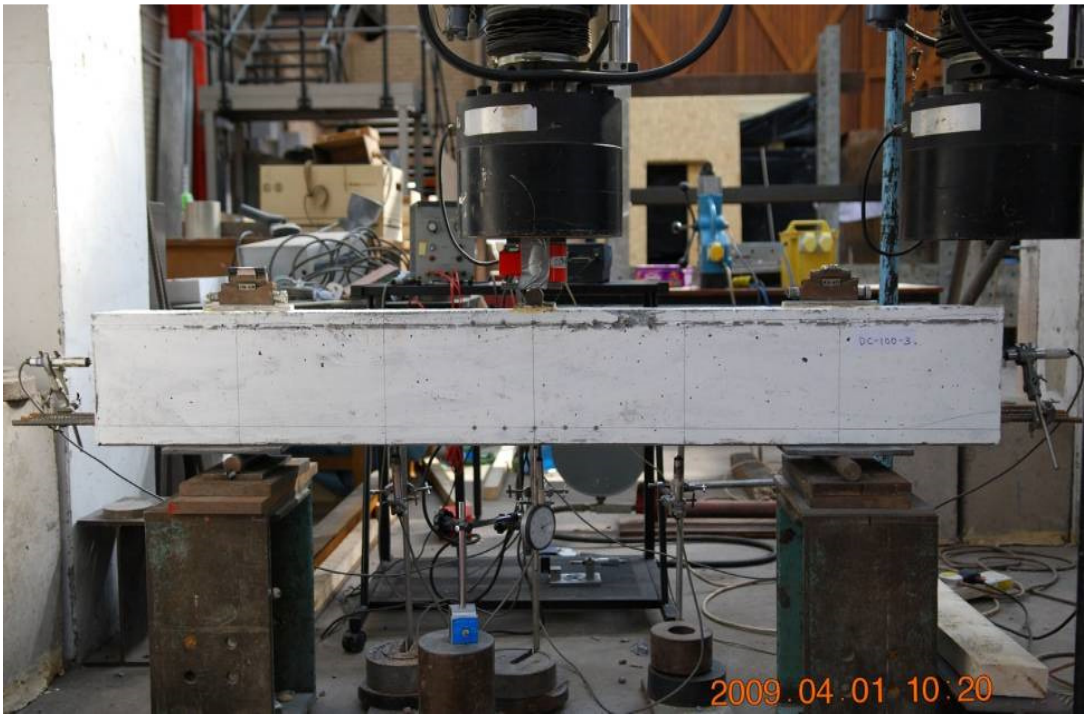

Figure 6.5: Ductility testing

6.2.4 Results and discussion

6.2.4.1 General Behaviour

Load-deflection curves for each group of beams are presented in figures 6.6 - 6.9. Results of the maximum deflection, yield & ultimate loads and the maximum rotations are summarized in Table 6.3. It has been found that, although the difference was insignificant, most DC-100 and DC-150 specimens achieved slightly higher ultimate load than their respective counterparts, and the excesses are 14% and 3%, respectively. This is because bar C has a high proof stress and ultimate strength than bar C`.

The onset and the propagation of cracks were recorded at each loading increment. Figures 6.10 -13 present photos for cracks distribution at different loading levels for each type of reinforcement and shear links spacing. Yield loads were between 91 and 100 KN and the ultimate load reached the range of 99 to 121 KN. Continuingly loading all beams beyond the ultimate load resulted in various failure modes: DC'-100-1, DC'-100-3, DC-150-1 and DC-150-3 failed by fracturing all their tension reinforcement bars while others failed with bars deformed extensively. DC'-150 beams exhibited noticeable shear failure feature evidenced by the inclined critical cracks. Failing modes are shown in Figures 6.14-17.

Ultimate yield ratio, i.e. ultimate load / yield load, as presented in Table 6.3, was in the range of 1.05 to 1.14 for all specimens except DC'-100-1, DC'-100-2 and DC'-100-3 being 1.21, 1.17, 1.17, respectively.

Table 6.3 also present the maximum deflection at the mid-span point and maximum rotation when the bar fractured or loading dropped to 40% of its ultimate value. The total rotation experienced at the mid-span point is calculated by the mid-span deflection divided by a quarter of the beam span. The DC'-150 group had the smallest rotation capacity, which was attributed to its shear-related failure nature. All other specimens had achieved a rotational capacity above 0.16 rad, i.e. the ratio of the mid-span deflection is great than span/25.

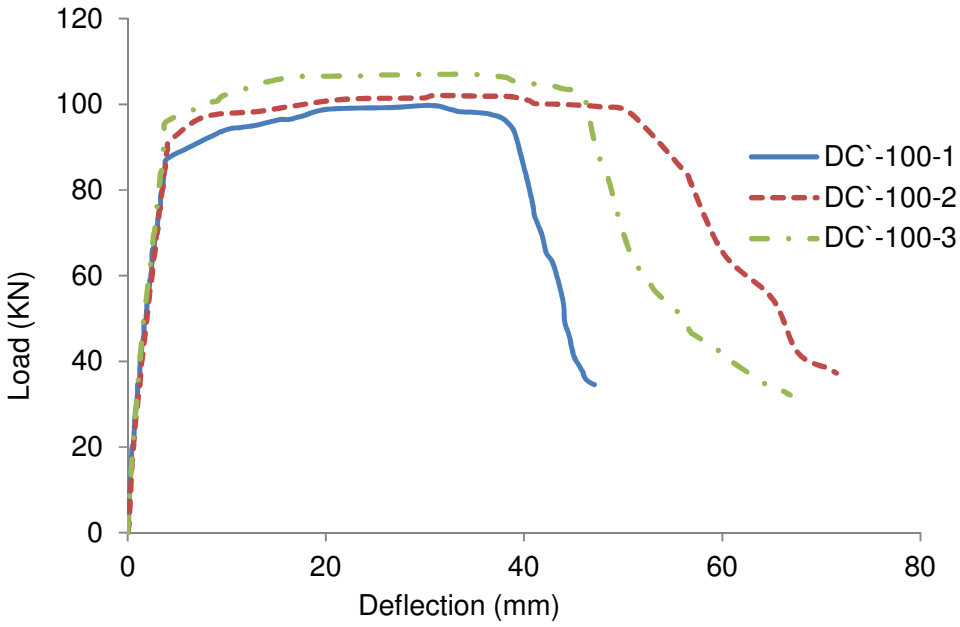

Figure 6.6: Load versus deflection for beam with C` class reinforcement @ 100 mm shear links spacing

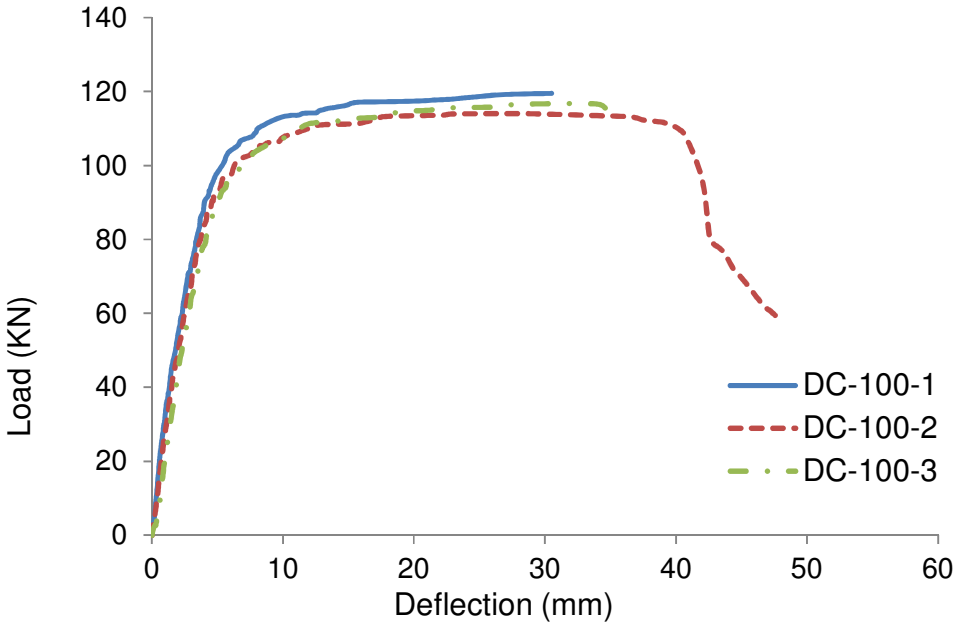

Figure 6.7: Load versus deflection for beam with C class reinforcement @ 100 mm shear links spacing

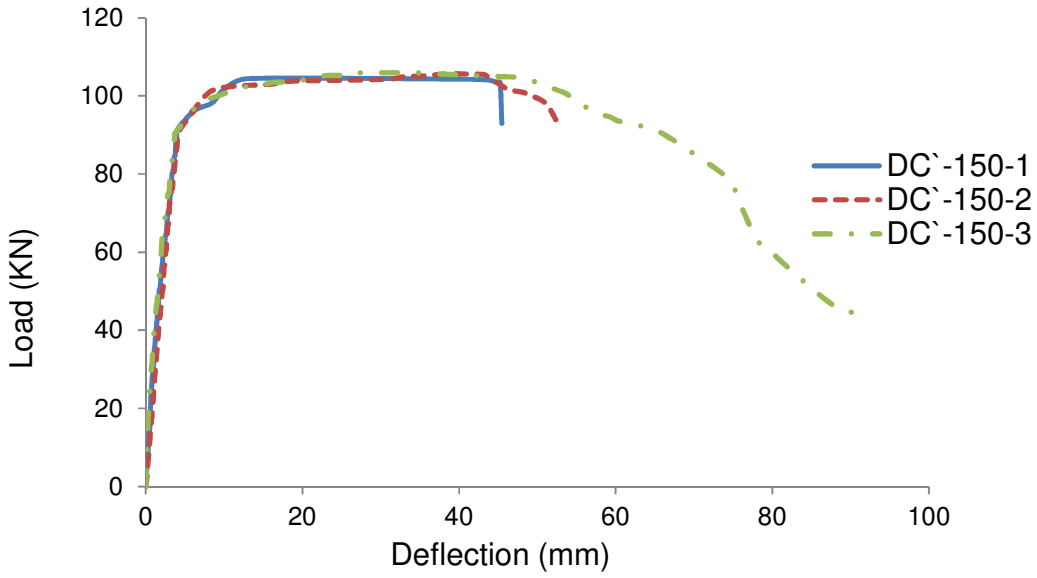

Figure 6.8: Load versus deflection for beam with C` class reinforcement @ 150 mm shear links spacing

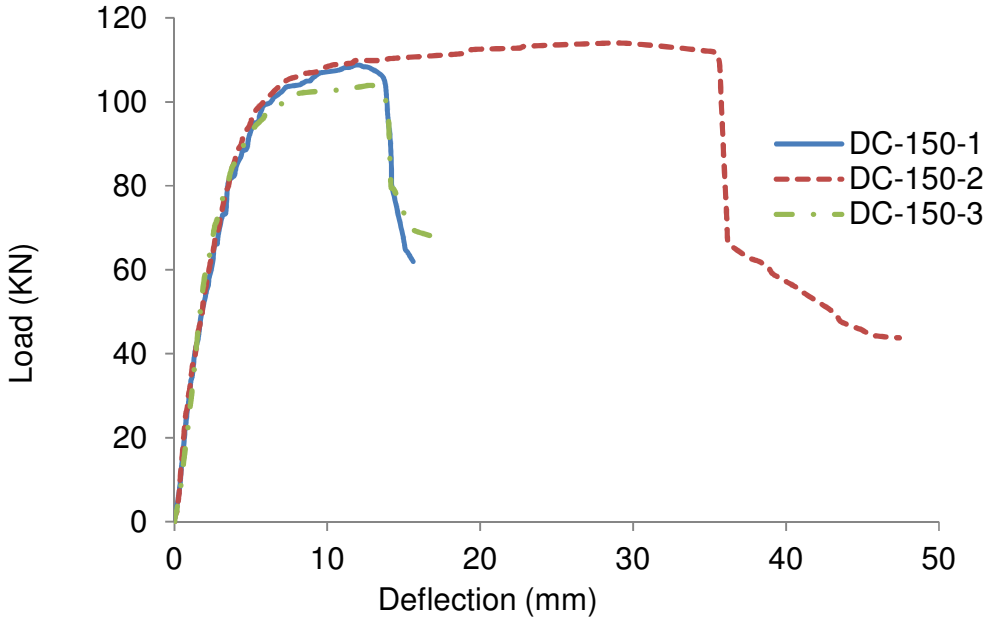

Figure 6.9: Load versus deflection for beam with C class reinforcement @ 150 mm shear links spacing

Table 6.3: Ductility test results

Beam group	Test beam	Beam age (Days)	Compressive strength (N/mm^2)	Indirect tensile strength (N/mm^2)	Modulus of rupture (N/mm^2)	Yield load (KN)	Ultimate load (KN)	Ultimate load/ yield load	Maximum deflection	Maximum rotation (rad)
DC`-100	DC'-100-1	22	33.2	3.06	4.52	100.5	121.30	1.21	48.50	0.19
	DC'-100-2	23	36.0	3.37	4.50	97.18	114.10	1.17	45.00	0.18
	DC'-100-3	24	36.4	3.80	4.74	99.17	116.70	1.17	35.00	0.14
	Avg. value	**23**	**35.2**	**3.41**	**4.59**	**98.95**	**117.36**	**1.18**	**42.75**	**0.17**
DC`-150	DC'-150-1	18	40.3	3.31	4.26	98.00	108.70	1.11	15.00	0.06
	DC'-150-2	19	39.5	3.38	4.63	99.40	113.90	1.14	35.75	0.14
	DC'-150-3	19	37.5	3.25	4.72	98.27	103.90	1.05	17.50	0.07
	Avg. value	**19**	**39.1**	**3.32**	**4.54**	**98.56**	**108.83**	**1.10**	**22.75**	**0.09**
DC-100	DC-100-1	14	33.2	2.71	4.33	93.00	99.71	1.07	42.50	0.17
	DC-100-2	15	37.9	3.04	4.67	91.10	102.00	1.11	61.25	0.25
	DC-100-3	18	39.9	3.47	4. 50	93.24	107.00	1.14	51.00	0.20
	Avg. value	**17**	**37.0**	**3.07**	**4.50**	**92.78**	**102.93**	**1.11**	**51.50**	**0.21**
DC-150	DC-150-1	19	44.3	3.39	4.84	94.14	104.40	1.11	47.25	0.19
	DC-150-2	20	45.3	3.01	4.56	92.40	105.70	1.14	52.50	0.21
	DC-150-3	21	45.3	2.84	4.61	95.60	105.90	1.11	77.50	0.31
	Avg. value	**20**	**45.0**	**3.08**	**4.67**	**94.05**	**105.33**	**1.12**	**58.75**	**0.24**

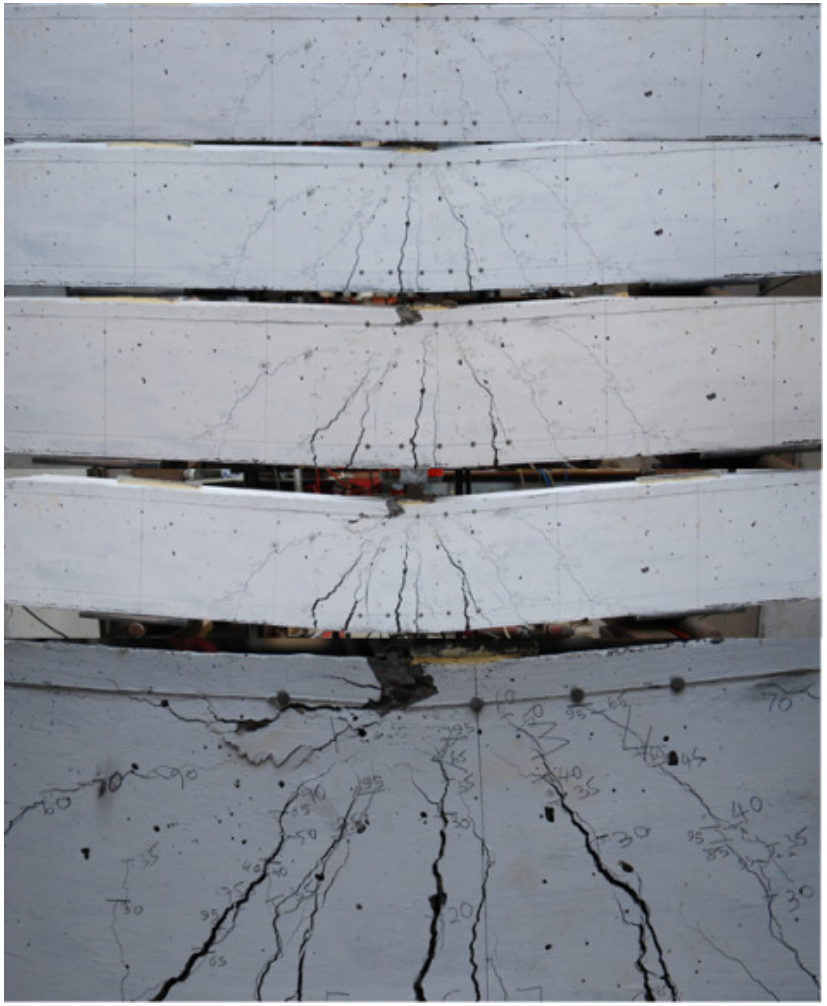

Figure 6.10: Example for cracks development of DC`-100

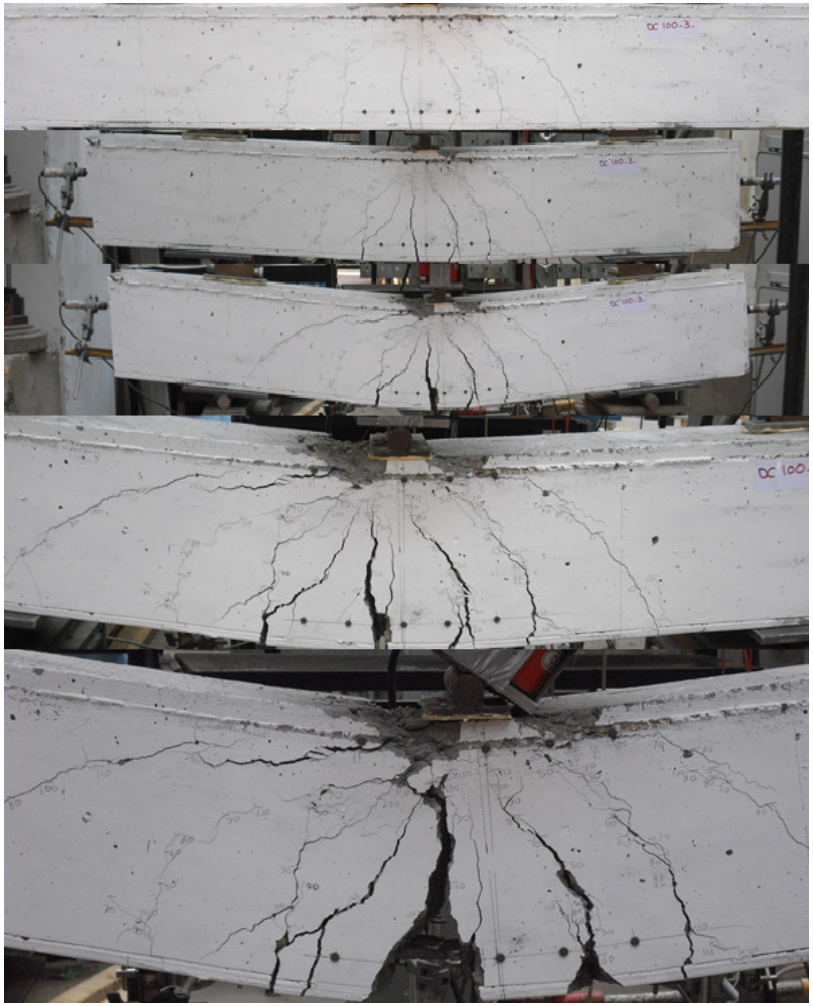

Figure 6.11: Example for cracks development of DC-100

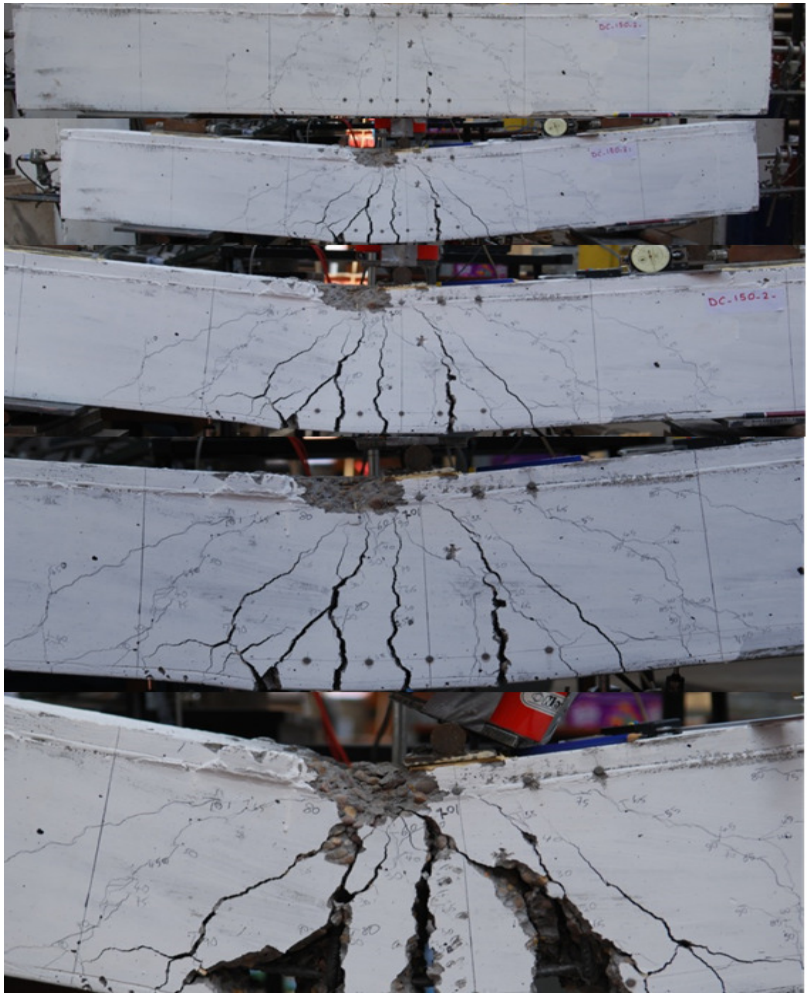

Figure 6.12: Example for cracks development of DC-150

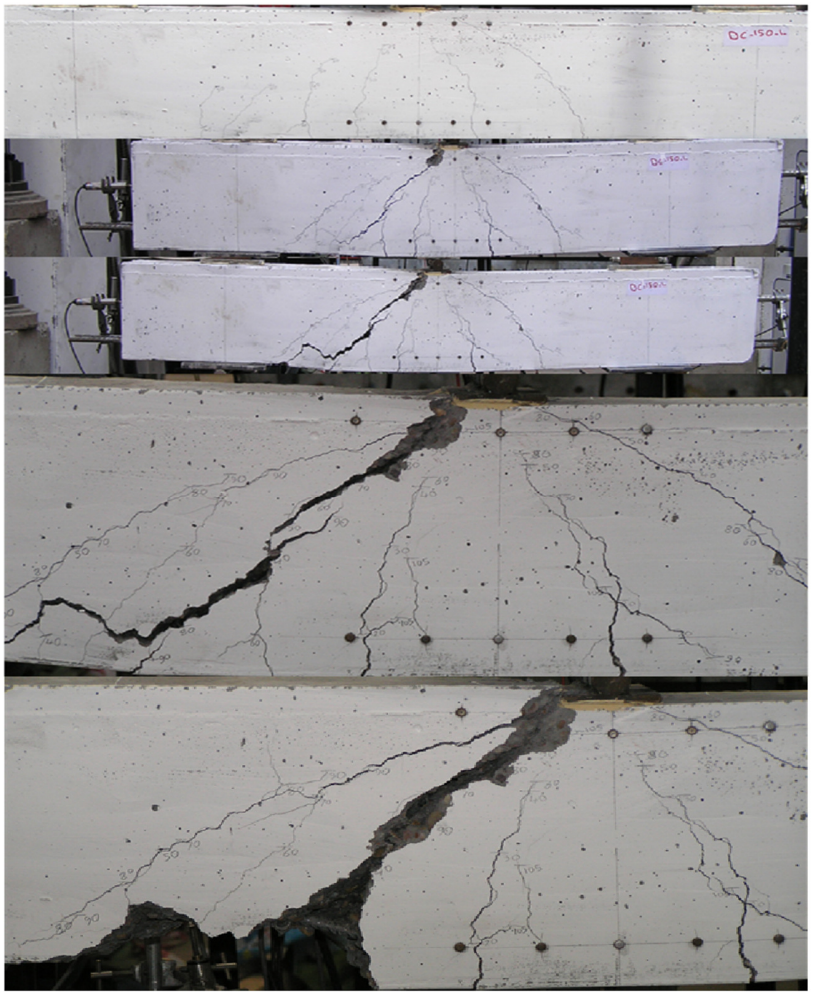

Figure 6.13: Example for cracks development of DC`-150

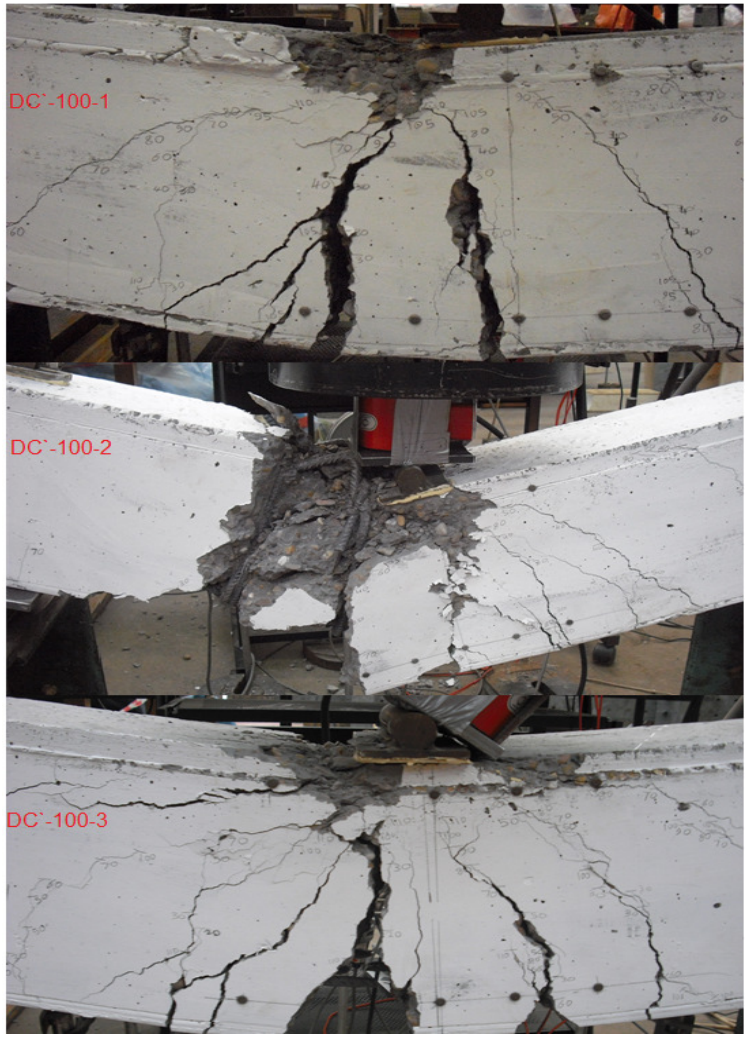

Figure 6.14: Failure modes for DC`-100 beams

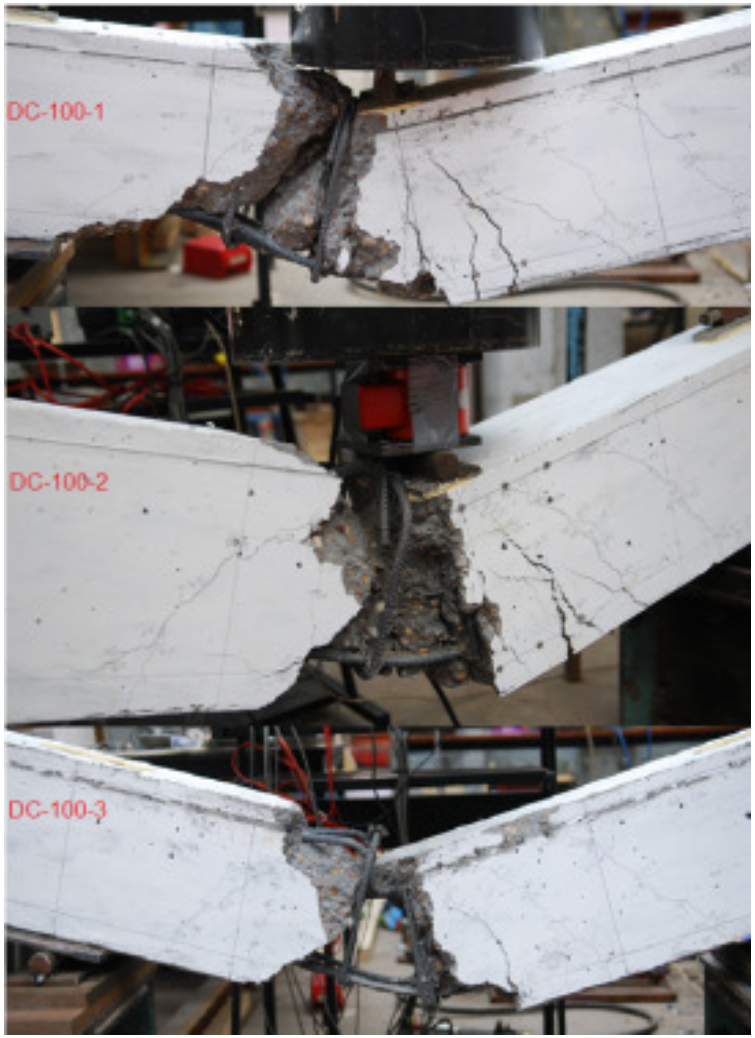

Figure 6.15: Failure modes for DC-100 beams

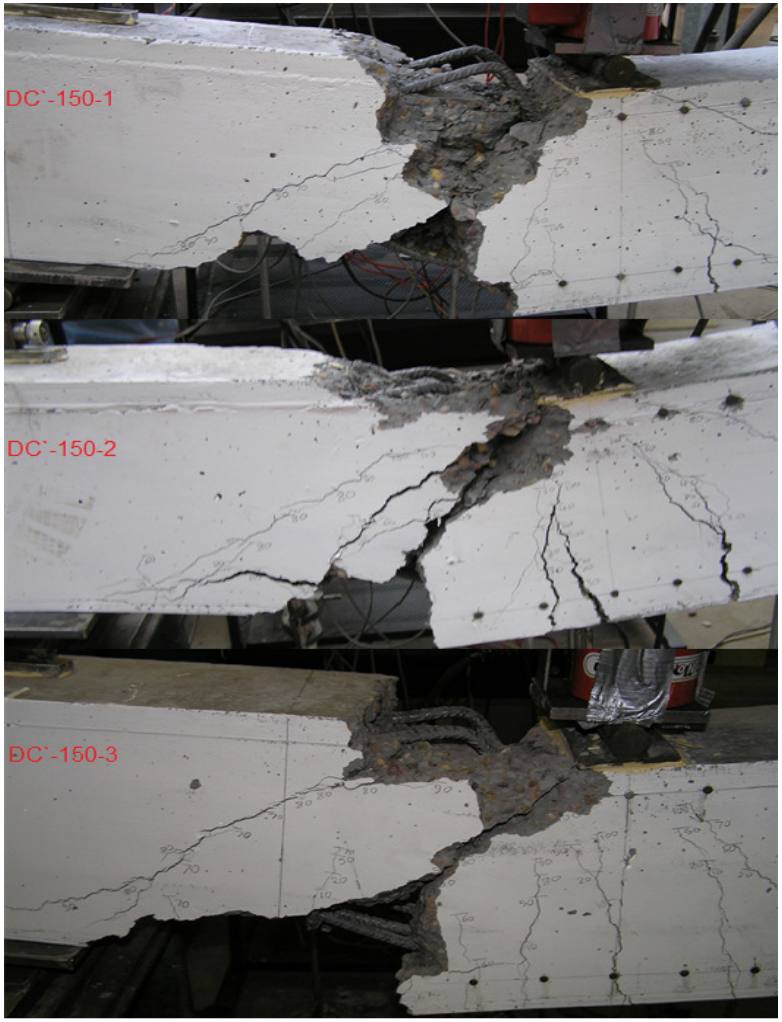

Figure 6.16: Failure modes for DC`-150 beams

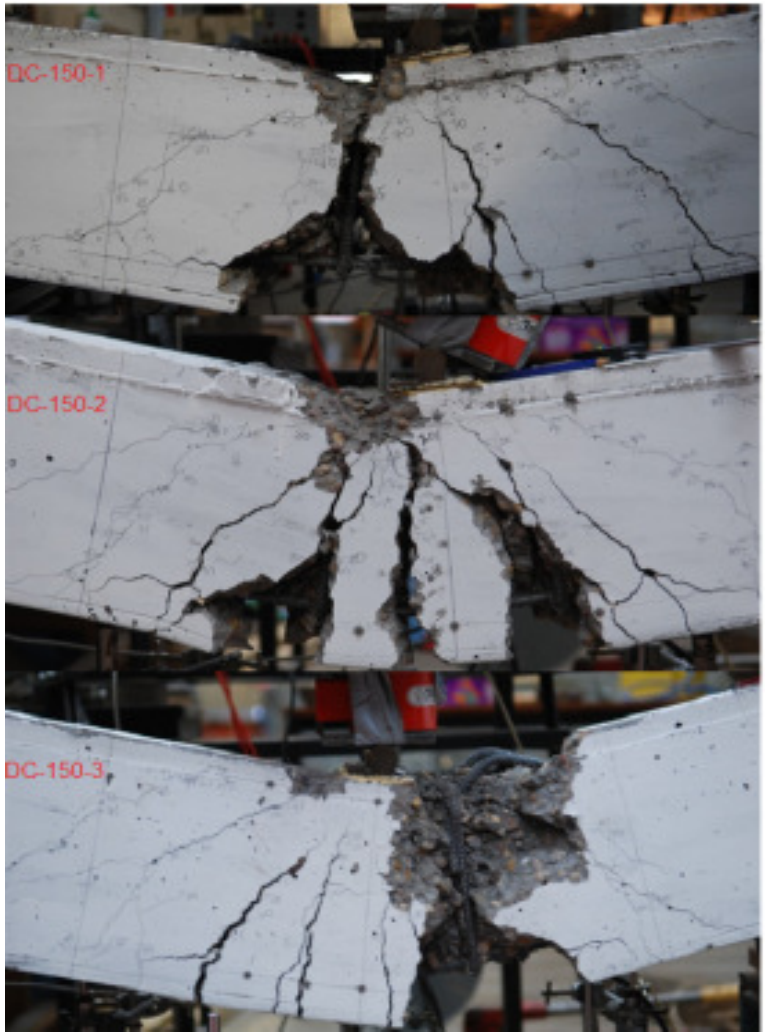

Figure 6.17: Failure modes for DC-150 beams

6.2.4.2 Discussion of test results

Test results were examined with regard to the following two variables: reinforcement type and shear link spacing. Table 6.4 presents rotations at yield and ultimate loading levels in addition to the ductility of each tested beam. As mentioned previously in section 2.2.3 of Chapter two, ductility is considered as the ratio of the maximum curvature to the curvature at the yield load. The beam rotation is considered to be the curvature in calculating the ductility of tested beams as listed in Table 6.4.

Comparing the ratio of the maximum rotation and the rotation at ultimate load between DC-100 and DC-150, it can be seen that decreasing the shear links spacing by third has increased the ductility of RC beam by 12%, but has a negligible effect on the ultimate loads, provided that both failure modes were in flexure.

The comparison between DC-100 and DC'-100 showed that bar C' resulted in a reduced ductility (around 11%) but increased the ultimate load by around 14%. DC-100 reached yield point at a smaller rotation than DC'-100 but both beams had comparable rotation at the ultimate load.

DC'-150 had shear-related failure and therefore it had reduced ultimate load as its failure was governed by shear resistance and hence exhibited a brittle failure mode. The reason that DC-150 still remained the flexure-related failure was because that it had higher concrete strength.

Table 6.4: Ductility of tested beams

Beam set	Tested beam	Rotation at yield load (rad)	Rotation at ultimate load (rad)	Maximum rotation (rad)	Ductility (Maximum rotation/Rotation at ultimate load)
DC-100	DC-100-1	0.010	0.118	0.194	1.64
	DC-100-2	0.009	0.100	0.180	1.80
	DC-100-3	0.011	0.118	0.140	1.19
	Avg. value	**0.010**	**0.115**	**0.171**	**1.54**
DC-150	DC-150-1	0.009	0.049	0.060	1.23
	DC-150-2	0.010	0.110	0.143	1.31
	DC-150-3	0.011	0.050	0.070	1.41
	Avg. value	**0.010**	**0.070**	**0.091**	**1.30**
DC`-100	DC`-100-1	0.006	0.099	0.170	1.71
	DC`-100-2	0.005	0.125	0.245	2.00
	DC`-100-3	0.006	0.136	0.204	1.50
	Avg. value	**0.006**	**0.119**	**0.206**	**1.74**
DC`-150	DC`-150-1	0.009	0.150	0.189	1.22
	DC`-150-2	0.011	0.150	0.210	1.40
	DC`-150-3	0.007	0.150	0.310	2.10
	Avg. value	**0.009**	**0.150**	**0.235**	**1.56**

6.2.4.3 Effect of shear link spacing and reinforcement type

Figures 6.18 & 6.19 illustrate the link spacing versus maximum deflection at the failure load & ultimate load, respectively. Each point in both figures represents the average for three identical beams. Beams reinforced with C` steel has higher ultimate load when confined with shear links at 100 mm spacing than 150 mm; that is due to the fact that the dense shear links will provide more confining effect and hence increase the concrete strength. Both sets of beams reinforced with C' and C bars showed almost the same yield loads in both link spacing cases.

In the case of DC series, as DC-150 beams had a considerably higher concrete strength than DC-100 at test (45kN/mm^2 vs. 37kN/mm^2), DC-150 beams had a higher ultimate load despite of the enhanced confining effect. If the maximum deflections at failure for both sets of beams DC-100 & DC-150 are normalized by the concrete strength, the values of (1.391 & 1.305) respectively are resulted. That can explain the reason why DC-150 beams had higher deflections comparing with DC-100.

In general, beams reinforced by C` steel with 100 mm links has the highest yield and ultimate loads among all tests and C` reinforced beams with 150 mm links had higher yield and ultimate loads than all other beams reinforced with C-class steel. This can be explained as C` steel has higher loading capacity than standard C-class which gives more resistance to the beams reinforced with C` bars.

High rotation values were noticed for beams reinforced with C` bars rather than C with shear links at 100 mm spacing at yield and the maximum load points, whereas C` beams with 150 mm had the highest maximum rotation among all tests.

Due to the various confining effect of the shear links of different spacing, The effective RR ratio for the 100mm shear link spacing case is lower than the 150mm case even the amount of the longitudinal bars remain the same. This agrees with the observations made by Beeby (1997) that “ductility reaches the maximum when the reinforcement ratio RR is set at a relatively low level and goes lower when RR increases after pass this level”.

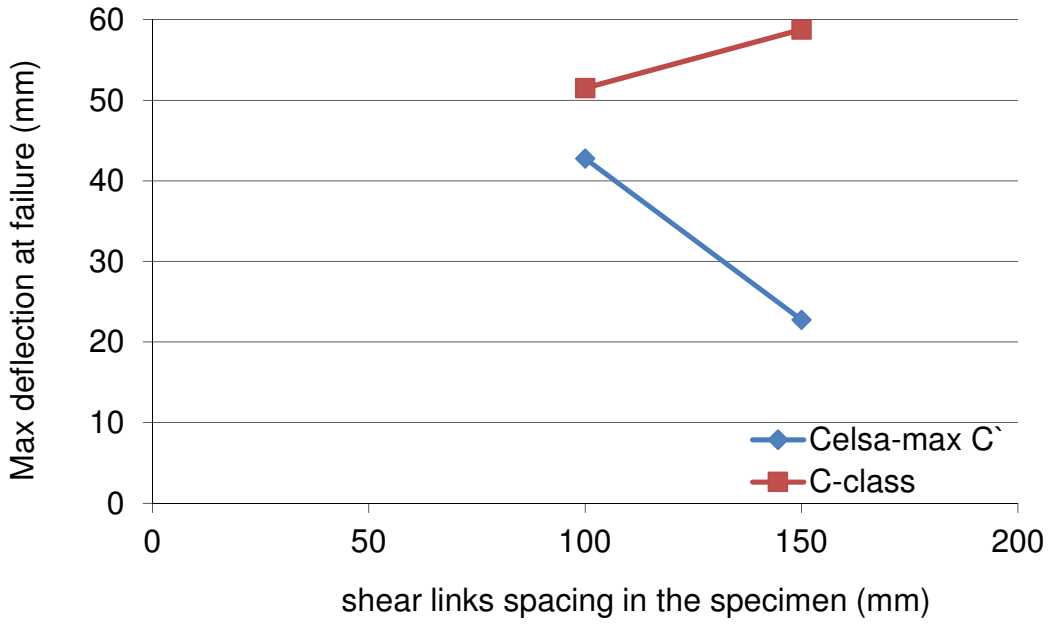

Figure 6.18: Maximum deflection at failure versus number of shear links for C & C’ reinforcement

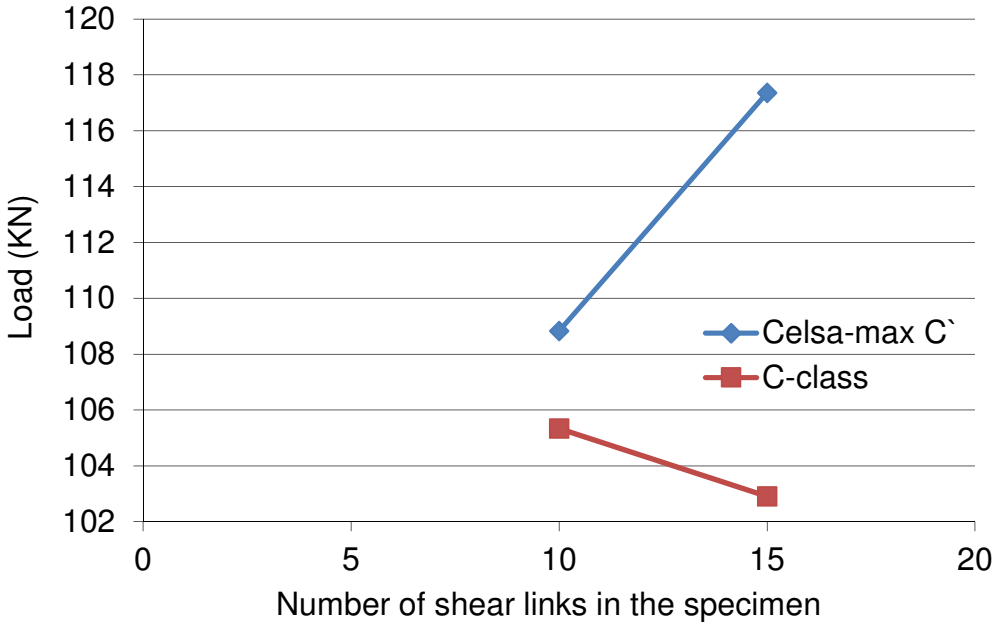

Figure 6.19: Ultimate load versus link spacing for C & C' reinforcement
Note: 15 links were used in beams with 100 mm spacing
& 10 links in beams with 150 mm spacing

6.2.4.4 Analytical predictions and comparison with experimental results

The predictions for both ultimate load and the failure mode of tested beams were carried out by using the model proposed by BS EN 1992-1-1:2004 in order to compare the laboratories tests with the code predictions. Based on the analytical predictions, the tested RC beams will be checked whether they comply with the codes and can identify any odd behaviour or results of the tested beams.

Beam failure can also be identified for flexure or shear. Calculations were made to determine the failure load for each case and the lower value were considered as the predicted ultimate load. DC'-100-1 is used to illustrate the calculation for the

flexural and shear capacities, where: f_{ck}= 27 N/mm^2, d =192 mm, b = 150 mm, A_s = 235.5 mm^2, A'$_s$ = 157 mm^2.

6.2.4.8.1 Flexural capacity

Status of tension steel bars needs to be checked whether they are in under-reinforced, balanced or over-reinforced. For that purpose, concrete compression force F_c, reinforcement tensile force F'$_s$ and reinforcement compression force F_s will be calculated to check if $F_c + F'_s \geq F_s$ or not. The previous three forces are given by the following equations:

Actual x can be calculated by equating the forces as follows: $F_c + F'_s = F_s$. However, the equations for F_c, F'$_s$, and Fs are going to be calculated by ignoring all partial factors for the purpose of having maximum loads:

$$F_c = f_{ck} b x \tag{6.1}$$

$$F'_s = f_{sc} A'_s \tag{6.2}$$

$$f_{sc} = 717.5\left[\frac{(x - d')}{x}\right] \tag{6.3}$$

$$F_s = f_{yk} A_s \tag{6.4}$$

where:

d: Effective depth – depth to the centre of the tension steel. In this case = 192 mm

f_{ck}*:* Characteristic strength of concrete in compression (cylinder). In this case = 35.28 N/mm^2

f_{yk}*:* Characteristic yield strength of tension/compression steel bar. For C` = 538.4 N/mm^2

A_s: Area of the longitudinal tension reinforcement. For 10 mm bars = 78.5 mm^2

A_{sw}: Area of shear reinforcement. For 8 mm bars = 50.24 mm^2

Finally, the resistance of bending moment is:

$$M = F'_s (d - d') + F_c (d - 0.4x) \quad (6.5)$$

The recorded ultimate moment M_u = 24.58 KN.m.

As a simply support beams with three points loading: $M_u = \frac{PL}{4}$

Therefore the point load (P) = $4M_u$ = 98.33 KN as L=1 m.

where:

M: the moment resistance for the cross section of examined beams

P: point load value at the center of beam span where load is applied

L: span length of the beam between the two supports

6.2.4.8.2 Shear capacity

a) The resistance is provided by the less value between the following two equations results:

$$V_{Rd,s} = \frac{0.9 A_{sw} f_{yk} d \cot\theta}{s} \quad (6.6)$$

$$V_{RD,\max} = \frac{0.9 b d f_{cd}}{\cot\theta + \tan\theta} \quad (6.7)$$

Where:

$V_{Rd,s}$: Design shear resistance governed by the yielding of shear reinforcements

$V_{Rd,\max}$: Design shear resistance governed by the crushing of concrete struts

The angle between the concrete compression strut and the beam axis required to resist the shear design force θ should be determined by considering the following two conditions:

- The maximum resistance should be achieved
- It should fall into this region: $21.8^0 \leq \theta \leq 45^0$

By Substituting Equation 6.2 into Equation 6.3, θ can be found to be:

$$\theta = \tan\left[\sqrt{1 + \frac{s.f_{cd}.b}{A_{sw}.f_{yk}}}\right] \tag{6.8}$$

where:

s: the spacing between shear links

f_{cd}: the designed compression value of concrete

In this case, θ is 0.445 rad.

Therefore, $V_{Rd,s}$ = 131 KN

Also, $V_{RD,s} = \frac{P}{2}$

Therefore the Point load (P) = 2 x $V_{Rd,s}$ = 262 KN

The lower value of the point loads between the flexural moment resistance and shear resistance will be considered as the ultimate failure load, which is the flexural failure load 100.32 kN.

Table 6.5 presents results of the theoretical prediction of all beams. It is worth noting that in this test, the beam mid-span section experienced both high bending moment and shear force, and whereas the above methods predict the resistance under the sole flexural or shear action. There is possibility that a joint action of

flexure and shear will lead to a mixed failure mode. This is particularly the case when the ratio of resistance due to sole shear and sole flexure is low. This perhaps explain why the failure mode for DC'-150 beam has shear-failure nature. Table 6.6 presents both experimental and theoretical failure loads and the ratio P_{exp}/P_{the}, where P_{exp} & P_{the} are the experimental and theoretical failure loads respectively. All beams have exceeded their predicted failure load.

Table 6.5: Theoretical load failure predictions for beams reinforced with single bars

beam	Neutral axis depth (x) (mm)	Theta (ɵ) (degree)	Flexural moment failure load (KN)	Shear failure load (KN)	Shear failure load/Flexural moment failure load
DC`-100-1	37.7	30.71	96.57	322	3.33
DC`-100-2	36.22	29.68	97.35	346	3.55
DC`-100-3	36	29.54	97.45	348	3.57
DC`-150-1	34.43	22.9	98.36	311	3.16
DC`-150-2	34.74	23	98.20	309	3.15
DC`-150-3	35.53	23.47	97.74	302	3.09
DC-100-1	36	30.71	90	322	3.58
DC-100-2	33.82	29	91.24	354	3.88
DC-100-3	33	28.54	91.63	362.5	3.96
DC-150-1	31.66	22.13	92.56	323.3	3.49
DC-150-2	31.31	21.9	93	326.6	3.51
DC-150-3	31.31	21.9	93	326.6	3.51

Table 6.6: Comparison between theoretical and experimental ultimate loads for beams reinforced with single bars

Beam	Theoretical ultimate load P_{the} (KN)	Experimental ultimate load P_{exp} (KN)	P_{exp} & P_{the}
DC`-100-1	96.57	121.3	1.26
DC`-100-2	97.35	114.1	1.17
DC`-100-3	97.45	116.7	1.20
DC`-150-1	98.36	108.7	1.11
DC`-150-2	98.20	113.9	1.16
DC`-150-3	97.74	103.9	1.06
DC-100-1	90	99.71	1.11
DC-100-2	91.24	102	1.12
DC-100-3	91.63	107	1.17
DC-150-1	92.56	104.4	1.13
DC-150-2	93	105.7	1.14
DC-150-3	93	105.9	1.14

6.3 RC Beams with Steel Mesh Test

6.3.1 Introduction

All tests were done using beams with a length of 1400 mm, breadth of 300 mm and height of 100 mm. Reinforcement consists of welded steel meshes with main bars along the specimen length and secondary welded bars along the

specimen breadth. Figure 6.20 shows a detailed drawing for a typical tested beam reinforced with steel mesh, it can be seen in the drawing that steel meshes are welded so secondary bars locate below the main bars. The concrete cover from bottom face of the beam to the secondary bars is 20 mm. All secondary bars have a diameter of 8 mm while main bars are 8, 10 or 12 mm, respectively. As the previous test for ductility, all beams were casted using a vibration table in two layers and covered after casting with polythene sheeting in order to be de-moulded after 48 hours and stored in a curing tank till testing day.

As all other experimental tests in this study, all specimens in this test are identified with an alpha numeric designation. The first letter D indicates ductility test, followed by letter F which stands for fabric, as beams are reinforced with steel fabrics. The last letter is C` or A to refer to the steel class of main bars in the steel mesh. Two numbers follow the alphabets indicating the main bar diameter size in mm and number of the tested beam in each group. Table 6.7 includes details about all tested beams and their reinforcement.

A simple drawing for RC beam with steel mesh is shown in Figure 6.20. As it can be seen in the drawing the beam is simply supported with one pint load in the middle.

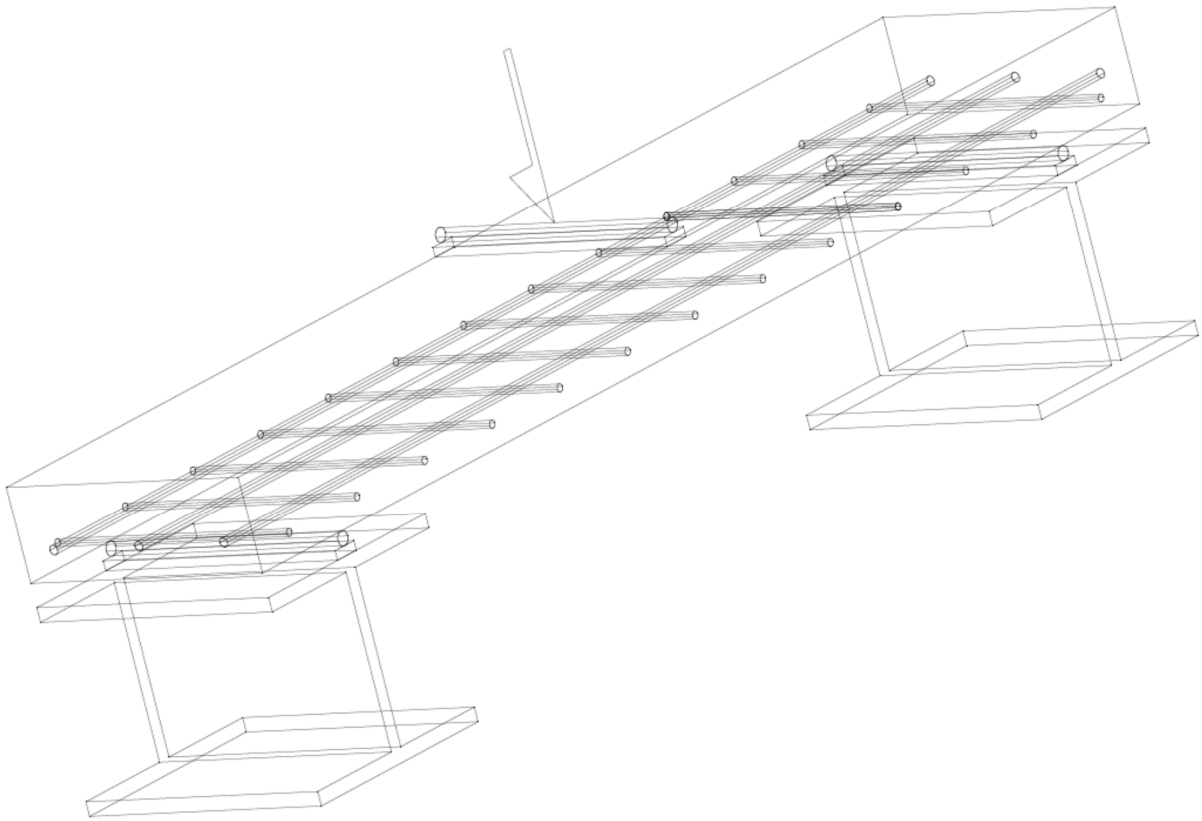

Figure 6.20: Detailed drawing for a tested beam reinforced with steel mesh

Table 6.7: Test beams and reinforcement details

Test specimen	Number of tested beams	Main steel class & size	Secondary bar size
DFA-8	2	Bar A, 8 mm	8 mm
DFA-10	2	Bar A, 10 mm	8 mm
DFC`-8	3	Bar C', 8 mm	8 mm
DFC`-10	3	Bar C', 10 mm	8 mm
DFC`-12	3	Bar C', 12 mm	8 mm

6.3.2 Test instruments

Same instruments as in ductility test for beams reinforced with confined single bars are used in the current test. Only one more strain reading has been added using strain gauges.

Strain gauges are placed at the middle of the main longitudinal bars and connected to the data logger so precise readings for reinforcement strain can be recorded. In order to get an accurate reading using strain gauges, a few steps are needed to be followed to mountain the strain gauges properly on the steel surface. The mounting process is widely explained in the next section.

6.3.3 Mounting strain gauge

There are five steps for the process of mounting a strain gauge in this study: prepare the surface of the steel bar, mark the surface for gauge orientation, prepare the gauge for mounting, position the gauge on the bar, and apply protection for the strain gauge.

A special kit is needed to mountain the strain gauge properly which includes:

- Degreaser
- Acid and basic solution
- An adhesive to install the strain gauge
- Laboratory grinder and different grades of sand papers
- Scissors, strip chart paper and permanent marker for the strain
- Tweezers, Teflon sheet, tape strips and razor blade to glue the gauge to the steel bar.
- Wire strippers/cutters.

Starting with applying the degreaser to the area of the bar where the strain gauge will be placed. Then a grinder is used to remove the ribs at that area. After that, an emery cloth and sand papers of grades 180, 220, 360 and 440 are used in order to smooth the surface of the steel bar after cutting the ribs as much as it can be done so the strain gauge can be perfectly glued to the steel bar.

Acidic solution then is applied to the steel surface followed by applying 400 grade of sand paper to perform wet sand surface. After that, a prep-conditioner is applied to rinse the steel surface where the wet sand is performed followed by applying the prep-neutralizer, basic solution. A cloth is used to clean the treated area of the steel bar.

The bar surface is marked for gauge orientation. Using a tweezers, the strain gauge is placed on a clean small box and a piece of tape is cut and folded from both sides. Then by placing the thumb over the tape and quickly in one motion, the tape is slid over the strain gauge. After that, the tape piece that includes the strain gauge it pulled off one side to apply special glue, catalyst C, at the bottom of strain gauge and let it dry for around 60 seconds. Then, the tape and strain gauge are placed on the steel bar surface and using a Teflon sheet pressure is applied using thumb for 60 seconds to make sure of mounting the strain gauge properly. Finally the tape is gently pulled off to remove the tape and keep the gauge placed on the bar.

For protecting the strain gauge and making sure that the casting process will not affect the strain gauge itself or the wires connecting it to the data logger, the strain gauge wire is tied to the bar. After that, a plastic sleeve of same length as the strain gauge is inserted to cover the gauge and silicon is applied on and around the sleeve to make sure that the strain gauge is isolated and the effect of casting and

vibration on the gauge is minimised as much as it can be. Figure 6.21 shows (a-e) steps for mounting a strain gauge starting by removing the steel bar ribs till final stage which is covering the strain gauge with silicon.

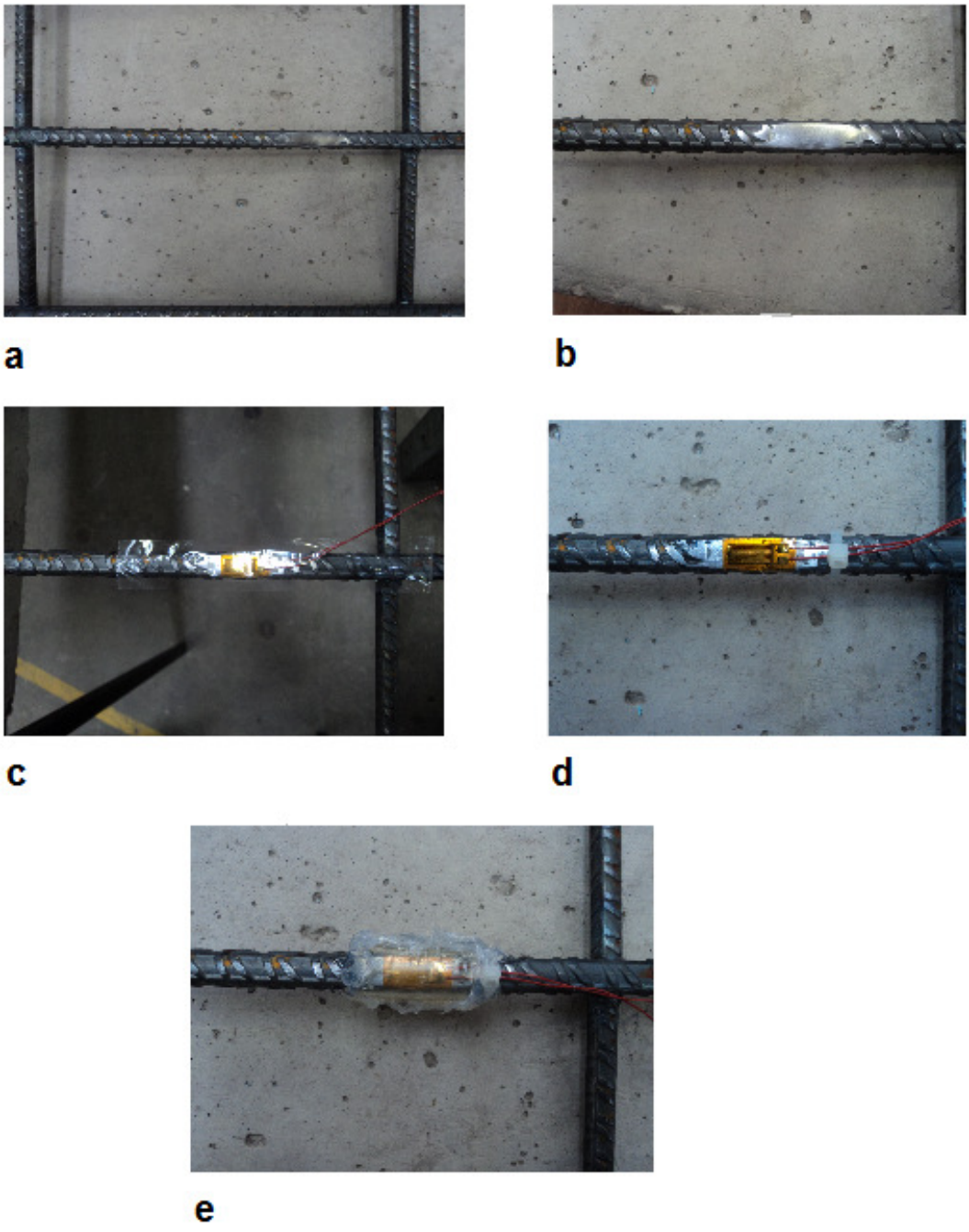

Figure 6.21: Mounting strain gauge on a steel bar

6.3.4 Test procedure

Control specimens are prepared and casted at the same day of beam cast using same concrete mix. Three cubes, three cylinders and three prisms are casted for each tested beam in order to determine the compressive strength, indirect tensile strength and modulus of rupture respectively. Testing results for all the control specimens are provided in Table 6.8 for each beam, control specimens are tested at same day along with reinforced beams.

Table 6.8: Control specimen's results for RC beams with steel meshes

Set of beams	Tested beam	Compressive strength $f_{cm,cube}$ (N/mm^2)	Characteristic cylinder strength f_{ck} (N/mm^2)	Indirect tensile strength (N/mm^2)	Modulus of rupture (N/mm^2)
DFA-8	DFA-8-1	43.8	38.0	3.4	6.4
	DFA-8-2				
DFA-10	DFA-10-1	39.1	34.0	3.1	5.3
	DFA-10-2				
DFC`-8	DFC'-8-1	32.1	19.7	2.2	5.3
	DFC'-8-2				
	DFC'-8-3				
DFC`-10	DFC'-10-1	26.9	23.5	2.5	4.1
	DFC'-10-2				
	DFC'-10-3				
DFC`-12	DFC'-12-1	28.7	25.0	2.6	3.9
	DFC'-12-2				
	DFC'-12-3				

Same loading procedure as in the ductility test for beams reinforced with confined single bars is followed in the current test as well. Results analysis and discussion are explained widely in the next section. Figure 6.22 shows test arrangements and loading conditions applied for each beam at testing day.

Figure 6.22: set up of concrete beam reinforced with steel mesh for ductility test

6.3.5 General behaviour and results

Table 6.9 shows the results for all ductility tests for beams reinforced with steel meshes. In addition to that, results for control specimens are included in Table 6.9 for all tested beams. Graphs for load versus deflection have been produced based on test results and shown in Figures 6.23, 6.24, 6.25, 6.26 and 6.27. It is shown in the mentioned graphs that all identical beams follow the same trend, only in Figure 6.26, one beam, DFC`-10-1 had a ductile behaviour while the other two identical beams DFC`-10-2 and DFC`-10-3 did not show a ductile failure as they has

a shear failure. The presence of shear failure can be explained as a joint action of moment and shear happens near the loading which can lead the beam to fail in shear instead of moment.

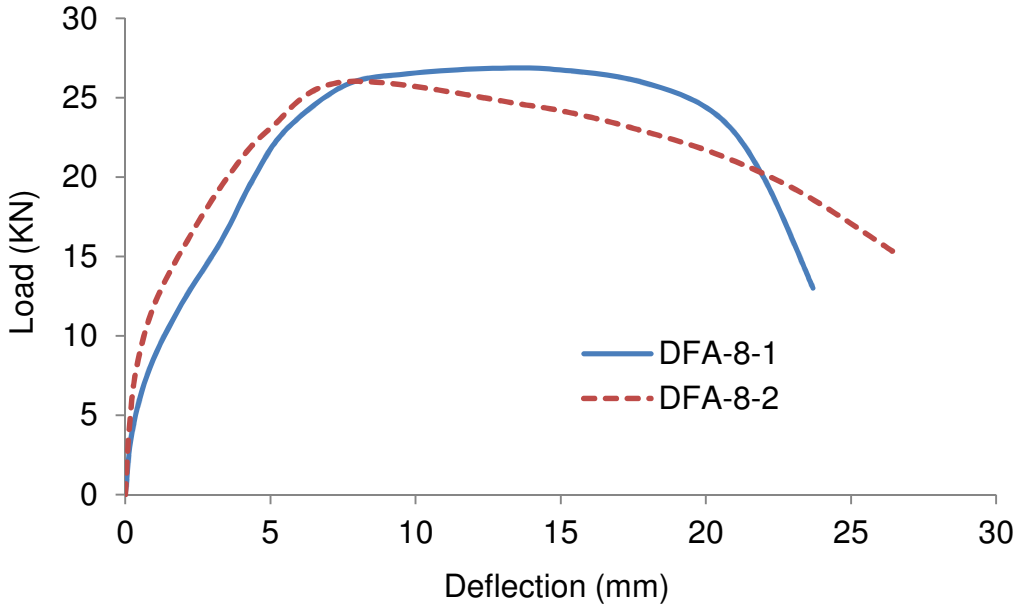

Figure 6.23: Behaviour of RC beams with class A steel meshes and main bar diameter of 8 mm

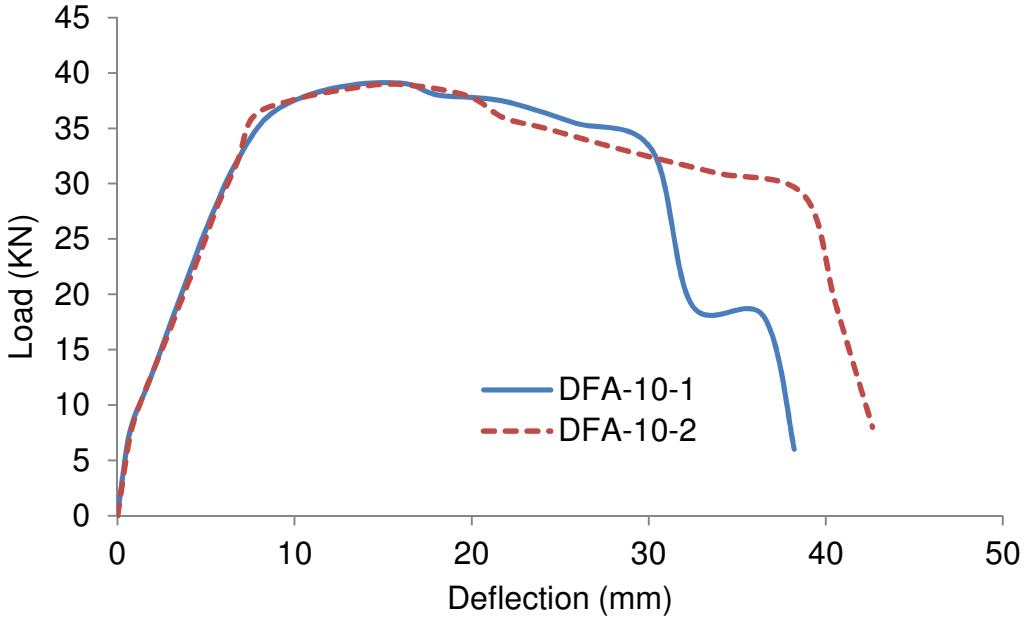

Figure 6.24: Behaviour of RC beams with class A steel meshes and main bar diameter of 10 mm

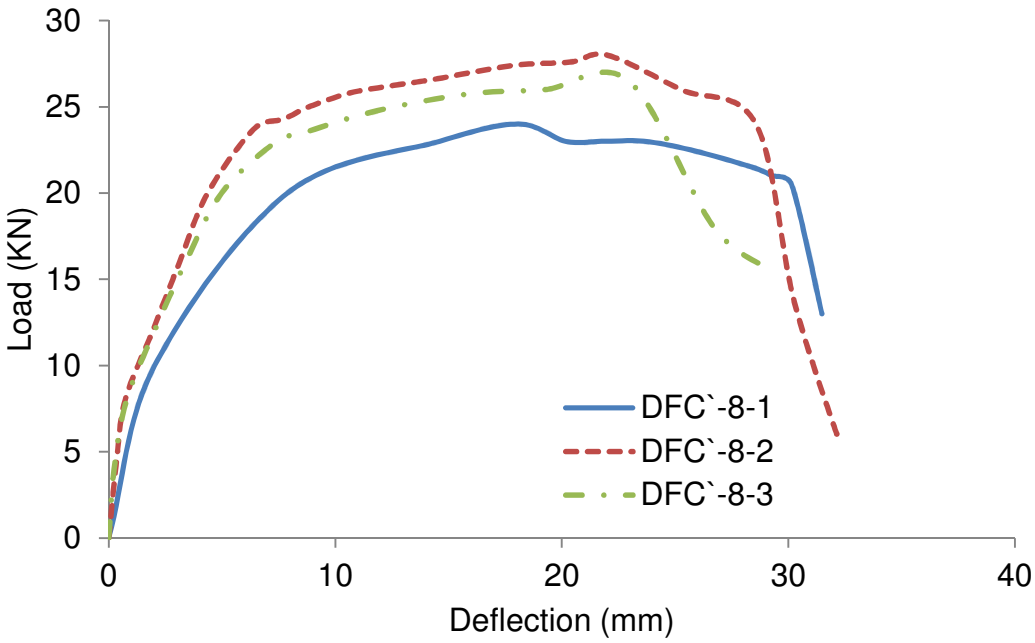

Figure 6.25: Behaviour of RC beams with class C` steel meshes and main diameter of 8 mm

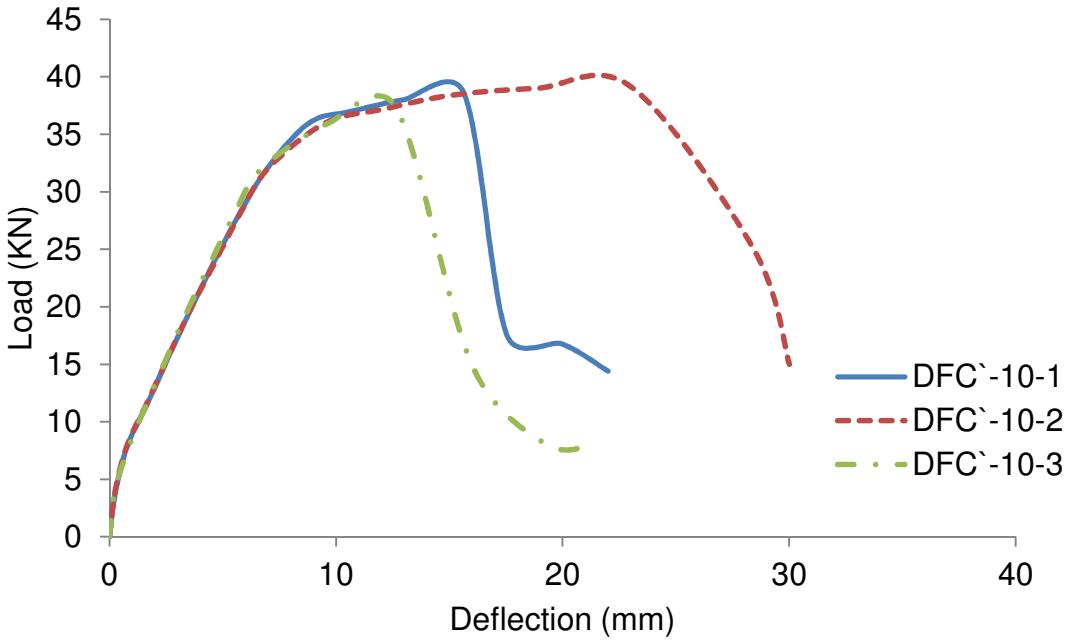

Figure 6.26: Behaviour of RC beams with class C` steel meshes and main diameter of 10 mm

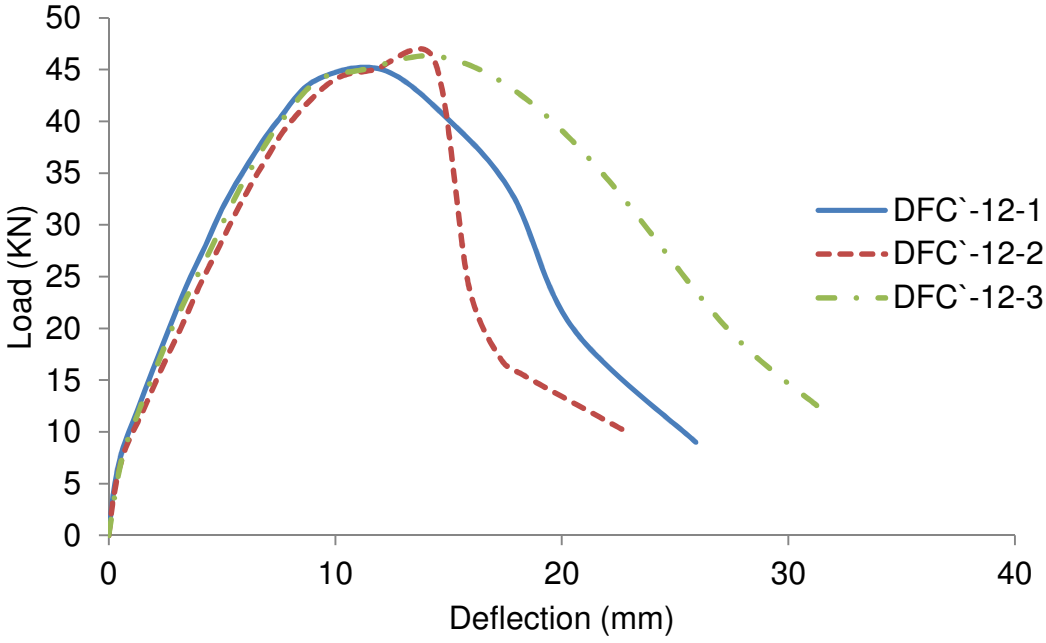

Figure 6.27: Behaviour of RC beams with class C` steel meshes and main diameter of 12 mm

Table 6.9: Properties of ductility tests for RC beams with steel meshes & properties of control specimens

Beam set	Tested beam	Compressive strength (N/mm^2)	Indirect tensile strength (N/mm^2)	Modulus of rupture (N/mm^2)	Yield load (KN)	Ultimate load (KN)	Ductility (ultimate load/ yield load)	Maximum deflection	Maximum rotation (rad)
DFA-8	DFA-8-1	43.8	3.38	6.39	25.5	28	1.1	22.95	0.20
	DFA-8-2				23.8	25.7	1.08	26.16	0.22
	Avg. value				24.65	26.85	1.09	24.55	0.20
DFA-10	DFA-10-1	39.13	3.14	5.31	36.7	40.9	1.11	38.24	0.30
	DFA-10-2				36.4	41.14	1.13	42.24	0.34
	Avg. value				36.55	41	1.12	40.24	0.32
DFC'-8	DFC'-8-1	32.05	2.18	5.34	23.3	25.23	1.08	31.48	0.30
	DFC'-8-2				24.7	29.24	1.18	32.26	0.36
	DFC'-8-3				24.33	27.3	1.12	29.29	0.34
	Avg. value				24.11	27.26	1.13	31.01	0.32
DFC'-10	DFC'-10-1	26.86	2.48	4.14	36.5	40.66	1.12	21.97	0.20
	DFC'-10-2				36.4	39.5	1.08	30.17	0.24
	DFC'-10-3				34.8	37.5	1.08	21.11	0.16
	Avg. value				35.9	39.22	1.09	24.41	0.20
DFC'-12	DFC'-12-1	28.65	2.6	3.86	39.6	46.4	1.17	26	0.20
	DFC'-12-2				39.2	46.75	1.19	22.23	0.18
	DFC'-12-3				39.53	46.6	1.18	30.61	0.24
	Avg. value				39.44	46.6	1.18	26.28	0.22

6.3.6 Comparison based on main bar diameter

Examples for the behaviour of RC beams reinforced with steel meshes which vary in main bar diameters are presented in Figures 6.28 & 6.31. Figure 6.28 shows two different series, the first series is for steel mesh reinforcement with 8 mm diameter size for both main and cross bars while the second series is for steel mesh reinforcement with 8 mm diameter size for cross bars and 10 mm diameter size for main bars. Bars in both series are A class steel bars; it is observed that mesh with 10 mm main bars can sustain higher load and undergoes more deflection after peak load comparing with the other mesh.

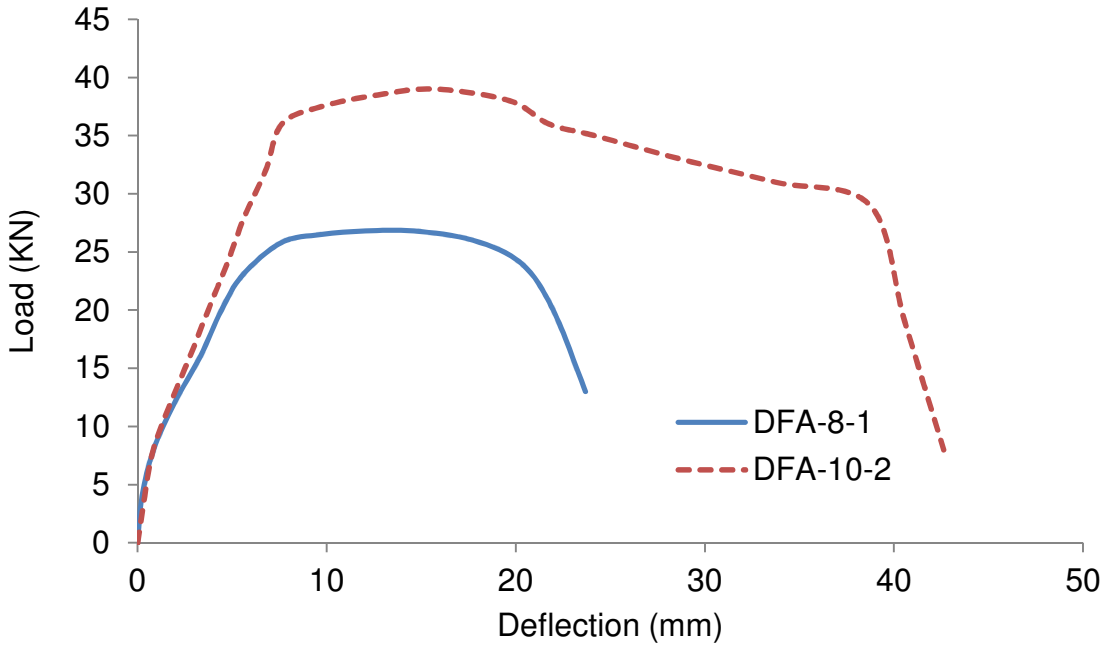

Figure 6.28: Behaviour of different main bar diameters for DFA-8 & DFA-10

Three RC beams with different main bar diameters 8, 10 and 12 mm respectively are shown in Figure 6.31. Beams reinforced with 12 mm main bars achieved the highest load while beams with 10 mm main bars showed more ductility

comparing to other beams in terms of behaviour and deflection. The deflection of RC beams with 10 mm main bars had the highest deflection when load drops to 80 % of the maximum load value. Failure modes for both beams presented in in the previous Figure are shown in Figures 6.29 & 6.30.

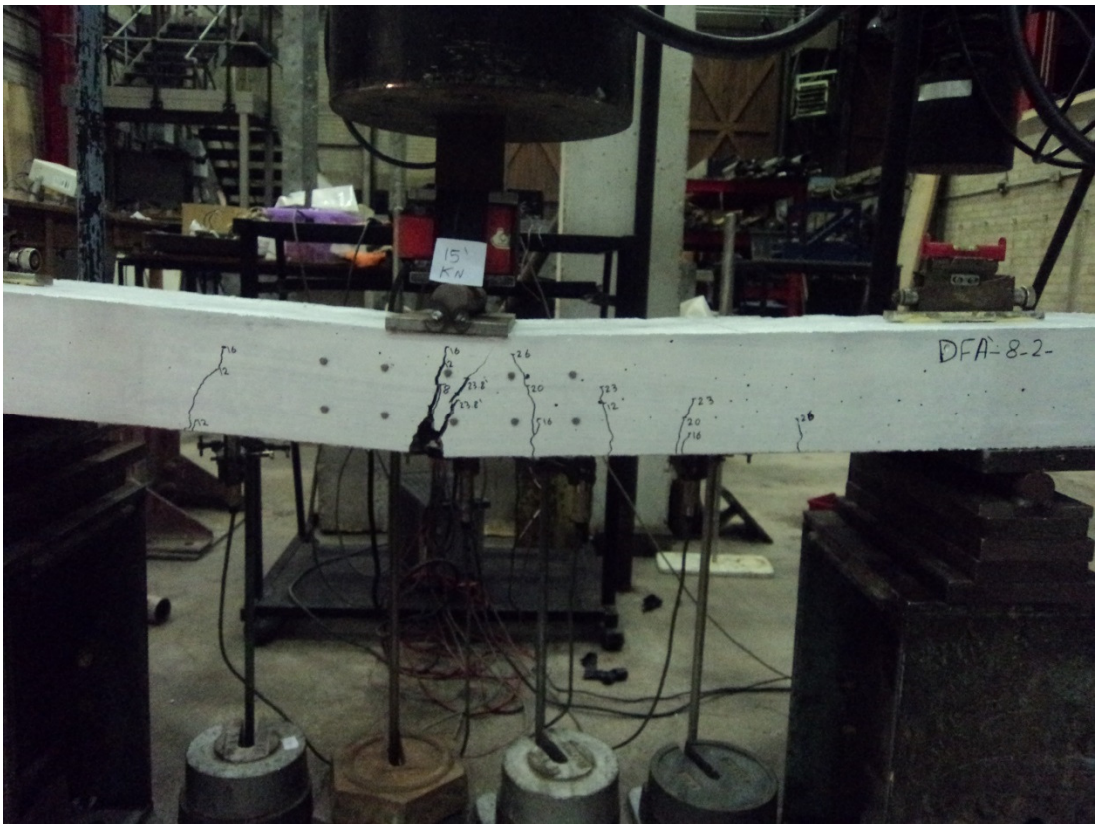

Figure 6.29: Ductility test failure mode for DFA-8

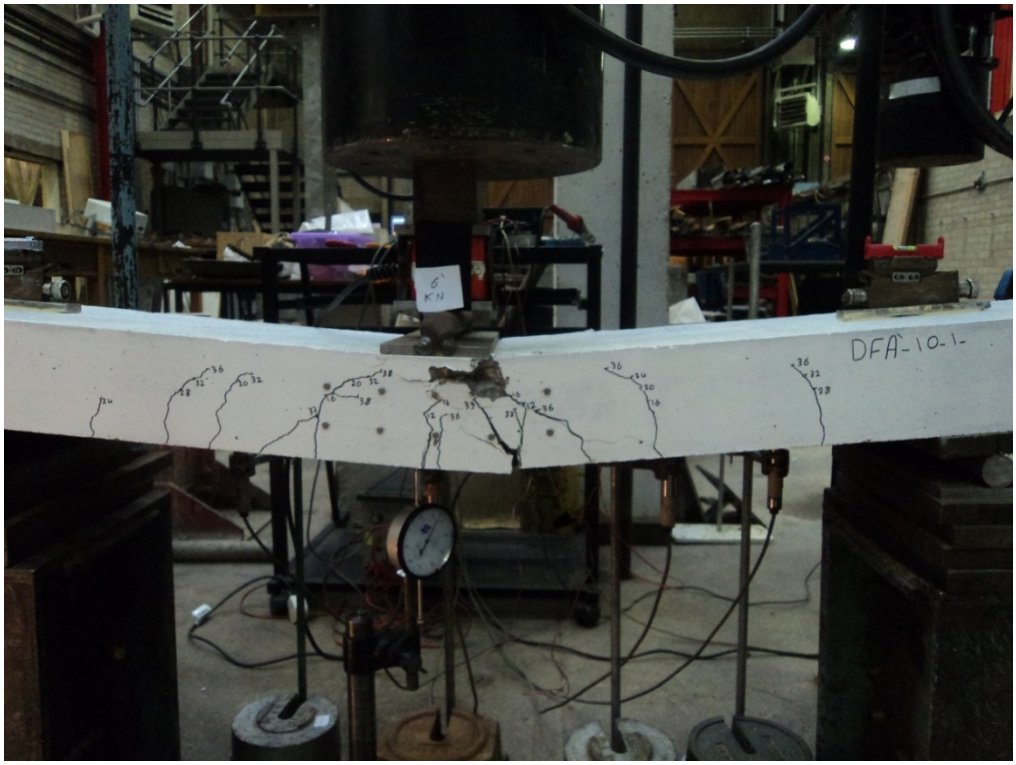

Figure 6.30: Ductility test failure mode for DFA-10

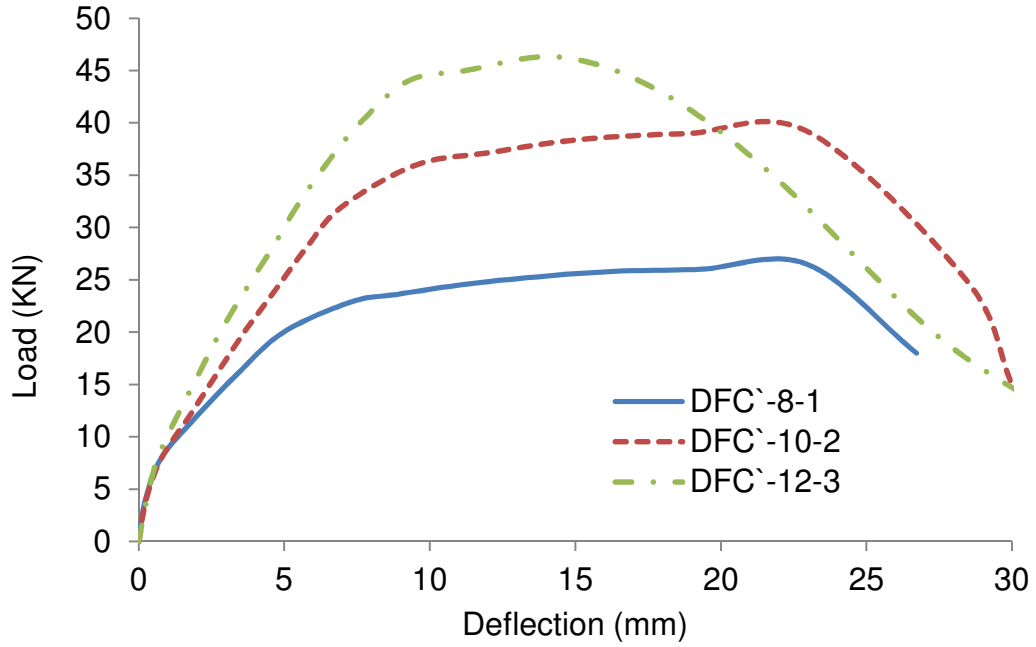

Figure 6.31: Behaviour of different main bar diameters for RC beams with class C` steel meshes and 8, 10 & 12 mm main bars diameters

The reason that the RC beam reinforced with mesh of 10 mm bars provided the best ductility is the fact that 10 mm bars provide a better moment resistance comparing to 8 mm bars. With comparison between 10 & 12 mm bars it is noticed that 12 mm bars might have reached the highest loads but with a modulus of rupture and compressive strength similar to the 10 mm mesh, that will initiate cracks easier and trig the damage of concrete more quickly, which can lead to shear failure as shown in Figure 6.34. On the other hand, beams reinforced with meshes of 10 mm main bars have suffered a joint action of moment and shear failure together; Figure 6.33 shows an example for this type of failure according to the tests done for this study. The ductile behaviour is shown in Figure 6.32 which represents the failure mode for beams reinforced with meshes of 8 mm main bars.

Analytical prediction for beams failure loads have also been carried out using same method which has been mentioned previously in section 1.2.2.5. For beams reinforced with steel meshes of 12 mm main bars, the moment failure load is between 23.8 and 43.32 KN which is less than the maximum experimental load for all beams as shown in Table 6.10

Table 6.10: Comparison between theoretical and experimental ultimate loads for beams reinforced with steel meshes

Beam	Predicted shear failure load (KN)	Predicted moment failure load (KN)	Experimental failure load (KN)
DFA-8-1	223.6	23.8	28
DFA-8-2	223.6	23.8	25.7
DFA-10-1	221.2	33.4	40.9
DFA-10-2	221.2	33.4	41.14
DFC'-8-1	259.7	23	25.23
DFC'-8-2	259.7	23	29.24
DFC'-8-3	259.7	23	27.3
DFC'-10-1	282.2	32.8	40.66
DFC'-10-2	282.2	32.8	39.5
DFC'-10-3	282.2	32.8	37.5
DFC'-12-1	269.8	43.32	46.4
DFC'-12-2	269.8	43.32	46.75
DFC'-12-3	269.8	43.32	46.6

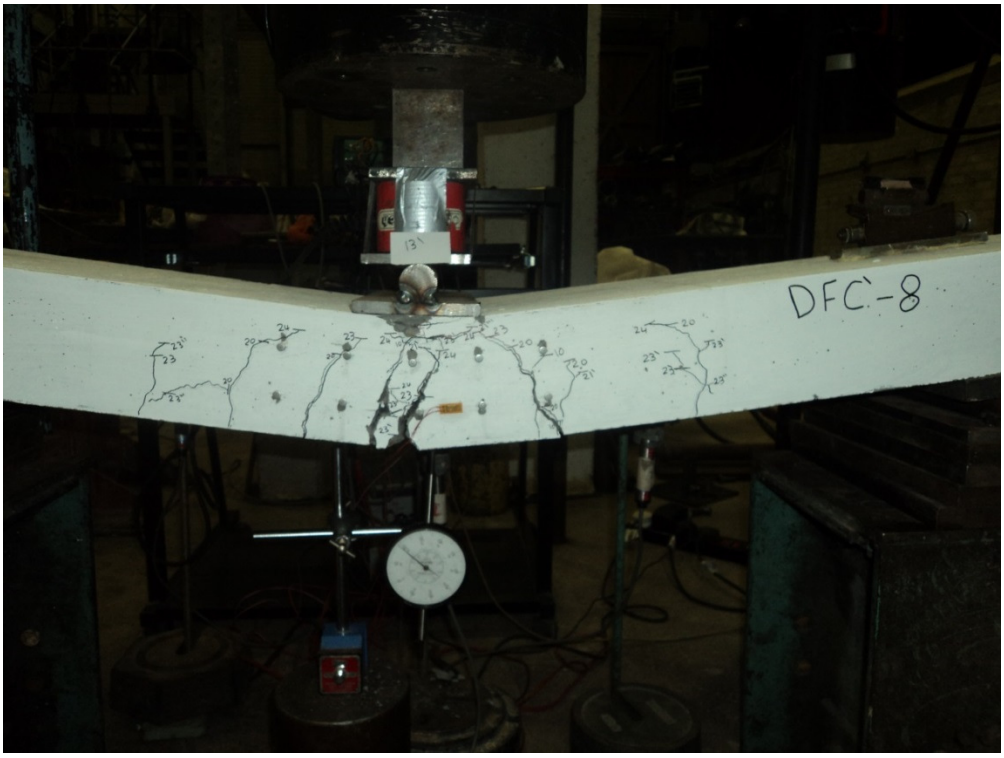

Figure 6.32: Ductility test failure mode for DFC`-8-1

Figure 6.33: Ductility test failure mode for DFC`-10-2

Figure 6.34: Ductility test failure mode for DFC`-12-2

6.3.7 Comparison based on the reinforcement steel class

Each of the Figures 6.35 & 6.36 shows the behaviour of two beams with different main steel classes

In the case of 8 mm main bars diameter, as shown in Figure 6.35, it can be noticed that the behaviour of both beams is similar although the beam reinforced with C` class can withstand slightly higher load and tolerate larger deflection. This is due to the fact that reinforcement class C` is more ductile and able to carry higher loads comparing to class A steel bars. That was proofed by testing both bar classes using Denison machine for tensile purposes and shown in Chapter 4.

By looking at the previous Figures 6.29 & 6.32 which illustrate the failure modes for both beams presented in Figure 6.35, it is obvious that beam with C` class has more cracks and larger deflection as the beam suffered higher load that during testing comparing to the beam with A class reinforcement

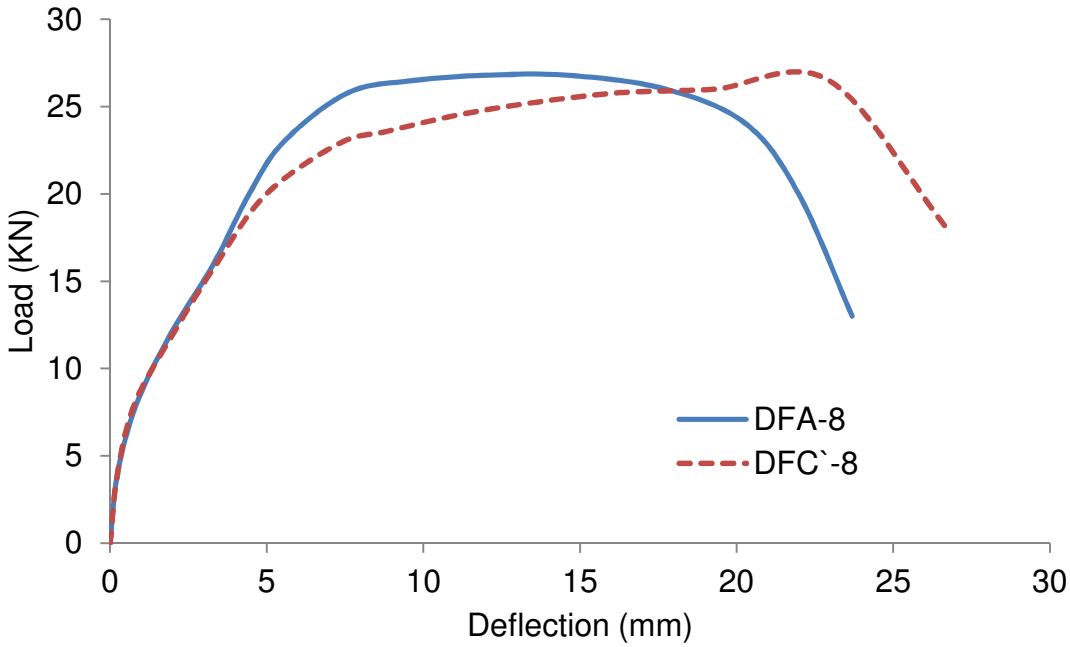

Figure 6.35: Behaviour of RC beams with meshes of classes C` & A

Beams with C` steel class and 10 mm diameter for main bars suffered a shear failure as presented in Figure 6.33, while beams with A class reinforcement had a failure which is close to moment failure as clear in Figure 6.32. This can be explained as beams with A class bars are due to fail before the deterioration of concrete which allow them to fail in a ductile manner. Figure 6.36 shows the behaviour for two beams with two different main bar classes of A and C` respectively.

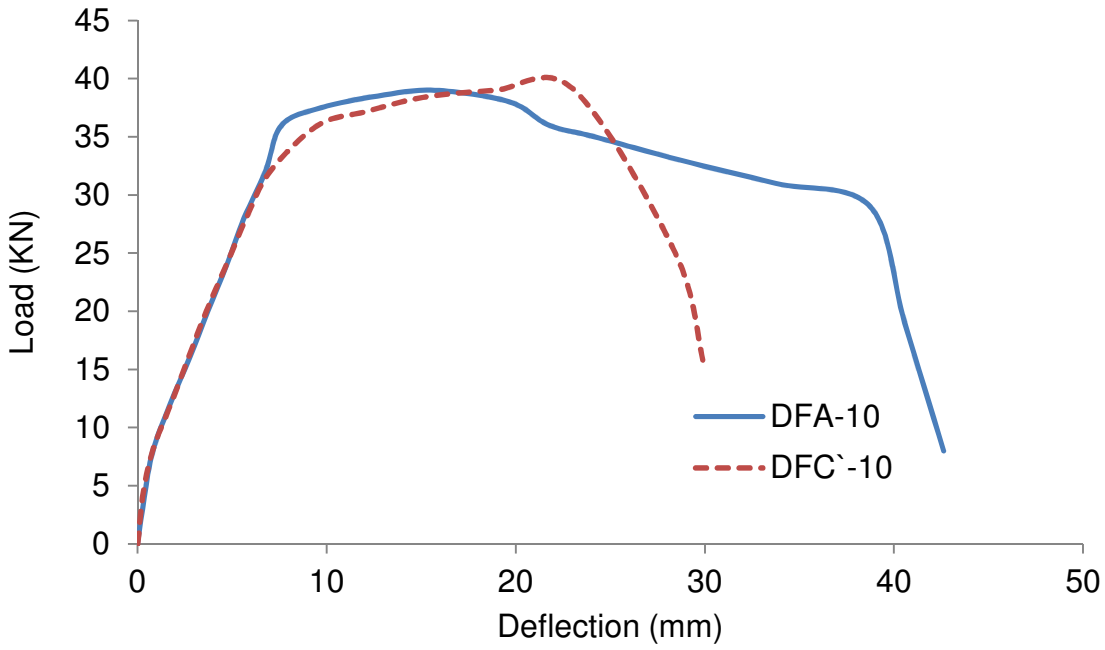

Figure 6.36: Behaviour of RC beams with meshes of classes C` & A and main bar diameter of 10 mm

6.3.8 Strain measurement of main steel bar and concrete surface

The strain of main steel bars of the reinforcing steel meshes was measured using strain gauges. Mechanical Demec gauge was used also to measure the strain of concrete. An explanation about the instruments used and installation process have been mentioned earlier in this study.

Each of the graphs in Figures 6.37 and 6.38 shows the series for two strain measurements. The first one is for the strain gauge regarding steel strain measurements which is connected to the data logger while the second series is for the concrete strain which was chosen to be at same level with the strain gauge.

It is not possible to let the strain gauge records the maximum strain value for steel as due to loading, beams will start to bend and steel will elongate which will affect either the strain gauge itself or the wires connecting it to the data logger. That will not allow keeping measuring the steel strain till end of the test as after a certain point the received readings for strain gauges will not represent the real values due to damage of wires or gauges.

It is obvious from the graphs in Figures 6.37 and 6.38 that the concrete and steel strains almost follow the same trend although higher strain values are recorded for concrete comparing to steel at failure load. This is the reason for having wider and more cracks in case of reinforcing identical beams with larger bar diameter as the concrete will be forced to sustain larger strain to comply with higher steel strain due to the larger steel diameter.

Larger steel bars can sustain larger strains and a result of that the concrete as a non-ductile material will be prone for more cracks and degradation which may lead to shear failure as happened in some tests in this study as in DFC`-10-2 & DFC`-12-2 and shown in Figures 6.28 and 6.29 respectively.

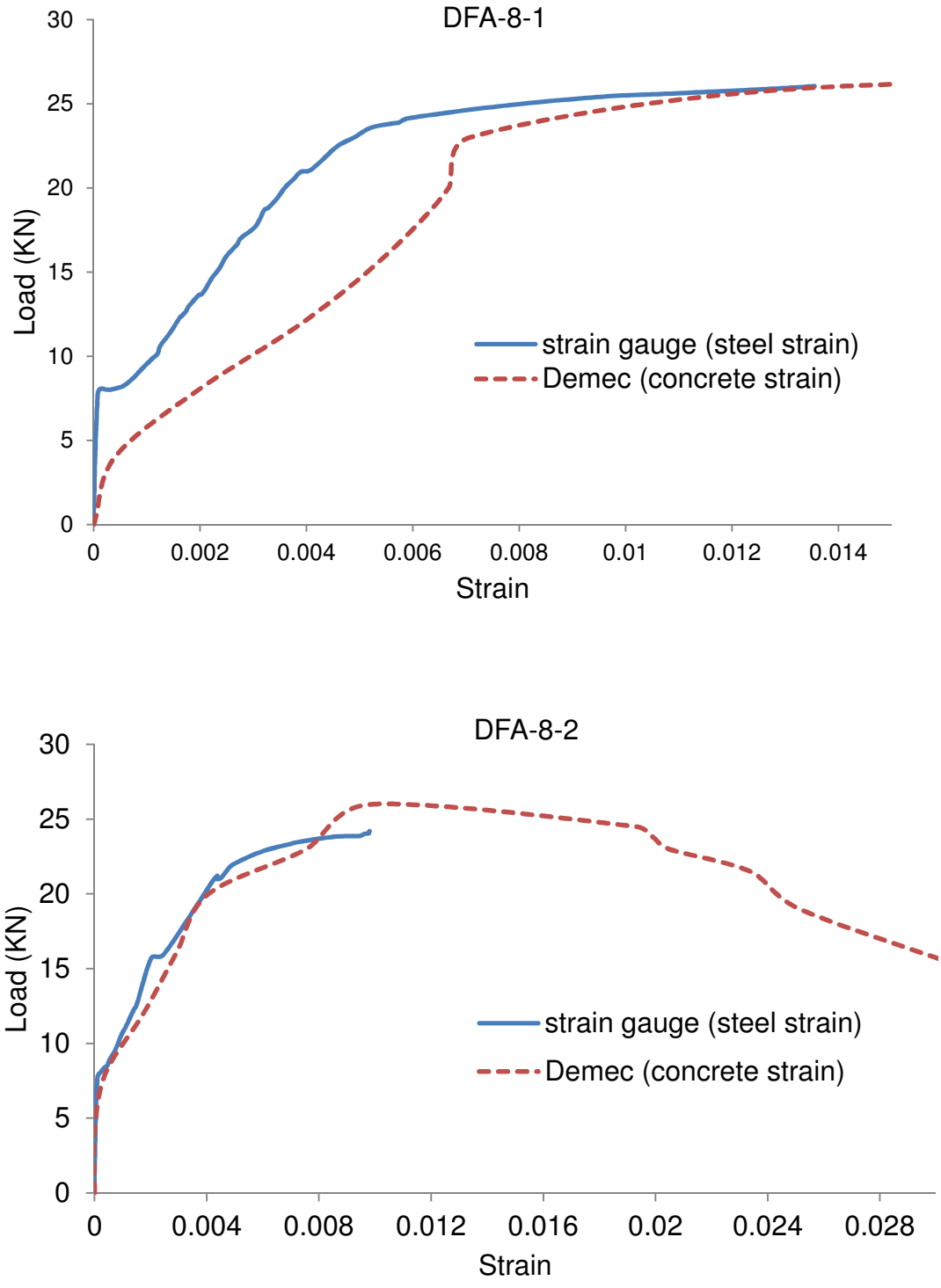

Figure 6.37: steel strain vs concrete strain graphs for RC beams with steel mesh of 8 mm main bars and steel of class A

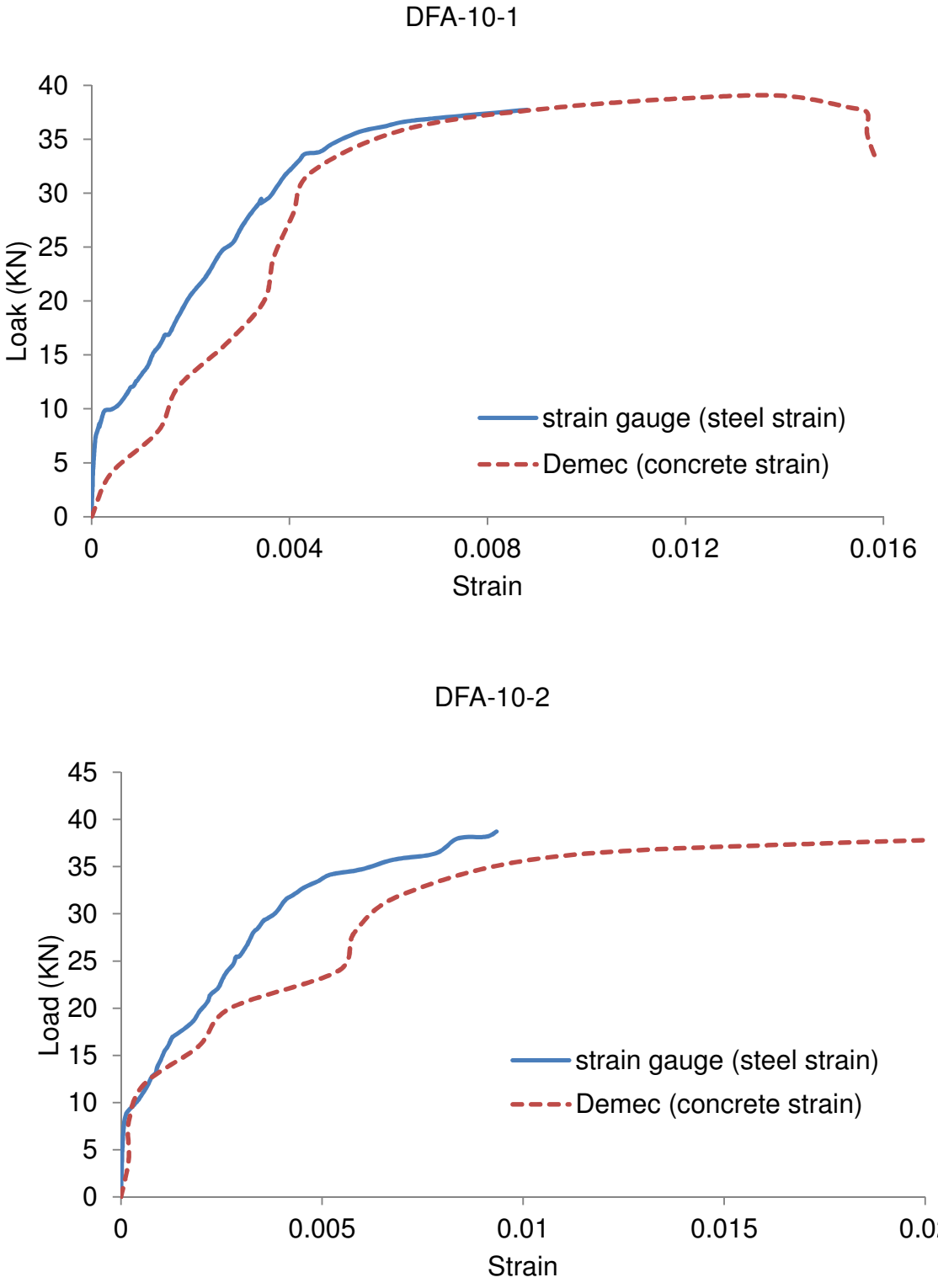

Figure 6.38: steel strain vs concrete strain graphs for RC beams with steel mesh of 10 mm main bars and steel of class A

6.4 Summary

The key findings of this chapter can be summarized as follows:

1. Ductility or rotational capacity is not related to capacity of reinforcing steel while beams with more ductile behaviour showed high yield loads.
2. Load capacities of beams reinforced with C steel are higher than beams reinforced with C` steel.
3. There is a positive correlation between the ultimate load and link spacing for C` bars, while C steel achieved almost similar ultimate load for both 100 & 150 mm link spacing with insignificant difference of 2 KN.
4. Beams reinforced with C` steel bars showed more ductility than those reinforced with standard C bars.
5. Beams with 150 mm link spacing tend to be more ductile than those confined with links at 100 mm spacing.
6. A better ductility performance is not associated with the use of larger bars as more cracks will appear due to suffering higher loads as larger bars diameters have been used.
7. RC beams with steel meshes are more ductile than beams reinforced with single bars and showed better performance in the post-peak region when load starts to drop down after reaching the maximum point.

Chapter 7: Comparison of Rotational Capacity with Existing Analytical Model

7.1 Introduction

This chapter includes calculations of rotational capacity of all beams which have been tested and presented previously in Chapter 6. Two methods are followed to calculate the rotational capacity.

Firstly, the rotational capacity is determined using the mid span deflection of each tested beam. The mid span deflection can be found in Tables 6.3 and 9 of Chapter 6. Rotational capacity is calculated by dividing the mid span deflection by half of the length of the plastic hinge zone. The suggested length of the plastic hinge zone is specified in BS EN 1992-1-1:2004 as 1.2 times beam height and shown in Figure 7.1.

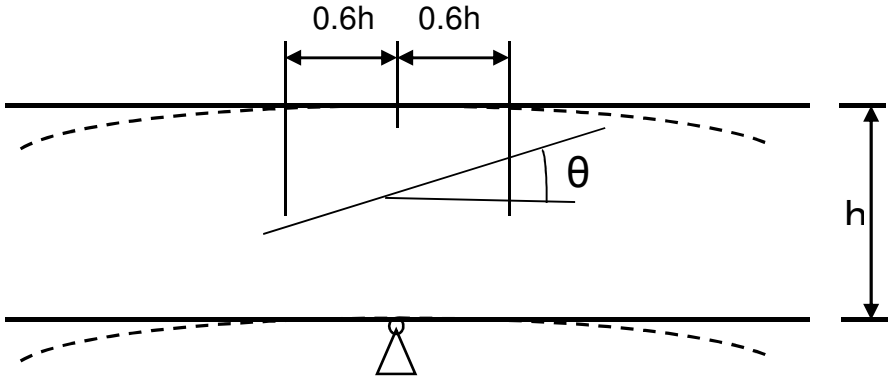

Figure 7.1: Detailed drawing for plastic hinge zone of RC continuous beams and one way slabs (BS EN 1992-1-1: 2004)

Secondly the rotational capacity is determined using numerical model developed in Hestbech's PhD thesis (2013). Hestbech has investigated the ductility of reinforced concrete structures and proposed a model to determine the rotational capacity of flexural elements.

7.2 The Concept of Hestbech Model

The concept of the model of Hestbech is shown in Figure 7.2. Hestbech has made a number of assumptions in order to develop the model as follows:

- The tensile reinforcement should yield.

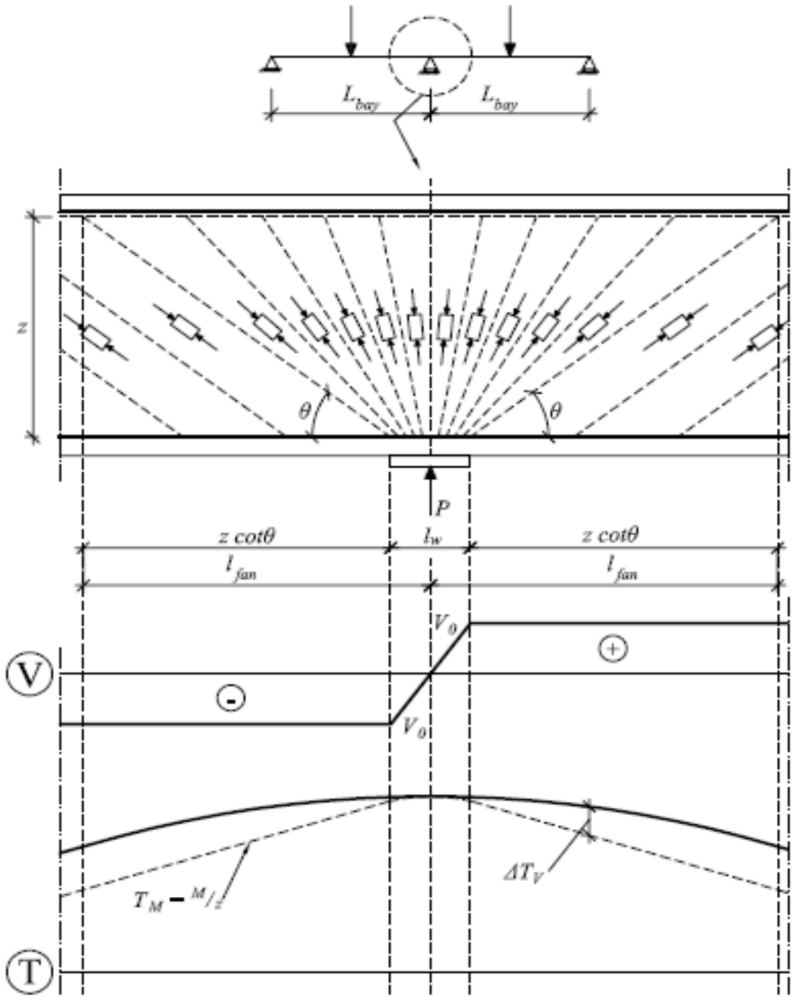

Figure7.2: The basis of the Lars model (Hestbech, 2013)

- The stress-strain relationship for reinforcement in the tension zone is bi-linear as presented in Figure 7.3. The stiffness E_{sy} and stress σ_s of the post-yield stage are determined by Equations 7.1 and 2 as follows:

$$E_{sy} = \frac{f_u - f_y}{\varepsilon_{su} - \varepsilon_{sy}} \quad (7.1)$$

$$\sigma_s = f_y + E_{sy}(\varepsilon_s - \varepsilon_{sy}) \quad (7.2)$$

where:

E_{sy}: post yield stiffness

f_u: ultimate stress of tension reinforcement

f_y: yield stress of tension reinforcement

ε_{su}: ultimate strain of tension reinforcement

ε_{sy}: yield strain of tension reinforcement

σ_s: stress of the tension reinforcement in post yield region

ε_s: strain of tension reinforcement at the point where σ_s is calculated

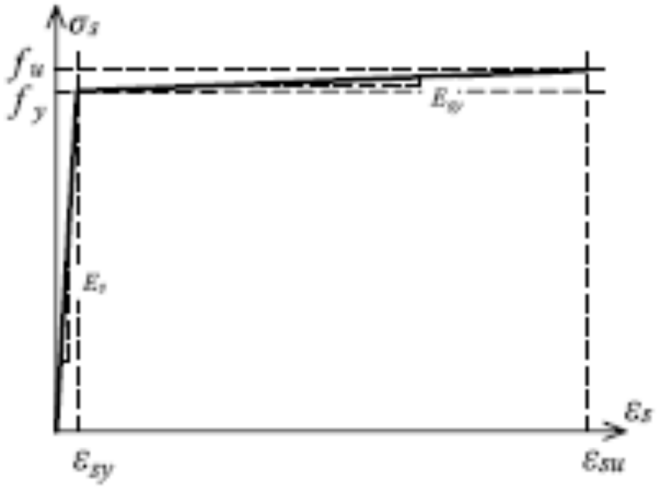

Figure 7.3: Bi-linear stress-srain relationship for tension reinforcement

- Loading plates are used at supports and loading points with specific dimensions, b & l_w. where b is the breadth of the loading plate and l_w is the width.
- The yield and failure of shear reinforcement are not allowed.
- The stresses are constant and equally distributed in shear reinforcement.
- The value of the neutral axis depth is considered from the critical cross section.

7.3 Rotational capacity calculation using numerical modelling

An example of determining the rotational capacity for one of the beams which has been examined for the purpose of this study is shown below. Explanation of the steps is also presented.

7.3.1 Procedure of determining the rotational capacity

In this section, it is demonstrated how to calculate the rotational capacity using the numerical model developed by Hestbech. The rotational capacity is determined using the following steps:

- Determine the maximum tension force T_{max}.
- Find out the variation in the tension force curve $T_{(\eta)}$.
- Consider the tension stiffening effect and adjust the tension force curve according to that.
- Calculate the rotational capacity using integration along the plastic hinge length

The maximum tension force is found from Equation 7.3 as follows:

$$T_{max} = A_s \left[f_y + E_{sy} (\varepsilon_{cu} \frac{1-\beta}{\beta} - \varepsilon_{sy}) \right] \quad (7.3)$$

Where:

A_s : area of tension reinforcement

ε_{cu}: ultimate strain of concrete

β: steel rupture

The steel rupture can be found as a relative neutral axis depth limit. The definition of the relative neutral axis limit can be found from the following expression (neutral axis depth / d).

The variation of tension force is defined in Equation 7.4 and then the tension stiffening is calculated from Equation 7.5 taking into consideration the average stiffening effect ΔT_{Ts} in Equation 7.6.

$$\Delta T_v(\eta) = \frac{V_0}{2zl_{fan}} \eta^2 \quad (7.4)$$

$$\Delta T_{TS} = \frac{1}{4} \tau x_0 O \quad (7.5)$$

$$T_{TS}(\eta) = T_{max} - \Delta T_v(\eta) - \Delta T_{TS} \quad (7.6)$$

Where:

L_{fan}: length of the stress fan.

O: summation of the circumferences of the steel reinforcement in the beam.

V_0: shear force that is related to the moment equilibrium for the critical cross section of the beam.

x_0: crack spacing (spacing between cracks).

z: distance between the centre of tension and compression reinforcement.

η: the local beam axis. It is introduced from the critical section where shear equals to zero.

Then the strain in plastic hinge zone is calculated from Equation 7.7:

$$\varepsilon_{s,p}(\eta) = \frac{\frac{T_{TS}(\eta)}{A_S} - f_y}{E_{sy}} \tag{7.7}$$

After that the cracks spacing (plastic slip) within the plastic hinge zone is calculated using integration in Equation 7.8 and finally the rotational capacity is calculated by dividing Equation 7.8 with the distance to the neutral axis as shown in Equation 7.9

$$s_p = \int_{-1/2L_p}^{1/2L_p} \varepsilon_{s,p}\ (\eta) d\eta \tag{7.8}$$

$$\alpha_p = \frac{s_p}{d - y_0} \tag{7.9}$$

The length of the plastic hinge L_p equals to double the value of η when $T(\eta)$ equals to the yield force in steel T_y.

7.3.2 Comparison between experimental and numerical rotational capacity

Tables 7.1 and 7.2 show the rotational capacities for beams reinforced with single bars and steel meshes respectively. It is shown in Table 7.1 that the predicted values of the rotational capacity are similar to the experimental values of beams reinforced with single steel bars and confined with shear links. On the other hand, it is noticed from Table 7.2 that the predicted and experimental values of the rotational

capacity of beams reinforced with steel meshes are not very close and there is a big difference revealed between both of the values. That can be explained as the model has been based on double reinforced beams confined with shear links, while beams reinforced with steel meshes can be considered as single reinforced beams, for which the model is not applicable. The other reason is that the model is based on the analysis of cracks caused by the tensile reinforcement. In case of beams reinforced with steel meshes, the cross bars cannot provide same confinement as shear links do in the other beams. Based on that, beams with mesh reinforcement are prone to more cracks and concrete deterioration which will not allow the beams to achieve the predicted rotational capacity as the predicted value is based on a proper confinement of the concrete using shear links.

Table 7.1: Rotational capacity of double reinforced beams reinforced with single steel bars

Beam set	Tested beam	Rotation based on analytical model (rad)	Rotation based on deflection (rad)
DC`-100	DC'-100-1	0.460	0.434
	DC'-100-2	0.462	0.346
	DC'-100-3	0.462	0.434
DC`-150	DC'-150-1	0.512	0.546
	DC'-150-2	0.571	0.526
	DC'-150-3	0.562	0.468
DC-100	DC-100-1	0.474	0.572
	DC-100-2	0.545	0.574
	DC-100-3	0.563	0.584
DC-150	DC-150-1	0.623	0.546
	DC-150-2	0.684	0.420
	DC-150-3	0.684	0.420

Table 7.2: Rotational capacity of beams reinforced with steel meshes

beam	Rotational capacity based on analytical model (rad)	Rotation based on deflection (rad)
DFA-8-1	0.58	0.20
DFA-8-2	0.58	0.22
DFA-10-1	0.602	0.30
DFA-10-2	0.602	0.34
DFC'-8-1	0.456	0.30
DFC'-8-2	0.456	0.36
DFC'-8-3	0.456	0.34
DFC'-10-1	0.507	0.20
DFC'-10-2	0.507	0.24
DFC'-10-3	0.507	0.16
DFC'-12-1	0.384	0.20
DFC'-12-2	0.384	0.18
DFC'-12-3	0.384	0.24

7.4 Summary

Comparison between the experimental rotational capacities of RC beams which have been recorded from tests with the rotational capacity of same beams calculated based on an analytical model. It has been found that the results are similar when beams are reinforced with steel bars and confined with shear links as the model has been developed on RC beams with same specifications as the beams used for investigation in this study. In the case of beams reinforced with steel meshes the results of the analytical model did not match with the experimental results, which indicates the need of extending the current model to include different types of reinforcement such as steel meshes.

Chapter 8: Conclusions

8.1 Introduction

This research aims to investigate the impact of steel bar properties on the bond and ductility performance of RC members. This chapter summarizes the work of the studies which have been carried out for the purpose of fulfilling the aims and objectives that were set at the very early stage of this research and stated in the first chapter of this thesis.

8.2 Main findings of this thesis regarding bond performance

It is found based on the investigations that steel bar properties can significantly affect the bond performance of RC members. The key findings of this study regarding bond interaction between steel and concrete can be stated as follows:

- Different rib patterns for steel bars of the same class, i.e. C & C`, can affect the bond performance and failure behaviour of reinforced concrete. It has been found in this study that additional longitudinal ribs can smooth the friction between steel and concrete and lead to the pull-out failure instead of splitting failure mode.
- The presence of shear links tends to increase the confinement of concrete surrounding the reinforcing bar and thus result in higher bond strength and more likely to fail with the steel bar pulled out instead of splitting failure.
- Examining the effect of shear links with different spacing finds that a notable increase in bond strength when the smaller spacing is applied.

- Bars with “better bond conditions” have better performance in terms of bond interaction. Better conditions here can be defined as: adequate concrete cover, bars placed far from the casting surface and concrete surrounding the bar to be properly compacted.
- Smaller slips are recorder for mesh reinforcement compared with the single bar reinforcement. That is due to the additional confinement that is provided by the welded cross bar.
- Larger concrete cover will render the pull-out failure and large covers will delay the splitting failure resulting in a ductile pull-out failure.

8.3 Main findings regarding ductility

Three point load test on simply supported beams reinforced with steel bars and steel meshes were conducted to investigate the effect of steel properties on the ductility behaviour and load resistance of reinforced concrete members. The outcome of this work can be categorised as follows:

- Smaller shear links spacing or in other words more shear links in RC beam results in higher failure loads for identical RC beams.
- Ductility reaches the maximum when the reinforcement ration, RR, set at relatively low level. An evidence of that are the beams reinforced with shear links at 150mm spacing exhibit larger rotations compared to the beams with identical reinforcement with shear links at 100mm spacing.
- All beams have achieved the predicted load. The maximum ratio of experimental load to the predicted load was recorded to be 1.26.

- RC beams with C` bars and shear links at 150mm spacing experienced a shear failure. That is due to the joint action of shear and flexural which result in a mixed failure.
- RC beams with steel meshes show higher peak loads when larger diameters of main bars are used.
- Beams reinforced with steel meshes of class C` and 10mm main bars showed the best ductile behaviour compared to other steel meshes consisting of 8 or 10mm main bar.
- RC beams with C class steel meshes show higher load resistance and larger deformations than beams with C class steel which suggest that the ductility and class of reinforcement can positively affect the ductility behaviour and load resistance of reinforced concrete members.
- Beams reinforced with steel meshes show better performance in terms of ductility comparing to beams with single bars reinforcement.

8.4 Comparison with analytical modelling findings

Experimental results of RC beams with single steel bars and shear links showed similarity to the predictions based on an analytical model which has been developed by Hastbech (2013). However, a large discrepancy was observed for RC beams with steel meshes. The model was derived for RC beams only containing longitudinal bars with or without shear links. Modifications of the model are required to allow for the RC beams containing steel meshes.

8.5 Future work recommendations

This work has produced important key findings for addressing the effect of different reinforcement properties on the behaviour of RC beams. Future work can be divided into two parts: first part includes an extension to the current tests to improve the statistical significance of the observations; second part concerns the establishment of numerical and analytical models.

The existing codes deal with bond or ductility as separate properties without linking them. This study showed that both of the properties are linked. For that, more tests and numerical modelling as mentioned earlier are required in order to revise the existing codes. Different amendments to the codes can be decided based on the results of the future work.

8.5.1 Extending the scope of the current tests

The current work can be extended in order to have more investigation variables and testing data. The extension of the current work can be summarized as follows

- It is recommended to test beams reinforced with steel meshes and large concrete covers to investigate their impact on the ductility of RC beams and compare with the similar study for RC beams with single bars and large concrete cover.
- Use strain gauges in pull-out tests to monitor the strain and stress distribution along the reinforcing bars during the process of testing. That gives more detailed results of bond stress distribution and can improve the understanding of the bond behaviour of steel bars during the pull-out testing.

- Study the bond behaviour of concrete blocks wrapped with FRP sheets to examine the effect of external confinement.

8.5.2 Numerical and analytical modelling

In order to gather more information that is difficult to have from the physical test, it is necessary to develop a numerical model that can reproduce the test. The model can be further extended to the RC beams reinforced with steel meshes.

The model should also be able to predict cracks development and distributions and capture the behaviour in the post-peak zone and hence investigate the effect of cracking behaviour due to the interaction of bond and the ductility performance of RC members.

An analytical model can be developed and verified using the numerical modelling and laboratory results presented in this work for the engineering estimation use. The analytical model can predict the rotational capacity of RC beams reinforced with meshes and include the effect of bond behaviour on the ductility.

References

1. ACI (American Concrete Institute). (1992) **State-of-the-Art Report on High Strength Concrete. American Concrete Institute.** Committee 363R-92, Detroit.
2. ACI (American Concrete Institue). **(1995) ACI Building Code Requirements for Reinforced Concrete**. ACI 318-95, 1995.
3. ACI 318-02 (American Concrete Institute). (2002) **Building Code Requirements for Structural Concrete and Commentary**. ACI, Farmington Hills, USA .
4. ACI 318R-02 (American Concrete Institute). (2002) **Building Code Requirements for Structural Concrete and Commentary**. ACI, Farmington Hills, USA.
5. Ahmad, S. H. Khaloo, A. R. and Poveda, A. (**1986) Shear Capacity of Reinforced High-Strength Concrete Beams**. ACI Journal, Proceedings, Vol. 83, No. 2, March-April 1986, pp. 297-305.
6. Ahmad, S.H., Lue, D.M. (1984) **Flexure-shear interaction of reinforced high-strength concrete beams**. ACI Structural Journal, Vol .84, No. 4, pp. 330-341.
7. Ahmad, S. H. and Barker, R. (1991) **Flexural Behaviour of Reinforced High-strength lightweight concrete beams**. ACI Structural Journal, Vol. 88, pp. 69-77.

8. Ahmad, S. H. et al. (1995) **Shear Ductility of Reinforced Lightweight Concrete Beams of Normal and High Strength Concrete**. Cement & Concrete Composites Vol. 17, pp. 147-159.
9. Ahmad, S. H. Hino, S. Chung, W. and Xie, Y. (1995) **An experimental technique for obtaining controlled tension failure of shear critical reinforced concrete beams**. Materials and Structures, Vol. 28, No. 1, January, pp. 8-15.
10. Ahmad S., et al (1995) **Shear Ductility of Reinforced Lightweight Concrete Beams of Normal and High Strength Concrete**. Cement & Concrete Composites (17), 147-159.
11. Almusallam, A. A. Al-Gahtani A. S. and Aziz, A. R. (1996) **Effetcs of Reinforcment Corrosion on Bond Strength**. Construction and Building Materials, Vol. 10, No. 2, pp. 123-129.
12. Al-Sulaimaini, G. J. Kaleemullah, M. Basumbal, I. A. and Rasheeduzzafar (1990) **Influence of Corrosion and Cracking on Bond Behavior and Strength of reinforced Concrete Members**. ACI Structural Journal, Vol. 87, No. 2, pp. 220-231.
13. American Concrete Institute ACI-318 (2002) **Building Code Requirements for Structural concrete and commentary**. ACI, Farmington Hills, USA.
14. American Concrete Institute ACI-408R (2003) **Bond and Development of Straight Reinforcing Bars in Tension**. ACI, Farmington Hills, USA.
15. Amleh, L. and Mirza, M. S. (2002) **Effects of Concrete W/C Ratio and Corrosion in Concrete Mix on Bond Between Steel and Concrete**.

Proceedings of the Third International Symposium on Bond in Concrete-From Research to Standards. Budapest, Hungary, pp. 285-292.

16. Azizinamini, A. Stark, M. Roller, J. J. and Gosh, S. K. (1993) **Bond Performance of Reinforcing Bars Embedded in High-Strength Concrete**. ACI Structural Journal, Vol. 90, No. 5, September-October, pp. 554-561.
17. Azizinamini, A. Chisala, M. Roller, J. H. and Ghosh, S. K. (1995) **Tension Development Length of Reinforcing Bars Embedded in High-Strength Concrete**. Journal of Engineering Structures, Vol. 17, No. 7, pp. 512-522.
18. Bamonte, P. Coronelli, D. and Gambarova, P.G. (2002) **Size Effect in High-Bond Bars**. Proceedings of the Third International Symposium on Bond in Concrete-From Research to Standards. Budapest, Hungary, pp. 43-52.
19. Beeby, A.W. (1997) **Ductility in Reinforced Concrete; Why is it needed and How is it Achieved?** The Structural Engineer, Vol. 75, No.18, pp. 311-318.
20. Beeby, A. W. (1998) **Tests to Investigate the Influence of Reinforcement Parameters on Rotation Capacity**. CEB Bulletin d' Information No. 242, Ductility of Reinforced Concrete Structures, pp. 309-332.
21. Beeby, A.W. (2004) **Why Do We Need Ductility in Reinforced Concrete Structures?** The Structural Engineer, Vol. 38, No. 5, pp. 27-29.
22. Baker, A. L. and Amarakone, A. M. (1967) **Inelastic Hyperstatic Frame Analysis**. American Concrete Institute.
23. Bartos, P. (1982) **Bond in Concrete**. London: Applied Science.

24. Bazant, Z. P. and Desmorat, R. (1994) **Size Effect in Fiber or bar Pull-out with Interface Softening Slip.** ASCE Journal of Engineering Mechanics, Vol. 120, No. 9, pp. 1945-1962.
25. British Standard Institution (1997) BS 8110-1:1997 **Structural Use of Concrete**. Part 1: Cod of Practice for Design". London
26. British Standard Institution (2007) BS EN 10079:2007 **Definition of Steel Products**. London
27. British Standard Institution (2004) **UK National Annex to EN 1992-1-1:2004: UK National Annex to Euro code 2**, Design of Concrete Structures. London
28. British Standard Institution (1997). BS 8110-1:1997: **Structural Use of Concrete. Part 1: Code of Practice for Design**.
29. British Standard Institution (2004). **UK National Annex to EN 1992-1-1:2004:" UK National Annex to Euro code 2**, Design of Concrete Structures.
30. British Standard Institution (2006). **Welding of Reinforcing Steel, BS EN ISO 17660-1:2006,** Part 1: Load-bearing Welded Joints.
31. British Standard Institution (2009). **Testing hardened Concrete, BS EN 12390-2:2009,** Part 2: making and Curing Specimens for Strength Tests.
32. British Standard Institution (2009). **Testing hardened Concrete, BS EN 12390-3:2009,** Part 3: Compressive Strength of Test Specimens.
33. British Standard Institution (2009). **Testing hardened Concrete, BS EN 12390-5:2009,** Part 5: Flexural Strength of Test Specimens.
34. British Standard Institution (2009). **Testing hardened Concrete, BS EN 12390-6:2009,** Part 6: Tensile Splitting Strength of Test Specimens.

35. British Standard Institution (2013).**Concrete-Specification, Performance, Production and Conformity, BS EN 206-2013**.
36. Cairns J. and Abdullah R. (1994) **Fundamental Tests on the Effect of an Epoxy Coating on Bond Strength**. ACI Materials Journal, July-August, No.91, pp. 331-338.
37. Cairns J. and Abdullah R. (1996) **Bond strength of Black and epoxy-coated reinforcement-A theoretical approach**. ACI Materials Journal, July-August, No.93, pp. 1-9.
38. Cairns J. and Jones, K. (1995) **Influence of Rib Geometry on Strength of Lapped Joints: An Experimental and Analytical Study**. Magazine of Concrete Research, V. 47, No. 172, September, pp. 253-262.
39. Cairns J. and Jones K. (1995) **The Splitting Forces Generated by Bond**. Magazine of concrete research, Vol. 47, No. 171, pp. 153-165.
40. Cairns J. and Plizzari G. A. (2003) **Towards a Harmonized European Bond Test**. Materials and Structures, Oct, Vol.36, pp. 498-506.
41. Cairns, J. and Plizzari, G. A. (2002) **Do We Need a Standard Test for Bond**. Proceedings of the Third International Symposium on Bond in Concrete-From Research to Standards. Budapest, Hungary, pp. 259-267
42. Carreira, D. J. and Chu, K. H. (1986) **The Moment–Curvature Relationship of Reinforced Concrete Members**. ACI Structural Journal, Vol. 83, No. 2, pp. 191–198.
43. CEB-FIP (1990) **Model code for Concrete Structures**. Comite Euro-International du Beton. c/o Thomas Telford, London.

44. CEB-FIP (1999) **Lightweight Aggregate Concrete, Codes and Standards**. State-of-Art Report prepared by Task Group 8.1, Federation Internationale du Beton. Lausanne, Switzerland.
45. CEB-FIP (2000) **Bond Reinforcement in Concrete**. State-of-Art Report prepared by Task Group 2.5, Federation Internationale du Beton. Lausanne, Switzerland.
46. Clark L.A. and Cope R.J. (1984) **Concrete Slabs Analysis and Design** Elsevier Applied Science Publishers Ltd., London.
47. Committee Euro-International du Beton (1967). **Recommendations for Design and Construction of Large Panel Structures**. CEB-FIP Bulletin d' information No. 60.
48. Corley, W. G. (1966) **Rotational Capacity Of Reinforced Concrete Beams**. Journal of the Structural Division, ASCE, Vol. 92, No. ST5, pp. 121-146.
49. Darwin, D. and Graham, E. K. (1993) **Effect of Deformation Height and Spacing on Bond Strength of Reinforcing Bars**. ACI Structural Journal, November-December, Vol. 90, No. 6, pp. 646-657.
50. Darwin, D. and Graham, E. K. (1993) **Effect of Deformation height and Spacing on Bond Strength of Reinforcing Bars.** SL-Report, University of Kansas Center for Research, Lawrence, kansas, January, pp. 68.
51. Darwin, D. Idun, E. K. Zuo, J. and Tholen, M. L. (1998) **Reliability-Based Strength Reduction Factor for Bond**. ACI Structural Journal, July-August, Vol. 95, No. 4, pp. 434-443.
52. Darwin, D. McCabe, S. L. Idun, E. K. and Schoenekase, S. P. (1992) **Development Length Criteria: Bars Not Confined by Transverse**

Reinforcement. ACI Structural Journal, November-December, Vol. 89, No. 6, pp.709-720.

53. Darwin, D. McCabe, S. L. and Brown, C. J. (1993) **Fracture Analysis of Steel-Concrete Bond**. Structural Engineering and Engineering Materials, SM report No. 36.
54. Darwin, D. Tholen, M. L. Idun, E. K. and Zuo, J. (1996a) **Splice Strength of High relative Rib Area Reinforcing Bars**. ACI Structural Journal, January-February, Vol. 93, No. 1, pp.95-107.
55. Darwin D. Tholen, M. L. Idun, E. K. and Zuo, J. (1996b) **Development length criteria for conventional and high relative rib area reinforcing bars**. ACI Structural Journal, May-June, Vol. 93, No. 3, pp. 347-359.
56. Darwin D. and Zuo, J. (2002) **Discussion of Proposed Changes to ACI 318 in "ACI 318-02 Discussion and Closure**. Concrete International, January, Vol. 24, No. 1, pp. 97-101.
57. Du, Y. et al (2008). **The Ductility of Concrete Beams Reinforced with Reinforcement of Ductility Classes A, B and C**. University of Birmingham.
58. Duthinh D. Carino, N.J. (1996) **Shear design of high-strength concrete beams: a review of the state-of-the-art**. Building and Fire Research Laboratory. National Institute of Standards and Technology.
59. Elzanaty, A.H. Nilson, A. H. and Slate, F.O. (1986). **Shear Capacity of Reinforced Concrete Beams Using High-Strength Concrete**. ACI Journal, Proceedings, Vol. 83, No. 2, March-April, pp. 290-296 **.**

60. Esfahani, M. R. and Vijaya Rangan, B. V. (1996) **Studies on Bond between Concrete and Reinforcing Bars**. School of Civil Engineering, Curtin University of technology, Perth, Western Australia, 315 pp.

61. Esfahani, M. R. and Vijaya Rangan, B. V. (1998a) **Local Bond Strength of Reinforcing Bars in Normal Strength and High-Strength Concrete (HSC)**. ACI Structural Journal, March-April, Vol. 95, No. 2, pp. 96-106.

62. Esfahani, M. R. and Vijaya Rangan, B. V. (1998b) **Bond between Normal Strength and high-Strength Concrete (HSC) and reinforcing Bars in Splices in Beams**. ACI Structural Journal, May-June, Vol. 95, No. 3, pp. 272-280.

63. Euro code 2 (2004) BS1992-2:2004, **Design of Concrete Structures.**

64. Gilbert, R. I. (2006) **Ductility of Reinforced Concrete Slabs, the Effects of Strain Localization**. Federation International du Béton. Proceedings of the 2nd International Congress, June 5-8, 2006 – Naples, Italy, pp. 12.

65. Gilbert, R. I. and Smith, S. T. (2006) **Strain Localization and its Impact on the Ductility of Reinforced Concrete Slabs Containing 500 MPa Reinforcement**. Advances in Structural Engineering, Vol. 9 No. 1, pp. 117–127.

66. Giroldo, F. and Bailey, C. G. (2008) **Experimental bond behavior of welded mesh reinforcement at elevated temperature.** Magazine of Concrete Research, Vol. 60, No. 1, February, pp. 23-31.

67. Gjorv, O. E. Monteiro, P. J. M. and Mehta, P. K. (1990) **Effect of Condensed Silica Fume on the Steel-Concrete Bond**. ACI Materials Journal, November-December, Vol. 87, No. 6, pp. 573-580.

68. Gorst, N. and Clark, L. (2003) **Effects of traumatize on bond strength of reinforcement in concrete**. Cement & Concrete Composite, Vol. 25.

69. Goto Y. (1971) **Cracks formed in concrete around deformed tension bars**. ACI Structural Journal. Vol. 68, No. 4, pp. 241-251.

70. Hamad S. (1995) **Bond strength improvement of reinforcing bars with specially designed rib geometries**. ACI Structural Journal, January-February, No. 92, pp. 3-13.

71. Hamad S. (1995) **Comparative bond strength of coated and uncoated bars with different rib geometries**. ACI Materials Journal, November-December, No. 92, pp. 579-590.

72. Hamad S. (1998) **Bond strength improvement of reinforcement in high-performance concrete: the role of silica fume, casting position and super plasticizer Dosage**. ACI Materials Journal, September-October, No. 95, pp. 499-511.

73. Hamad S. (2004) **Experimental and analytical evaluation of bond strength of reinforcement in fiber-reinforced polymer-wrapped high-strength concrete beams**. ACI Structural Journal, November-December, No. 101, pp. 747-754.

74. Hamad S. et al. (2004) **Bond strength improvement of reinforcing bars with specially designed rib geometries**. Journal of Composites for Construction © ASCE, January-February, pp. 14-21.

75. Haskett, M. Oehlers, D. J. and Mohamed Ali, M. S. (2008) **Local and Global Bond Characteristics of Steel Reinforcing Bars**. Engineering Structures, No. 30, pp. 376-383.

76. HO, J .C .M. KWAN, A. K. H. and PAM, H. J. (2003) **Theoretical Analysis of Post-Peak Flexural Behaviour of Normal- and High-Strength Concrete Beams**. Structural Design of Tall and Special Buildings, Vol. 12, No. 2, pp. 109–125.

77. HO, J. C. M. KWAN, A. K. H. and PAM, H. J. (2004) **Minimum Flexural Ductility Design of High-Strength Concrete Beams**. Magazine of Concrete Research, Vol. 56, No. 1, pp. 13–22.

78. HO, J. C. M. AU, F. T. K. and KWAN, A. K. H. (2005) **Effects of Strain Hardening of Steel Reinforcement on Flexural Strength and Ductility of Concrete Beams**. Structural Engineering and Mechanics, Vol. 19, No. 2, pp. 185–198.

79. Ian, G. R. and Sakka, Z. I. (2010) **Strength and Ductility of Reinforced Concrete Slabs Containing Welded Wire Fabic and Subjected to Support Settlement**. Engineering Structures, Vol. 32, March, pp. 1509-1521.

80. Izzuddin, B. A. et al. (2004) **Ductility Assessment for an Idealized Elastic-Plastic Structural System Subject to an Instantaneous Applied Load**. Imperial College London.

81. Joop A. den Uijl, Agnieszka J. Bigaj (1996) **A bond model for ribbed bars based on concrete confinement**. Heron, Vol. 41, No. 3, pp. 201-226.

82. Jirsa, J. O. and Breen, J. E. (1981) **Influence of Casting position and shear on Development and Splice Length Design Recommendation**. Research Report No. 242-3F, Center for Transportation research, the University of Texas at Austin, Texas.

83. Kachlakev, D. and McCurry, D. D. (2000) **Behavior of Full-Scale Reinforced Concrete beams Retrofitted for Shear and flexural with FRP laminates**. Composites part B: Engineering, Vol. 31, April, pp. 445-452.

84. Kuang, J. S. and Atanda, A. I. (2005) **Enhancing Ductility of Reinforced Concrete Frame Buildings**. Proceedings of the Institution of Civil Engineering, Vol. 158, No. SB4, August, pp. 253-265.

85. Kulkarni, S. M. and Shah S. P. (1998) **Response of Reinforced Concrete Beams at High Strain Rates**. ACI Structural Journal, Vol. 95, No. 6, November-December, pp. 705-715.

86. Kwan, A. K. H. Ho, J. C. M. and Pam, H. J. (2002**) Flexural Strength and Ductility of Reinforced Concrete Beams.** Proceedings of the institution of Civil Engineer Structures & Buildings Vol. 152, No. 4, November, pp. 361-369.

87. Kwan, A. K. H. HO, J. C. M. and PAM, H. J. (2004) **Effects of Concrete Grade and Steel Yield Strength on Flexural Ductility of Reinforced Concrete Beams**. Australian Journal of Structural Engineering, Vol. 5, No. 2, pp. 119–138.

88. Kwan, A. K. H. AU, F. T. K. and CHAU, S. L. (2004) **Theoretical Study on Effect of Confinement on flexural Ductility of Normal and High-Strength Concrete Beams**. Magazine of Concrete Research, Vol. 56, No. 5, pp. 299–309.

89. Kwan, A. K. H. Chau, S. L. Au, F. T. K. (2006**) Improving Flexural Ductility of High-Strength Concrete Beams.** Proceedings of the institution of Civil Engineer Structures & Buildings, Vol. 159, No. SB6, December, pp. 339-347.

90. Lars, H. (2013) **Ductility of Reinforced Concrete Structures in Flexure.** Department of Engineering, Faculty of Science, AARHUS University, Denmark.

91. Leon R., (1998) **Bond and Development of Reinforcement**. Farmington Hills, Michigan, American Concrete Institute.

92. Li, Z. Ohno, Y. and Suzuki, K. (1994) **Effects of Bond Creep and Shrinkage on Long-term Crack Width of Reinforced Concrete beams**. Proceedings of Japan Concrete Institute, Vol. 16, No. 2, pp. 407-412.

93. Luke, J. J. Hamad, B. S. Jirsa, J. O. and Breen, J. E. (1981) **Influence of Casting position and shear on Development and Splice Length of Reinforcing Bars**.

94. Lutz, L. A. Gergely, P. and Winter, G. (1966) **The Mechanics of Bond and Slip of Deformed reinforcing Bars in Concrete**. Report No. 324, Department of Structural Engineering, Cornell University, Ithaca, New York, November, pp. 711-721.

95. MacGregor, J. G. and Bartlett. (2000) **Reinforced Concrete: Mechanics and Design**. 1st Canadian Edition. Prentice Hall Canada Inc., Scarborough, Ontario.

96. Malvar, J. (1992) **Bond of Reinforcement under Controlled Confinement**. ACI Materials Journal. Vol. 89, No. 6, pp. 593-601.

97. Mander, B. J. Priestley, J. N. M. and Park, R. (1988) **Theoretical Stress-Strain Model for Confined Concrete**. ASCE Journal of Structural Engineering, Vol. 144, No. 8, 1804-1826.

98. Mansur M, A. Chin, M. S. and Wee, T. H. (1997) **Flexural Behaviour of High-Strength Concrete Beams**. ACI Structural Journal, Vol. 94, No. 6, pp. 663–674.

99. Mendis P. A. and French C. W. (2000) **Bond Strength of reinforcement in High Strength Concrete**. Advances in Structural Engineering Journal, Vol. 3, Vo. 3, pp. 245-253.

100. Mirza, S. A. and Macgregor, G. (1981) **Strength and Ductility of Concrete Slabs Reinforced with Welded Wire Fabric**. Proceedings of the ACI Structural Journal, Vol. 78, No. 5, September-October, pp. 374-381.

101. Mo, Y. L. and Chan, J. (1996) **Bond and Slip pf Plain Rebar in Concrete**. Journal of material in Civil Engineering, Vol. 8, No. 4, pp. 208-211.

102. Moghaddam, H. A. and Samadi, M. (2009) **On the Effect of Ductility of Confining Material on Concrete Ductility**. Proceedings of the Structures Congress: Do not Mess with Structural Engineers, pp. 259-269.

103. Mphonde, Andrew G. and Franz, Gregory C. (1984) **Shear Test of High and Low-Strength Concrete Beams without Stirrups**. ACI Structural Journal, Vol. 81, No. 4, pp.350-357.

104. National Institution of Standards and Technology, (NISTIR 7396). (2007) **Best Practices for Reducing the Potential for Progressive Collapse in Buildings**. USA: Department of Commerce.

105. Neville, A. M. and Brooks, J. J. (1987) **Concrete technology**. New York: John Wiley & Sons, Inc.

106. Neville, A. M. (1995) **Properties of Concrete.** 4th ed. London: Wiley.

107. Okelo R., Yuan, R. (2005) **Bond strength of fiber reinforced polymer rebar in normal strength concrete**. Journal of Composites for Construction, May-June, pp. 203-213.

108. Ogura, N. Bolander, J. E. and Ichinose, T (2008) **Analysis of Bond Splitting Failure of Deformed bars within Structural Concrete**. Journal of Engineering Structures, Vol. 30, pp. 428-435.

109. Orangun, C. O. Jirsa, J. O. and Breen, J. E. (1975) **The Strength of Anchored Bars: A reevaluation of Test Data on Development length and Splices**. Research report No. 154-3F, Center for Highway Research, the University of Texas at Austin, Texas, January, 18 pp.

110. Orangun, C. O. Jirsa, J. O. and Breen, J. E. (1977) **Reevaluation of Test Data on Development Length and Splices**. ACI Journal, March, Vol. 74, No. 3, pp. 114-122.

111. Pam, H. J. Kwan, A. K. H. Islam, M. S. (2001) **Flexural Strength and Ductility of reinfored Normal- and High-Strength Concrete Beams**. Proceedings fo the Institution fo Civil Engineering, Vol. 146, No. 4, November, pp. 381-389.

112. PAM, H. J. KWAN, A. K. H. and HO, J. C. M. (2001) **Post-Peak Behaviour and Flexural Ductility of Doubly Reinforced Normal- and High-Strength Concrete Beams**. Structural Engineering and Mechanics, Vol. 12, No. 5, pp. 459–474.

113. Park, R. and Paulay, T. (1975) **Reinforced Concrete Structures**. John Wiley & Sons, New York.

114. Park, R. and Gamble, W. L. (1980) **Reinforced Concrete Slabs**. John Wiley and Sons, New York, pp. 618.

115. Park R. (1988) **Ductility Evaluation from Laboratory and Analytical Testing.** Proceedings of the 9th World Conference on Earthquake Engineering, Vol. VIII, Tokyo–Kyoto, pp. 605–616.

116. Pecce, M. (1998) **Experimental Evaluation of Rotation Capacity of HPC Beams**. CEB Bulletin d' Information No. 242, pp. 197-210.

117. Prakhya, G. K. V. and Morley, C. T. M. (1990) **Tension stiffening and moment-curvature relations of reinforced concrete elements**. ACI Structural Journal, 1990, 87, No. 5, pp. 597–605

118. Purkiss, J. (2006) **Concrete Design. Second edition**, Butterworth-Heinemann pp. 115-119.

119. Plizzari G. A., Deldossi M. A., Massimo S. (2002) **Transverse reinforcement effects on anchored deformed bars**. Magazine of concrete, April, Vol. (50), pp. 161-177.

120. Skorobogatov, S. M. and Edwards, A. D. (1979) **The Influence of the Geometry of Deformed Steel Bars on Their Bond Strength in Concrete**. The Institution of Civil Engineers, Vol. 67, Part 2, June, pp. 327-339.

121. Rudi, M. (2008) **Progressive Collapse for Connections in Reinforced Concrete structure.** Department of Engineering, faculty of Science University of Birmingham, United kingdom.

122. Research Report No. 242-1, Center for Transportation research, the University of Texas at Austin, Texas, June, 153 pp.

123. Saatcioglu, M. and Razvi, S. R. (1992) **Strength and Ductility of Confined Concrete.** Journal of Structural Engineering, ASCE, Vol. 118, No. 6, pp. 1590–1607.

124. Sanad, A. I. Saka, M. P. (2001) **Prediction of ultimate shear strength of reinforced concrete deep beams using neural networks**. Journal of Structural Engineering, July 2001.

125. Sebastian, W. and Zhang, C. (2008) **Analysis of Concrete Structures Axross the Ductility Spectrum**. Magazine of Concrete Research, Vol. 60, No. 9, November, pp. 685-690.

126. SHIN, S. W. GHOSH, S. K. and MORENO, J. (1989) **Flexural Ductility of Ultra-High Strength Concrete Members**. ACI Structural Journal, Vol. 86, No. 4, pp. 394–400.

127. Skorobogatov, S. M. and Edwards, A. D. (1979) **The Influence of the Geometry of Deformed Steel Bars on Their Bond Strength in Concrete**. The Institution of Civil Engineers, Vol. 67, Part 2, June, pp. 327-339.

128. Sule, M. and van der Veen, C. (2002) **Development of Bond Between Reinforcemetn Steel and early Age Concrete**. Proceedings of the Third International Symposium on Bond in Concrete-From Research to Standards. Budapest, Hungary, pp. 277-284.

129. Tastani, S. P. and Pantazopoulou, S. J. (2002) **Experimental Evaluation of the Direct Tension Pullout Bond Test**. Proceedings of the Third International Symposium on Bond in Concrete-From Research to Standards. Budapest, Hungary, pp. 268-276.

130. Tastani, S. P. and Pantazopoulou, S. J. (2010) **Direct tension Pullout Bond Test: Experimental results**. Journal of Structural Engineering, Vol. 136, No. 6, pp. 731-743.

131. Tastani, S. P. and Pantazopoulou, S. J. (2013) **Reinforcement and Concrete Bond: State determination along the Development length**. Journal of Structural Engineering, September, Vol. 139, pp. 1567-1581.

132. Tepfers, R. (1973) **A Theory of Bond Applied to Overlapping Tensile Reinforcement Splices for Deformed Bars**. Division of Concrete Structures, Chalmers University of Technology, Goteborg, Sweden, 328 pp.

133. Tepfers R. (1979) **Cracking of concrete cover along anchored deformed reinforcing bars**. Magazine of concrete research, Sep, Vol. 32, No.112.

134. Tepfers R. (1980) **Bond stress along lapped reinforcing bars**. Magazine of concrete research, March, Vol. 31, No.106.

135. Tepfers R., et al (2000) **State of art report, bond of reinforcement in concrete, CEB Bulletin d' Information**. International federation of structural engineering (fib). Lausanne, Switzerland. Chapters 1 & 8.

136. Tepfers R., L. De Lorensiz (2003) Bond of FRP reinforcement in concrete- A challenge. Mekhanika Kompozitnykh Materialov, Vol. 39, No. 4, pp. 477-496.

137. Vogel, T. and Schenkel, M. (2002) **Bond Behavior of reinforcement with Inadequate Cover**. Proceedings of the Third International Symposium on Bond in Concrete-From Research to Standards. Budapest, Hungary, pp. 359-366.

138. Wafa, F. F. and Ashour, S. A. (1992) **Mechanical Properties of High-Strength Fiber Reinforced Concrete**. ACI Materials Journal, September-october, V. 89, No. 5, pp. 449-455.

139. Zekany, A. J. Neumann, S. Jirsa, J. O. and Breen, J. E. (1981) **The Influence of Shear on Lapped Splices in Reinforced Concrete**. Research Report 242-2, Center for Transportation Research, Bureau of Engineering Research, University of Texas at Austin, Texas, July, 88 pp.

140. Walker, P. R. Batayneh, M. K. and Regan, P. E. (1997) **Bond strength tests on deformed reinforcement in normal weight concrete**. Journal of Materials and Structures, August-September, Vol. 30, pp. 424-429.

141. Wang, H. (2009) **An Analytical Study of Bond Strength Associated with Splitting of Concrete Cover**. Journal of Engineering Structures, Vol. 31, pp. 968-975.

142. Williamson S. (1999). **The influences of concrete cover properties on the effect of reinforcement corrosion**. PhD thesis, University of Birmingham.

143. Wu, Y. F. and Zhao, X. M. (2013) **Unified Bond Stress-Slip Model for reinforced Concrete**. Journal of Structural Engineering, November, Vol. 139, pp. 1951-1962.

144. Yamao, Y. Chou, L. and Niwa, J. (1984) **Experimental Study of Local Bond-Slip Relationship**. Proceedings of Japan Society of Civil Engineers, No. 343, pp. 219-228.

145. Yalciner, H. Eren, O. and Sensoy, S. (2012) **An Experimental Study on the Bond Strength Between Reinforcement bars and Concrete as a**

Function of Concrete Cover, Strength and Corrosion Level. Cement and Concrete Research, Vol. 42, pp. 643-655.

146. Zsutty, T. C. (1968) **Beam Shear Strength Prediction by Analysis of Existing Data**. ACI Journal, Proceedings, Vol. 65, No. 11, November, pp. 943-951.

147. Zuo, J. Darwin, D. (2000) **Splice strength of conventional and high relative rib area bars in normal and high-strength concrete**. ACI Structural Journal, July-August, No.97, pp. 630-641.

148. Zuo, J. and Darwin, D. (1998) **Bond Strength of High Relative Rib Area Reinforcing Bars**. SM Report No. 46, University of Kansas Center for Research, Lawrence, Kansas, 350 pp.

149. Zuo, J. and Darwin, D. (2000) **Splice Strength of Conventional and High Relative Rib Area Bars in Normal and High-Strength Concrete**. ACI Structural Journal, July-August, Vol. 97, No. 4, pp. 630-641.